

Towards the generation of recombinant and pharmaceutically relevant target proteins:

Phage display-based isolation of specific scFv antibodies
against metastasizing pancreatic carcinoma
for clinical application and
development of novel fluorescent reporter tags
for on-line monitoring during target protein production

**Von der Fakultät für Mathematik, Informatik und Naturwissenschaften
der RWTH Aachen University zur Erlangung des akademischen Grades einer
Doktorin der Naturwissenschaften genehmigte Dissertation**

vorgelegt von

Eva-Maria Siepert (M.Sc.)
aus Bad Säckingen

Berichter: Universitätsprofessor Dr. rer. nat. Dr. rer. medic. Stefan Barth
 Universitätsprofessor Dr. rer. nat. Lothar Elling

Tag der mündlichen Prüfung: 22. November 2013

Diese Dissertation ist auf den Internetseiten der Hochschulbibliothek online verfügbar.

In Erinnerung an meine Großmutter

Data presented in this thesis has partially been published in a peer-reviewed journal:

“Siepert, E.M., et al., *Short-chain fluorescent tryptophan tags for on-line detection of functional recombinant proteins*. BMC Biotechnol, 2012. 12(1): p. 65.

This DFG-funded project was performed in co-operation with Esther Gartz und Prof. Dr. Jochen Büchs at the Department of Biochemical Engineering (AVT) at RWTH Aachen University.

All bioengineering experiments, and subsequent data analysis, were conducted by Esther Gartz at the Department of Biochemical Engineering (AVT) at RWTH Aachen University at the head of Prof. Dr. Jochen Büchs

Index

1	Introduction.....	1
1.1	Pancreatic cancer	2
1.1.1	Statistics	2
1.1.2	Risk factors.....	3
1.1.3	Diagnosis.....	3
1.1.4	Therapy.....	4
1.2	Immunotherapy	6
1.2.1	Immunotoxins.....	9
1.2.2	Monoclonal antibodies	9
1.3	Phage display technology	12
1.3.1	M13KO7 bacteriophage	12
1.3.2	<i>In vitro</i> selection procedure	14
1.3.3	Tomlinson Libraries I and J.....	16
1.3.4	L3.6pl target cell line.....	18
1.3.5	Epidermal growth factor receptor.....	19
1.3.6	Monoclonal anti-EGFR antibody fragment 425(scFv).....	19
1.3.7	Generation of 14.1(scFv).....	20
1.4	Protein expression.....	20
1.4.1	Prokaryotic protein expression	20
1.4.2	Eukaryotic protein expression	21
1.5	Protein tags	22
1.5.1	Affinity tags.....	22
1.5.2	Reporter proteins	23
1.5.3	Synthetic labels and SNAP-tag technology.....	26
1.5.4	Tryptophan and potential tryptophan-based tags	28
1.6	On-line monitoring of micro-scale shaking cultures	28
1.7	Objective.....	30
2	Material.....	33
2.1	Chemicals and consumable supplies.....	33
2.2	Equipment and software	33
2.3	Bacterial strains and media	35
2.4	Eukaryotic cell lines and media	36

2.5	Enzymes and their buffers	37
2.6	Reaction kits	37
2.7	Buffers, solutions and antibiotics.....	37
2.8	Antibodies and enzyme-conjugated antibodies	39
2.9	Primer	39
2.10	Plasmid vectors	40
2.11	Molecular weight markers	41
2.12	Single chain antibody libraries and helperphage	41
3	Methods.....	42
3.1	Molecular biological and DNA cloning techniques.....	42
3.1.1	Polymerase chain reaction.....	42
3.1.2	DNA restriction digest.....	44
3.1.3	DNA ligation	44
3.1.4	DNA sequencing and sequencing analysis	44
3.1.5	Analytical and preparative agarose gel electrophoresis	44
3.1.6	Determination of DNA concentration	45
3.1.7	Plasmid DNA isolation from <i>E.coli</i>	45
3.1.8	Design of tryptophan tag (W-tag).....	46
3.1.9	Cultivation of <i>E.coli</i>	46
3.1.10	Preparation of bacterial cryo stock cultures	49
3.1.11	Heat shock transformation of <i>E.coli</i>	49
3.2	Tissue culture and cell processing	49
3.2.1	Cultivation of eukaryotic cell lines.....	49
3.2.2	Cryopreservation and reactivation of eukaryotic cell lines	50
3.2.3	Eukaryotic recombinant protein expression in HEK293T cells	51
3.2.4	Isolation of peripheral blood mononuclear cells	52
3.2.5	Preparation of membrane fractions	53
3.3	Protein chemical and immunological methods	54
3.3.1	SDS-PAGE.....	54
3.3.2	Western blot analysis.....	54
3.3.3	Determination of protein concentration.....	54
3.3.4	Immobilized metal-ion affinity chromatography	55
3.3.5	Extraction of recombinant protein after prokaryotic expression	57
3.3.6	Dialysis of scFv-protein solutions and crude lysate	58
3.3.7	Concentrating protein solutions.....	58

3.3.8	Mass spectrometrical analysis	59
3.3.9	Enzyme-linked immunosorbent assay (ELISA)	59
3.3.10	Flow cytometric analysis	62
3.3.11	Fluorescence-based internalization assays	63
3.4	Phage Display Technology	66
3.4.1	Cultivation of Tomlinson Libraries I and J	66
3.4.2	Phage infection and production	66
3.4.3	Phage precipitation	67
3.4.4	Titer determination	67
3.4.5	Biopanning	67
3.4.6	Site-directed mutagenesis	72
3.5	Methods of bioengineering	74
3.5.1	Micro-scale on-line measurement	74
3.5.2	2D-scan analysis	75
3.6	Analytical and statistical software	75
3.7	Documentation and image editing	75
4	Results: Antibodies against pancreatic cancer	77
4.1	Experiments prior to phage display selection	77
4.1.1	Quality assessment of Tomlinson Libraries I and J	77
4.1.2	Testing of blocking and washing conditions	78
4.2	Isolation of L3.6pl-specific scFv-phage particles	79
4.2.1	Enrichment of scFv-phage particles on adherent cells	79
4.2.2	Enrichment of scFv-phage by suspension panning	81
4.2.3	Enrichment of scFv-phage particles on membrane fractions	83
4.2.4	Identification of unique L3.6pl-specific scFv-phage binders	85
4.2.5	Monoclonal phage ELISA of 14.1(scFv)	89
4.3	Sequence analysis of isolated L3.6pl-specific scFv	90
4.3.1	Whole cell ELISA	92
4.3.2	Cross-reactivity analysis	93
4.4	QuikChange Mutation of stop codons	95
4.5	Production and purification of soluble scFv antibodies	95
4.5.1	Prokaryotic expression in HB2151 <i>E.coli</i> via pIT2 phagemid	96
4.5.2	Prokaryotic expression in BL21 Rosetta 2 (DE3) via pMT plasmid	97

4.5.3	Eukaryotic expression in HEK293T via pMS-SNAPMut plasmid	98
4.5.4	IMAC purification and SNAP-tag labeling with fluorescent dyes.....	99
4.6	Characterization of soluble scFv antibodies	100
4.6.1	Protein ELISA	100
4.6.2	Flow cytometric analysis.....	101
4.6.3	Internalization assays	105
5	Results: Design of novel fluorescent W-tag.....	112
5.1	Generation of W-tag constructs	112
5.1.1	Sequence design and cloning	112
5.1.2	Vector assembly of W-tag constructs.....	114
5.2	Expression of W-tag fusion proteins.....	115
5.2.1	Protein expression in bacterial pellet.....	115
5.2.2	Protein secretion into cultivation medium.....	116
5.2.3	Protein expression in different types of media	117
5.2.4	Percentage of over-expressed Wx-Ki-4(scFv)	117
5.3	On-line measurement data	118
5.3.1	On-line fluorescence intensity measurements	119
5.4	Protein purification of Wx-Ki-4(scFv) proteins	123
5.4.1	Protein recovery by TES buffer lysis	123
5.4.2	IMAC protein purification.....	124
5.5	Measurement of protein binding activity.....	125
5.5.1	Wx-M12(scFv) binding analysis on MCF7 and MDA-MB-231.....	125
5.5.2	Protein ELISA of Wx-Ki-4(scFv) fusion proteins	126
5.5.3	Flow cytometric analysis of Wx-Ki-4(scFv) on L540cy.....	126
5.5.4	Competitive FACS	127
5.6	2D fluorescence measurement of Wx-Ki-4(scFv)	129
6	Discussion.....	130
6.1	Isolation and characterization of pancreas-specific scFv antibodies	130
6.1.1	Enrichment of L3.6pl-specific binders.....	131
6.1.2	The Tomlinson Phage Library.....	139
6.1.3	Protein Expression.....	143
6.1.4	Soluble protein ELISA analysis	144

6.1.5	Flow cytometric binding and cross-reactivity observations	145
6.1.6	Hypothesis on clones D5(scFv) and D9(scFv)	146
6.1.7	Internalization behavior	147
6.2	Design of optically active W-tags	149
6.2.1	W-tag design	150
6.2.2	W-tag protein expression and purification	151
6.2.3	Online measurement of fluorescence intensity	153
6.2.4	2D-scans	155
6.2.5	Flow cytometric binding analysis	156
7	Outlook	157
7.1	Pancreas-specific scFv antibody fragments	157
7.2	Characterization of optically active W-tag	158
8	Summary	160
9	References	162
10	Appendix	178
10.1	QuikChange Mutagenesis primers	178
10.2	Amino acids (IUPC letter codes)	179
10.3	List of approved therapeutic mABs in Germany	179
10.4	Abbreviations	181
10.5	List of figures	186
10.6	List of tables	189
10.7	Publications, presentations and posters	192
10.8	Curriculum Vitae	193
10.9	Acknowledgement	195

1 Introduction

Cancer is the second most common cause of death in Germany (total incidence of 469,800 in 2008 [1]) as well as in the rest of the Western world [2, 3]. Each type of cancer is classified by the specific tissue initially affected. With an incidence of 71,660 (32.1%) breast cancer is most common in women, whereas in men prostate cancer is most frequent with an incidence of 63,440 (25.7%) [1]. In general, cancerous cells emerge due to mostly age-dependent genetic modifications resulting either in up-regulated gene function or in down-regulated tumor suppression [4]. Due to demographic changes as well as increasing obesity, a dramatic rise of cancer incidence rates is expected over the next decades [1].

Based on the assumption that practically all mammalian cells share a similar molecular repertoire of pathways controlling their proliferation, differentiation and death, literature suggests a multi-step process of events progressively leading to neoplastic development. During tumorigenesis malignant cells acquire a set of novel capabilities which successfully disrupt tissue-own cancer defense mechanisms [4, 5]. Literature states six main characteristics that apply for the formation of virtually all malignant cells (Table 1-1):

Table 1-1 Six generally applicable characteristics for development of malignant tumor cells. [4, 5]

Characteristic property	Mechanisms
Self-sufficiency in growth signals	Well-controlled proliferative pathways are misregulated due to signals governing cell growth-and-division cycle. This is can be caused by autocrine production of growth factors or over-expression of receptors (e.g. tyrosine kinases such as the epidermal growth factor receptor (EGFR) (I.3.4.4)) answering to growth signals [6].
Evasion of growth-inhibiting signals	Tumor suppressor genes, such as RB (retinoblastoma-associated) [6], process extracellular signals necessary for cell cycle activation. The TP53 protein acts as a DNA damage sensor [7] and receives intrinsic stress signals (e.g. O ₂ or growth factor levels). As a result, it can halt the cell cycle or induce apoptosis. Defective or missing genes result in uncontrolled proliferation.
Evasion of apoptosis	Typically apoptosis is activated by various physiologic stresses [8] but is inactivated in high-grade malignant cells by pro- and antiapoptotic regulatory proteins. For example blocking of caspases 8 and 9, as well as activation of the Bcl-2 family apoptosis inhibitor oppresses programmed cell death [9, 10].
Replicative immortality	Due to absent telomerase, telomers of healthy cells become shorter with each replication cycle. Elevated telomerase levels in about 90% of all cancers ensure addition of hexanucleotide tandem repeats to telomers thus creating immortal cells [11].
Sustained angiogenesis	Cancer cells and tumors possess an exorbitant need for nutrients and oxygen which leads to never-ending neovascularization. Angiogenesis is for example induced by up-regulation of the vascular endothelial growth factor A (VEGF-A) or by inactivation of the angiogenic inhibitor thrombospondin-1 (TSP-1) [12].
Tissue invasion and metastasis	Alterations in cell attachment and changes in the extracellular matrix, e.g. inactivation of the adhesion molecule E-cadherin [13], induce detachment of cells which then evade surrounding tissues, or release of malignant cells that build metastasis at different locations.

Tumors do not merely comprise a cluster of abnormal cells, but develop an organ-like complexity. Multiple distinct cells are recruited by malignant cells creating a tumor microenvironment which for example provides necessary signals and growth factors, or

structural foundation (fibroblasts). During the hyperproliferative phase of a tumor, even whole subpopulations of cancer stem cells (CSC) are formed that promote malignant growth and metastasis [14, 15]. [4, 5]

1.1 Pancreatic cancer

The pancreas is an organ of mainly glandular tissue located behind the stomach. Its exocrine gland comprises more than 95% and produces the pancreatic juice containing enzymes to digest fats, proteins and carbohydrates. The remaining parts are endocrine cells arranged in small clusters (islets of Langerhans) responsible for hormone release, for example insulin, into the blood. Tumors originated from glandular tissue are classified as adenocarcinomas. [16, 17]

1.1.1 Statistics

The pancreatic adenocarcinoma is a rare but very aggressive type of cancer. In 2008, the morbidity in Germany was 18/100,000 people with a total incidence of 14,960, which corresponds to only 3% of all cancers (Table 1-2). Despite its low incidence rate, pancreatic cancer is the 4th most common cause of cancer-related deaths [1].

Table 1-2 Statistical data on pancreatic cancer in Germany in 2008 with a prognosis for 2012. [1]

	2008		2012	
	♂	♀	♂	♀
Incidence	7,390	7,570	7,800	7,600
Deaths by pancreatic cancer	7,327	7,508	N/A	N/A
Morbidity¹	18.4	18.1	19.5	18.3
Age at diagnosis²	70	76	N/A	N/A
Mortality rate¹	18.2	17.9	N/A	N/A
Relative 5-year survival rate	8	7	N/A	N/A

¹ per 100,000 persons, ² median

The main reason for this high mortality is its distinctly invasive growth behavior in addition to an enormous potential for premature lymphogenic and hematogenic metastasis into neighboring organs, such as liver, lymph nodes, and lung [16, 18, 19]. Fast metastatic spread and high tumor resistance towards radiation and chemotherapy result in a mortality rate of nearly 100% (Table 1-2) [1, 16, 19]. This implies that the prognosis of a patient is strongly dependent on the progression of disease at the time of diagnosis. Except for very early diagnosis, pancreatic cancer is always lethal resulting in an average 5-year patient

survival rate of 1 – 5% and a median life expectancy of 4 – 6 months when diagnosed after metastasis or local spread [1, 16, 18, 20, 21].

1.1.2 Risk factors

Definite reasons for pancreatic cancer are not exactly known, but classified risk factors are excessive abuse of alcohol and cigarettes, as well as obesity in combination with type 2 diabetes [22-24]. In 5 – 10% of the patients, malignant pancreatic cancer is due to a genetically induced risk, inherited from a likewise diseased first-degree relative with cancer or hereditary pancreatitis [16, 25]. Currently identified genetic alterations include amongst others, mutations in codon 12 of the oncogene KRAS2 which is involved in the regulation of cellular growth factor signal transduction [26] or inactivating mutations of the tumor suppressor genes TP53 (inactivated in approximately 60% of pancreatic cancers) or p16 (inactivated in 90% of pancreatic cancers). Normally, TP53 is activated after DNA damage occurs thus inducing apoptosis in the G1-phase of the cell cycle, whereas active p16 acts as cyclin-dependent kinase inhibitor. Its inactivation leads to unhindered cell proliferation. Mutations, which result in deviant methylation patterns of for example FoxE1, NPTX2, CLDN5 or SPARC [19, 27, 28], influence rates of receptor-ligand signal transduction. Prevalence of mutations for the hereditary and sporadic pancreatic carcinoma is evaluated similarly. Moreover, a genetic predisposition to develop pancreatic cancer originates in the mutation of gametes [19, 27, 28]. Altogether, all genetic factors account for approximately 20% of all cases but could also lead to a differential diagnosis.

1.1.3 Diagnosis

The asymptomatic disease pattern of early-stage pancreatic cancer and the lack of adequate and reliable cancer markers in combination with poor molecular imaging techniques complicate an early and correct diagnosis. Primary tumors are located deep inside the body and cannot be seen or felt during routine examinations. Acute clinical symptoms, for example severe pain, weight loss and jaundice, usually do not arise before metastasis has occurred and the tumor has reached an irresectable stage [16, 19]. In case of suspected pancreatic cancer, classical sonography and CT examinations (optionally with contrast agents) are employed to visualize tumor growth. By means of additional tests, such as endoscopic retrograde cholangiopancreatography combined with tissue biopsy, MRI or laparoscopy, the tumor spread is estimated preoperatively. Other examination methods may include intraductal or endoscopic sonography (possibly combined with a Fine-Needle-

Aspiration biopsy), angiography or positron emission tomography (PET) [16]. Tumors are staged according to the American Joint Committee on Cancer (AJCC) using the Tumor-Nodus-Metastasis system [29]. At time of diagnosis, the disease is exclusively localized to the pancreas in 20% of the patients, another 40% are diagnosed with local spread whereas visceral metastasis are found in the rest of the patients [30]. Malignant tumors of the exocrine pancreas originate predominantly (95%) within the ductal epithelium [20, 31].

Many pancreatic tumors express carbohydrate antigen (CA 19-9), carcinoembryonic antigen (CEA), cytokeratins 7, 8, 13, 18 and 19, as well as B72.3 (TAG-72), CA 125, DUPAN2 or mucins (Muc 1, 3, 4 or 5AC). These markers can be detected via immunohistochemistry staining techniques of biopsy tissue or blood samples. CA 19-9 is the most commonly used tumor marker (gold standard) for serum and tissue analysis with a sensitivity of 80% for asymptomatic pancreatic cancer and 55% at occurrence of small resectable tumors < 3 cm. However, no diagnostically significant results are possible from CA 19-9 serum concentrations in asymptomatic patients with invasive lesions [19]. Therefore, CA 19-9 is mostly only used for follow-up examinations during medical treatment. Genetic testing rarely appears promising since inherited DNA mutations are often linked to many different kinds of cancers.

1.1.4 Therapy

Despite marked advancements in molecular tumor biology, the treatment efficiency of pancreatic cancer has not significantly increased within the last 25 years [1, 20]. Basically, three main types of treatment are available: (a) Surgery, (b) chemotherapy and (c) radiation therapy. Surgical tumor removal (pancreatico-duodenectomy or Whipple procedure) is currently the only curative treatment with prospects of success [16, 32]. It can be performed in 15 – 20% of the patients; but even if R₀ resection of the tumor was successful, the 5-year survival rate amounts to only 25 – 30%. Survival decreases to 10% after lymph nodes have been invaded [16, 33]. Only approximately 5% of all tumors are truly resectable at the time of diagnosis.

Nowadays, adjuvant therapeutic approaches consisting of systemic chemo- or radiation therapy, or a combination of both, are employed to reduce the mortality rate [34, 35]. Best results are currently obtained by combining the cytostatic adjuvant Gemcitabine (2', 2'-Difluordesoxycytidin, Gemzar[®]) with resection [36-38]. Since its approval in 1996, it is applied during first-line treatment of advanced and metastasized pancreatic carcinoma

but with limited success. Besides a pain-reducing and weight-gaining effect, Gemcitabine was successfully applied during adjuvant treatment of operable tumors. In comparison to 5-FU (5-Fluorouracil, Efudex[®]), used until the late 1990s, Gemcitabine is better tolerated and results in an improved treatment outcome with a 1-year survival rate of 18% instead of 2% [37, 39, 40]. Both adjuvants are cytostatic pyrimidine analogues and belong to the family of antimetabolites. They intervene during DNA synthesis, especially in highly proliferating tumor cells, leading to cell cycle arrest and subsequent apoptosis. While Gemcitabine is metabolized intracellular to Gemcitabine-triphosphate and inserted into the DNA instead of the human cytidine, 5-FU irreversibly blocks the enzyme thymidylate synthase thus inhibiting thymidine and DNA synthesis.

Since 2007, Erlotinib (Tarceva[®]) is approved for chemotherapeutic treatment of pancreatic cancer. It is a selective inhibitor targeting the tyrosine kinase domain of the epidermal growth factor receptor (EGFR) and is mostly applied in combination with Gemcitabine [41, 42]. EGFR is highly expressed, and sometimes mutated, in a lot of cancerous cells. Erlotinib reversibly attaches to the adenosine triphosphate (ATP) binding site of EGFR thus interrupting cell signal transduction. Usually two EGFR molecules have to form a homodimer for signal transmission. This linking process which activates cellular pathways is induced by ATP. Its blocking consequently results in a missing signaling cascade.

During adjuvant radiation therapy, ionizing high-energy X-rays (photons) or charged particles are used to eliminate cancer cells as pre-operative or post-operative tumor treatment. Ionization of atoms either damages ssDNA and dsDNA of cancerous or dividing cells directly leading to apoptosis. On the other hand, free radicals (hydroxyl radicals) are formed after ionization of water molecules which indirectly damage cellular DNA. Computer-controlled radiation is focused on the tumor by external beam radiation devices, such as intensity-modulated radiation therapy (IMRT) or the robotic arm CyberKnife[®]. They place precise multiple-directioned doses of radiation on the tumor according to its 3D shape to minimize exposure of normal tumor-surrounding tissue [43, 44]. Post-surgery radiation therapy combined with chemotherapy, currently yields the best prognosis for pancreatic cancer patients [31].

Due to the high resistance of pancreatic cancer towards conventional chemotherapeutics and radiation therapy, repeated high-dosage treatment causes unspecific damage to healthy tissue surrounding the tumor. Subsequently this leads to various adverse side effects, such as nausea, hair and weight loss. Chemotherapeutics also damage the bone marrow and the

subsequent production of new blood cells causing an increased chance of infection (lymphocytes) as well as bleeding and bruising after minor injuries (platelets), or fatigue (erythrocytes). This dramatically reduces a patient's life quality [17, 45, 46].

1.1.4.1 Prognosis

Residual tumor cells (minimal residual disease (MRD)) are responsible for a high relapse rate featuring liver metastasis as dominating recurrence in 50 – 70% of the patients [16]. Current treatment options are rarely curative and mostly palliative and life-prolonging. The prognosis remains devastating, especially considering the increasing tendency towards malignant diseases as a result of demographic change (incidence of pancreatic cancer peaks between 7th and 8th decade of life) [1]. Therefore, the need to investigate clinical and tumor biological factors that enable an improved targeted therapeutic approach becomes apparent.

1.2 Immunotherapy

Immunotherapy is a relatively novel but fast advancing field of targeted cancer therapy. It exploits characteristics of cancerous cells, which specifically distinguish them from healthy ones, to eliminate malignant cells with minimal side effects. Within the last 20 years various strategies for targeted tumor treatment have been developed. Immunotherapeutics [31, 47] in form of antibody-drug-conjugates (ADC) present a promising alternative approach which has already led to an increased therapeutic specificity for other types of cancer [48, 49]. Moreover, specific antibodies conjugated to an imaging molecule (e. g. fluorophore, Fe²⁺-particles) may be applied for tumor diagnostics [50-52] in addition to targeted therapeutic drug delivery.

Active immunotherapy stimulates the immune system directly into attacking diseased cells by induction of an efficient cytotoxic T lymphocyte (CTL) response. Moreover, innate mechanisms of the immune system to initiate, program and regulate tumor specific immune responses are exploited [53], including dendritic cells (DCs) as powerful antigen-presenting cells. DCs process unfamiliar endogenous proteins to antigenic peptide fragments and present them on their surface as MHC class I complexes for CD8⁺ T-cell recognition [31, 54]. Exogenous antigens, on the other hand, are digested by proteases after uptake via lysosomes, presented as MHC class II complexes and recognized by CD4⁺ T-cells [31, 54]. T-cells then secrete interferons (e. g. IFN- γ) or cytokines (e. g. tumor necrosis factor TNF- α) as well as interleukins (e. g. IL-4, IL-10) to activate DCs and CTLs

[31, 55, 56]. T-cell activation is often additionally linked to a humoral antibody-based immune response. Known and frequent surface antigen mutations of pancreatic cancer, such as KRAS [57], CEA [58], p53 [59] or human telomerase reverse transcriptase (hTERT) [60], are perfect targets for immunotherapeutic approaches [31]. Particularly interesting targets concerning pancreatic cancer therapy are its treatment-suppressing mechanisms, caused by immune suppressive cells within the tumor microenvironment. Among other mechanisms, this comprises the expression of surface molecules suppressing immune response (e. g. vascular endothelial growth factor) [61], which repress CD8⁺ CTL function by IL-10 secretion [31]. Vaccines, consisting of inactive whole tumor cells as vehicle, can be utilized to deliver specific tumor-associated antigens (TAA) into the body. Another possibility are peptide vaccines mimicking a small immunogenic region of a defined TAA, which induce a TAA-specific T-cell mediated immune response [31]. For cell-based vaccines, synthetic peptides from known tumor antigens are inserted into DC for MHC class I and MHC class II complex presentation [31]. Other options include insertion of tumor cell lysates or transfection with whole tumor cell DNA or RNA [31]. Immunogenicity of tumor cells can be increased by transfection of DCs with genes coding for example for the co-stimulating granulocyte macrophage colony-stimulating factor [62]. In a variation of cell-based immunotherapy, certain cell types (DCs, CTLs) from a cancer patient are amplified, modified *ex vivo* and re-injected into the patient [63, 64]. As a direct result, these molecules inhibit tumor growth, indirectly act anti-angiogenic or increase immune response (progress was shown during melanoma therapy by injection of tumor infiltrating lymphocytes (TIL) [65-67]). As for pancreatic cancer, these active immunotherapeutic approaches are currently under preclinical and clinical investigation.

During a passive immunotherapeutic approach, recombinant monoclonal antibodies (mAB) specifically recognize tumor-associated antigen (TAA) structures on target cells ideally over-expressed on the tumor as well as its metastasis [68, 69]. This specific activity is associated with a reduction of side effects and poses a huge advantage for therapeutic mABs. Their therapeutic effector mechanisms can be direct or indirect. The direct effector function only depends on the binding performance of the mAB to a specific target antigen. Binding recombinant mABs disrupt receptor-ligand interactions by blocking either receptor (e. g. EGFR) or ligand (e. g. TNF- α , VEGF). Similarly, disabling of surface structures also prevents interactions between cells, for example after transplantations (e. g. IL-2 against CD25). An additional direct effector function is the mediation of intracellular

apoptotic impulses by cross-linkage of two surface receptors. Indirect effector mechanisms are dependent on the Fc-moiety of a mAB and thus the antibody isotype. Effector cells (e. g. macrophages, T-cells) are recruited via the Fc-effector function, resulting in the elimination of a diseased cell by apoptosis, phagocytosis or activation of the complement system. Complement-dependent cytotoxicity (CDC) is induced after opsonisation with mAB leading to complement activation and cell lysis [70]. So-called antibody-dependent cellular cytotoxicity (ADCC) is stimulated by attachment of the Fc-part of bound mABs to receptors on effector cells [70, 71]. These cells then secrete substances, such as perforin and Granzyme B, or mediate phagocytosis. Table 1-3 exemplarily lists recombinant mAB with direct and indirect effector function.

Table 1-3 List of approved exemplarily mABs with a direct and indirect effector mechanisms.

mAB	Mechanism	Effector molecule	Application
Infliximab (Remicade®)	direct ligand-mediated	binding to cytokine TNF- α blocks receptor reaction, inhibition of proinflammatory signals	rheumatoid arthritis, Crohn's disease [72]
Adalimumab (Humira®)	direct ligand-mediated	binding to cytokine TNF- α blocks receptor reaction, inhibition of proinflammatory signals	rheumatoid arthritis, autoimmune diseases [73]
Basiliximab (Simulect®)	direct receptor-mediated	binding to IL-2 receptor CD25 prevents rejection after kidney transplants	organ transplantation [74]
Daclizumab (Zenapax®)	direct receptor-mediated	binding to IL-2 receptor CD25 prevents rejection after kidney transplants	organ transplantation [75]
Bevacizumab (Avastin®)	direct ligand-mediated	binding to secreted VEGF inhibits angiogenesis	advanced colorectal, lung, breast, kidney and cervix carcinoma [76]
Trastuzumab (Herceptin®)	Direct receptor-mediated indirect (ADCC)	binding to EGF blocks HER2/neu receptor, inhibits growth and proliferation-inducing signals	breast cancer [49, 71]
Rituximab (MabThera®)	direct receptor-mediated, indirect (CDC and ADCC)	Binding to and cross-linking of CD20 receptors on B-cell, induces apoptotic signals	lymphoma, leukemia, transplant rejection [48, 70, 71]

In Europe, currently twelve mABs are approved for cancer therapy (10.3) [77], for example Rituximab, Trastuzumab or Cetuximab [48, 49, 78], but none for an effective and specific treatment of pancreatic cancer. To improve their therapeutic effect, the natural binding function of mABs is enhanced by covalent conjugation to cytotoxic substances, such as low-molecular chemical compounds, to form radioimmunoconjugates (e. g. I¹³¹ or Y⁹⁰ [79, 80]) or non-radioactive chemoimmunoconjugates (e. g. Doxorubicin [81]), as well as macro-molecular protein-based immunotoxins (IT) [69, 82].

1.2.1 Immunotoxins

Immunotoxins (ITs), also known as cytolytic fusion proteins, are passive humoral immunotherapeutics. They consist of a tumor-specific binding moiety and a cytotoxic effector domain, where the mAB acts as a carrier molecule for targeted delivery. In order to reach complete cytotoxic potency and consequent selective elimination of malignant cells, ITs have to be internalized and translocated to the cytoplasm after surface binding [83]. Hence, the choice of target protein is important since not every binding ligand is also internalized and suitable to induce apoptosis with a limited number of receptors. Protein-based cytotoxic effector domains can be derived from plants (e. g. Ricin or Saporin (also called ribosome inactivating protein (RIP)) or bacteria (e. g. diphtheria toxin, Exotoxin A (ETA) [84, 85]). A frequently used bacterial toxin is the truncated version of the Exotoxin A (ETA') [85-87] from *Pseudomonas aeruginosa*, whose genetic mutation does not influence its catalytic activity but prevents unspecific toxicity caused by premature separation of ligand and toxin. Due to their high immunogenicity, plant and bacteria-derived toxins have their limitations during repeated treatment cycles since they may induce an immune response, ranging from fever to kidney toxicity and vascular-leak-syndrome [88]. Next generation toxins are of human origin, such as human RNase (angiogenin) [89], kinases (DAPK2) [90] or serin proteases (Granzyme B) [91, 92]. Human toxins are smaller than ETA' which is favorable for efficient protein expression and presents an advantage for tissue penetration during solid tumor treatment [31, 68, 69, 93-96].

1.2.2 Monoclonal antibodies

Antibodies are part of the natural immune reaction and responsible to mark foreign substances or mutated cancer-related protein structures on cells [97]. In cancer therapy, antibodies are used to detect tumor-specific target structures. While the idea of targeted cell toxins was already phrased by Paul Ehrlich in the 1800s [98], it was impossible to be realized until the invention of hybridoma technology [99], which was a huge mile stone in the field of specific recombinant mAB development. Hybridoma technology uses immunized mice to isolate antibody-secreting B-cells which are then fused to immortal myeloma cells (cancer B-cells) for antibody production.

Murine as well as human mABs belong to the immunoglobuline (Ig) superfamily [97]. An Ig consists of four poly-peptide chains with two identical light chains (L-chain) and two

identical heavy chains (H-chain) which are covalently inter-linked via disulfide bridges [97]. Each chain is divided into a constant region (C-region) and a variable region (V-region). The constant heavy chain (C_H) has three domains (C_{H1} , C_{H2} , C_{H3}), whereas the variable chain has just one domain (Figure 1-1). V-regions of both chains (V_H and V_L) are divided into three hypervariable regions, denoted complementarity determining regions (CDRs) which are stabilized by four genetically conserved framework regions (FWRs) with β -sheet structure [100, 101]. These CDRs are the specific antigen binding sites and identically presented on the two arms of the Y-shaped antibody protein. Antibody specificity is mainly determined by the amino acid sequence of the CDRs, whereas the three domains of the C-region mediate effector functions, such as the activation of the complement system or binding to surface receptors of macrophage.

The high level of immunogenicity in first-generation recombinant mABs, caused by their hybridoma technology-related murine origin, often resulted in a human anti-mouse antibody (HAMA) immune response during clinical studies [102]. HAMA is amplified when a therapeutic is applied repeatedly and antibodies are neutralized before they can take effect. This may cause severe side effects, from fever to life-threatening renal failure. Moreover, *in vivo* tumor penetration was impaired by the large size of full-length antibodies (150 kDa) [103]. Since 1975, the rapid progress in recombinant DNA technologies and antibody engineering has contributed fundamentally to overcome the problems of size and immunogenicity. Recombinant molecular biological techniques allowed the artificial *in vitro* generation of genetically modified antibody fragments with higher binding affinity, stability and less immunogenicity. To reduce antibody size and to improve mobility and diffusion properties through tumor tissue, different antibody fragments can be designed for therapeutic use [97, 104]. Besides the full-length antibody (150 kDa), monovalent Fab fragments (fragment of antigen binding, 50 kDa) are produced with protease treatment [105]. Another option are bivalent $F(ab)_2$ fragments (100 kDa) [97] or monovalent single chain fragment variables (scFv) (Figure 1-1) [97, 106]. With only 25 kDa, recombinant scFv molecules are the smallest antibody fragments. They consist of protein heterodimers with associated variable domains of V_H and V_L chains which are connected by a glycine-serine linker (GS-linker) for stabilization and proper folding.

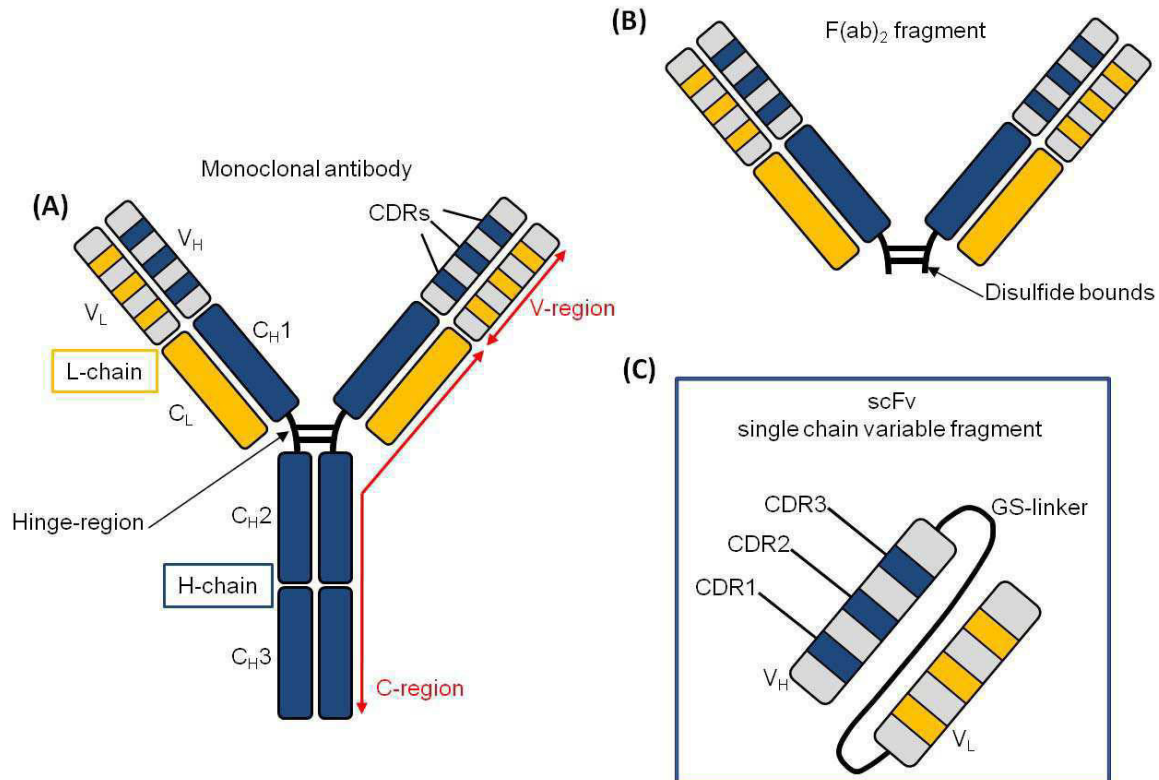


Figure 1-1 Schematic drawing of monoclonal antibody, F(ab')₂ fragment and scFv to illustrate the structure of immunoglobulins (Ig) and derived antibody fragments.

(A) shows the monoclonal full-length antibody (150 kDa) marked with its important regions: CDR = complementarity determining region (hypervariable regions), L-chain = light chain (yellow), H-chain = heavy chain (blue), C-region = constant region (red arrow), V-region = variable region (red arrow), V_L = variable light chain, V_H = variable heavy chain and the three constant domains of the heavy chain C_{H1}, C_{H2}, C_{H3}. (B) The F(ab')₂ fragment (50 kDa) shows two fragments of antigen binding connected via a disulfide bridge. (C) The scFv (single chain fragment variable) as the smallest recombinant antibody (25 kDa) linked with a glycine-serine (GS) linker for correct folding and stability.

To minimize the HAMA immune reaction caused by murine recombinant antibodies, second-generation chimeric antibodies are constructed by exchanging the murine C-region with a human sequence. Third-generation humanized antibodies are created by murine CDR-grafting into a human antibody framework. These antibodies still cause an immune reaction against the residual murine portion (HACA = human anti-chimeric antibody) or against allotypic epitopes and glycosylation of the foreign human C-region (HAHA = human anti-human antibody) [107, 108]. Nevertheless, these antibody formats are preferable since they only result in low antibody titers and may still be used for therapeutic applications. Latest-generation antibodies are composed of completely human antibody sequences acquired by immunization of transgenic mice carrying human Ig genes [109] or via isolation from human phage display libraries [110, 111].

All mentioned molecules can be constructed by means of recombinant antibody technologies, with the option for immunotoxin expression and *in vitro* as well as *in vivo*

analysis. For this thesis, only scFv antibody formats were utilized. Their low molecular size supports rapid and efficient tumor penetration but results in a shorter circulation time due to renal clearance from the system, which occurs up to about 60-70 kDa [112]. Larger constructs are cleared through the digestive system and consequently have a longer retention time [113]. Recombinant scFv antibodies lack the functional Fc effector moiety [114, 115] and are easy to produce in large high-quality quantities by means of prokaryotic and eukaryotic expression systems.

Essential parameters to choose a suitable molecule for tumor targeting are: (a) High specificity, (b) missing cross-reactivity towards undiseased tissues, and (c) high affinity (preferably in the low μ molar and nmolar range during *in vivo* targeting) [116].

1.3 Phage display technology

Phage display technology is a powerful, fast and efficient tool to select specifically binding antibodies or scFv fragments (also Fab fragments) against almost any antigen [111], for use in targeted immunotherapy or diagnostic optical imaging techniques. In contrast to the hybridoma technology [99], phage display is performed completely *in vitro*. A huge advantage of this technology is the potential to construct large phage libraries with high sequence diversity [110, 117]. Compared to traditional approaches, it allows for *in vitro* screening and selection of billions of scFv fragments or peptides/proteins to identify lead candidates of monoclonal therapeutic antibodies [110, 111, 118]. Moreover, it facilitates the construction of recombinant antibodies with a completely human framework, thus minimizing adverse immune reactions [118]. It is distinguished between immunized libraries constructed from antigen-reactive B-cells or naïve libraries created from B-cells without antigen contact [111]. In addition, CDRs can be artificially mutated to enhance diversity by means of polymerase chain reaction (PCR) and randomized oligonucleotide primers [119]. Once high-affinity antibodies have been identified from a phage library, their synthesis is straightforward and can be optimized by conjugation or cloning [120]. Besides the described system of antibody phage display (1.3.1, 1.3.2, 1.3.3), this method has also been established on yeast or ribosomes [121].

1.3.1 M13KO7 bacteriophage

Phage display technology is based on the fusion of a scFv antibody to a bacteriophage coat protein where the phage is responsible for presenting the scFv antibody for selection [122]. The M13KO7 bacteriophage (Figure 1-2), used in this thesis, is a ssDNA virus, and

belongs to the filamentous non-lytic bacteriophage that infects gram-negative bacteria, such as TG1F⁺ *E.coli*. M13KO7 decreases bacterial growth but keeps the host cell intact while producing and secreting scFv-phage particles into the surrounding medium. M13KO7 phage particles have a diameter of 6.5 nm and are 939 nm long with a viral mass of 16.3 kDa [123]. Its genetic information is contained on a circular ssDNA of 6407 nucleotides encapsulated inside the phage coat proteins. It encodes eleven proteins (pI - pXI) responsible for the coat proteins (pIII, pVI, pVII, pVIII, pIX), phage assembly (pI, pIV, pXI) and DNA replication (pII, pV, pX). Its flexible cylinder-shaped body is composed of approximately 2700 copies of coat protein pVIII and is capped by each five copies of the minor coat proteins pIX and pVII on one side, and by each five copies of pVI and pIII on the other side (Figure 1-2A). For most phage display applications, the pIII coat protein is N-terminally fused to a peptide, protein or scFv fragment, which is then presented on the phage particle exterior for selection. Moreover, the pIII protein is required for infection of the TG1F⁺ *E.coli* bacteria carrying the conjugative F-plasmid (F = fertility factor), which allows expression of F-pili essential for M13KO7 absorption. After attachment of the phage coat protein pIII to the tip of the F-pilus, it is drawn inwards; the phage genome is injected and translocated into the cytoplasm [124]. The complementary strand of the ssDNA is synthesized by the bacteria which results in a supercoiled dsDNA template for replication and protein translation inside the host cell. Proteins pVII, pIX, pVIII, pIII and pVI are directed to the periplasmic membrane where they are assembled and subsequently secreted after completion [125]. The oxidizing environment within the periplasm ensures correct folding and disulfide bond formation of fusion proteins for phage display. Phage proteins pII, pX and pV remain in the cytoplasm since they are only engaged in the replication process. Genetic information of the different scFv fragments fused to the pIII proteins is encoded on a plasmid-based phagemid. This merely carries the gene for the scFv-pIII fusion but none of the other phage genes and has been transformed into TG1F⁺ *E.coli*. Phagemids have an *E.coli* origin for expression as well as a phage origin locus and an ampicillin resistance. Additionally, a multiple cloning site is integrated in front of the pIII gene (gIII) to insert the scFv antibody fragment. The phagemid is missing all genetic information for assembly, coat proteins and DNA replication thus lacking the ability to build phage particle on its own. To achieve that, phagemid-containing bacteria are infected with “empty” helperphage which complements the missing genes including the pIII wild-type protein [126] thus combining genotype and phenotype. This process is called phage rescue. This non-complex phagemid system simplifies any

subsequent cloning procedures and enables the construction of larger and more diverse libraries. Moreover, this system allows adjusting the valency of the scFv-presenting phage.

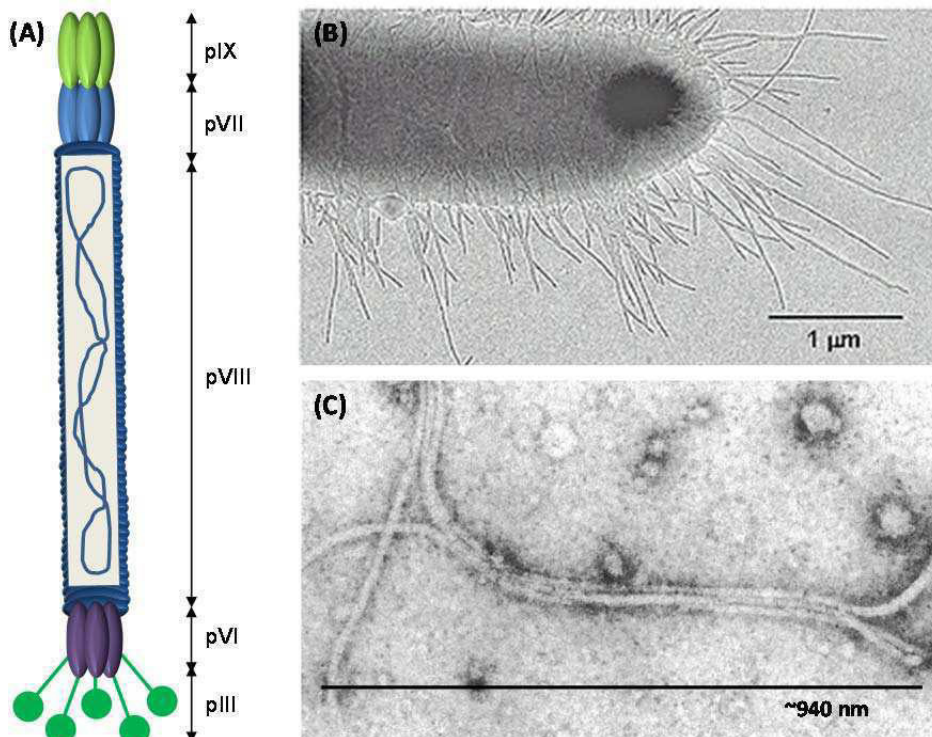


Figure 1-2 Schematic of filamentous M13 bacteriophage and E.coli with F-pili.

(A) Schematic drawing of filamentous M13 bacteriophage showing coat proteins pIII, pVI, pVII, pVIII and pIX as well as the ssDNA within the phage body (drawing adapted from [123]), (B) Electron microscopic picture of *E.coli* bacterium displaying F-pili [127], (C) Electron microscopic picture of filamentous bacteriophage [128].

Two types for M13KO7 phage exist: (a) Monovalent M13KO7 helperphage, which still contain genetic information for the pIII wild-type protein, can incorporate between zero and one copies of the pIII-scFv fusion protein during assembly [129], and (b) polyvalent M13KO7ΔpIII hyperphage, being a helperphage with a deletion of the pIII gene, can integrate five copies of pIII-scFv fusion protein during assembly to avoid heterogeneity [130]. Since the helperphage genome encodes the wild-type coat proteins, typically over 90% of rescued phages do not display the library protein at all. Nevertheless, monovalent display by using phagemid vectors may be essential when selecting antibodies of higher affinity [131].

1.3.2 *In vitro* selection procedure

The *in vitro* selection process of specifically binding scFv fragments by means of phage display is called biopanning. The selective antigens (purified proteins, viable cells, membrane fractions or sugars) are immobilized on immunotubes or microtiter plates

(MTPs) with maxisorb surfaces [110, 111, 119, 132-134]. Phage particles displaying the scFv-pIII fusion protein (scFv-phage) are expressed in TG1F+ bacteria and incubated on these antigen target structures. Unbound or low-affinity scFv-phage particles are removed during stringent washing cycles and bound antibody fusion proteins can be eluted via pH-shift. To complete the biopanning cycle, obtained scFv-phage binders are amplified by infection with fresh TG1F+ *E.coli* and the selection cycle is repeated three times [135, 136]. Washing stringency is increased with each selection round whereas the concentration of immobilized antigen is decreased. Figure 1-3 illustrates a biopanning selection cycle as performed during this work.

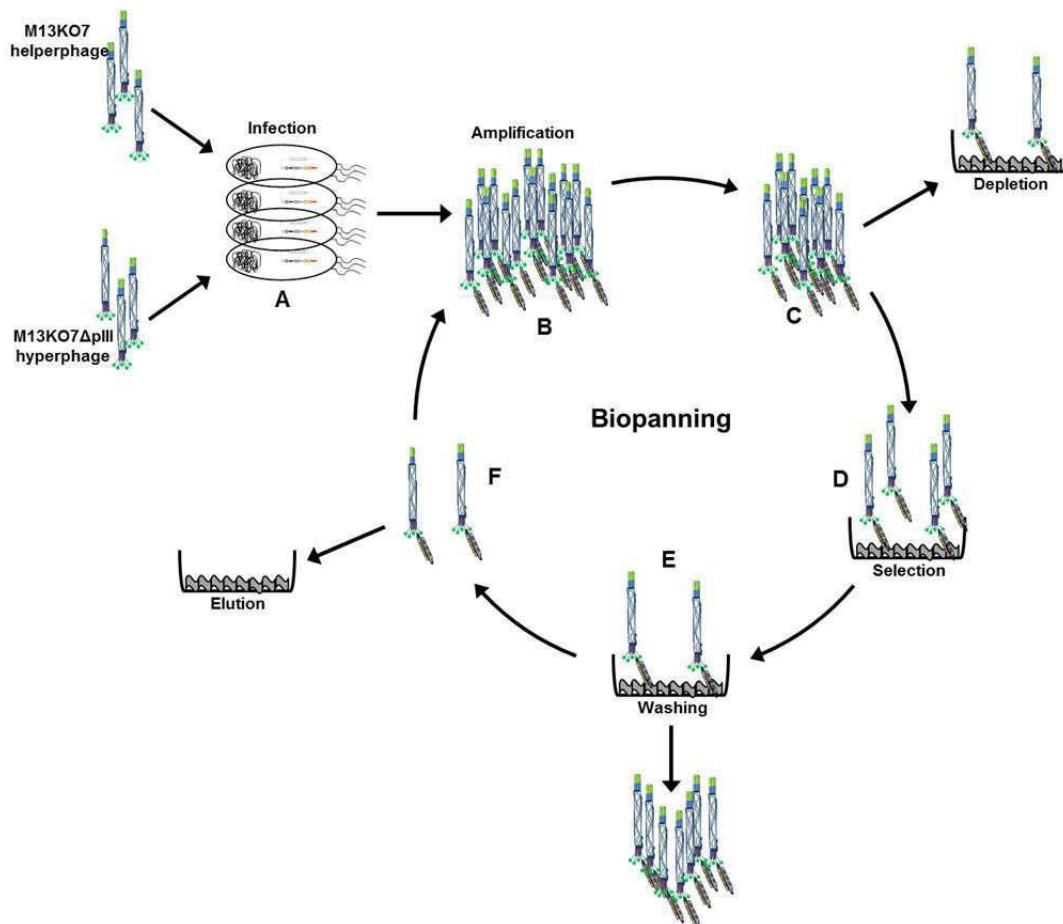


Figure 1-3 General schematic illustration of phage display panning procedure for the selection of specific scFv-phage particles.

(A) Infection of unselected TG1F+ *E.coli* library, transformed with the scFv-carrying phagemids. Either the monovalent M13KO7 helperphage or the polyvalent M13KO7ΔpIII are used for infection of the library. (B) Amplification of scFv-phage particles. (C) Subtractive selection of scFv-phage molecules that show unspecific binding to a depletion antigen (e. g. peripheral blood mononuclear cells (PBMCs)); unspecifically bound scFv-phage particles are discarded. (D) Positive selection of scFv-phage particles that specifically bind to the target antigen. (E) Unbound or weakly bound scFv-phage molecules are removed by several stringent washing steps supplemented with different detergents if necessary. (F) Specifically bound scFv-phage proteins are eluted via pH-shift and used to infect “empty” TG1F+ *E.coli* to amplify fresh scFv-phage particles for the next panning round. In order to isolate specific scFv-phage binders, the shown selection cycle is repeated three times.

Biopanning is ideally conducted on a certain homogeneous target protein in form of purified protein [137] but heterogeneous panning strategies are also feasible [134, 138]. Since surface proteins are integrated into the lipid layer of the membrane, selections are then performed on whole viable cells to preserve their native protein conformation or on membrane fractions which imitate the intact cell surface [134, 138]. A great advantage of selections on purified protein is that only one protein is targeted compared to the entire repertoire of membrane proteins, phospholipids, polysaccharides and glycoproteins on living cells or membrane fractions. Heterogeneous conditions favor enrichment of unspecific scFv-phage particles which can be removed by means of subtractive selection on different cells as well as vigorous washing [138]. A complementary selection strategy is concentrated on the isolation of internalizing scFv-phage particles since this attribute is essential for therapeutic approaches [139], such as immunotoxins or other antibody conjugates. All eukaryotic cells are able to take up extra cellular substances in vesicles via endocytosis. Ligand-binding receptors then transport cytolytic antibody immunoconjugates to their target location within the cell. Internalizing antibodies are best selected on viable cells where they mostly target surface proteins with a very high expression density. Isolation of a desired and specific scFv antibody from an antibody phage library may require a combination of different selection methods.

1.3.3 Tomlinson Libraries I and J

High diversity (normally 10^9 - 10^{11} clones/library) and quality of phage display libraries are essential for successful antibody selection [140-142] by phage display. It is generally distinguished between naïve and immunized libraries. Immunized libraries are constructed from V-genes of mice [128] or other animals whereas naïve libraries are either derived from natural human non-immunized or synthetic V-genes [143]. Random rearrangement of V_H and V_L genes of naïve human B-cells, enables the design of highly diverse libraries consisting of scFv antibody fragments. The probability to isolate a specific high-affinity binding peptide from an antibody phage display library increases with the structural diversity of the library [144]. Naïve libraries are advantageous over immunized libraries which are limited in their diversity [145]. Within several days, binders against any arbitrary antigen may potentially be generated from the same naïve phage library. This includes toxic substances, haptens and carbohydrates as well as intra- and extra-cellular proteins of cells and viruses, or body-own antigens which evade immunization through natural tolerance mechanisms [141].

This work uses the Tomlinson phage libraries I and J [135] for the isolation of recombinant monoclonal scFv antibody fragments. Both libraries are naïve semisynthetic filamentous phage display libraries of human origin with over 100 million diverse scFv fragments. Library size is only limited by transformation efficiency (10^7 - 10^9 clones/library) of the pIT2 phagemid vector (Figure 1-4) into the *E.coli* strain TG1F+ [135]. Each single chain is constructed of a polypeptide consisting of a V_H and V_L domain connected by a flexible synthetic glycine-serine [(Gly₄Ser)₃] linker [110] (1.2.2, Figure 1-1). All scFvs bind to protein A and L for detection, purification or immobilization purposes and in addition carry a *myc*-tag and His₆-tag. In order to maximize side chain diversity, CDRs of library I have been diversified via DVT triplets [135, 146], in a total number of 18 residues (D = adenine, guanine, thymine, V = adenine, guanine, cytosine, T = thymine). This results in a library size of 1.47×10^8 clones with 96% insert-carrying plasmids. For library J, CDR diversity was artificially enhanced by NKK triplet mutations (N = any base, K = cytosine, guanine) to a library size of 1.37×10^8 clones, comprising 88% insert-carrying plasmids. As a drawback, NNK diversification generates the *amber* stop triplet TAG with a statistical probability of 3% [147]. Besides incorporated side chain diversity both libraries are based on a single human framework with V_H (V3-23/DP-47 and J_H4b) [148, 149] and V_K (O12/O2/DPK9 and J_K1) [149, 150]. Expression patterns of these V-gene families dominate the human antibody repertoire [151] and feature high stability [152]. During scFv-phage expression in the *E.coli* suppressor strain TG1F+ the *amber* stop codon is translated as glutamine. This is necessary since the pIT2 phagemid system includes a systematically inserted TAG triplet that theoretically separates the scFv from the pIII fusion protein during soluble protein expression in a non-suppressor strain, such as HB2151 *E.coli*. Random *amber* stop codon insertion within the CDRs imposes a disadvantage during soluble protein production resulting in early protein termination or translation of non-sense proteins. Consequently, TAG triplets in CDRs have to be removed via site-directed mutagenesis before expression of soluble proteins. During this procedure thymine is exchanged against cytosine, thus encoding for a glutamine triplet instead of an *amber* stop codon [153, 154]. Protein expression in the pIT2 phagemid (Figure 1-4) is under the control of the IPTG-inducible *lac* promoter located up-stream of the ribosomal binding site (RBS). Down-stream of that, the N-terminally located bacterial *pectate lyase* B leader signal sequence (*pelB*) is responsible for transporting the expressed proteins into the periplasmic space for subsequent secretion of scFv-phage particles.

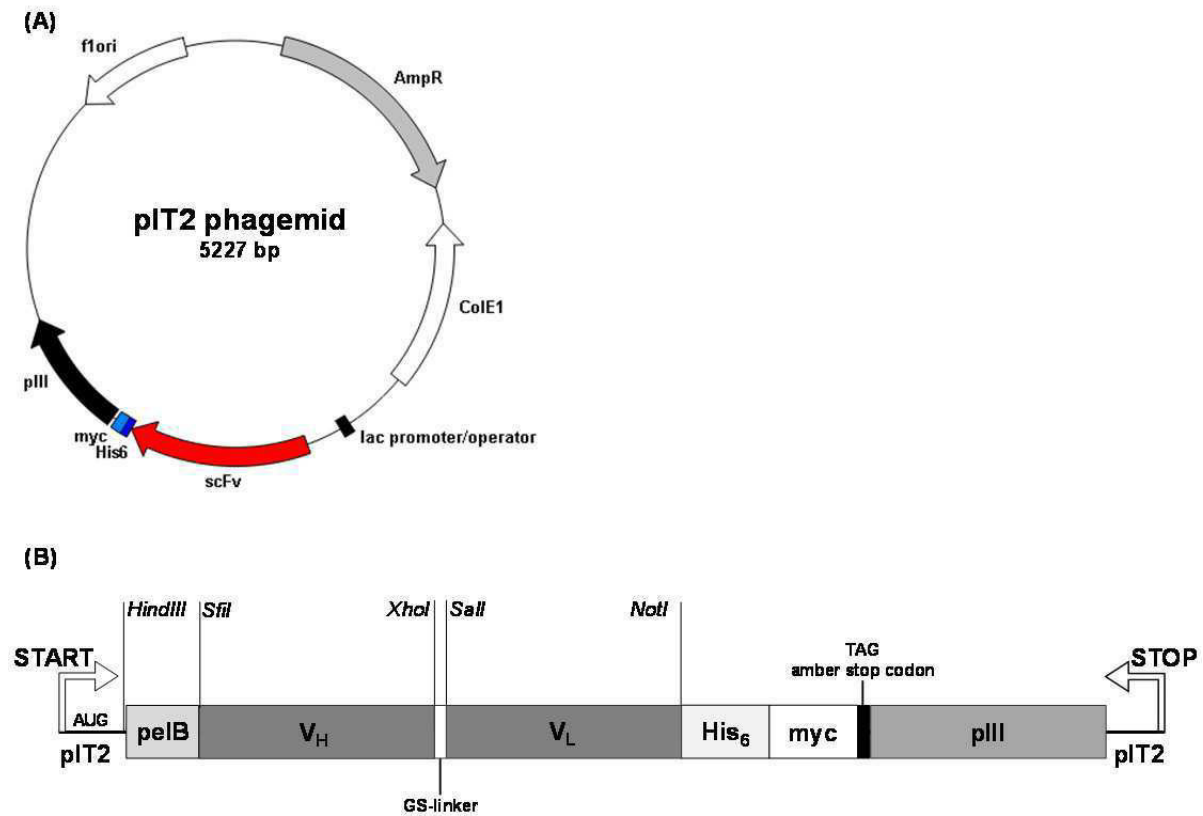


Figure 1-4 Schematic illustration of pIT2 phagemid and corresponding expression cassette for production of scFv-phage particles.

(A) pIT2 phagemid vector for production of scFv proteins fused to the pIII M13KO7 phage coat protein in TG1F+ *E. coli* as well as for soluble protein production in HB2151 *E. coli* without pIII-fusion controlled by an IPTG-induced lac-operon. Soluble protein expression ends after the His₆-tag and myc-tag as shown in (B). (B) Schematic of pIT2 expression cassette for prokaryotic expression of soluble proteins in HB2151 *E. coli*. A *pelB* signal peptide is located up-stream of the scFv sequence mediating periplasmic protein expression and eventual protein secretion into the culture medium. Within the scFv, the heavy chain V_H is connected to the light chain V_L through a glycine-serine (GS) linker peptide. IPTG-inducible scFv expression is controlled by a lac-operon. Down-stream of the scFv sequence a His₆-tag and myc-tag are integrated followed by the *amber* stop triplet TAG to separate the scFv and pIII phage coat protein. Potential restriction sites (*HindIII*, *SfiI*, *NotI*, *XhoI*, *SalI*) for subcloning into other expression vectors are indicated. [135]

The M13KO7 phage carries a kanamycin resistance so that infected bacteria carrying the ampicillin-resistant pIT2 phagemid grow and produce scFv-phage particles only in culture medium complemented with both antibiotics; hence uninfected and phagemid-lacking bacteria or contaminating organisms are sorted out.

1.3.4 L3.6pl target cell line

The pancreatic carcinoma cell line L3.6pl was chosen as phage display target cell line for its highly metastasizing properties and the existence of a well-established orthotopic mouse model [155]. L3.6pl was developed from the human ductal pancreas adenocarcinoma cell line COLO357. This generated the FG cell line (FG = fast growing) after several transplantation and selection cycles of *in vivo* pancreas-liver transplants in nude mice and

subsequent *in vitro* cultivation [156]. FG was then injected into the spleen of nude mice, and potentially developed liver metastasis were removed and cultivated *in vitro*. Several repetitions of this process resulted in the L3.6pl which exhibited very aggressive tumor growth and extreme potential for metastasis [155]. The L3.6pl-based orthotopic mouse model, developed by Bruns et al. [155], has proven useful to treat and image L3.6pl tumors, or to examine effects of novel proapoptotic therapeutics on pancreatic tumors [157, 158].

1.3.5 Epidermal growth factor receptor

Similar to many other cell lines derived from epithelial tumors, the pancreatic cancer cell line L3.6pl features an increased over-expression of the epidermal growth factor receptor (EGFR) [157, 159] which accounts for a very high proliferation index and inhibited apoptosis of malignant cells [160, 161]. EGFR is a membranous glycoprotein (MW = 170 kDa) with tyrosine kinase activity integrated into the cell membrane and is involved in signal transduction pathways. EGFR over-activation often coincides with increased resistance against conventional chemotherapeutic treatment options, as well as advanced tumor stages and a reduced survival rate [162]. Binding to an EGFR molecule causes dimerization of two receptor molecules, thus inducing autophosphorylation of tyrosine residues of the intracellular EGFR tyrosine kinase. This activates a signal transduction cascade and mediates the internalization of the EGFR-ligand-complex by endocytosis [163]. High internalization capability is also required for potentially therapeutic scFv antibodies isolated by phage display throughout this work. Therefore, the EGFR and its corresponding well-documented single chain antibody fragment 425(scFv) [164], offer an excellent positive control for all binding and internalization processes on the L3.6pl cell line used for comparison of the newly isolated scFv binders.

1.3.6 Monoclonal anti-EGFR antibody fragment 425(scFv)

During this work, the monoclonal anti-EGFR antibody fragment 425(scFv) [164], binding to the EGFR, was used as a positive control. Several studies have proven that anti-EGFR mAb can inhibit growth of some EGFR-positive (EGFR+) cell lines *in vitro* as well as EGFR+ tumor growth in transplanted immunodeficient mice [165, 166]. Selective tissue treatment was shown, resulting in the mAb IMC225 Cetuximab (Erbiximab®) against metastasizing colon carcinoma [167]. Cetuximab binds to a different surface epitope of the EGFR than 425(scFv) [164, 168]. The latter has not been approved for therapeutic use but

has proven very efficient in the lab when used as 425(scFv)-ETA' immunotoxin on EGFR+ cell lines, as for example A431 or L3.6pl [157-159, 169].

1.3.7 Generation of 14.1(scFv)

In addition to the clones selected from Tomlinson libraries I and J, the recombinant clone 14.1(scFv) was characterized in this work. It has originally been isolated from an immunized library created from murine B-cells by Beate Stadler at Fraunhofer IME (Aachen). Therefore, mice have been immunized, with a total of 1×10^7 L3.6pl cells or membrane fractions [134] in combination with GERBU Adjuvant 10, by applying six subcutaneous boosts within 13 weeks. Antibody saturation in serum was documented from weekly blood samples by ELISA analysis. After 15 weeks, spleens were dissected to isolate and prepare mRNA. After subsequent cDNA synthesis of V_H and V_L genes followed by SOE-PCR amplification, the generated scFv antibody fragments were cloned into the pHEN4II phagemid via the restriction sites *SfiI* and *NotI* and transformed into TG1F+ *E.coli*. The library (size $\sim 10^6$) construction process was carried out according to Tur et al, 2003 [134]. Analogous to the method described in chapter 0, the pancreas-specific antibody fragment 14.1(scFv) has been isolated on L3.6pl antigen via biopanning prior to this work.

1.4 Protein expression

1.4.1 Prokaryotic protein expression

Non-human proapoptotic proteins are often toxic for the host organism when produced in eukaryotes. Hence, recombinant cytolytic proteins are usually expressed in prokaryotes such as *E.coli*. This microorganism is one of the most commonly used hosts for the expression of recombinant proteins and well-studied as prokaryotic production system. It is easy to manipulate on genetic level and uncomplicated to handle during cultivation. Recombinant proteins can either be expressed in the cytoplasm or secreted into the periplasmic space of the bacteria [170].

Periplasmic expression: During this process, recombinant proteins are secreted into the periplasmic space via the inner membrane by means of signal peptides, such as *pelB* or *ompA*. The oxidizing environment of the periplasm in *E.coli* contains disulfide-oxidoreductases [171, 172] and chaperons [173], which favors the generation of disulfide bonds and consequently correctly folded proteins. Moreover, low content of contaminating

bacterial proteins presents an advantage for subsequent purification processes. Additionally, the periplasm comprises few proteases thus reducing proteolytic degradation to a minimum [174]. Improved expression protocols and systems increase production efficiency by use of compatible solutes and osmotic stress [175], facilitating the accumulation of up to 95% of functional protein in the periplasmic space. Combined with high expression vectors, for example pET-derived vectors [171], very high productivity rates are attained. Nevertheless, subsequent protein secretion from the periplasmic space into the culture medium is not always feasible but strongly depends on protein size and culturing conditions that increase membrane porosity.

Cytoplasmic expression: In comparison to the periplasmic production, the cytoplasmic expression produces considerably higher yields during recombinant protein production [176, 177]. However, these proteins are mostly stored within the cell as insoluble aggregates, known as inclusion bodies (IBs) [178]. Proteins in IBs exist in a denatured and cross-linked form with a strongly diminished biological activity of varying degree [178]. To reconstruct functional proteins, costly and elaborate back-folding is necessary which often leads to low recovery rates of functional protein as well as decreased protein stability and diminished aggregating behavior [179]. Nevertheless, the high concentration of recombinant protein in IBs can be an advantage, since they also protect proteins from degradation by cytoplasmic proteases [180].

During human protein production in *E.coli*, differences of codon usage in prokaryotes and eukaryotes have to be considered [181]. When neglected, the effect on translation efficiency and folding can be dramatic. Certain *E.coli* strain derivatives, such as BL21 Rosetta 2 (DE3), contain the pRARE2 plasmid supplying tRNAs for 7 rare codons (AGA, AGG, AUA, CUA, GGA, CCC, CGG) [182] enabling the bacteria to translate human triplets; thereby enhancing the yield for expression of mammalian proteins. Another limiting factor is the inability of bacteria to accomplish post-translational modifications and glycosylation, which may lead to misfolding and disturbed functionality of expressed proteins [172].

1.4.2 Eukaryotic protein expression

Alternatively to prokaryotic systems, recombinant protein expression in eukaryotes allows the production of a homogenous protein product in high quantity and quality with correct post-translational modifications. The existence of glycosylation and diverse other

modifications is of utmost importance for subsequent use in clinical applications. In addition, expression systems accomplish the production of larger and more complex proteins (e. g. 150 kDa full-length mAb). Responsible for proper protein folding and functionality are disulfidomerase and chaperones located in the endoplasmic reticulum (ER), which guarantees formation of disulfide bonds as well as clustering of protein domains [172]. Moreover, eukaryotic cells secrete recombinant proteins into the culture medium when directed by a signal sequence. This renders a continuous protein expression possible since the destruction of production cells becomes unnecessary. Media collection is sufficient and, due to low level of unwanted proteins, purification is simplified. One possible system for the secretion of eukaryotically expressed proteins is the pSecTag-derived pMS vector system (2.10) [183], where an N-terminal Ig-Kappa (Ig κ) signal sequence controls secretion of transfected protein from the cells and promotes fast production of high amounts of recombinant target protein. By using mutated cell lines, unsusceptible towards the catalytic domains of the cytotoxic proteins [184], it is also possible to employ eukaryotes for the production of functional recombinant cytolytic proteins when modified in their binding activity and cytotoxicity [92, 185]. Commonly used mammalian production cell lines are cos7 (monkey kidney cells), CHO (Chinese hamster ovary) and the human embryonic kidney cell line HEK293T. HEK293T and cos7 cells are equipped with the SV40 origin of replication (ori), expressing the large-T antigen of the SV40 virus. This supports high-copy production transfected plasmids and is especially suitable for transient transfections.

1.5 Protein tags

1.5.1 Affinity tags

In recent years, the field of high-yielding production of recombinant heterologous proteins has grown rapidly. To facilitate purification of a single target protein from a heterologous protein solution, protein fusion tags, called affinity tags, are applied. Commonly, these tags are employed for specific and efficient affinity purification by means of chromatography, for example during immobilized metal-ion affinity chromatography (IMAC), or immunodetection of proteins during Western blotting or analysis via enzyme-linked immunosorbent assays (ELISA). The most frequently used affinity tags, their use and amino acid sequence are listed in Table 1-4 below.

Table 1-4 List of common affinity tags including matrices, sequences and molecular size [186]

Name	Matrix	Sequence	Size (kDa)
Polyarginine-tag (poly-arg)	Cation-exchange resin	RRRRR	0.80
Polyhistidine-tag (poly-His)	Ni ²⁺ -NTA, Co ²⁺ -CMA (Talon)	HHHHHH	0.84
FLAG-tag	Anti-FLAG mAB	DYKDDDDK	1.01
Strep-tag II	Strep-Tactin	WSHPQFEK	1.06
c-myc-tag	mAB	EQKLISEEDL	1.20
S-tag	S-fragment of RNaseA	KETAAAKFERQHMDSD	1.75
HAT-tag Natural histidine affinity tag	Co ²⁺ -CMA (Talon)	KDHLIHNVHKEFHAAHANK	2.31

Larger affinity fusion tags that are well-established are: 3 x - FLAG-tag, calmodulin-binding peptide, cellulose-binding domains, streptavidin-binding peptide (SBP), chitin-binding domain, glutathione S-transferase (GST) or maltose-binding protein [186]. Moreover, the Fc-part of recombinant mABs may be utilized likewise as affinity tag.

1.5.2 Reporter proteins

Literature mostly features three major reporter systems. In 1980, the first article was published about reporter fusions with β -galactosidase (*lacZ* gene) [187] used to determine tissue-specific promoter activity, to perform blue/white screening by indicating bacterial colonies carrying a certain DNA region or to monitor transcriptional regulation in various biological processes [188]. Furthermore, luminescence-based reporter systems, for example in form of firefly luciferase (*luc*) or bacterial luciferase (*luxCDABE*), are state of the art [188, 189]. The third category of reporter proteins comprises the fluorescent proteins; such as the green fluorescent protein (GFP) and its derivatives, or flavin mononucleotide-based fluorescent proteins (FbFPs). They enable rapid and simple detection or even quantification of molecular and genetic occurrences since the system provides an easily measurable signal output after protein expression [190]. Fluorescence proteins have been used to study biofilm formation, protein expression in prokaryotes and eukaryotes *in vitro* as well as *in vivo*.

1.5.2.1 Fluorescent reporter tags

Green fluorescent protein (GFP) and its derivatives: Conventional fluorescent reporter proteins, such as GFP [191] and its derivatives are state-of-the-art and often used as fusion tags for detecting recombinant proteins during cultivation, screening and bioprocess optimization; or to analyze localization, movement and interaction of proteins *in vitro* and

in vivo. GFP was first described in 1961 [192, 193] as a protein originated from the jelly fish *Aequorea Victoria* emitting green fluorescence after excitation with blue or ultra violet light. Currently, GFP is an important tool for gene-specific fusions to investigate protein expression or protein targeting in living cells, tissue, or organs. Its protein sequence consists of 238 amino acids with a molecular mass of 26.9 kDa [191]. The chromophore, a *p*-hydroxybenzylideneimidazolinone, is formed by an autocatalytic reaction starting from the tripeptide sequence Ser₆₅–Tyr₆₆–Gly₆₇ within the native protein structure. For fluorescence formation, GFP folds into a nearly native conformation where the imidazolinone is formed by nucleophilic attack of the amide of Gly₆₇ on the carbonyl of residue 65, followed by dehydration. The molecular oxygen dehydrogenates the α - β -bond of residue 66 to connect its aromatic group with the imidazolinone [191]. Afterwards, the chromophore acquires visible absorbance and fluorescence ability. This mechanism requires atmospheric oxygen for fluorescence development. Fluorescence of anaerobically preformed GFP develops with a simple exponential time course only after air is readmitted. This means that fluorescence formation does not correlate with the concentration of the GFP itself. Considering the secondary structure of GFP, almost the whole primary sequence is used to build an 11-stranded β -barrel threaded by an α -helix running up the axis of the cylinder (Figure 1-5). The chromophore is attached to the α -helix and is buried in the center of the cylinder. A large number of polar groups and structured water molecules are adjoining the chromophore [191]. The excitation maxima of wild-type GFP occur at wavelengths 395 nm and 475 nm resulting in an emission at 509 nm. GFP mutants have been generated with optimized features or variations of fluorescent proteins have been discovered in other organisms, displaying other fluorescence spectra, such as CFP (cyan), YFP (yellow), mCherry or dsred (red), eGFP (enhanced GFP), color-switching FPs and many others [194]. The GFP gene itself comprises all necessary information for post-translational synthesis so that fluorescence formation is not based on external jellyfish-specific enzymes even though it requires an oxygen-sufficient environment.

However, some drawbacks discussed in literature may arise during the use of GFP as reporter protein. This may render on-line monitoring a challenging affair where fluorescent proteins are detected using non-invasive, specific and sensitive devices that monitor product formation and localization *in vivo*. One disadvantage of fluorescent proteins, based on GFP, is their relatively high molecular mass (26.9 kDa) compared to typical target proteins which might impose stress on the host metabolism during fermentation. Moreover, its oxygen-dependency may result in a lag-time between expression and fluorescence

detection rendering quantitative real-time measurement impossible. Detection of the GFP fluorophore can even be completely inhibited in an oxygen-limited or anaerobic environment [191, 195-197]. As a conclusion, on-line measurement of GFP is feasible, but not ideal in oxygen-insufficient fermentation systems or ones that yield active protein products, particularly for products with a low molecular weight. Moreover, hydrogen peroxide generation via oxidation with O₂ during fluorophore formation, at a stoichiometric 1 : 1 ratio with mature GFP, can be problematic during high-yield protein over-expression, since it imposes stress and damage to the host cell [191].

Flavin mononucleotide-based fluorescent proteins: Recently, flavin mononucleotide (FMN)-based fluorescent proteins (FbFPs), such as the blue light receptor Evoglow®, were developed as an alternative to GFP. FbFPs are derived from the blue light receptor of the light-oxygen-voltage family and are widely spread in prokaryotic and eukaryotic organisms as well as in plants [198, 199]. In contrast to plants, the physiological function of the receptors is practically unknown in bacteria. FMN (phototropin) serves as chromophore excitable by blue light. Following excitation, the thiol group of a preserved and photoactive cysteine residue bonds with FMN, thus forming a FMN-cysteine-C(4a)-thiol adduct. One example is the bacterial YtvA receptor from *B. subtilis* (Figure 1-5) [200]. It has a length of 261 amino acids including an N-terminal photoactive LOV-domain (residues 25 - 126) and a C-terminal sulfate transporter and anti-sigma factor antagonist domain (residues 147 - 258) carrying a nucleotide triphosphate-binding motif [199]. When excited at 450 nm, these FbFPs emit weak intrinsic auto-fluorescence at 495 nm. Using genetic manipulation, the respective photoactive cysteine was replaced by a non-polar alanine to enhance fluorescence performance as a result of reduced fluorescence quenching [200, 201]. In order to enhance fluorescence intensity in *E. coli* the N-terminal LOV-domain was adjusted to *E. coli* usage [200]. In comparison to GFP, which is limited to biological systems containing sufficient cellular oxygen, FbFPs also fluoresce under oxygen-limited and even anaerobic conditions, thus rendering *in vivo* labeling and detection without oxygen possible [200]. Furthermore, the genetically modified FbFPs are much smaller, only 15.7 kDa, (42% of GFP by molecular weight) [196, 200, 202] which presents an advantage for the host organism during protein synthesis.

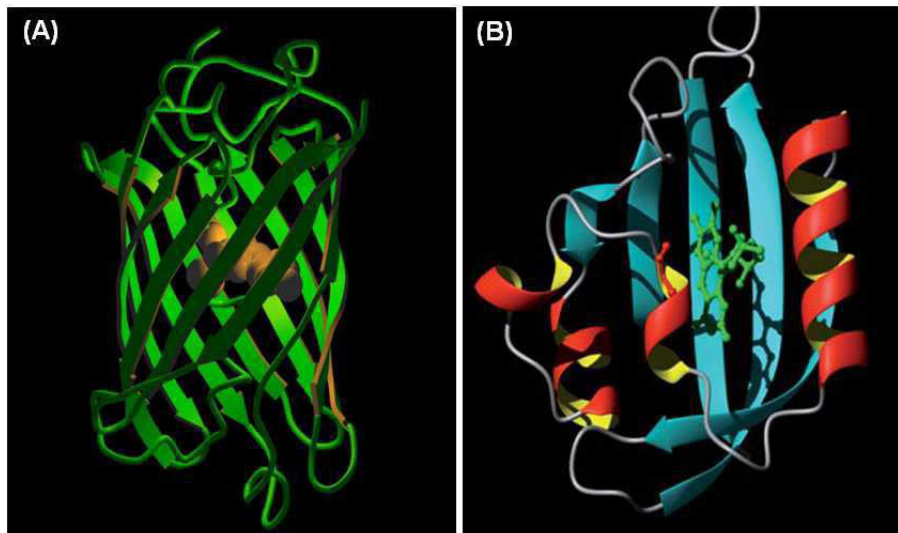


Figure 1-5 Illustrated protein structure of GFP and YtvA LOV domain from *Bacillus subtilis* exemplarily for the FMN-based fluorescent proteins. (A) Figure displays the 11-stranded β -barrel (green) and the chromophore attached to the α -helix in its center (brown) [203]. (B) Its FMN-binding domain consists of five β -sheet structures (blue) that are flanked by two α -helices (red and yellow). The chromophore is indicated in green, and the photoactive cysteine in the center is colored red [200].

1.5.3 Synthetic labels and SNAP-tag technology

Artificial post-expression coupling of a target protein to a particle, small molecule or dye, is an essential method for some targeting approaches. Conveniently, proteins and peptides naturally display four different reactive groups that are used for chemical conjugation, such as amino, sulfhydryl, carboxyl and carbonyl groups in glycoproteins. These groups can be modified with a variety of available cross-linking reagents. Such labeling reactions are random and may change or interrupt protein activity. Especially small scFv antibody fragments often do not tolerate chemical modifications as they consist only of the antigen binding variable domains where the majority of residues is involved in antigen recognition or essential for scFv structure. Due to difficulties in site-specific coupling causing alterations in protein activity, scFv antibodies are less frequently used for post-expression labeling than mABs or peptides, despite their excellent affinity, specificity and flexibility to the respective antigen. Therefore, coupling via predefined residues has been introduced, such as cysteine residues or unnatural amino acids, with unique reactive groups. Tag-based systems are available for the labeling of proteins with fluorophores including the Halo-tag and the lumio-tag [204, 205] or enzyme-based tags including trans-linked systems by the biotin holoenzyme synthetase, sortases and the Sfp phosphopantetheinyl transferase [206-208]. Still, the use of these systems for *in vivo* applications is limited since they are not broadly applicable, unspecific and labor intensive.

Another excellent alternative to direct genetic labeling is the SNAP-tag (Figure 1-6) [209]. It is an artificial post-expression labeling technique and allows coupling of a protein of interest to all kind of dyes, nanoparticles, radioactive labels or even the generation of theranostics. The SNAP-tag is a genetically engineered version of the human DNA-repair enzyme *O*(6)-alkylguanine DNA alkyltransferase (hAGT) [210], which allows substrates containing *O*(6)-benzylguanine (BG) derivatives to be covalently linked to a recombinant protein thus providing a strategy to equip an antibody with various imaging reagents [211]. The benzylguanine (BG) derivatives are substituted with a label at position 4 of the benzyl ring and guanine is cleaved off during the covalent labeling process. The label itself is chemically attached to the free amines of BG which react with commercially available activated carboxyl esters, such as N-hydroxysuccinimide (NHS) attached to a fluorescent dye [209, 212]. Its molecular size is approximately 20 kDa and either N- or C-terminal fusion proteins can be generated. In its natural function, hAGT supports DNA integrity. It scans DNA for alkyl adducts on guanine and thymine bases and removes them by a nucleophilic substitution reaction, thus inactivating the enzyme followed by its degradation [213].

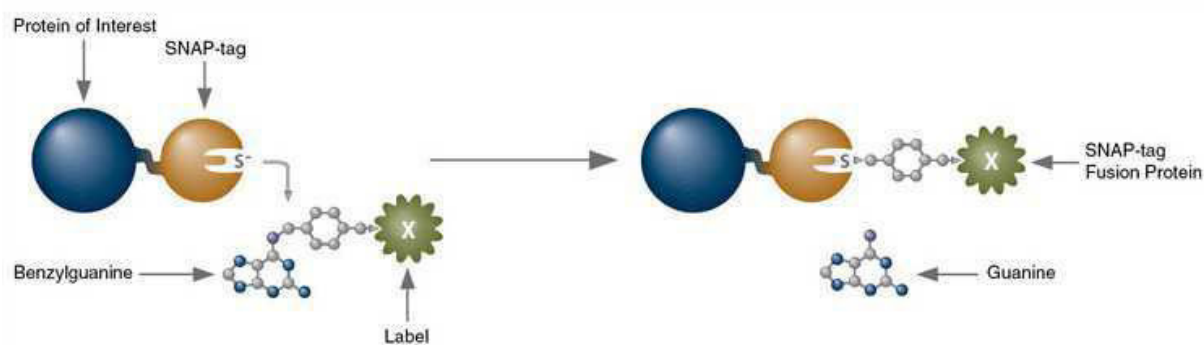


Figure 1-6 Schematic illustration of SNAP-tag coupling mechanism. [214]

This technology has been employed in a multitude of experimental applications ranging from labeling of proteins within living cells with cell-permeable BG-fluorophore dye [212] to protein immobilization on BG-modified chip surfaces [215]. Specific scFv antibodies labeled with the near infrared dye BG-747 were shown to accumulate rapidly and specifically at tumor sites. Its small size ensured efficient renal clearance, thus generating a much higher signal-to-background ratio than the full-length antibody [158]. The coupling reaction is highly efficient and specific for any kind of substrates modified for covalent binding (e. g. particles, radioactives or fluorescent dyes). Similarly to the SNAP-tag, an *O*(2) benzylcytosine reactive tag, called CLIP-tag has recently been described [216].

1.5.4 Tryptophan and potential tryptophan-based tags

Although FbFPs are an improvement over GFP, considering its suitability for anaerobic environments, even smaller fluorescent protein tags are preferable to further reduce the impact on host strain metabolism. This would allow more resources to be committed to the production of the recombinant target protein. In general, larger tags are less favorable due to increased protein interactions, disturbance of proper protein folding or production related stress on the host organism. One possible solution is to develop novel and even shorter tags based on the auto-fluorescent properties of aromatic amino acids such as tryptophan (W), tyrosine (Y) or phenylalanine (F) [217]. Within these amino acids, delocalized π -electrons in the aromatic ring structures are excited to higher energy states when exposed to certain wavelengths of light, emitting fluorescence in the UV-range when returning to their ground state. All three amino acids depict hydrophobic properties but feature differing Stoke's shifts. Tryptophan displays a larger Stoke's shift (~70 nm) than the other two aromatic amino acids which is combined with a relatively high quantum yield with an excitation maximum at 280 nm and an emission maximum at 350 nm.

These characteristics make tryptophan a suitable choice for the design of a novel protein reporter tag with auto-fluorescent optical activity. Moreover, its fluorescence is highly sensitive to the properties of the surrounding environment (i. e. polarity) and arrangement of neighboring amino acids [218]. Spectral characteristics of tryptophan may also be enhanced in the presence of tyrosine [219] since it is able to share its delocalized π -electrons. Most proteins are statistically likely to contain tryptophan but the number and distribution of residues vary [220]. Tags with tryptophan residues have previously been used to improve protein isolation by creating a hydrophobic affinity patch rather than a fluorescent label [221].

1.6 On-line monitoring of micro-scale shaking cultures

Generation of novel pharmaceutically relevant target proteins has led to a constantly growing demand for efficient and high-throughput screening systems in the field of molecular biotechnology. Complex gene and protein libraries allow the identification of new lead candidates for the drug industry by initial screening [222]; for example in microtiter plates (MTPs) followed by scale-up for industrial production. MTPs are frequently used for the high-throughput parallel characterization of microbial cultures under identical conditions, small-scale screening and as a lab-scale model for shaking

bioreactors. Simple and functional design makes them a cost-efficient and fast tool for parallel experiments (MTPs with 48, 96, 384 and 1536 up to 3456 wells) during multiple fermentation parameter analysis, such as measurement of temperature, oxygen transfer rates (OTR), dissolved oxygen tension (DOT), pH value and biomass. The recently developed BioLector® technology [223] even allows monitoring of continuously shaking *E.coli* cultures via on-line measurements using specially adapted MTPs [224, 225].

In the late 1990s, the first shaking high-throughput systems were engineered from Erlenmeyer flasks equipped with standardized pH and DOT sensors for real-time monitoring [226] in form of a fed batch system connected to feeding lines consisting of 16 parallel flasks (20-300 mL). The Respiration Activity Monitoring System (RAMOS) is another advanced shaking system [227] where the head of the flasks is equipped with an oxygen and a pressure sensor to assess the oxygen transfer rate (OTR), carbon dioxide transfer rate (CTR) and the resulting respiratory quotient (RQ). RAMOS can operate up to eight flasks simultaneously on an orbital shaker with working volumes of 10 – 50 mL in 250 mL flasks. To reduce developmental periods and to increase throughput, the design of new micro bioreactors with minimized sample volumes and higher number of simultaneous samples was necessary. This resulted in a progression from Erlenmeyer flasks to microtiter plates [228], for example systems consisting of 48-well (SimCell system, Bioprocessors Inc., MA, USA) [229] and 24-well (Micro-24 system, Microreactor Technologies Inc., CA, USA) [230]. MTPs were developed that were aerated by rising bubbles assisted by additional orbital shaking. Nevertheless, integration of on-line sensors into those bubble columns proved difficult due to strong foaming and uneven oxygen distribution. With the BioLector® technology [223, 224], used in this work as a modified device, 96 samples and more can be analyzed in parallel at a sample volume of 100 - 200 μ L and continuously shaken during measurements. Supplementary equipment, such as multipipetes, pipetting robots, microscale readers and autosamplers, ensure reproducible results [228]. Aeration of microtiter cultures is primarily influenced by the ratio of gas-liquid exchange area to volume, and secondly by surface tension. Latter counteracts liquid movement and flow under impact of g-forces caused by orbital shaking so that the air-liquid surface area is sustainably reduced in wells of less than 8 mm diameter. Nevertheless, a satisfactory OTR can be achieved in small vessels, when small volumes are combined with high rotational velocity thus antagonizing surface tension [228]. An additional essential aspect of fermentation systems in MTPs, and subsequent quantitative and statistical analysis, is the sealing method of the individual wells to prevent

cross-contamination and to limit evaporation. Very often semi-permeable adhesive plastic foil is successfully used, ensuring sufficient oxygen exchange from the outside and tight well closure to minimize water loss at the same time. The production of recombinant protein products, during cultivation in non-invasive fermentation systems, is often monitored using fluorescent fusion proteins [231], classically GFP or one of its derivatives. Common measurement systems for fluorescence intensity documentation are microplate readers.

1.7 Objective

The thesis at hand is focused on two different topics:

- (1) The phage display-based isolation of novel recombinant scFv antibodies as potential tools for early diagnosis or as prospective therapeutic approach against metastasizing pancreatic cancer, and
- (2) the design of a short optically active reporter tag based on the auto-fluorescent properties of tryptophan for on-line monitoring of product formation during micro-scale fermentation.

In the first part of this work, the primary scientific goal aims at the development of novel recombinant scFv antibodies for possible future application as efficient diagnostic tools in early stage tumor detection or post-operative disease monitoring of pancreatic cancer. Moreover, such novel recombinant proteins provide the opportunity for a therapeutic approach to specifically remove residual metastatic pancreatic carcinoma cells thus significantly increasing the average survival rate and life quality of patients.

Pancreatic cancer is characterized by a mortality rate of nearly 100%. This is due to a high relapse rate, as a result of very aggressive tumor metastasis and incomplete elimination of malignant cells after treatment, as well as insufficient reliable options for early diagnosis. Extensive surgery, radiation and chemotherapy are state-of-the-art treatments but unspecific and hardly add to an improved prognosis. As a consequence the demand for novel and efficient therapeutic options is very high and research advances for early diagnosis are desperately needed. Recombinant antibodies are a promising tool and already established for diagnosis and specific targeted immunotherapy of other types of cancer.

During a three-step panning strategy, the scFv libraries Tomlinson I and J are selected by means of phage display technology on living cells and functional membrane fractions of the metastasizing pancreatic cancer cell line L3.6pl to isolate new and highly specific scFv antibodies against unknown tumor-associated antigens *in vitro*. Their potential as

diagnostic imaging tool is evaluated by functionalizing scFv antibodies via SNAP-tag fusions by means of *in vitro* binding analysis. Additional *in vitro* investigations of internalization behavior assess the drug delivery potential for prospective fusions of the recombinant scFv ligand to a toxic effector domain to generate cytolytic fusion proteins for therapy.

The second part of this thesis is focused on the development of short-chained optically active reporter tags based on the accumulation of tryptophan residues (W) and their ability to auto-fluoresce. These tags will be evaluated with regard to their applicability as non-invasive on-line monitoring tool for production of antibody-based therapeutics.

Production up-scaling of recombinant pharmaceutically relevant therapeutical proteins still poses a bottle neck. Laboratory-scale fermentation systems, for example with the BioLector® device, simulate large-scale fermentation conditions thus rendering time-saving and cost-efficient parallel high-throughput characterization and screening of microbial cultures under identical conditions in microtiter plates (MTPs) possible. Commonly, the product formation of recombinant proteins during cultivation is monitored off-line after sampling, or on-line using conventional genetically fused fluorescent reporter proteins, such as green fluorescent protein (GFP) and its derivatives, or flavin mononucleotide-based fluorescent proteins (FbFPs). A major drawback of those conventional reporter proteins is their relatively high molecular size which imposes stress on the host metabolism during fermentation and possibly causes steric hindrance during protein folding and secretion. Moreover, the strong oxygen-dependency of GFP for fluorophore formation is problematic. In general, smaller fluorescent tags are preferable since this minimizes occurrence of potential problems. Therefore, five low-molecular-weight protein tags (W-tags) will be designed comprising different numbers of tryptophan residues, thus exploiting the auto-fluorescence of tryptophan-clustering. A genetic in-frame fusion of these newly designed W-tags with the anti-CD30 antibody fragment Ki-4(scFv) serves as proof-of-concept model to assess bacterial growth versus target protein formation. One aim is to visualize tryptophan fluorescence intensity during on-line monitoring in *E.coli* cultures as well as the dependency of fluorescence on the number of involved tryptophan residues. Besides that post-expression *in vitro* functionality and specificity analyses, are intended to demonstrate the potential of these novel W-tags as an alternative tagging method during fermentation of recombinant pharmaceutical proteins in comparison to conventional reporter proteins.

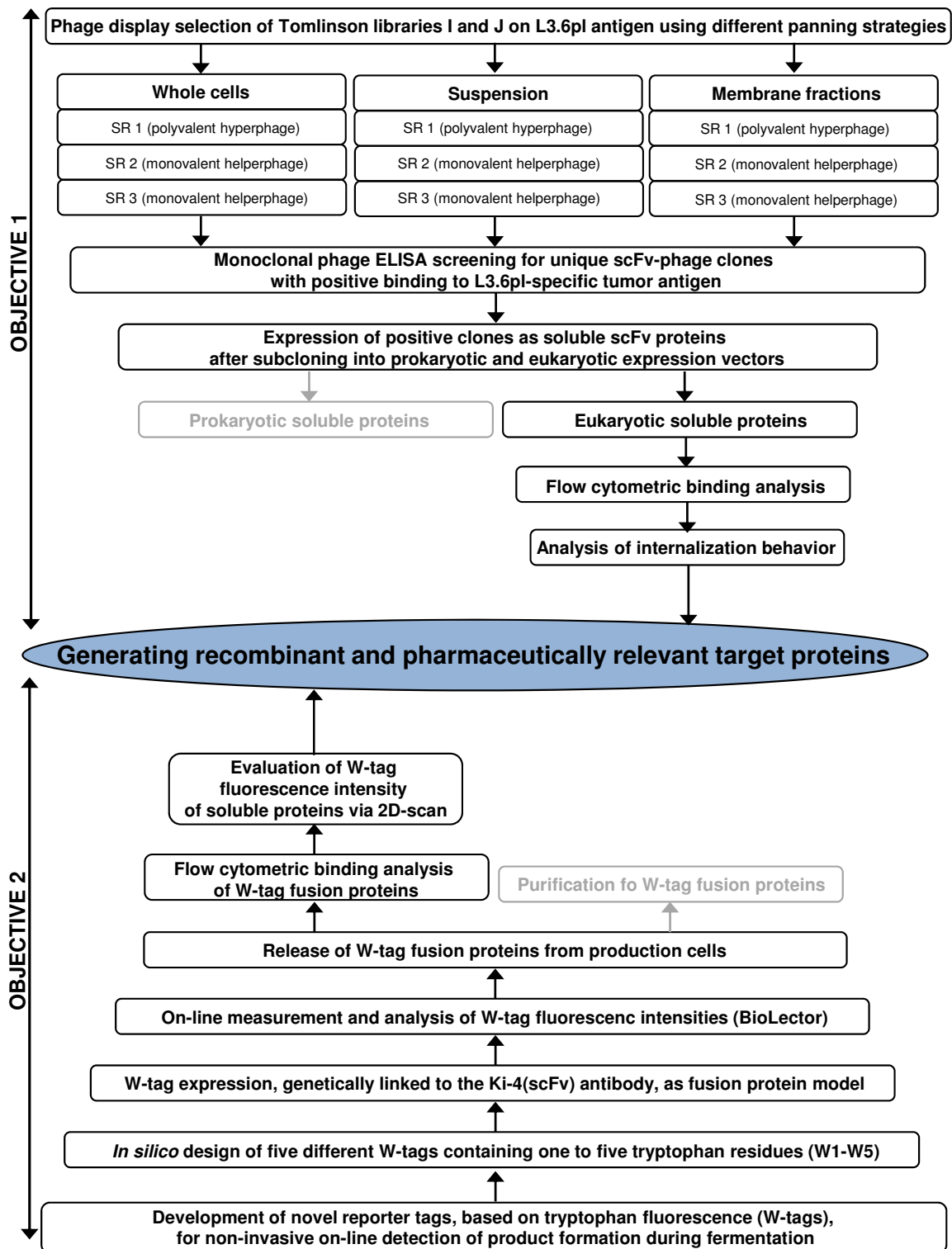


Figure 1-7 Flow chart illustrating the two objectives of this thesis and their experimental approach.

2 Material

2.1 Chemicals and consumable supplies

Chemicals and consumable supplies used in this work were purchased from the following companies: Applichem (Darmstadt), Becton, Dickinson & Co., BD Bioscience (Heidelberg), Biocompare (San Francisco, CA, USA), Carl Roth GmbH & Co. KG (Karlsruhe), Clontech (Saint-Germain-en-Laye, France), Eppendorf AG (Hamburg), GE Healthcare (München), Greiner Bio-One GmbH (Solingen), Invitrogen (Darmstadt), Merck KGaA (Darmstadt), Millipore (Darmstadt), Nerbe plus GmbH (Winsen/Luhe), New England Biolabs (Frankfurt am Main), Nunc GmbH & Co. KG (Wiesbaden), Otto Fischar GmbH & Co. KG (Saarbrücken), Promega GmbH (Mannheim), Roche Diagnostics Deutschland GmbH (Mannheim), Sarstedt AG & Co. KG (Nümbrecht), Sigma-Aldrich (Seelze), Thermo Scientific (Langenselbold), TPP Techno Plastic Products AG (Trasadingen, Switzerland), VWR International GmbH (Darmstadt) and Whatman GmbH (Dassel). All chemicals and consumables were applied according to manufacturers' instructions if not indicated otherwise. Purchase from different suppliers is possible if requirements necessary for a successful and reproducible outcome are fulfilled.

2.2 Equipment and software

Table 2-1 List of software, its application and corresponding supplier

Software	Application	Supplier
Adobe Photoshop CS4	Image editing	Adobe System, München
AIDA 4.27.039 Advanced Image Data Analyzer	Protein concentration analysis	Raytest Isotopenmessgeräte GmbH, Straubenhardt
ArgusX	Agarose gel analysis	Argus Software, London, UK
CellQuest Pro 3.3	Flow cytometry	Becton, Dickinson & Co., BD Bioscience, Heidelberg
Cyflagic 1.2.1	Flow cytometry	Perttu Terho & Cyflo Ltd., Turku Finland
Evoshell	Confocal microscopy, OPERA	Evotec Technologies, Hamburg
Geneious 5	DNA sequence analysis	Biomatters Ltd., Auckland, New Zealand
GraphPad Prism 5.01	Statistics	GraphPad software, Inc., LaJolla, CA, USA
i-control	Tecan reader	Tecan Group Ltd., Männedorf, Switzerland
Image J 1.42q	Image editing	National Institutes of Health, Bethesda, MD, USA
MassLynx v4.0	Mass spectrometry	Micromass, Water Corporation, Eschborn
MS Office 2010	Text and statistics	Office 2012, Microsoft Corp., Redmont, WA, USA
Origin 8	Statistics	ADDITIVE Soft- und Hardware für Technik und Wissenschaft GmbH, Friedrichsdorf
QuantityOne Basic 1-D Analysis software v.4.2.1	Fluorescence documentation	Bio-Rad, Offenbach
Vector NTI 11	DNA sequence analysis	Invitrogen, Darmstadt
WinMDI 2.9	Flow cytometry	Build 2, Joe Trotter, La Jolla, CA, USA

Table 2-2 List of hardware with corresponding suppliers

Equipment/Hardware	Supplier/Manufacturer
Agarose Electrophoresis Device	mini-SUB/SUB-CELL® GT, Bio-Rad, München
BioLector-like shaking device	self-made at Aachener Verfahrenstechnik (AVT) at RWTH Aachen University, adaptation from m2p-Labs, Baesweiler
Cell washer	Dade Serotec, Baxter, Unterschleißheim
Cytospin centrifuge	Cytospin 2 Centrifuge, Shandon, Thermo Scientific, Braunschweig
Centrifuges	Centrifuge 5804R, Eppendorf AG, Hamburg Biofuge Haemo, Heraeus Instruments & Co. KG, Hanau Multifuge 3 L-R, Heraeus Instruments & Co. KG, Hanau Multifuge 3 S-R, Heraeus Instruments & Co. KG, Hanau
Confocal microscope	Opera HCS System, Evotec Technologies, Hamburg
Flow cytometer	FACScalibur, Becton, Dickinson & Co., BD Bioscience, Heidelberg
Fluorescence documentation	VersaDoc MP System, Bio-Rad, Offenbach
Incubator (37 °C)	GFL 3031, GFL-Gesellschaft für Labortechnik G mbH, Burgwedel
Mass spectrometer	ESI-MS/MS Mass Spectrometer Micromass Electrospray Q-TOF-2, Waters Corporation, Eschborn
MilliQ system	MilliQ Synthesis QuantumEX Ultrapure Organex Cartridge, Millipore, Darmstadt
Orbital shaker	POLYMAX 1040, Heidolph Instruments GmbH & Co. KG, Schwabach
PCR Thermo Cycler	GeneAmp PCR System 9700, Applied Biosystems by LifeTechnologies Corp., Darmstadt
96-well plate shaker	TIMIX, Edmund Bühler GmbH, Hechingen
Power supply	PowerPac® HC, Bio-Rad, München
2D-scanner	FluoreMax-4P, Horiba Jobin Yvon Instruments Inc., USA
SDS-PAGE + Western blot devices	BioRad miniProtean III device, additional equipment for gel casting, Bio-Rad, München
Shaking incubator (variable T)	Innova Incubator Shaker 4430, New Brunswick Scientific, Wesseling-Berzdorf
Sonification device	Sonoplus HD 2070, tip: UW 2070, KE76, Bandelin Electronic GmbH & Co. KG, Berlin
Spectro-photometer	BioPhotometer plus, Eppendorf AG, Hamburg
Tecan reader	Tecan Multiplate-Reader Infinite M200, Tecan Group Ltd., Männedorf, Switzerland
Thermo shaker (variable T)	Thermomixer comfort, Eppendorf AG, Hamburg
Tissue culture clean bench	HeraSafe HS18, Heraeus Instruments & Co. KG, Hanau
Tissue culture incubator (37 °C)	HeraCell 150, Thermo Scientific, Braunschweig
Tube rotator	Tube Rotator, VWR International GmbH, Darmstadt
Ultracentrifuge	Aventi Centrifuge J-25i, Beckman Coulter, Krefeld

2.3 Bacterial strains and media

Following *E. coli* strains (Table 2-3) were used during this thesis.

Table 2-3 List of *E. coli* strains, their genotypes and corresponding suppliers

<i>E. coli</i> strain	Genotypes	Supplier
BL21 Rosetta 2 (DE3) Supercompetent Cells	F ⁻ <i>ompT hsdS_B(r_B⁻ m_B⁻) gal dem</i> (DE3) pRARE2 (Cam ^R)	Merck KGaA, Darmstadt
HB2151	K12 <i>ara Δ(lac-proAB)thi/F' proA+B lacIq lacZAM15</i>	MCR, Cambridge, UK
TG1 Tr	K12 <i>Δ(lac-proAB) supE thi hsdD5/F' traD36 proA⁺B lacI^f lacZAM15</i>	MCR, Cambridge, UK
XL1 Blue Supercompetent Cells	<i>recA1 endA1 gyrA96 thi-1 hsdR17 supE44 relA1 lac [F' proAB lacI^fZAM15 Tn10 (Tet^r)]</i>	Agilent Technologies, Waldbronn

Bacterial growth media and agar (Table 2-4) were prepared with ddH₂O (deionized water) and autoclaved as 250 mL or 300 mL aliquots in 500 mL bottles, appropriate antibiotics and/or sterile glucose were added directly prior to use.

Table 2-4 List of cultivation media and agars and their exact formulae

Cultivation media/agar	Composition
2 x TY medium	16 g tryptone, 10 g yeast extract, 5 g NaCl, ad 1 L ddH ₂ O
2 x TY _{amp}	100 µg/mL ampicillin in 2 x TY medium
2 x TY _{amp} , 2 x TY _{kan}	100 µg/mL ampicillin or 50 µg/mL kanamycin in 2 x TY medium
2 x TY _{gluc,amp}	1% glucose, 100 µg/mL ampicillin in 2 x TY medium
2 x TY induction medium	100 µg/mL ampicillin, 50 µg/mL kanamycin, 0.25 mM IPTG in 2 x TY medium
Cryo medium	15% (v/v) sterile glycerol, appropriate antibiotic in 2 x TY medium
Lysogeny Broth (LB) medium	10 g tryptone, 5 g yeast extract, 10 g NaCl, ad 1 L ddH ₂ O
LB _{amp} , LB _{kan}	100 µg/mL ampicillin or 50 µg/mL kanamycin in LB medium
LB auto-induction medium	0.5 g/L glucose, 2 g/L lactose, 5 g/L glycerol in LB medium
Lysogeny broth (LB) agar	5 g yeast extract, 5 g NaCl, 10 g Bacto-Agar, ad 1 L ddH ₂ O
LB _{amp} , LB _{kan} agar	100 µg/mL ampicillin or 50 µg/mL kanamycin in LB agar
LB _{gluc,amp} agar	1% glucose, 100 µg/mL ampicillin in LB agar
M9 minimal agar (1 L final volume)	Solution A: 15 g Bacto-Agar in 780 mL ddH ₂ O Solution B: 2.5 g NaCl, 5 g NH ₄ Cl, 33.9 g Na ₂ HPO ₄ , 15 g KH ₂ PO ₄ in 1 L ddH ₂ O Solution C: 1 M MgSO ₄ Solution D: 1 M CaCl ₂ x 6 H ₂ O Solution E: 20% glucose Solution F: 0.001 g thiaminhydrochlorid in 10 mL ddH ₂ O Autoclave solutions A – D, sterile filtrate solutions E and F Mix 780 mL Solution A, 200 mL Solution B, 2 mL Solution C, 100 µL Solution D, 20 mL Solution E and 400 µL Solution F.
SOC medium	Agilent Technologies, Waldbronn
Modified Wilms-Reuss medium (1 L final volume) [232]	Solution I: 5 g (NH ₄) ₂ SO ₄ , 0.5 g NH ₄ Cl, 3 g K ₂ HPO ₄ , 2 g Na ₂ SO ₄ , 41.85 g MOPS (3-(N-morpholino)propanesulfonic acid buffer) in 947 mL ddH ₂ O (pH 7.5) Solution II: 0.027 g ZnSO ₄ x 7 H ₂ O, 0.024 g CuSO ₄ x 5 H ₂ O, 0.015 g MnSO ₄ x H ₂ O, 0.027 g CoCl ₂ x 6 H ₂ O, 2.088 g FeCl ₃ x 6 H ₂ O, 0.099 g CaCl ₂ x 2 H ₂ O, 1.67 g Na ₂ EDTA x 2 H ₂ O in 50 mL ddH ₂ O Solution III: 250 g glucose in 500 mL ddH ₂ O Solution IV: 5 g MgSO ₄ x 7 H ₂ O in 100 mL ddH ₂ O Solution V: 0.1 g thiaminhydrochlorid in 10 mL ddH ₂ O Autoclave solutions I, III, IV and sterile filtrate solutions II and V. Mix 947 mL Solution I, 1 mL Solution II, 40 mL Solution III, 10 mL Solution IV, 1 mL Solution V and add appropriate antibiotic

2.4 Eukaryotic cell lines and media

The EGFR+ and highly metastasizing pancreatic cancer cell line L3.6pl was chosen as selection cell line. Thus, the well-published anti-EGFR 425(scFv) single chain antibody fragment [159, 164] could be exploited as positive control during characterization experiments. The Hodgkins' lymphoma-derived cell line L540cy over-expressing the CD30 surface receptor was used as positive cell line for the Ki-4(scFv) antibody fragment [132]. Table 2-5 and Table 2-6 list all cell lines and necessary reagents used for the characterization of scFv fragments or W-tagged fusion proteins.

Table 2-5 List of cell lines, their originating tissue, supplier and cultivation medium

Cell line	Characteristics	Supplier/Reference	Medium
A431	Human epidermoid carcinoma	ATCC, Manassas, VA, USA	RPMI/10/1
FG	Human pancreatic carcinoma	Munich, Bruns et al. 1999 [155]	RPMI/10/1
HEK293T	Human embryonal kidney	ATCC, Manassas, VA, USA	RPMI/10/1
L3.6pl	Human pancreatic carcinoma	Munich, Bruns et al. 1999 [155]	RPMI/10/1
L540cy	Human Hodgkins' Lymphoma	ATCC, Manassas, VA, USA	RPMI/10/1
LNCaP	Human prostate carcinoma	DSMZ, Braunschweig	RPMI/10/1
MCF7	Human breast adenocarcinoma	DSMZ, Braunschweig	RPMI/10/1
MDA-MB-231	Human breast adenocarcinoma	ATCC, Manassas, VA, USA	RPMI/10/1
MIA PaCa-2	Human pancreatic cancer	ATCC, Manassas, VA, USA	DMEM/10/1
PancTul	Human pancreatic carcinoma	Kiel University, Prof. Kalthoff [189]	RPMI/10
PancTul-CBRL	Human pancreatic carcinoma	Kiel University, Prof. Kalthoff [189]	RPMI/10
PT-46	Human pancreatic carcinoma	Kiel University, Prof. Kalthoff	RPMI/10
S2-0028	Human pancreatic carcinoma	Ulm University	RPMI/10/1
SiHa-BTH35	Human cervix carcinoma	ATCC, Manassas, VA, USA	RPMI/10/1
Su86.86	Human pancreatic carcinoma	ATCC, Manassas, VA, USA	DMEM/10/1

(RPMI: RPMI 1640 Glutamax, DMEM: DMEM Glutamax, 10: 10% fetal bovine serum (FBS), 1: 1% penicillin-streptomycin (P/S))

Table 2-6 List of tissue culture media and supplementary components for tissue culture

Media and supplementary components	Supplier/Manufacturer
Accutase®	PAA Laboratories GmbH, Pasching, Austria
DMEM (Dulbecco's Modified Eagle Medium) Glutamax	Invitrogen/Gibco, Life Technologies GmbH, Darmstadt
DMSO (99%) for tissue culture	Sigma-Aldrich, Seelze
1 x DPBS (Dulbecco's Phosphate Buffered Saline), pH 7.4	Invitrogen/Gibco, Life Technologies GmbH, Darmstadt
Fetal bovine serum (FBS)	Invitrogen/Gibco, Life Technologies GmbH, Darmstadt
Penicillin-Streptomycin Liquid	Invitrogen/Gibco, Life Technologies GmbH, Darmstadt
RPMI (Roswell Park Memorial Institute) 1640 Glutamax, containing phenol red	Invitrogen/Gibco, Life Technologies GmbH, Darmstadt
RPMI 1640 Glutamax, without phenol red	Invitrogen/Gibco, Life Technologies GmbH, Darmstadt
Trypan blue	Invitrogen/Gibco, Life Technologies GmbH, Darmstadt
0.25% trypsin-EDTA (1x), containing phenol red	Invitrogen/Gibco, Life Technologies GmbH, Darmstadt
Zeocin®	Invivogen, Toulouse, France

2.5 Enzymes and their buffers

All enzymes (Table 2-7) for restriction digests, dephosphorylation, ligations or DNA amplification were applied according to distributor's manual. Enzyme reaction buffers and reaction components essential for enzyme activity were supplied with enzyme purchase.

Table 2-7 List of enzymes and corresponding suppliers

Enzymes	Supplier/Manufacturer
Antarctic phosphatase	New England Biolabs, Frankfurt am Main
GoTaq Flexi DNA Polymerase	Promega GmbH, Mannheim
<i>Pfu</i> DNA polymerase	Fermentas, St. Leon-Rot
<i>DpnI</i>	Fermentas, St. Leon-Rot
<i>HindIII</i>	New England Biolabs, Frankfurt am Main
<i>NcoI</i>	New England Biolabs, Frankfurt am Main
<i>NdeI</i>	New England Biolabs, Frankfurt am Main
<i>NotI</i>	New England Biolabs, Frankfurt am Main
<i>SfiI</i>	New England Biolabs, Frankfurt am Main
T4 DNA Ligase	Invitrogen/Gibco, Life Technologies, Darmstadt

2.6 Reaction kits

Following kits (Table 2-8) were applied according to the manufacturer's instructions.

Table 2-8 List of commercially available kits and corresponding suppliers

Name	Supplier/Manufacturer
ABTS substrate	Roche Diagnostics Deutschland GmbH, Mannheim
FuGene HD Transfection	Roche Diagnostics Deutschland GmbH, Mannheim
Nucleo Bond PC 100 Kit	Macherey & Nagel, Düren
Nucleo Spin Plasmid Kit	Macherey & Nagel, Düren
QIAquick Gel Extraction Kit	Qiagen GmbH, Hilden
QuikChange® Site-Directed Mutagenesis Kit	Agilent Technologies, Waldbronn
Uptima BC Assay Protein Quantification	Interchim, Sankt-Augustin-Buisdorf

2.7 Buffers, solutions and antibiotics

All buffers and solutions (Table 2-9) were prepared with ddH₂O if not indicated otherwise. Antibiotics (Table 2-10) were prepared with ultra-pure water (MilliQ) from the MilliQ Synthesis System (specifications: 18.2 MΩ/cm at 25 °C, pyrogen content <0.0001 EU/mL and bacteria content <1 KBE/mL), sterile filtrated, aliquoted and frozen at -20 °C until use.

Table 2-9 List of composition of buffers and solutions

Buffer	Composition
10 x colony PCR buffer	500 mM KCl, 100 mM Tris-HCl (pH 9.0), 1% (v/v) TritonX100
Destaining solution	100 mL acetic acid (100% glacial), 200 mL methanol, 700 mL ddH ₂ O
ELISA coating buffer	5.3 g Na ₂ CO ₃ in 900 mL ddH ₂ O, add 4.2 g NaHCO ₃ , 1 g NaAc, ad 1 L ddH ₂ O (pH 9.6)
Homogenization buffer	25 mM Tris-HCl (pH 7.4), 320 mM sucrose, 1 Complete Protease Inhibitor tablet/50 mL
IPTG solution	1 M IPTG stock solution in MilliQ
10 x Laemmli running buffer	31 g Tris, 144 g glycine, 10 g SDS, ad 1 L ddH ₂ O (pH 8.6)
1 x Laemmli running buffer	1 : 10 dilution of 10 x Laemmli running buffer in ddH ₂ O
Lysis buffer	50 mM Tris, 300 mM NaCl, 10 mM EDTA (pH 8.0), 1 Complete Protease Inhibitor tablet/50 mL (pH 7.5)
Lysis buffer with lysozyme	300 µg/mL lysozyme in lysis buffer
Lysis buffer with NP-40	10 mM NP-40 in lysis buffer
2% MPBS, 5% MPBST, 5% MRPMI	2% or 5% (w/v) milk powder dissolved in 1 x PBS, 1 x PBST or RPMI Glutamax
10 x PBS (phosphate buffered saline)	80 g NaCl, 2 g KCl, 14.4 g Na ₂ HPO ₄ , 2.4 g KH ₂ PO ₄ (pH 6.9), ad 1 L ddH ₂ O
1 x PBS	1 : 10 dilution of 10 x PBS with ddH ₂ O (pH 7.4)
1 x PBST	1 x PBS, 0.05% (v/v) Tween20
PEG/NaCl	20% (w/v) PEG6000, 2.5 M NaCl
4% PFA fixing solution	4 g (w/v) paraformaldehyde, ad 100 mL 1 x PBS
Phage elution buffer	200 mM glycine-HCl (pH 2.2)
Phage neutralization buffer	1M Tris-HCl (pH 9.1)
5 x protein loading buffer	62.5 mM Tris-HCl (pH 6.8), 30% (v/v) glycerol, 4% (w/v) SDS, 0.05% (w/v) bromophenol blue, 10% (v/v) β-mercaptoethanol
Resuspension buffer	50 mM Tris-HCl (pH 7.4)
4% PAA stacking gel (2 gels)	650 µL Rotiphorese Gel 30, 625 µL 1 M Tris-HCl (pH 6.8), 50 µL 10% (w/v) SDS, 50 µL 10% (w/v) APS, 5 µL TEMED, 3.645 mL ddH ₂ O
12% PAA separation gel (2 gels)	4 mL Rotiphorese Gel 30, 3.75 mL 1 M Tris-HCl (pH 8.8), 100 µL 10% (w/v) SDS, 50 µL 10% (w/v) APS, 10 µL TEMED, 2.11 mL ddH ₂ O
50 x TAE buffer (Tris-Acetate-EDTA)	242 g Tris, 57.1 mL pure acetic acid, 100 mL 0.5 M EDTA at pH 8.0 (working pH 8.3)
4 x TALON wash buffer	0.2 M NaH ₂ PO ₄ , 1.2 M NaCl, ad 1 L ddH ₂ O (pH 7.0)
1 x TALON wash buffer	1 : 4 dilution of 4 x TALON wash buffer with ddH ₂ O (pH 7.0)
1 x TALON elution buffer	250 mM imidazole in 1 x TALON wash buffer (pH 7.0)
TEA buffer	0.1 M TEA in ddH ₂ O (pH 12.0)
1 x TES buffer	50 mM Tris, 20% (w/v) sucrose, 1 mM EDTA (pH 8.0), 1 Complete Protease Inhibitor tablet/50 mL
0.2 x TES buffer	1 : 5 dilution of 1 x TES buffer with ddH ₂ O, 1 Complete Protease Inhibitor tablet/50 mL
10 x Western blot transfer buffer	25 mM Tris, 192 mM glycine, ad 1 L ddH ₂ O
1 x Western blot transfer buffer	100 mL 10 x Western blot transfer buffer, 200 mL methanol, 700 mL ddH ₂ O

Table 2-10 List of antibiotics

Antibiotics	Supplier	Stock concentration	Working concentration
Ampicillin	Sigma-Aldrich, Seelze	50 mg/mL	100 µg/mL
Chloramphenicol	Sigma-Aldrich, Seelze	34 mg/mL	34 µg/mL
Kanamycin	Sigma-Aldrich, Seelze	50 mg/mL	50 µg/mL
Penicillin	Invitrogen/Gibco, Life Technologies GmbH, Darmstadt	10 mg/mL	100 µg/mL
Streptomycin	Invitrogen/Gibco, Life Technologies GmbH, Darmstadt	10 mg/mL	100 µg/mL
Zeocin®	Invivogen, Toulouse France	100 mg/mL	100 µg/mL

2.8 Antibodies and enzyme-conjugated antibodies

Table 2-11 lists antibodies for specific proteinchemical detection of recombinant scFv-phage particles or scFv fusion proteins during ELISA (3.3.9), flow cytometry (3.3.10), Western blotting (3.3.2) and immunofluorescence staining (3.3.11.2).

Table 2-11 List of antibodies for immunological analysis

Antibodies	Host	Application	Supplier	Dilution
HRP/anti-M13 monoclonal conjugate	mouse	E	GE healthcare, München	1:5000
Penta-His Alexa Fluor 488 conjugate	mouse	F	Qiagen GmbH, Düren	1:300
Monoclonal anti-polyHis IgG	mouse	E, WB	Sigma, Seelze	1:2000
Anti-rabbit Fc specific IgG HRP conjugate	goat	E, WB	Sigma, Seelze	1:5000
Anti-mouse-peroxidase conjugate	goat	E, WB	Sigma, Seelze	1:5000
Polyclonal anti-SNAP-tag IgG	rabbit	E, IF	Genescript, Aachen	1:5000
anti-rabbit IgG (H+L) F(ab) ₂ Fragment Alexa Fluor 647	goat	IF	Cell Signaling Technology Inc., Boston, MA, USA	1:5000

E: ELISA, IF: immunofluorescence, F: flow cytometry, WB: Western blot

2.9 Primer

All primer sequences (Table 2-12) used for sequencing reactions or PCR amplification were ordered from Invitrogen (Darmstadt) as lyophilized powder, reconstituted in MilliQ to a concentration of 100 pmol and stored at -20 °C until use.

Table 2-12 Primer sequences and corresponding vectors for sequencing and PCR

Primer name	Vector	Sequence 5' 3'	Direction of sequencing
fdseq1	pIT2	GAA TTT TCT GTA TGA GG	reverse down-stream of scFv
LMB3	pIT2	CAG GAA ACA GCT ATG AC	forward up-stream of scFv
mSNAP forward	pMS-SNAPMut	CGA CTC ACT ATA GGG AGA CCC AAG C	forward up-stream of scFv
mSNAP reverse I	pMS-SNAPMut	CCT TTG CCC AGC AGC TTG ATC TCG	reverse down-stream of scFv
mSNAP reverse II	pMS-SNAPMut	GCA ACT AGA AGG CAC AGT CG	reverse down-stream of SNAP
T7 promoter	pMT	TAA TAC GAC TCA CTA TAG GG	forward up-stream of scFv
T7 terminator	pMT	TAC AGG GCG CGT CCC ATT CG	reverse down-stream of scFv

2.10 Plasmid vectors

Table 2-13 Plasmid vectors/phagemids, corresponding background information and suppliers

Vectors	Background information	Supplier
pIT2	Phage display vector of Tomlinson libraries I and J. Phagemid vector for pIII-scFv fusion protein production in <i>E.coli</i> TG1F+ or expression of soluble scFv proteins in <i>E.coli</i> HB2151. Ampicillin 40ancreati, <i>lac</i> -promoter/IPTG controlled.	MRC, Cambridge, UK
pMT	Vector for prokaryotic protein expression of soluble scFv proteins or Wx-scFv fusion proteins. Derived from pET27b+ vector [171]. Kanamycin resistant, T7 promoter/IPTG controlled.	FhG IME, Aachen
pET27b+	Vector for prokaryotic protein expression, used as negative control during on-line measurements. Kanamycin resistant, T7 promoter/IPTG controlled.	Merck KgaA, Darmstadt
pMS-SNAPMut	Vector for eukaryotic soluble protein expression. Bicistronic construct combined from vectors pSecTag2 (Invitrogen, Darmstadt) and pIRES2-eGFP (Clontech, Saint-Germain-en-Laye, France). Ampicillin and Zeocin [®] resistant, CMV promoter controlled [183].	FhG IME, Aachen
pMA	Cloning vector for W-tags, ampicillin resistant	GENEART, Regensburg
pCR4Blunt-TOPO	Cloning vector for W-tags, ampicillin and kanamycin resistant	GENEART, Regensburg

Detailed plasmid maps of pMT and pMS-SNAPMut vectors are illustrated in Figure 2-1 displaying highlighted coding sequences for the single genetic components. Schematics of corresponding expression cassettes are outlined in 4.5 and 5.2 including all restriction sites required for cloning.

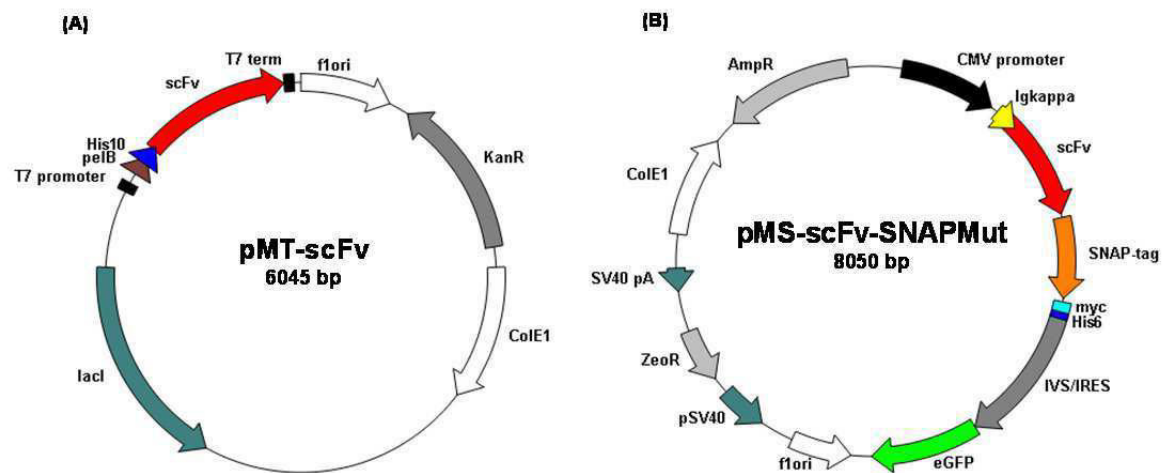


Figure 2-1 Schematic drawing of plasmid maps of expression vectors pMT and pMS-SNAPMut.

(A) pET-derived pMT plasmid for the prokaryotic production of soluble scFv protein in BL21 Rosetta 2 (DE3) *E.coli* promoting *lac*-operon controlled protein expression via T7 promoter and T7 terminator. Recombinant proteins are transported into the periplasmic space and eventually secreted via the *pelB* leader peptide. Detection and purification is performed via the His₁₀-tag. Figure 4-9 describes the expression cassette in more detail. (B) Bicistronic pMS-SNAPMut vector for eukaryotic expression of recombinant proteins after transient transfection into HEK293T cells. Protein expression is CMV-controlled (cytomegalovirus promoter) and an *Igkappa* (immunoglobulin *kappa*) signal sequence promotes secretion of soluble proteins. Detection and purification is achieved with the His₆-tag, *myc*-tag or SNAP-tag. An internal ribosomal entry site (IVS/IRES) mediates co-translation of eGFP (enhanced green fluorescent protein) during cultivation in Zeocin-supplemented medium. Cloning and prokaryotic expression is carried out during Ampicillin pressure. Figure 4-10 explains the expression cassette in more detail. F1 ori: replication origin f1 phage, pSV40: SV40 replication origin, SV40 pA: SV40 polyadenylation signal, ColE1: *E.coli* origin of replication, AmpR: Ampicillin resistance, KanR: Kanamycin resistance, ZeoR: Zeocin resistance.

2.11 Molecular weight markers

Table 2-14 Molecular DNA and protein markers and corresponding suppliers

DNA Ladder/Protein Marker	Supplier/Manufacturer
MassRuler DNA Ladder Mix, 100 – 10,000 bp	Fermentas, St. Leon-Rot
Spectra Multicolor Broad Range Protein Ladder, 10 – 260 kDa	Fermentas, St. Leon-Rot
Novex Sharp Pre-stained Protein Standard, 3.5 – 260 kDa	Invitrogen, Darmstadt
Prestained Protein Ladder Broad Range, 10 – 230kDa	New England Biolabs, Frankfurt am Main
Orange G, 6 x DNA loading dye, 50 bp	New England Biolabs, Frankfurt am Main

2.12 Single chain antibody libraries and helperphage

Phage display libraries, used for selections during this thesis, were the human single-fold scFv Tomlinson Libraries I and J, originally obtained from the Medical Research Council (MRC) Center for Protein Engineering in Cambridge (UK). Both are encoded on the pIT2 phagemid vector as scFv proteins fused to the pIII phage coat protein. Transformed into *E.coli* TG1 Tr (TG1F+), the phagemids were stored as cryo stocks at -80 °C. TG1F+ bacteria can be infected by filamentous M13KO7 phage particles to produce scFv-phage units. A detailed instruction and description of the Tomlinson Libraries I and J is found in 1.3.3. Following phage types were used (Table 2-15).

Table 2-15 Description of different types of phage particles and corresponding suppliers

Phage	Characteristics	Supplier
M13KO7 helperphage	It codes for genetic information of all wild-type coat proteins. After infecting phagemid-carrying bacteria, pIII-scFv fusion proteins are produced as well as unfused pIII coat proteins. During phage assembly, the coat proteins are joined at random so that between one and two pIII-scFv fusion proteins are presented on the surface of 1 – 10% of all produced phage particles. Kanamycin resistant.	New England Biolabs, Frankfurt am Main
M13 KO7 Δ pIII hyperphage	It is a M13KO7-derived gIII-deficient version which misses the pIII gene (gIII) completely. During phage assembly, only the scFv-pIII coat protein is present, and as a consequence, produced phage particles present five incorporated pIII-scFv on their protein coat. Kanamycin resistant.	PROGEN Biotechnik GmbH, Heidelberg

3 Methods

3.1 Molecular biological and DNA cloning techniques

General recombinant DNA techniques, as well as methods for cell cultivation, transfecting mammalian cells and transforming bacteria, were based on standard of “Molecular Cloning: A laboratory manual” from Sambrook et al., 2001 [233]. Individual components for experiments are listed below. Phosphate buffered saline solution, here called PBS was used at a concentration of 1 x PBS. Same applies for PBS supplemented with 0.05% Tween20, called PBST. Recombinant cloning techniques were used to subclone DNA fragments into the plasmid/phagemid vectors pIT2 or pMT for prokaryotic expression, or into pMS-SNAPMut for eukaryotic expression (2.10). General cloning was performed with *E.coli* strain XL1 Blue (3.1.2, 3.1.3).

3.1.1 Polymerase chain reaction

Polymerase chain reaction (PCR) [233, 234] is an important standard technique in molecular biology. DNA fragments were exponentially amplified by PCR, for subsequent sequencing (3.1.4) or restriction digest (3.1.2), but also to introduce mutations in a DNA fragment (3.4.6) by means of the *taq*-polymerase from *Thermus aquaticus* bacterium [234]. Besides *taq*-polymerase, a *pfu*-polymerase was used with 3'-5'-exonuclease proof-reading activity to correct potential sequence errors during DNA assembly of the elongation step. PCR products were examined by analytical and preparative agarose gel electrophoresis (3.1.5). PCR reaction mixtures were prepared on ice; autoclaved ddH₂O was used as negative control.

3.1.1.1 PCR based on DNA template

A PCR reaction can be started from a DNA template, such as chromosomal DNA or a plasmid. PCR reactions were set up in 200 µL tubes of a PCR-strip (25 µL/tube reaction volume). It was tested whether positive L3.6pl-binding scFv-phage particles, after screening in the monoclonal phage ELISA (3.3.9.2) contained a scFv-insert. Right-sized scFv-inserts were excised from the agarose gel (3.1.5), extracted and sequenced (3.1.4). Primers LMB3 (forward) and fdseq1 (reverse) attached to the insert template at a distance of 134 and 119 base pairs (bp), respectively, resulting in a PCR product 976 bp long. Table 3-1 states conditions for the thermo cycler and the reagents for the PCR reaction mixture.

Table 3-1 Reaction conditions of DNA template-based PCR amplification reaction.

(A) PCR reaction mixture, (B) thermo cycler program.

(A)		(B)		
Reagent	Volume [μL]	Temperature [$^{\circ}\text{C}$]	Time [min]	Cycles
DNA template	1	94	03:00	1
5 x <i>gotaq</i> buffer	5	94	01:00	
DMSO (99%)	2	50	00:45	
dNTP mix (25 mM)	0.3	72	02:00	30
LMB3 (10 pmol)	1	72	10:00	
fdseq1 (10 pmol)	1	4	∞	
50 x <i>gotaq</i> polymerase	0.15			
ddH ₂ O	ad 25 μL total volume			

DNA fragments for restriction digest were extracted by same PCR procedure.

3.1.1.2 Bacterial colony PCR

Instead of a DNA template, PCR can be started from a bacterial colony. Therefore, a single colony was picked from an agar plate with a sterile pipet tip, saved on a second agar plate by slightly touching and transferred to a 200 μL tube as PCR. Table 3-2 lists the colony PCR reaction mix and thermo cycler set-up.

Table 3-2 Reaction conditions of colony-based PCR amplification reaction.

(A) PCR reaction mixture, (B) thermo cycler program.

(A)		(B)		
Reagent	Volume [μL]	Temperature [$^{\circ}\text{C}$]	Time [min]	Cycles
Bacterial colony	1 colony	95	10:00	1
10 x colony PCR buffer	5	95	01:00	
MgCl ₂ (25 mM)	3	50	01:00	
dNTP mix (25 mM)	0.3	72	01:30	30
LMB3 (10 pmol)	1	72	10:00	
fdseq1 (10 pmol)	1	4	∞	
50 x <i>gotaq</i> polymerase	0.2			
ddH ₂ O	ad 50 μL total volume			

The colony PCR method was used to check for presence of scFv-inserts or to test whether a ligation (3.1.3) during cloning has been successful.

3.1.2 DNA restriction digest

Plasmids or PCR products were digested with restriction endonucleases (2.5) according to enzyme concentrations, buffers and temperature given in manufacturers' manual. Typically, 500 – 100 ng DNA material was digested in 50 μ L total volume applying one unit enzyme/1000 ng DNA, except for supercoiled plasmid DNA where a 4-fold enzyme concentration was used to achieve complete digestion. Isolated L3.6pl-specific scFv fragments (3.4) were subcloned into pMT and pMS-SNAPMut expression vectors through restriction sites *SfiI* and *NotI*. Newly designed W-tags (3.1.8) with *pelB* leader were subcloned from GENEART vectors into the pMT expression vector [171] via *NcoI* and *HindIII* restriction sites, whereas W-tags without *pelB* leader were transferred using *NdeI* and *HindIII*. To prevent relegation, vector backbones were additionally dephosphorylated at 37 °C for 1 h after digest using Antarctic phosphatase, followed by a 20 min deactivation step at 65 °C. Digested DNA fragments were separated by preparative agarose gel electrophoresis (3.1.5), gel-purified (2.6) and ligated (3.1.3) into the desired DNA vector construct.

3.1.3 DNA ligation

To ligate scFv fragments and W-tags into their respective vector backbones, 50 – 100 ng vector were ligated to the insert at a molecular ratio of 1 : 3 using the enzyme T4 ligase (2.5). Ligation was carried out with T4 ligation buffer at RT for 3 h as instructed in the manual.

3.1.4 DNA sequencing and sequencing analysis

PCR products, site-directed mutations or correct ligations, as well as DNA fragments or plasmids were sequenced at MWG Eurofins (Ebersberg, Germany) by dideoxy chain termination according to Sanger et al. [235]. 15 μ L of purified PCR product (5 ng/ μ L) or purified plasmid DNA (50 – 100 ng/ μ L) were transferred to an Eppendorf tube, sent for sequencing and subsequently analyzed with the Vector NTI software (Table 2-2).

3.1.5 Analytical and preparative agarose gel electrophoresis

For preliminary analysis, 5 – 10 μ L samples of undigested plasmid DNA, PCR products or restricted DNA were mixed with DNA loading dye and loaded onto an analytical agarose gel to check the length of the DNA fragments. Gels were prepared with 0.8 – 1% (w/v)

agarose in 1 x TAE buffer (2.7), containing 0.1 µg/mL ethidium bromide, and run at 80 - 120 V. Size and integrity of a DNA fragment were evaluated with a DNA molecular marker (2.11). DNA-embedded ethidium bromide was visualized via a UV transilluminator at 312 nm, documented by a black and white camera attached to the top of the transilluminator and analyzed using the ArgusX program (2.2).

For subsequent DNA excision and purification, a preparative agarose gel was run separately using the entire DNA solution. No picture was taken to prevent DNA damage by UV-light but the desired DNA fragment was quickly excised from the gel (under a UV transilluminator lamp) and gel-purified using the QIAquick Gel Extraction Kit (2.6).

3.1.6 Determination of DNA concentration

DNA was diluted at 1 : 30 or 1 : 50 in ddH₂O and transferred to a UV cuvette to measure DNA concentration in a spectro-photometer (2.2) via the extinction at $\lambda = 260$ nm. DNA purity was evaluated at wavelengths 260 and 280 nm. Whereas the DNA absorbs UV light at both wavelengths, residual proteins absorb UV light at 280 nm only. DNA samples free of protein contamination have a 260/280 ratio of 1.8, whereas a contaminated sample displays a 260/280 ratio <1.8.

3.1.7 Plasmid DNA isolation from *E.coli*

Plasmid DNA was isolated from *E.coli* cultures using the Macherey & Nagel Kits (2.6) NucleoSpin Plasmid (mini-preparation) or NucleoBond PC100 (midi-preparation). Quality and quantity of isolated DNA was confirmed by spectrophotometric analysis (3.1.6). Isolated plasmid DNA was used for sequence analysis of bacterial clones (3.1.4), control digests (3.1.2) or long term storage at -20 °C. To prepare very pure DNA for transfection of eukaryotic cells, the eluted DNA was precipitated with isopropanol and washed with 70% ethanol. The pellet was resuspended in 150 µL ddH₂O, and then 1 / 10 volumes 3 M NaOAc and 2.5 volumes 100% ethanol were added. The tube was placed at -80 °C O/N and thawed at RT for 10 min. Precipitated DNA was spun down (12,000 x g, 4 °C, 30 min). The supernatant was removed, the transparent pellet washed with 1 mL 80% ethanol (12,000 x g, 4 °C, 10 min) and dried at RT for 5 – 10 min after the supernatant was removed with a pipet. DNA was resuspended in 50 – 100 µL TE-buffer.

3.1.8 Design of tryptophan tag (W-tag)

Following the expertise of Dr. Heinrich Delbrück from Fraunhofer IME in Aachen, five short and optically active tags, called W tags, were modeled by integrating the aromatic auto-fluorescent amino acid tryptophan (W) into a naturally occurring β -sheet motif from *Bacillus caldolyticus* cold shock protein (Bc *Csp*) [236].

This special β -sheet motif was found by screening the Protein Data Bank (PDB) for small motifs with the appropriate distribution of hydrophobic amino acids. Bc *Csp* [PDB: 1C9O] is a small protein (66 amino acids) comprising two β -sheets that form a β -barrel. The first β -sheet (30 amino acids) consists of three β -strands connected by two loops, with a hydrophobic core and one tryptophan and two phenylalanine residues exposed on the surface. Starting from the third residue, the sequence was systematically mutated *in silico* to increase the number of tryptophan residues within the loop using CHARMM (<http://www.CHARMM.org>) in Discovery Studio (<http://www.accelrys.com>) the free energy of each model was minimized and models with the lowest free energy for each number of substituted tryptophan residues were selected.

W-tags were synthesized at GENEART (Regensburg, Germany) with *E.coli*-compatible base triplets as DNA sequence in pMA and pCR4Blunt TOPO cloning vectors containing restriction sites *NheI*, *NcoI* and *HindIII*, an His₆-tag, a GS-linker and a cleavable enterokinase site (EK). W-tags were subcloned into the pMT expression vector upstream of the Ki-4(scFv) [237] or M12(scFv) [238] (3.1.3) and transformed into BL21 Rosetta 2 (DE3) *E.coli* (3.1.9.3). Untagged Ki-4(scFv) or M12(scFv) were introduced as positive expression control (EC), the empty pET-27b+ vector served as negative control (NC).

3.1.9 Cultivation of *E.coli*

Different *E.coli* strains were used for infection of the Tomlinson libraries I and J, and subsequent production of M13KO7-based scFv-helperphage units (3.4.2), for DNA amplification and isolation (3.1.9.2), or for the prokaryotic production of proteins (3.1.9.3, 3.1.9.4). For a list of all bacterial strains, their suppliers and the distinct characteristics see chapter 2.3.

3.1.9.1 Phage infection and production in TG1F+

TG1F+ *E.coli* (2.3) is an *amber* stop codon (TAG) suppressor strain, commonly used as host strain of filamentous M13KO7 helperphage and M13KO7 Δ pIII hyperphage during biopanning (3.4.5). These TG1F+ cells have no antibiotic resistance and were grown on a M9 minimal media agar plate at 37 °C. For infection, a single TG1F+ colony was picked, transferred into 5 mL 2 x TY media (no antibiotics, no glucose) and grown at 37 °C, shaking at 250 rpm O/N. The O/N culture was diluted 1 : 100 into fresh 2 x TY medium and grown (37 °C, 250 rpm) to an optical density measured at 600 nm (OD₆₀₀) of 0.4 – 0.5. This indicates the logarithmical growth phase when the bacterial F-pili are formed and efficient infection with M13KO7 phage is possible. After each cultivation step, TG1F+ samples were plated on LB_{amp} and LB_{kan} control agar to check for contaminating unspecific M13KO7 phage or plasmids.

3.1.9.2 DNA amplification and isolation in XL-1Blue

XL1 Blue *E.coli* (2.3) were employed for general cloning, plasmid DNA amplification and isolation. Transformed XL1 Blue clones were picked from an agar plate for cultivation in 5 mL (mini-preparation) or 25 mL LB medium (midi-preparation) at 37 °C and 250 rpm containing the plasmid-appropriate antibiotic. Important: No glucose was added since it clogs the membrane during DNA isolation (3.1.7).

3.1.9.3 Prokaryotic recombinant protein expression in BL21 Rosetta 2(DE3)

Large-scale expression of Wx-Ki-4(scFv) and Wx-M12(scFv) fusion proteins: Large quantities of the W-tag proteins fused to Ki-4(scFv) or M12(scFv) (5.2) as well as the negative and positive expression control proteins (5.2) were fermented in BL21 Rosetta 2 (DE3) using 1L-Erlenmeyer flasks. Clones were inoculated from cryo stocks, grown O/N as pre-cultures in 10 mL modified Wilms-Reuss synthetic medium [232] (2.3) supplemented with 20 g/L glucose using 250 mL shake flasks sealed with cotton plugs at 37 °C, a shaking frequency of 350 rpm and 50 mm shaking diameter. 80 mL fresh Wilms-Reuss synthetic medium containing 20 g/L glucose and 50 μ g/mL kanamycin were inoculated at an OD₆₀₀ adjusted to 0.1 (same culturing conditions as above). After 4 h, the bacterial cultures were induced with 1 mM IPTG, cultivated for another 6 h and harvested after 10 h (4000 x g, 4 °C, 30 min).

Micro-scale expression of Wx-Ki-4(scFv) and Wx-M12(scFv) fusion proteins: W-tagged fusion proteins were also expressed in BL21 Rosetta 2 (DE3) *E.coli* during the on-line measurement in microtiter plates (MTPs). Pre-cultures were prepared as described above. 200 μ L main cultures were inoculated at OD₆₀₀ 0.1 and grown in 96-well MTPs (lumox, black, μ -clear, Greiner Bio-One, Kremsmünster, Austria) sealed with a gas-permeable membrane (AB-0718; Abgene, Epsom, UK) to allow aeration while minimizing evaporation. Cultivation took place in a temperature-controlled room (37 °C) under an aerated hood with humidified air to minimize evaporation, at 950 rpm and 3 mm shaking diameter. When entering the exponential growth phase ($t = 3.2$ h), cultures were induced with 1 mM IPTG. The maximum oxygen transfer rate in Erlenmeyer and MTP system was always maintained by a high shaking frequency with an appropriate shaking diameter using small culture volumes in a large shaking volume [239, 240].

5 mL expression of recombinant scFv, Wx-Ki-4(scFv), and Wx-M12(scFv) proteins: W-tagged fusion proteins and isolated scFv clones (after *amber* stop codon mutation (3.4.6) and subcloning into the pMT vector) were expressed in BL21 Rosetta 2 (DE3). Expression was either performed using a 25 mL flask in 5 mL Wilms-Reuss synthetic medium followed by IPTG induction (as described above) or in a special auto-induction medium (2.3) [241]. Therefore, a pre-culture of 5 mL LB_{kan} was inoculated from a cryo stock, shaken O/N at 37 °C and 250 rpm. Then 100 μ L/sample were inoculated into 10 mL main culture (LB auto-induction medium, 50 μ g/mL kanamycin) and cultivation was continued O/N.

L3.6pl-specific scFv antibodies were also cultivated in BL21 Rosetta 2 (DE3) to produce soluble protein for protein ELISA analysis (3.3.9.3).

3.1.9.4 Prokaryotic recombinant protein expression in HB2151

Soluble scFv proteins were produced with the non-suppressor strain HB2151 *E.coli* (3.3.9.3) via the pIT2 phagemid vector using the same expression protocol as in 3.3.9.3. No subcloning into an expression vector was needed and the scFv fragments were expressed at microtiter scale, directly after QuikChange Mutation of the *amber* stop codons in CDR2 (3.4.6). Produced soluble scFv proteins were analyzed for binding activity in a protein ELISA (3.3.9.3).

3.1.10 Preparation of bacterial cryo stock cultures

For all bacterial strains and clones, 5 mL cultures were grown O/N at 37 °C shaking at 250 rpm in LB or 2 x TY medium supplemented with the plasmid-appropriate antibiotic. Cells were pelleted (4500 x g, 4 °C, 10 min) and resuspended in 1 mL cryo medium (2.3). This bacterial suspension was quickly transferred into a labeled cryo tube, placed on ice and frozen at -80 °C for long-term storage.

3.1.11 Heat shock transformation of *E.coli*

Heat-shock transformation was used to introduce genetic material into chemically competent bacteria. Competent cells were thawed on ice for 10 min, 25 µL/sample bacterial suspension were transferred into a pre-chilled Eppendorf tube and 1 µL plasmid DNA (2 µL for ligations) were added. Cells were incubated on ice for 30 min, then heat-shocked in a 42 °C water bath for exactly 45 s since the duration of the heat pulse is the critical step for maximum transformation efficiency. Tubes were quickly placed back on ice for additional 2 min, then filled up with 250 µL SOC medium (pre-warmed to 42 °C) and incubated at 225 – 250 rpm for 1 h to allow for development of respective antibiotic resistance during cell division. Afterwards 50 – 100 µL bacterial suspension (250 µL for ligations) were plated out on LB agar plates supplemented with the plasmid-appropriate antibiotic to grow cell colonies in an incubator at 37 °C for 12 – 16 h.

3.2 Tissue culture and cell processing

3.2.1 Cultivation of eukaryotic cell lines

All mammalian cells were incubated at 37 °C in a 5% CO₂ atmosphere and 95% relative humidity using 75 cm² tissue culture flasks. Confluency dependent, cells were passaged and supplied with fresh media every three to four days. Dulbecco's Phosphate Buffered Saline (DPBS) (2.4) was used for all cell lines. Depending on the cell line, cells were cultivated in RPMI 1640 Glutamax or DMEM Glutamax (2.4) media supplemented with 10% FBS (fetal bovine serum) and 1% penicillin/streptomycin (P/S). For full list of media composition and components for cultivation and passaging see Table 2-5.

Adherent cell lines were cultivated in the respective media (2.4). For passaging, cells were washed with 4 mL DPBS and detached from the bottom of the flask with 2 mL Accutase[®] at RT. Cell suspension was filled up with 8 mL medium and centrifuged (1200 rpm, 4 °C,

5 min). Pellet was resuspended in fresh medium and diluted to the optimal cell density (between 1 : 3 and 1 : 10).

The Hodgkins' lymphoma-derived suspension cell line L540cy, expressing the CD30 receptor for Ki-4(scFv) binding, was grown in complex RPMI/10/1. Cells were cultivated at a density of $0.5 - 1.5 \times 10^6$ cells/mL in a 10 mL volume.

Transfected HEK293T cells, used for the production of soluble scFv-SNAP proteins, were cultivated in RPMI/10/1, supplemented with 100 µg/mL Zeocin[®] for selection pressure (RPMI/10/1/Zeo). Cells were passaged every 2 weeks at a 1 : 5 dilution.

3.2.2 Cryopreservation and reactivation of eukaryotic cell lines

For freezing, cells were grown in 75 cm² flasks until log-phase for several days to reach about 60 – 80% confluence. Adherent cells were detached from flask using Accutase[®] before counting. Viable cells in a 10 mL cell suspension were counted in a Neubauer haemocytometer. A haemocytometer is a thick glass slide with two counting chambers, each 0.1 mm deep. Each chamber is divided into nine large squares delineated by triple white lines. The center square is divided into 25 squares which are subdivided into 16 squares. The entire reticulated part has an area of 9 mm². Trypan blue was used to determine the vital cell count. Non-viable cells absorb the dye and appear blue and asymmetrical under the microscope, while healthy viable cells are refractory to the dye and rounded. 10 µL cell suspension were mixed with 10 µL trypan blue and incubated for 5 min. A cover slip was placed over the two chambers of the haemocytometer and 10 µL of the cell mixture with trypan blue were pipetted to one chamber. Viable cells in the four squares at the corners were counted, the average was calculated and the cell concentration per mL was calculated using the following formula: cells/mL = average number of counted cells x dilution factor x 10⁴.

Then 10 mL cell suspension were pelleted (1,200 x g, 4 °C, 10 min) and cells were resuspended in freezing medium, consisting of 70% RPMI 1640 Glutamax or DMEM medium containing adequate antibiotics, 20% FBS and 10% DMSO, to a concentration of $5 \times 10^6 - 1 \times 10^7$ cells/mL, depending on the cell line. 1 mL of this suspension was transferred into sterile labeled cryo tube, closed tightly and placed on ice immediately. After 5 min the cryo tube was placed into the -20 °C freezer for 2 h, then at -80 °C O/N and after that into the liquid nitrogen tank for long-term storage.

For thawing, a 75 cm² tissue culture flask was prepared with 10 mL respective medium (pre-warmed to 37 °C). A tube with the cryo-preserved cells was removed from the liquid nitrogen, thawed at 37 °C until cell suspension was free of ice and cells were immediately transferred to the flask with the pre-warmed medium. Cells were left to settle for two days, then the media was refreshed and cells were passaged as described in 3.2.1.

3.2.3 Eukaryotic recombinant protein expression in HEK293T cells

Isolated L3.6pl-specific scFv antibody fragments, after monoclonal phage ELISA screening and site-directed mutagenesis of *amber* stop codons were subcloned into the eukaryotic pMS-SNAPMut expression vector (4.5.3) via *SfiI* and *NotI* restriction sites. Constructs were transfected into HEK293T cells, to produce soluble scFv protein under Zeocin[®] selection pressure. Soluble scFv-SNAP proteins were used for protein ELISA analysis (3.3.9.3), flow cytometrical binding analysis (3.3.10) and internalization assays (3.3.11.1).

3.2.3.1 Transfecting HEK293T cells

All pMS-scFv-SNAPMut DNA constructs were transfected into HEK293T cells via lipofection [242] with the lipofection reagent FuGene HD (Roche Diagnostics GmbH, Mannheim) according to manufacturers' instructions. With this method, exogenous DNA is introduced into a cell via cationic lipid vesicles. These vesicles complex the negatively charged DNA and create large clusters which are internalized through the cell membrane by endocytosis. This transfection process is most efficient in the log-phase when the mitosis metabolism in the cell is at its peak and DNA is transported to the nucleus and taken up. HEK293T cells were split into a 12-well plate at 6×10^4 cells/well and cultivated in RPMI/10/1, for about 24 h or to reach 80% confluency. 2.5 µg purified DNA per transfection (3.1.7) were mixed gently with 3 µL FuGene transfection reagent, to reach the recommended ratio of approximately 1 : 3, and filled up with 100 µL serum-free RPMI Glutamax medium. This mixture was incubated at RT for 15 min to allow formation of the transfection complex. Meanwhile 1.5 mL/well fresh RPMI/10/1 was transferred into the 12-well plate. Afterwards the transfection mixture was added dropwise, incubated at RT for 5 min. Then plates were incubated at 37 °C for another 48 – 72 h to allow transfection.

The pMS-425(scFv)-SNAPMut plasmid was used as positive transfection control, ddH₂O as negative.

3.2.3.2 Cultivation of transiently transfected HEK293T for protein production

Following 48 – 72 h incubation, the transiently transfected HEK293T cells were supplied with 1.5 mL fresh RPMI/10/Zeo for selective pressure to remove untransfected cells. Two days later, all transfected HEK293T cells were detached from the 12-well plate using Accutase[®], transferred to a 75 cm² tissue culture flask without splitting and placed at 37 °C and 5% CO₂ to settle and grow for one week under selective pressure. By then, several colonies with transfected HEK293T cells had developed which were singularized with Accutase[®] and placed into a fresh 75 cm² flask for passaging and collection of supernatant containing soluble scFv-SNAP proteins (3.2.1). Tissue culture supernatant was harvested once a week and stored at 4 °C for up to 6 months since the proteins were stabilized by the FBS in the medium.

Protein production of secreted scFv-SNAP proteins was examined via SDS-PAGE (3.3.1) and Western blotting (3.3.2). In addition, the pMS-scFv-SNAPMut vector contains an eGFP sequence separated from the scFv-SNAP expression cassette by an IVS/IRES sequence. As a result, scFv-SNAP protein expression was monitored under a fluorescence microscope (data not shown).

3.2.4 Isolation of peripheral blood mononuclear cells

Peripheral blood mononuclear cells (PBMC) were isolated from buffy coats by means of density gradient centrifugation, to use for the preparation of membrane fractions (3.2.5), for depletion during biopanning (0, 3.4.5.2) or as negative control during flow cytometrical analysis (3.3.10). PBMCs were prepared freshly for each experiment. Buffy coats (45 – 50 mL) were obtained from the Department of Transfusion Medicine at Aachen University Hospital. Blood was carefully withdrawn from the transfusion bag using a syringe and transferred to a 50 mL falcon tube where it was mixed with PBS (free of Ca²⁺ and Mg²⁺!!) at a ratio of 1 : 1. Ficoll Paque PLUS (GE healthcare) was mixed thoroughly; 15 mL were removed with a syringe and placed in 50 mL falcon tube. Ficoll Paque is an aqueous solution of a high molecular weight polysaccharide adjusted to a density of 1.077 ± 0.001. Next, 30 mL of the blood-PBS mixture were carefully transferred onto the Ficoll Paque without disturbing the lower layer forming two phases. The falcon was centrifuged (800 x g, 18 – 20 °C, 30 min, brakes switched off). Ficoll-Paque acts as a separation medium and during centrifugation cells migrate to form layers containing different cell types. Erythrocytes and granulocytes aggregate at the bottom of the flask

together with cell debris. At the interface between plasma and Ficoll-Paque layer, mononuclear cells are found beside slowly sedimenting particles, such as platelets. After separation, the mononuclear ring containing the PBMCs was collected from the falcon. Cells were washed three times with 10 mL PBS (200 x g, RT, 5 min) to remove contaminations of platelets and cell material. Clean PBMCs were resuspended in PBS or homogenization buffer (2.7).

3.2.5 Preparation of membrane fractions

Biologically active membrane fragments were produced from different cell lines as a source for undefined antigen during solid-phase panning and as coating antigen on 96-well plates during screening and ELISA experiments. Cell lines were cultivated, sonicated and membrane fractions were isolated using ultra centrifugation [134].

Cell lines were cultivated in 75 cm² flasks using the appropriate media. About 10 flasks per cell line were harvested and 1.8 x 10⁷ cells/preparation/cell line were processed to membrane fractions. Adherent cells were detached from the flask with 2 mL Accutase[®]. Cells were washed with 3 x 10 mL PBS (200 x g, 4 °C, 10 min). Cells were resuspended in 8 mL ice-cold homogenization buffer (2.7), counted and incubated on ice for 10 min. This cell suspension was sonicated twice for 60 s with intensity of maximum 70% or until the cell suspension appeared clear (depending on morphological properties of cell line). The clear suspension was centrifuged (1,000 x g, 4 °C, 12 min). The supernatant was transferred to ultra-centrifuge tubes and centrifuged (100,000 x g, 4 °C, 20 min). Pelleted membrane fractions were taken up in 10 mL ice-cold resuspension buffer (50 mM Tris HCl (pH 7.4)) and were ultra-centrifuged again under the same conditions. Finally, the membrane fraction pellet was resuspended in 1.2 mL/tube PBS and stored as 300 µL aliquots at -80 °C. For L3.6pl and FG membrane fractions ELISA coating buffer was used instead of PBS.

3.3 Protein chemical and immunological methods

3.3.1 SDS-PAGE

Denaturing discontinuous sodium dodecylsulfate polyacrylamide gel electrophoresis (SDS-PAGE) was performed for protein analysis, detection and size separation [233]. Protein samples were mixed with 5 x protein loading dye containing β -mercaptoethanol, heated to 99 °C for 5 – 10 min for complete denaturation, centrifuged and loaded on a 12% polyacrylamide gel next to a pre-stained protein marker for size comparison. Protein separation was carried out in a BioRad MiniProtean III Electrophoresis chamber at 100 – 150 V for 1 – 2 h. Then glass plates were removed and separated protein bands were stained with Coomassie Brilliant Blue (SERVA, Heidelberg, Germany). The gel was destained until protein bands became clearly visible using Destaining Solution (2.7) and a sponge. For buffer compositions, stacking and separating gel mixtures see 2.7. Completed Coomassie-stained gels were scanned for documentation and subsequent automatic imaging data analysis (AIDA) (3.3.3.1).

3.3.2 Western blot analysis

Proteins from a duplicate SDS-PAGE (3.3.1) were transferred and immobilized onto a nitrocellulose membrane (GE healthcare, UK) with a cooled BioRad Mini Trans-Blot device. This method specifically verifies proteins by means of immunochemical visualization. Following protein transfer, the membrane was blocked with 2% MPBS for 2 h at RT, washed 3 x 5 min with PBST and incubated with a penta-anti-His IgG mouse primary antibody (2.8) (dilution: 1 : 2000 in PBS) for 1 h at RT. Washing was repeated as above and the secondary goat-anti-mouse peroxidase conjugated antibody (2.8) was incubated (dilution: 1 : 5000 in PBS) for 1 h at RT. The signal was developed with 3,3'-diaminobenzidine tetrahydrochloride (DAB) activated with 30% H₂O₂. Several washing steps with PBS stopped the substrate reaction and the blot was scanned for documentation and AIDA analysis (3.3.3.1).

3.3.3 Determination of protein concentration

Protein concentrations were determined using two different methods: (1) Densitometric analysis of protein bands on Coomassie-stained gels by the AIDA Image Analyzer software (3.3.3.1) and (2) colorimetric determination with a BC-assay (3.3.3.2).

3.3.3.1 AIDA analysis

Protein samples on the Coomassie-stained gel (3.3.1) were analyzed against a BSA standard dilution series (10 µg/mL – 500 µg/mL) run in parallel. AIDA visually compares staining density of protein bands and protein concentrations were calculated in relation to the BSA standards. Thus, overall protein concentrations as well as the concentration of a certain target protein can be calculated.

3.3.3.2 BC-Assay

Total protein concentration of purified scFv-SNAP proteins was determined colorimetrically with a BC-assay (2.6). In this method, Cu^{2+} ions are reduced to Cu^+ ions and proteins are quantitatively chelated to the monovalent copper ions in presence of bicichoninic acid to form a purple and water soluble complex. The color signal was developed for 1 h at 60 °C and its absorption was measured at $\lambda = 562$ nm. The result was interpreted and calculated in Excel based on a straight calibration line from a BSA protein standard dilution series (2 – 500 µg/mL). The reaction protocol was carried out in a microtiter plate according to the manufacturers' instructions for the "enhanced protocol".

3.3.4 Immobilized metal-ion affinity chromatography

Eukaryotically expressed soluble scFv-SNAP proteins, as well as prokaryotically expressed Wx-Ki-4(scFv) proteins, were purified via the C-terminal His₆-tag using immobilized metal-ion affinity chromatography (IMAC) [243]. This method facilitates small-scale purification of non-denatured prokaryotic and eukaryotic proteins by means of batch preparation with a suspended matrix. Its principle is based on the reversible interaction between various amino acid side chains (e. g. present in His₆-tag) and bivalent immobilized metal-ions, such as Co^{2+} , Ni^{2+} or Zn^{2+} , usually embedded into pockets of an iminodiacetic acid (IDA) matrix. His-tagged proteins act as electron donor and transition metal ions as electron acceptor, thus forming a reversible ionic bond. Nickel-based resins tend to bind host proteins with histidine residues, having an adverse effect on protein purity. Instead, cobalt-based TALON resin was employed here to purify the His₆-tagged proteins under native conditions. Competitive elution with excess imidazole recovers resin-bound proteins by replacing all His₆-tagged proteins on the TALON resin.

3.3.4.1 IMAC purification protocol

Collected tissue culture supernatant (TCSN) containing eukaryotically expressed scFv-SNAP proteins (3.2.3) or bacterial crude lysate from prokaryotic expression after cell disruption with a combination of TES buffer lysis (3.3.5.2) and sonication (3.3.5.4) were processed during IMAC. Cell debris was removed from solutions (4,500 x g (15,000 x g for crude lysate), 4 °C, 30 min). Moreover, EDTA was removed from bacterial lysate in an additional dialysis step (3.3.6) to prevent it from disturbing the IMAC purification set-up. The whole purification process was carried out at RT. For purification, 9 mL TCSN or dialyzed crude lysate were mixed with 4 mL 4 x Equilibration buffer (2.7) in a 15 mL falcon tube. 150 – 200 µL TALON resin were transferred to a 1.5 mL Eppendorf tube, centrifuged (6,000 rpm, 1 min) and washed with 1 mL 1 x Equilibration buffer. Supernatant was always removed by dunking the pipet tip into the resin pellet and carefully aspirating the liquid. Equilibrated matrix and TCSN or dialyzed lysate were mixed and incubated for 1 h on a rotator to allow the His₆-tagged proteins to attach to the Co²⁺ ions on the TALON matrix. This suspension was centrifuged (1,000 x g, 5 min), and after discarding the supernatant the resin was washed twice with 1 mL 1 x Equilibration buffer as above. To elute matrix-bound proteins, the matrix was incubated with 150 µL Elution buffer containing 250 mM imidazole (2.7) for 20 min on a rotator. The matrix was pelleted (6,000 rpm, 2 min), the supernatant containing the eluted protein transferred to a fresh Eppendorf tube and stored at 4 °C.

Purified proteins were analyzed via SDS-PAGE (3.3.1) and Western blotting (3.3.2) to determine protein purity and concentration for following protein ELISA (3.3.9.3) and flow cytometric binding analysis (3.3.10) as well as internalization assays (3.3.11.1, 3.3.11.2).

3.3.4.2 SNAP-tag labeling of scFv-proteins with fluorophore dyes

For subsequent fluorescence-based binding and internalization experiments scFv antibody fragments were genetically fused to an engineered version of the human DNA-repair enzyme O₆-alkylguanine DNA alkyltransferase (hAGT), known as SNAP-tag (1.5.3), by subcloning into the pMS-SNAPMut vector [209, 210, 212, 213]. Substrates containing O₆-benzylguanine derivatives can be covalently linked to SNAP fusion proteins providing a strategy to equip scFv antibodies with various fluorescent dyes or other imaging reagents [209, 211, 215]. The SNAP-tag labeling reaction is highly specific and efficient (stoichiometrically 1 : 1) but independent of the label's nature. Substrates BG-Vista Green (BG-VG), BG-Alexa Fluor 488 (BG-AF488) and BG-Alexa Fluor 647 (BG-AF647) were

purchased from New England BioLabs as lyophilized products, resuspended in 50 μL DMSO (stock concentration: 1 nmol/ μL) and stored at $-20\text{ }^{\circ}\text{C}$ protected from light. For the labeling reaction scFv-SNAP proteins were IMAC-purified as described in 3.3.4.1. Right before the elution step, matrix-bound proteins were additionally incubated with 150 μL 1 x Equilibration buffer containing 1.5 μL BG-dye for 1 h at RT on a rotator protected from light. Afterwards the resin was washed with 3 x 1 mL 1 x Equilibration buffer, eluted and analyzed as described in 3.3.4.1. Successful fluorescence labeling was checked on the SDS-PAGE before Coomassie staining under a VersaDoc device. Fluorescence-labeled proteins always have to be protected from light to avoid fading of fluorescence intensity.

3.3.5 Extraction of recombinant protein after prokaryotic expression

Bacteria-produced periplasmic recombinant proteins were released from the cells by application of several methods. Recovered proteins were used for soluble protein ELISA (3.3.9.3) or flow cytometric binding analysis (3.3.10), or 2D scans of Wx-Ki-4(scFv) proteins (3.5.2).

3.3.5.1 Lysozyme extraction

One method for protein extraction after prokaryotic expression was the enzyme-based lysozyme extraction. Lysis buffer (2.7) was freshly mixed with 300 $\mu\text{g}/\text{mL}$ lysozyme (stock solution: 10 mg/mL in 10 mM Tris-HCl, pH 8.0) and the bacterial pellet was resuspended. This mixture was incubated at $37\text{ }^{\circ}\text{C}$ for 30 min, then the suspension was centrifuged (15,000 x g, $4\text{ }^{\circ}\text{C}$, 30 min) and the lysate was transferred to a fresh tube.

3.3.5.2 TES buffer extraction

Osmotic shock extraction uses the sudden change of solute concentration from high to low around the cells. Due to the lower salt concentration, large amounts of water enter the cell very rapidly, causing it to swell and burst, thereby releasing the proteins contained in the periplasmic space. To release periplasmic proteins from 50 mL pelleted bacterial culture (3.1.9.3), they were resuspended in 8 mL 1 x Tris-EDTA-sucrose (TES) buffer (2.7). The suspension was incubated for 15 min on ice, then 12 mL 0.2 x TES buffer at RT were added and the mixture was incubated for 15 min shaking at RT to keep suspension intact. Osmotic lysate with periplasmic proteins was recovered after centrifugation (15,000 x g, $4\text{ }^{\circ}\text{C}$, 30 min), transferred to a fresh 15 mL falcon tube.

3.3.5.3 Extraction with NP-40

As third method, the non-denaturing detergent Nonidet-P40 (Applichem, A1694 0250, 99% pure), normally a detergent for recovery of cytoplasmic proteins was tested. Therefore, lysis buffer (2.7) was supplemented with 10 mM of NP-40, the bacterial pellet was resuspended and the mixture was incubated on ice for 5 – 10 min. The lysate was spun down (15,000 x g, 4 °C, 30 min) and the lysate was collected in a clean tube.

3.3.5.4 Extraction via sonication

Harvested bacteria were resuspended in lysis buffer (2.7) and the suspension was sonicated five times for 60 s at 70% amplitude (Sonoplus, Bandelin, Berlin, Germany) until the solution appeared transparent. The mixture was kept on ice to prevent protein degradation. The solution was centrifuged (15,000 x g, 4 °C, 30 min) and released proteins were transferred to a fresh tube.

3.3.6 Dialysis of scFv-protein solutions and crude lysate

To remove salts, EDTA or imidazole, protein samples and crude cell lysates were passed through PD10-desalting columns (GE Healthcare, Munich) thus exchanging the buffer with PBS prior to down-stream analysis. This method is based on gravity-flow gel filtration for collecting size-sorted molecules. For dialysis, sample volume was adjusted to 2.5 mL, then columns were calibrated with 2 x 10 mL ddH₂O and samples were loaded onto the column. The flowthrough with the low-molecular contaminants was discarded and protein was eluted from gel filter with 3 – 3.5 mL PBS, whereas salts remain on the column.

3.3.7 Concentrating protein solutions

Samples of large volume and low protein content were concentrated by means of Vivaspin 6 (15 mL) or Vivaspin 20 (50 mL) ultrafiltration spin columns with a protein cut-off at 5 or 30 kDa depending on protein size. Molecules below cut-off pass the polyethersulfon membrane in the concentration centrifugators. A large volume of a protein solution was transferred to the upper compartment of the spin columns and centrifuged according to the manufacturers' instructions at 4 °C to the desired volume and concentration. Contaminants were removed efficiently by refilling the protein solution with PBS to 5 or 10 mL and repeated centrifugation. Final protein concentrate was recovered directly from the spin column and transferred to a fresh tube to determine protein content.

3.3.8 Mass spectrometrical analysis

As analytical method to determine molecules and molecule fragments mass spectroscopy was employed to verify the identity of W-tagged and non-tagged scFv antibody fragments. A protein band was excised from a Coomassie-stained SDS-PAGE (3.3.1), shredded and decolorized by adding ammonium hydrogen carbonate (NH_4HCO_3) and acetonitrile. After denaturation with dithiothreitol (DTT) and alkylation with iodine acetamide, mass spectrometric analysis was performed by Michael Küpper from Fraunhofer Institute IME (Aachen). Molecules were analyzed with an ESI-MS/MS mass spectrometer (Micromass Electrospray Q-TOF 2, Waters Corporation, Eschbor) after proteolytic cleavage with trypsin and gel extraction in a nanoHPLC (Dionex, Germering). Identified molecule fragments were evaluated using the protein data base MASCOT (Matrix Science, London, UK).

3.3.9 Enzyme-linked immunosorbent assay (ELISA)

The enzyme-linked immunosorbent assay (ELISA) is a common antibody-dependent detection assay based on an enzymatic color change reaction, thus identifying binding activity to an immobilized antigen on an MTP. ELISA was used to show enrichment of L3.6pl-binding scFv-phage particles (3.3.9.1), to screen for sequence-unique L3.6pl-specific scFv-phage particles (3.3.9.2) and to test cross reactivity to other cell lines (3.3.9.2). Moreover, specific binding activity of soluble scFv-SNAP proteins after eukaryotic expression was documented (3.3.9.3) by ELISA. Membrane preparations (3.2.5) of L3.6pl and PBMC cells were coated as antigen, as well as membrane preparations of several other cell lines during cross reactivity testing (4.3.2).

General information for all ELISA experiments: (a) All blocking and incubation steps were performed out on an orbital shaker (400 rpm), (b) bacterial MTP cultures were covered with a semi-permeable membrane to ensure sufficient oxygen supply for bacterial growth and (c) MTPs with phage-containing solutions or bacterial cultures were covered with an air-tight plastic seal to avoid phage-related cross-contamination to neighboring wells or the incubator.

3.3.9.1 Polyclonal phage ELISA

After each selection round, polyclonal phage pools were analyzed for enrichment of L3.6pl-specific scFv-phage fragments. The scFv-phage pools of all three selection rounds, as well as the original Tomlinson Libraries, were precipitated with PEG/NaCl (2.7) and

resuspended in PBS to reach a phage concentration (3.4.4) of 1×10^{11} pfu/mL. A 96-well MTP was coated with 100 μ L/well L3.6pl membranes (dilution: 1 : 100 in ELISA coating buffer) and 100 μ L/well FG or PBMC membranes, respectively, at the same antigen dilution. Antigen was immobilized on MTPs by incubation at 4 °C for 12 – 16 h without shaking. Then the antigen was quickly washed with 3 x 200 μ L/well PBS and blocked with 200 μ L/well 2% MPBS for 2 h at RT. In parallel, the polyclonal scFv-phage pools were blocked with 2% MPBS at a ratio of 1 : 1. Afterwards, wells were washed as above and 100 μ L/well blocked scFv-phage solution was added to the respective wells. After incubation of the scFv-phage solution for 1 h at RT unbound scFv-phage particles were removed with 3 x 200 μ L/well PBST and 100 μ L/well secondary HRP/anti-M13 monoclonal conjugated antibody (dilution: 1 : 5,000 in 2% MPBS) were incubated for 1 h at RT. Then wells were washed as before and 100 μ L/well fresh ABTS (2,2'-azino-bis(3-ethyl-benzothiazoline-6-sulphonic acid) substrate solution were added and incubated at RT for 15 – 60 min. ABTS absorbance was measured in a Tecan Reader (2.2) at 405 nm (reference wavelength 490 nm) every 15 min.

To verify results, all polyclonal scFv-phage pools were analyzed as triplicates. Moreover, every assay was performed twice with M13KO7 helperphage and repeated once with M13KO7 Δ pIII hyperphage.

3.3.9.2 Monoclonal phage ELISA

After biopanning a population of scFv-phage particles was screened by a monoclonal phage ELISA to identify unique scFv-phage clones with L3.6pl-specific binding activity. A 5 mL 2 x TY_{gluc,amp} culture was inoculated from TG1F+ *E.coli* glycerol stocks resulting from the third selection round and grown for 8 h at 37 °C and 250 rpm. 1 : 100 dilutions ranging from 10^{-2} to 10^{-8} were prepared with 2 x TY_{gluc,amp} medium, then 10 μ L/dilution was plated on an LB_{amp} agar plate and incubated O/N at 37 °C. Single colonies carrying the information for one unique phagemid were picked to produce a single scFv-presenting clone for monoclonal phage ELISA analysis. Individual clones were each inoculated into a 96-well MTP with 150 μ L/well 2 x TY_{gluc,amp} medium and grown at 37 °C and 250 rpm O/N. A cryo stock was prepared from this original 96-well MTP (3.1.10) from which a small inoculum (~1 – 2 μ L/well) was transferred to a fresh 96-well MTP containing 200 μ L/well 2 x TY_{gluc,amp} medium. Cultures were grown at 37 °C and 250 rpm for 2 h to reach an approximate OD₆₀₀ of 0.4 – 0.5, then 25 μ L/well 2 x TY_{gluc,amp} medium were added containing 1×10^9 pfu/well M13KO7 helperphage. Wells were infected at 37 °C

without shaking for 30 min and another 30 min shaking at 37 °C and 250 rpm. Then the MTP was centrifuged (1,800 x g, 4 °C, 10 min), the supernatant was discarded and the bacterial pellet resuspended in 200 µL/well 2 x TY induction medium (2.3) to induce phage production. The MTP was placed at 30 °C and 250 rpm for 18 – 20 h to promote phage production. Next, scFv-phage cultures were centrifuged as above and the supernatant containing the scFv-phage was blocked with 2% MPBS (ratio 1 : 1) for 2 h before monoclonal phage ELISA analysis. For the monoclonal ELISA procedure the same protocol was used as for the polyclonal phage ELISA (3.3.9.1).

One sample was analyzed per well, and thus each monoclonal phage ELISA was repeated three times to ensure reproducibility of the results.

Antigen coating: Membrane fractions of L3.6pl and other cell lines were coated on the 96-well MTP in 100 µL/well (dilution: 1 : 100 in ELISA coating buffer or PBS) and immobilized at 4 °C O/N. Living cells were coated 24 h previous to the ELISA experiment. 100 µL/well cell suspension, at 20,000 cells/well, were seeded out in RPMI/10/1 and grown. PBMCs were isolated (3.2.4), diluted to a concentration of 20,000 cells/well and centrifuged to the MTP bottom, first at 500 x g for 5 min, then with increased centrifugation force for 30 min at 4,500 x g. The supernatant covering all cells was discarded and wells were air-dried for 2 min. Then 100 µL/well of ice-cold EtOH (-20 °C) were incubated on ice (under a hood) for 10 min to fix cells onto MTP.

3.3.9.3 Protein ELISA

After monoclonal phage ELISA screening (3.3.9.2) and site-directed mutagenesis of *amber* stop codons (3.4.6), L3.6pl-specific scFv antibodies were analyzed as soluble protein expressed in: (1) A prokaryotic system via pIT2 vector in HB2151 or pMT vector in BL21 Rosetta 2 (DE3) *E.coli*, or (2) via the eukaryotic pMS-SNAPMut vector transfected into HEK293T cells (3.2.3). Binding activity and specificity without an attached phage particles, possibly interfering with the specific scFv-binding, was tested on L3.6pl membrane fractions (antigen coating as in 3.3.9.2). Samples were analyzed in triplicates and the soluble protein ELISA was repeated twice to confirm reproducibility of binding results.

Prokaryotic expression: Soluble scFv proteins were expressed as 5 mL cultures as described in 3.1.9.3. Bacteria were pelleted (4,500 x g, 4 °C, 15 min) and periplasmic proteins were recovered via TES buffer lysis (3.3.5.2). The lysate was analyzed via

SDS-PAGE (2.7) before performing the ELISA experiment. Blocking, washing and incubation steps were analogous to the polyclonal phage ELISA (3.3.9.1), but different antibodies were applied. Specific L3.6pl-binding scFv antibodies were detected with a monoclonal anti-poly His mouse IgG antibody (dilution: 1 : 2500 in PBS) against His₆-tag which was then bound by a goat-anti-mouse peroxidase-conjugated IgG secondary antibody (dilution: 1 : 5000 in PBS). ABTS substrate was added to develop a signal (3.3.9.1). The W-tagged Ki-4(scFv) proteins, after dialysis (3.3.6) and Vivaspin concentration (3.3.7), were treated likewise.

Eukaryotic expression: TCSN containing scFv-SNAP proteins (3.2.3) was collected and the protein concentration analyzed via SDS-PAGE. Blocking, washing and incubation steps were analogous to the polyclonal phage ELISA (3.3.9.1). Bound scFv-SNAP proteins were captured with a commercial polyclonal anti-SNAP-tag rabbit IgG (dilution: 1 : 5,000 in PBS). For specific detection a goat-anti-rabbit HRP-conjugated IgG antibody (dilution: 1 : 5,000 in PBS) was applied followed by signal development with 100 µL/well fresh ABTS (3.3.9.1).

3.3.10 Flow cytometric analysis

Binding activity of L3.6pl-specific scFv-SNAP proteins and Wx-Ki-4(scFv) fusion proteins on a native antigen conformation was analyzed via flow cytometry. PBMCs were used as negative control. Samples were centrifuged at 1,200 x g at 4 °C for 5 min. Mean fluorescence intensity values (MFI) and geometrical mean values (%G mean) of the flow cytometry measurements were displayed as percent changes in relation to 425(scFv) positive control or Ki-4(scFv) expression control (100%). MFI was calculated by CellQuest Pro or WinMDI 2.9 software (Table 2-1). All measurements were performed with a FACScalibur flow cytometer (Table 2-2).

3.3.10.1 Binding analysis of scFv-SNAP proteins

50 µL L3.6pl and PBMC cell suspensions (2×10^5 cells/mL) were transferred into FACS tubes and washed with 1 mL ice cold PBS. 300 µL/tube unpurified TCSN containing scFv-SNAP proteins (3.2.3) or 2 µg IMAC-purified protein (3.3.4) were added and incubated on ice for 1 h. Cells were washed once with 1 mL PBS, incubated on ice with 100 µL/tube penta-anti-His Alexa Fluor 488 conjugated antibody (dilution: 1 µg/mL) for 30 min and washed again twice. Cell pellet was resuspended in 500 µL/tube ice cold PBS containing 1 µg/mL propidium iodide to sort out dead cells. The fluorescence signal of

bound proteins was measured and analyzed. The same conditions were employed during flow cytometric cross-reactivity testing to other cell lines.

3.3.10.2 Binding analysis of BG-coupled scFv-SNAP proteins

L3.6pl and PBMC cells were transferred into FACS tubes and treated as in 3.3.10.1. Then 2 μg IMAC-purified BG-coupled protein (3.3.4) were added and incubated on ice for 1 h. Used scFv-SNAP proteins were either coupled to BG-VG or BG-AF488 for measurement of green fluorescence or to BG-AF647 for red fluorescence documentation. Cells were washed twice with 1 mL PBS and resuspended in 500 μL /tube ice-cold PBS containing 1 $\mu\text{g}/\text{mL}$ propidium iodide to sort out dead cells (propidium iodide staining was not used for measurement of BG-AF647 coupled scFv proteins since the signal of propidium iodide interfered with the measurement). The fluorescence signal of bound proteins was measured and analyzed as in 3.3.10.1.

3.3.10.3 Binding analysis of Wx-Ki-4(scFv) fusion proteins

L540cy and PBMC cell suspensions (2×10^5 cells/mL) were transferred into FACS tubes and treated as described in 3.3.10.1. Then 2 μg of each Wx-Ki-4(scFv) fusion protein, present in bacterial crude extract after TES-lysis (3.3.5.2) were incubated on ice for 1 h. Binding of Wx-Ki-4(scFv) fusion proteins to L540cy cells was detected via the His₆-tag as described in 3.3.10.1.

3.3.11 Fluorescence-based internalization assays

When developing therapeutic treatment options it is essential to isolate scFv antibodies with internalizing properties. Internalization into a diseased target cell after binding to its cellular surface is a very basic requirement for cytolytic cancer therapeutics (e. g. immunotoxins) to unfold their full effect within the cell. Moreover, rapid degradation of the medicine in the body is prevented leading to better treatment results. Newly isolated scFv antibodies isolated from the Tomlinson Libraries I and J were characterized for internalization behavior by means of flow cytometry (3.3.11.1) and OPERA-based confocal microscopy on living cells (3.3.11.2) as well as on immunofluorescence-stained fixed and permeabilized cells (3.3.11.2). The well-documented and rapidly internalized EFGR-binding 425(scFv) antibody fragment [158, 159] was used as positive control throughout all internalization experiments.

3.3.11.1 Flow cytometry-based internalization testing

All incubations at 4 °C were performed in 1% NaN₃ to prevent too rapid internalization. Incubations at 37 °C were carried out in serum-free RPMI medium to create a most viable environment encouraging internalization. For washing, cells were resuspended in 1 mL ice-cold PBS and pelleted (1,200 rpm, 4 °C, 5 min). To test for surface binding and internalization, 1 x 10⁶ L3.6pl cells/tube were incubated for 1 h with 300 µL NaN₃ or RPMI 1640 Glutamax medium, containing 3 µg AF647-coupled scFv-SNAP protein. Incubation was conducted at 4 °C to allow cell surface attachment only, and another in parallel at 37 °C to promote internalization of 647-labeled scFv-SNAP proteins. Then cells were washed with 1 x 2 mL PBS and the red fluorescence signal of 4 °C and 37 °C incubations was measured using a FACScalibur device. For measurements, cells were always resuspended in 500 µL/tube 0.5% PFA. Afterwards surface-bound scFv-SNAP proteins were digested off with 500 µL/tube 0.25% trypsin-EDTA at 37 °C for 5 – 10 min. Trypsin reaction was stopped by addition of 500 µL/tube RPMI medium supplemented with 20% FBS. Then, cells were washed once and the fluorescence signal was measured again. For 4 °C incubations, no fluorescence signal was expected after trypsinization. However, for 37 °C incubations the fluorescence signal should still be present from inside the cells if the internalization process has been successful. As additional control, L3.6pl cells before and after trypsinization were incubated with a penta-anti-His Alexa Fluor 488 conjugated IgG as secondary detection antibody to confirm removal of all surface-bound scFv-SNAP proteins by trypsinization. Therefore, cells were resuspended in 100 µL/tube NaN₃ containing 1 µg/mL secondary antibody, incubated on ice for 30 min., washed twice, measured and analyzed as described in 3.3.10. This protocol has been adapted from Xiao et al., 2008 [244].

3.3.11.2 OPERA-based confocal microscopy

Real-time observation of living L3.6pl cells: All scFv-SNAP fusion proteins with a positive internalization outcome in 3.3.11.1 were examined further during live cell imaging with OPERA-based confocal microscopy at Fraunhofer IME (Aachen). The OPERA measurement device is a fully automated system for confocal microscopy able to measure several samples and their replica wells in parallel and to visualize internalization kinetics for several hours in real-time under cell cultivating conditions. The laser analysis system was able to focus on different layers throughout the cell and to stack the pictures for subsequent documentation and analysis. L3.6pl cells were split onto a 96-well MTP

(Greiner, black, μ -clear) at 20,000 cells/well, and placed at 37 °C to settle and adhere O/N in RPMI/10/1. Afterwards, culture medium was exchanged with serum-free medium for 2 – 4 h. Then, wells were washed twice with 200 μ L ice-cold PBS and 3 μ g scFv-SNAP protein labeled with BG-AF647 were incubated at 4 °C in 50 μ L/well RPMI medium without phenol red (color would disturb measurement) for 30 – 60 min to visualize binding to the cell surface. Again wells were washed with 3 x 200 μ L PBS to remove excess dye or unbound proteins. The MTP was then placed at 37 °C to induce internalization. Internalization was observed and measured with the OPERA system after 30, 60 and 80 min via AF647 fluorescence. To remove background fluorescence related to free AF647 dye, wells were washed repeatedly with PBS. AF647-labeled Ki-4(scFv)-SNAP protein, without internalizing properties on L3.6pl cells, served as negative control. Samples were measured as triplicates and pictures were taken of surface-bound as well as internalized scFv-SNAP proteins.

Immunofluorescence staining: L3.6pl cells were seeded into a 96-well MTP (Greiner, black, μ -clear) at 20,000 cells/well and grown O/N in full media. Medium was exchanged to serum-free and cells were incubated for another 3 – 4 h. Wells were washed twice with 200 μ L PBS and 150 μ L/well unpurified TCSN containing soluble scFv-SNAP proteins were added. Proteins incubated at 37 °C for different time periods (4 h, 3 h, 2 h and 1 h) to examine internalization behavior. In parallel, the same scFv-SNAP proteins were incubated at 4 °C for 1 h to confirm cell surface binding. Next, wells were washed twice with 200 μ L ice-cold PBS, fixed with 200 μ L 4% PFA for 10 min at RT and washed again with PBS (2 x 5 min and 3 x fast). Half of the wells were permeabilized with 100 μ L 0.1% TritonX100 in PBS for 10 min at RT and washed with PBS (3 x 5 min). Unspecific sites were blocked with 200 μ L/well 3% BSA/PBS (BSA: IgG-free fraction V) for 1 h at RT or at 4 °C O/N. Wells were cleaned with PBS (3 x fast) and the polyclonal anti-SNAP-tag rabbit IgG secondary antibody (dilution: 1 : 5,000 in 1% BSA/PBS) was incubated for 1 h at RT or at 4 °C O/N. Afterwards, cells were washed again with PBS (2 x fast, 3 x 5 min.). Next, the anti-rabbit IgG (H+L), F(ab)₂ Fragment (Alexa®647) tertiary detection antibody (dilution: 1 : 1,000 in 1% BSA/PBS) was incubated for 1 h at RT. Wells were washed using same washing conditions as above and 100 μ L/well DAPI solution (dilution: 1 : 10,000 in PBS) were added for counter-staining of nuclei. Fluorescence intensity of bound scFv-SNAP proteins was detected via the OPERA system. Measurement parameters were adjusted with the OPERA software Evoshell with the help of Dr. Stefano

Di Fiore at Fraunhofer IME (Aachen). Figures were evaluated and edited using the ImageJ 1.42q software.

3.4 Phage Display Technology

In this work, the naïve human and semi-synthetic Tomlinson Phage Libraries I and J (1.3.3) were used for the isolation of L3.6pl-specific scFv antibody fragments using phage display technology. To avoid confusion between clones selected from the two libraries, biopanning was performed separately.

3.4.1 Cultivation of Tomlinson Libraries I and J

Each library was received as a 500 μ L cryo stock containing phagemid-carrying TG1F+ *E.coli*. 200 mL pre-warmed 2 x TY_{gluc,amp} medium (2.3) were inoculated with it and grown O/N at 37 °C and 250 rpm. Bacteria were pelleted (4,000 x g, 4 °C, 10 min), resuspended in 10 mL 2 x TY cryo medium (2.3), aliquoted (500 μ L/tube) and stored at -80 °C (3.1.10).

Tomlinson library cultures for phage display selection were inoculated from these stocks and grown O/N as 5 mL 2 x TY_{gluc,amp} medium pre-culture at 37 °C and 250 rpm. 25 mL fresh 2 x TY_{gluc,amp} medium were inoculated with 500 μ L pre-culture and grown in a sterile 250 mL Erlenmeyer flask at 37 °C and 250 rpm to OD₆₀₀ of 0.5. This optical density indicates the logarithmic growth phase of TG1F+ *E.coli* when phage infection via extended F-pili is possible (1.3.1).

3.4.2 Phage infection and production

5 mL of this culture (3.4.1) were infected with M13KO7 helperphage or M13KO7 Δ pIII hyperphage, at a multiplicity of infection (MOI) \geq 20, and incubated for 30 min at 37 °C without shaking followed by 30 min shaking at 37 °C and 250 rpm. The infected culture was centrifuged (4,000 x g, 4 °C, 5 min), the supernatant discarded and the infected bacterial pellet was resuspended in 25 mL 2 x TY induction medium (2.3) to promote phage production. The suspension was sealed in air-tight Erlenmeyer plastic flasks and incubated at 30 °C and 250 rpm for 18 – 20 h. As infection control, 50 μ L of this suspension were also plated on LB_{kan} agar and incubated at 37 °C O/N. Phage pools were prepared freshly before each selection round.

3.4.3 Phage precipitation

The bacterial culture (3.4.2) was spun down (4,500 x g, 4 °C, 30 min), the phage-containing supernatant transferred to a 50 mL falcon tube and 1/5 volume ice-cold PEG/NaCl (2.7) was added. At low temperatures, the presence of PEG shifts the solubility constant of the phage particles in solution, thus precipitating phage particles during incubation on ice for 1 h. Precipitated phage were pelleted (12,000 x g, 4 °C, 30 min) and the phage pellet was resuspended in 200 – 1000 µL PBS (depending on the selection round and strategy). Phage solutions were stored at 4 °C until use.

3.4.4 Titer determination

Before and after each selection round, the phage input and output titer was determined with the colony method, where ampicillin-resistant TG1F+ cultures were counted after infection with a dilution series of M13KO7 helperphage. Therefore, 10 mL 2 x TY_{gluc,amp} medium were inoculated with a single uninfected TG1F+ colony from an M9 minimal agar plate (2.3) and grown at 37 °C and 250 rpm to an OD₆₀₀ of 0.5. Then phage suspensions, either after PEG-precipitation or elutions after panning, were diluted 1 : 100 in 200 µL PBS (dilutions: 10⁻² to 10⁻¹⁶) and used to infect fresh TG1F+ *E.coli* by incubation for 1 h at 37 °C and 250 rpm. 10 µL of each dilution were spotted on an LB_{gluc,amp} agar plate and incubated at 37 °C for 12 – 16 h. Plaque forming units (pfu), i. e. resistant bacterial colonies, were counted and phage concentration was calculated as follows:

$$\text{phage concentration [pfu/mL]} = \frac{n \text{ [pfu]} \times 5}{(\text{DF} \times \text{volume [mL]})}$$

(n = counted number of ampicillin-resistant colonies on one plate (e.g. plate with 10⁻⁶ dilution); DF = dilution factor of phage suspension from plate with counted colonies (e.g. at 10⁻⁶ dilution); volume = plated volume of phage-bacteria mixture of 10 µL; 5 = dilution of phage-bacteria mixture; pfu = plaque forming units)

3.4.5 Biopanning

L3.6pl-specific scFv antibody fragments were selected via three panning strategies:

- (1) Solid-phase panning on adherent viable cells under internalizing conditions (3.4.5.1),
- (2) suspension panning on living cells under internalizing conditions (3.4.5.2) and
- (3) solid-phase panning on membrane fractions for selection of surface-binding scFv fragments (3.4.5.3).

Each complete selection consisted of three panning rounds. First selection rounds were always performed with the polyvalent M13KO7ΔpIII hyperphage. This particular phage is

missing the gene coding for the pIII coat protein (Δ pIII), hence displaying five copies of a specific scFv fragment fused to pIII when produced in TG1F+ *E.coli*. It shows a much stronger binding affinity to a specific surface protein than phage particles with only one copy. By this a maximum amount of scFv fragments with unspecific binding to the depletion antigens were removed whereas the ones displaying L3.6pl-specific binding were rescued to the next selection round. Second and third selection rounds were carried out with the monovalent M13KO7 helperphage carrying one scFv-pIII protein on its surface. Antigen concentrations were reduced with continuing selection rounds along with increasing washing stringency to eliminate scFv-phage particles with unspecific binding properties. For detailed instructions to phage display technology, the Tomlinson libraries and a general panning schematic see Figure 1-3.

3.4.5.1 Panning on adherent L3.6pl cells under internalization conditions

Two days prior to panning 1×10^6 L3.6pl cells were split into a 25 cm² tissue culture flask with RPMI/10/1 medium. The same was done for the FG cell line. To avoid cell loss during panning, cells had to be adhered to the bottom of the flask. The same cell concentration was used for each selection round.

Throughout selection rounds, 1 mL precipitated scFv-phage particles (3.4.3) were blocked with 5% MRPMI (ratio 1 : 1). This mixture was transferred to an empty 25 cm² tissue culture flask and incubated at RT for 2 h on a shaker to block the unspecific binding sites and to eliminate plastic binders. Simultaneously, FG and L3.6pl cells were washed three times with 2 mL PBS and were each blocked with 2 mL 5% MRPMI for 2 h at RT.

Cross-reactive scFv-phage particles were separated from L3.6pl-specific binders via depletion on FG cells, before selection on L3.6pl cells. Therefore, blocked phage solution was transferred onto the FG cells and incubated for 1 h at RT shaking slightly.

This solution containing the non-bound phage after subtractive selection on FG cells was transferred onto the L3.6pl cells for positive selection. The phage mixture was incubated at 37 °C for 1 h shaking slightly. The supernatant was discarded and L3.6pl cells were washed with PBS and PBST according to washing steps listed in Table 3-3.

Table 3-3 Washing steps with increasing stringency applied during solid phase selection on adherent whole cells.

	Selection round 1	Selection round 2	Selection round 3
Washing steps	3 x PBST quick 2 x PBST 5 min on shaker 3 x PBS quick 2 x PBS 5 min on shaker	1 x PBST quick 4 x PBST 5 min on shaker 1 x PBS quick 4 x PBS 5 min on shaker	1 x PBST quick 4 x PBST 5 min on shaker 1 x PBS quick 4 x PBS 5 min on shaker

Phage were collected via proteolytic elution with 600 μL 0.2 M glycine HCl (pH 2.2) incubated on L3.6pl cells for 10 min at RT shaking slightly. The eluate was neutralized with 1500 μL 1 M Tris-HCl (pH 7.4), transferred to a fresh tube. L3.6pl cells were dissolved in 600 μL 0.1 M TEA (pH 12) by incubation for 10 min at RT and subsequently neutralized with 1500 μL 1 M Tris-HCl (pH 7.4). Output titers of phage eluate and lysate were determined (3.4.4) and two falcons with 14 mL *E.coli* TG1F+ suspension at an OD_{600} of 0.5 were infected with the phage eluate and lysate, respectively. Infected cultures were centrifuged (4,000 x g, 4 $^{\circ}\text{C}$, 10 min) and the pellet was resuspended in 600 μL 2 x $\text{TY}_{\text{gluc,amp}}$ medium. The bacterial suspension was plated on four LB_{amp} agar plates and incubated at 37 $^{\circ}\text{C}$ for 12 – 16 h. Afterwards ampicillin-resistant colonies were scraped from the plate with 1.5 mL 2 x TY cryo medium and 1 mL/tube bacterial suspension were placed at -80 $^{\circ}\text{C}$ for long term storage.

Figure 3-1 visualizes the selection strategy for the isolation of specific scFv fragments on adherent L3.6pl cells.

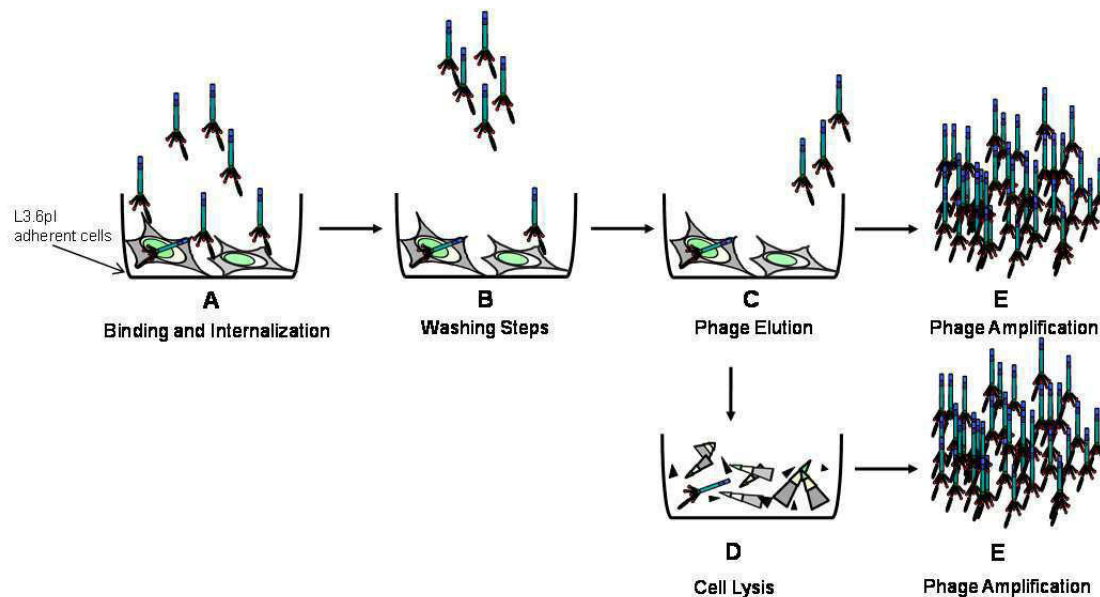


Figure 3-1 Schematic for phage display selection on adherent whole L3.6pl cells.

(A) Complete phage pool is incubated on the adherent L3.6pl cells for binding and internalization at 37 $^{\circ}\text{C}$, (B) unbound phage particles are washed away in several washing step of differing stringency, (C) surface-bound phage particles are eluted from the cells via a pH shift and I the eluted phage particles are amplified again so that they can be used for the next selection round starting again with (A) or for further characterization. (D) Phage particles that have been internalized during incubation at 37 $^{\circ}\text{C}$ are recovered via cell lysis. I Phage particles from lysis fraction are amplified again.

3.4.5.2 Suspension panning on L3.6pl cells under internalizing conditions

1 x 10^6 L3.6pl cells and same amount of PBMC cells were harvested, washed twice with 5 mL PBS and transferred to a 15 mL falcon tube. PBMCs were freshly isolated before each selection round (3.2.4). The same cell concentration was used for all three selection

rounds, all centrifugation steps were carried out at 200 x g at 4 °C for 2 min. To ensure that the cells were able to survive shear stress implied by repeated centrifugation, the third selection round was simulated previous to this panning strategy (Table 3-4).

Table 3-4 Washing steps with increasing stringency used for selection rounds one, two and three during suspension panning with whole L3.6pl cells

	Selection round 1	Selection round 2	Selection round 3
Washing steps	3 x PBST quick 2 x PBST 5 min on shaker 3 x PBS quick 2 x PBS 5 min on shaker	1 x PBST quick 4 x PBST 5 min on shaker 1 x PBS quick 4 x PBS 5 min on shaker	1 x PBST quick 4 x PBST 5 min on shaker 1 x PBS quick 4 x PBS 5 min on shaker

The same protocol as described in 3.4.5.1 was used for panning, internalization, lysis and re-infection of scFv-phage fragments with the only difference that the phage-scFv particles were not eluted from the cells but lysis was performed right away. Figure 3-2 shows a schematic of the applied suspension panning strategy.

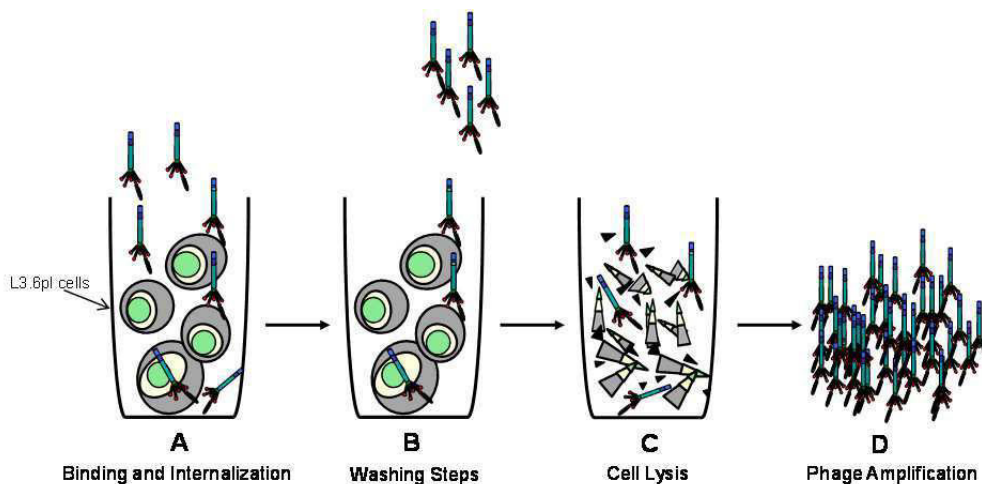


Figure 3-2 Schematic for phage display selection on L3.6pl cells in suspension.

(A) Complete phage pool is incubated on L3.6pl cells in suspension for binding and internalization at 37 °C, (B) unbound phage particles are washed away in several washing step of differing stringency, (C) surface-bound and internalized phage particles are recovered at the same time via total cell lysis without previous elution and (D) the recovered phage particles are amplified again so that they can be used for the next selection round starting again with (A) or for further characterization.

3.4.5.3 Panning on membrane fractions

100 μ L/well PBMC and L3.6pl membrane fractions were coated on a 96-well MaxiSorb MTP at 4 °C for 12 – 16 h to immobilize the depletion and selection antigens. Antigen concentration was decreased during the panning process as well as the number of coated wells (

Table 3-5). L3.6pl membrane fractions were diluted in ELISA coating buffer (pH 9.6), PBMC membrane fractions in PBS (pH 7.4).

Table 3-5 Dilution of membrane fraction antigen used for selection rounds one, two and three.

	Selection round 1	Selection round 2	Selection round 3
Antigen dilution	Undiluted	1 : 10	1 : 100
Number of coated wells	4	3	2

Precipitated phage solutions were resuspended in 600 μ L for the first, 400 μ L for the second and 200 μ L PBS for the third selection round. The precipitated phage pools were blocked with 5% MPBST (ratio 1 : 1). 200 μ L/well 5% MPBST-phage mixture was transferred to empty wells (number of wells according to selection round) on the MTP and incubated at RT for 2 h on a shaker to block the unspecific binding sites as well as to sort out plastic-binding scFv-phage units. Simultaneously, wells coated with PBMC and L3.6pl antigen were washed with 3 x 200 μ L PBS and were blocked with 200 μ L 5% MPBST for 2 h at RT.

Cross-reactivity to healthy human cells was eliminated by negative selection on PBMC membranes. Therefore, blocked phage solutions were transferred to the PBMC-coated wells and incubated for 1 h at RT on a shaker before positive selection on L3.6pl antigen. The depleted phage solution was transferred onto the L3.6pl membranes and incubated on a shaker for 1 h at RT. Afterwards the supernatant containing unbound scFv-phage particles was discarded and the antigen was washed with PBS and PBST at RT according to the washing steps listed in Table 3-6.

Table 3-6 Washing steps with increasing stringency applied during selections rounds one to three for all modes of selection.

	Selection round 1	Selection round 2	Selection round 3
Washing steps	3 x PBST quick	1 x PBST quick	10 x PBST quick
	2 x PBST 5 min on shaker	4 x PBST 5 min on shaker	5 x PBST 5 min on shaker
	3 x PBST quick	1 x PBST quick	10 x PBST quick
	2 x PBST 5 min on shaker	4 x PBST 5 min on shaker	5 x PBST 5 min on shaker

Surface-bound scFv fragment antibodies were eluted via a pH shift. 200 μL /well 0.2 M glycine-HCl (pH 2.2) were added to each antigen-coated well, incubated for 10 min at RT on a shaker and neutralized with 500 μL /well 1 M Tris-HCl (pH 7.4). The titer of each eluate was determined by drawing a 2 μL aliquot (3.4.4) and the phage were transferred to 14 mL TG1F+ suspension grown to an OD_{600} of 0.5. In parallel, 200 μL /well of the same TG1F+ culture were transferred into each phage-containing well on the MTP and both were incubated for 1 h at 37 °C without shaking to allow infection. Infected cultures were pooled and panning was finished as described in 3.4.5.1. Panning strategy on membrane fractions is illustrated in Figure 3-3.

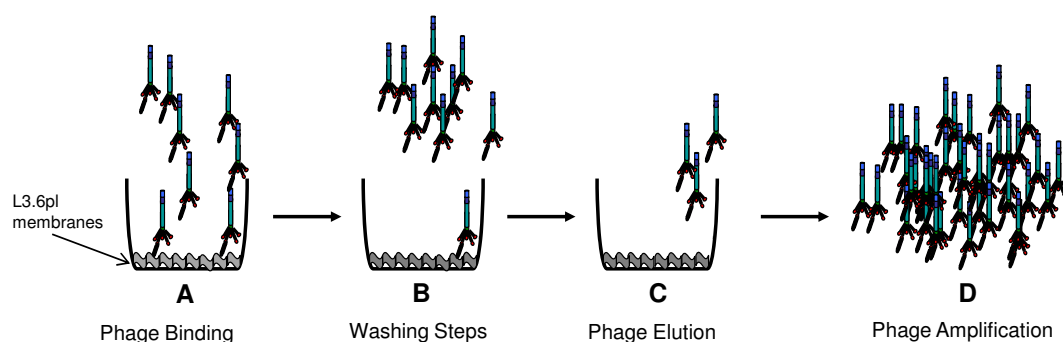


Figure 3-3 Schematic for phage display selection on L3.6pl membrane fractions.

(A) Complete phage pool is incubated on the membrane fractions for binding, (B) unbound phage particles are washed away in several washing step of differing stringency, (C) bound phage particles are eluted from the membrane fractions via a pH-shift and (D) the eluted phage particles are amplified again so that they can be used for the next selection round starting again with (A) or for further characterization.

3.4.6 Site-directed mutagenesis

The Tomlinson Library J has been artificially diversified by introduction of NNK triplets. As a consequence, about 3% of the scFv clones statistically contain a TAG triplet coding for the *amber* stop codon (1.3.3) within CDR2. *E.coli* suppressor strains, such as TG1F+, translate the TAG stop codon to the amino acid glutamine. To obtain fully functional scFv clones for soluble protein expression in non-suppressor strains or eukaryotes, the *amber* stop codon was mutated using the “QuikChange Site-Directed Mutagenesis Kit” (2.6). A point mutation exchanged the *amber* stop codon TAG to the triplet CAG directly coding for the neutral amino acid glutamine. The kit is based on a PCR reaction performed with the proof-reading *PfuTurbo* DNA polymerase from *Pyrococcus furiosus* and a temperature cycler. *PfuTurbo* DNA polymerase replicates both plasmid strands without misplacing the mutant oligonucleotide primers. Instead of the usual ssDNA template, the basic procedure makes use of the supercoiled dsDNA vector containing the insert of interest and two synthetic oligonucleotide primers containing the desired mutation. Primers were especially

designed for the mutation of each CDR2. The oligonucleotide primers, each complementary to opposite strands of the vector, were extended during temperature cycling and create a new and mutated circular dsDNA plasmid. The PCR product was digested with *DpnI*, which is an endonuclease specific for methylated and hemimethylated DNA. Thus the parental bacteria DNA template was removed without damaging synthesized and mutated DNA not displaying methyl groups.

3.4.6.1 QuikChange Mutation primers

Due to the high degree of variation within each CDR2 sequence, a different primer pair was designed for each mutation process using the QuikChange Primer Design software from Agilent Technologies Genomics. Primers were between 25 and 45 bases long with a melting temperature $T_m \geq 78$ °C and an optimal GC-content of at least 40%. T_m was calculated according to the following formula $T_m = 81.5 + 0.41(\%GC) - 675/N - \%mismatch$ (N =length of primer). Primers had to anneal at exactly the same sequence on opposite strands of the plasmid with the desired mutation in the middle of the primers and ~10 – 15 bases of correct sequence on both sides. Primers (10.1) were ordered from Invitrogen and delivered as lyophilized powder.

3.4.6.2 QuikChange Mutation protocol

Lyophilized primers were restored with sterile ddH₂O to a final concentration of 10 pmol and mixed for the PCR mutagenesis reaction with double-stranded phagemid DNA, reaction buffer, dNTPs and the *Pfu*Turbo DNA polymerase on ice. Table 3-7 shows the mutagenesis mix and thermo cycler set-up.

Table 3-7 Reaction conditions of site-directed mutagenesis of *amber* stop codons using the QuikChange Site-Directed Mutagenesis Kit.

(A) PCR reaction mixture, (B) thermo cycler program.

(A)		(B)		
Reagent	Volume [μ L]	Temperature [$^{\circ}$ C]	Time [min]	Cycles
Phagemid DNA (~20 ng/ μ L)	0.5	95	00:30	1
10 x <i>Pfu</i> reaction buffer	5	95	00:30	
dNTP mix (25 mM)	1	55	01:00	
Forward primer (10 pmol)	1	68-72	06:00	12
Reverse primer (10 pmol)	1	72	10:00	
<i>Pfu</i> DNA polymerase	1	4	∞	
ddH ₂ O	ad 50 μ L total volume			

The PCR product was placed on ice for 10 min, then 1 μ l *DpnI* restriction enzyme was added to each amplification reaction and immediately incubated at 37 °C for 1 h to digest non-mutated parental DNA. Mutated plasmids were transformed into XL1Blue *E.coli* (3.1.11) and plated on LB_{amp} agar. Single colonies were picked and tested for presence and correct size of the scFv-insert via colony PCR (3.1.1.2) using primers LMB3 and fdseq1 and subsequent agarose gel electrophoresis (3.1.5). Correct scFv-inserts were gel-purified with the QIAquick Gel Extraction Kit (2.6), sequenced with same primers (2.9, 3.1.4) and evaluated via alignment with non-mutated sequences (Vector NTI software). Successfully mutated scFv-clones were stored as cryo stocks at -80 °C (3.1.10).

3.5 Methods of bioengineering

The bioengineering part of this thesis was performed in cooperation with Esther Gartz at the Institute for Biochemical Engineering (AVT) at RWTH Aachen University lead by Prof. Dr. – Ing. Jochen Büchs. The modified BioLector [223, 224, 245] device, used for this thesis, has originally been developed at the AVT and is now commercially distributed by m2pLabs GmbH (Baesweiler). All continuous on-line measurements with the BioLector-like device were exclusively performed at the AVT by Esther Gartz. It was used to monitor product formation of a target protein fused to the short auto-fluorescent W-tag designed in this thesis [246].

3.5.1 Micro-scale on-line measurement

Continuous non-invasive micro-scale on-line measurement was performed on micro-scale cultures expressing the W-tagged Ki-4(scFv) and M12(scFv) fusion proteins (3.1.9.3). Biomass and product formation of induced and non-induced cultures were measured with the modified BioLector device containing an added fiber optical measurement moiety [223, 224]. The adapted device included a modified orbital shaker (Kühner, Basel, Switzerland), an x-y linear motion unit (BMG, Lab Technologies, Offenburg), a fluorescence spectrophotometer with filter wheels (Fluostar, BMG, Lab Technologies, Offenburg) and a computer. All filters had an optical band width of 10 nm. Biomass formed during fermentation was quantified using 180° back-scattered light at 620 nm. Increase in product formation during the fermentation process was observed via fluorescence intensity of the accumulated tryptophan residues within the designed W-tags which were fused to the Ki-4(scFv) or M12(scFv) target proteins. The auto-fluorescent W-tags were excited at 280 nm and detected at an emission wavelength of 350 nm. Both measurement variables were

obtained while the cultures were shaken continuously and without disturbing the fermentation system.

3.5.2 2D-scan analysis

After large scale protein production (3.1.9.3), the fluorescence intensity of 200 μL bacterial crude extract was analyzed in 96-well MTPs (lumox, black, μ -clear, Greiner Bio-One) using two dimensional (2D) fluorescence scanning. Bacterial cultures were centrifuged (4,500 \times g, 4 $^{\circ}\text{C}$, 30 min) and proteins were released with combined application of TES buffer lysis (3.3.5.2) and sonication (3.3.5.4). Buffer of the lysates was exchanged to PBS (3.3.6) to remove EDTA and colored bacterial contaminations to reduce disturbing factors during 2D-scan analysis. Then samples were concentrated (3.3.7) and fluorescence intensity of 3 $\mu\text{g}/\text{mL}$ W-tagged proteins was measured at excitation wavelengths of 250 – 300 nm and emission wavelengths of 300 – 400 nm using a modified FluoreMax-4P (Horiba Jobin Yvon, USA) with a Y-shaped optical fiber and an inlet for the MTP to measure from below. Integration time was set to 100 ms and the gap width was 2 nm for excitation as well as for emission.

3.6 Analytical and statistical software

All on-line fermentation and 2D-scan data was analyzed and statistically evaluated by Esther Gartz using Microsoft Office Excel 2010. Final data was obtained from the wells and the statistical mean was calculated of a 4-fold verified set of measurements. The relative percentage deviation was also calculated from this set of data. All results were proven to be reproducible in different experiments. Curve diagrams from this data were created with Origin. Calculation of the fitted power function in 5.3.1 was performed with MATLAB. ELISA data was statistically evaluated using Microsoft Office Excel 2010 or GraphPad Prism 5.0. Flow cytometric evaluation of mean fluorescence intensities and the geometrical mean was performed with the CellQuest Pro software (BD Biosciences, NJ).

3.7 Documentation and image editing

SDS-PAGE and Western blots were digitalized with a commercially available standard scanner. Photographs, scans and other pictures were edited and adapted in Adobe Photoshop CS4, with Microsoft Power Point 2010 or ImageJ. Both programs were used to optimize colors, black, white and grey shades or variations and intensities. Moreover, they were applied to sharpen contrast or adjust light intensities as well as to ensure sufficient

image resolution and the appropriate format of the filed pictures. Results were neither changed nor manipulated.

4 Results: Antibodies against pancreatic cancer

Treatment of cancer with antibody-based immunotherapy holds high potential as alternative adjuvant therapeutic approach. Since currently no recombinant antibodies are approved for treatment of pancreatic cancer [77] or adequate early diagnosis, the aim of this thesis was to isolate novel and sequence-unique scFv antibody fragments from the Tomlinson phage libraries I and J using phage display technology. The highly metastasizing pancreatic cancer cell line L3.6pl was exploited as target antigen to generate highly specific scFv binders against unknown tumor-associated antigens expressed on pancreatic cancer cells. The following chapter provides isolation results of three different panning strategies applied for scFv antibody selection and the screening of sequence-unique L3.6pl-specific scFv antibody fragments. Moreover, it states the *in vitro* characterization of isolated scFv antibodies, cross-reactivity data to other pancreatic cancer cell lines, native protein structure binding data on living cells and internalization properties.

4.1 Experiments prior to phage display selection

4.1.1 Quality assessment of Tomlinson Libraries I and J

Selection of highly specific scFv antibodies was performed using the naïve and semi-synthetic human Tomlinson phage libraries I and J (1.3.3) obtained from the Medical Research Council (MRC) Center for Protein Engineering (Cambridge, UK).

To assess infection rate and quality of phagemid-carrying bacteria, both libraries were infected separately with monovalent M13KO7 helperphage to produce scFv-presenting phage particles under antibiotic pressure with ampicillin and kanamycin (3.4.2). Titer determination (3.4.4) of precipitated phage molecules (3.4.3) showed a scFv-phage particle concentration of at least 4.9×10^{11} pfu/mL for the library I and 5×10^{12} pfu/mL for the library J. The minimum phage concentration necessary for successful selection is 1×10^{11} pfu/mL. Successful analysis of phagemid-carrying and infected bacteria allowed subsequent high-quality production of scFv-phage units for phage display selection with different panning strategies (0, 3.4.5.1, 3.4.5.2). As continuous quality controls, input and output titrations were performed throughout all panning processes to ensure sufficient infection rates and scFv-phage concentrations.

4.1.2 Testing of blocking and washing conditions

To observe potentially adverse effects of cell lysis and shear stress on living L3.6pl cells during suspension panning, the third selection round with the most stringent washing protocol (3.4.5.2) was simulated with five blocking/washing reagents (Table 4-1) prior to panning.

Table 4-1 Five different blocking/washing reagents tested for their adverse effects on L3.6pl cells

	Reagent	pH	Manufacturer
(a)	1 x PBS	7.4	lab stock (2.7)
(b)	1 x DPBS	7.4	Invitrogen/Gibco, Life Technologies GmbH, Darmstadt
(c)	1 x PBST	7.2	lab stock (2.7)
(d)	RPMI 1640 Glutamax	7 – 7.4	Invitrogen/Gibco, Life Technologies GmbH, Darmstadt
(e)	0.9% (w/v) NaCl isotonic solution	7 – 7.5	VWR, Darmstadt

The reagent with the least negative effect on L3.6pl cells was subsequently chosen for selection. Pellet size was documented after each step by marking the pellet border on the falcon tube resulting in Table 4-2.

Table 4-2 Documentation of negative effects for five different washing reagents tested on the cell line L3.6pl using panning conditions of third selection round.

Washing step	(a)	(b)	(c)	(d)	(e)
1	complete	complete	complete	complete	complete
2	complete	complete	complete	complete	complete
3	complete	complete	complete	complete	complete
4	complete	complete	complete	50%	75%
5	50%	complete	complete	25%	25%
6	0%	50%	complete	0%	0%
7		50%	complete		
8		25%	complete		
9		0%	50%		
10			50%		

Reagents (a), (d) and (e) had the strongest adverse effect on L3.6pl cells resulting in a complete cell loss caused by lysis after 6 washing steps, followed by reagent (b) with total cell loss after 9 washing cycles. The best cell yield was reached with 1 x PBST (reagent (c)) with 50% remaining cells after completed third panning round. PBST was consequently applied for all selection rounds with L3.6pl cells in suspension.

4.2 Isolation of L3.6pl-specific scFv-phage particles

This work employed the scFv-based Tomlinson libraries I and J to generate specific L3.6pl-binding scFv-phage units with the phage display technology. Successful isolation of specific binders depends on the scFv-phage library, the antigen source and the selection strategy. The next chapter describes the scFv-phage enrichment and selection results of three different panning strategies:

- (1) on adherent L3.6pl whole cells (3.4.5.1),
- (2) on L3.6pl cells in suspension (3.4.5.2),
- (3) on L3.6pl membrane fractions (3.4.5.3).

A general panning schematic applied to all three panning strategies is diagrammed in Figure 1-3. L3.6pl-binding scFv-phage molecules were isolated during three consecutive panning rounds. Unspecific particles binding to ubiquitous surface proteins or the MTP surface were eliminated via negative selection on FG or PBMC antigen. Enrichment of scFv-phage binders after each panning cycle was assessed by input and output titration (3.4.4) as well as via polyclonal phage ELISA analysis (3.3.9.1).

4.2.1 Enrichment of scFv-phage particles on adherent cells

Solid-phase panning on adherent L3.6pl cells (3.4.5.1) was performed exclusively with Tomlinson library J. All subtractive selection steps were carried out on FG cells and the hyperphage M13KO7 Δ pIII was applied for the first selection round. After phage rescue, eluted scFv-phage proteins were used for subsequent selection by elution only, whereas each lysis fraction was used for subsequent selection by elution and lysis. Elution fractions after the same selection rounds were combined before output titration. Sensitivity of L3.6pl cells towards the alkaline elution buffer and shear stress led to cell loss during washing and elution. Hence, to obtain complete titration result documented in Table 4-3, selection round two was repeated three times, and selection round three was repeated once for satisfying elution and lysis outcomes. The final lysis fraction showed a very low output titer but the infected culture on the harvest plate had enough colonies to stop the selection process. Based on input and output titrations, the enrichment factor (EF) ($EF = \text{output [pfu/mL]} / \text{input [pfu/mL]}$) was calculated for specifically binding scFv-phage units after elution and lysis for each selection round. Accordingly, the actual enrichment (AE) was calculated by dividing enrichment factors of two successive selection rounds ($AE = EF_x / EF_{x-1}$) as displayed in Table 4-3. For the elution fractions, practically no enrichment ($AE = 0.005$)

was documented from the first to the second panning round but an 11-fold enrichment of L3.6pl-binding scFv-phage particles was found after the third selection round. No significant enrichment of scFv-phage particles was documented for the lysis fractions, neither after the second ($AE_2 = 0.0004$), nor the third panning round ($AE_3 = 0.004$).

Table 4-3 Input and output titer of elution and lysis fractions during three consecutive panning rounds on adherent L3.6pl cells.

The input titer was over 1×10^{11} pfu/mL and output titers ranged from 6×10^8 pfu/mL after selection round one to 1.2×10^2 pfu/mL after the third round. In addition, calculations of enrichment factors (EF) and resulting actual enrichments (AE) after each selection round are stated. (A) Enrichment documentation of elution fractions, (B) enrichment documentation of lysis fractions.

(A)	Selection round	Elution		EF	AE
		Input [pfu/mL]	Output [pfu/mL]		
	1	5×10^{12}	4.2×10^7	8.4×10^{-6}	-
	2	8×10^{11}	3.3×10^4	4.1×10^{-8}	0.005
	3	5.2×10^{11}	2.4×10^5	4.6×10^{-7}	11

(B)	Selection round	Lysis		EF	AE
		Input [pfu/mL]	Output [pfu/mL]		
	1	5×10^{12}	6×10^8	1.2×10^{-4}	-
	2	1×10^{12}	4.8×10^4	4.8×10^{-8}	0.0004
	3	5.7×10^{11}	1.2×10^2	2.1×10^{-10}	0.004

In addition, enrichment of L3.6pl-binding scFv-phage particles was examined by means of polyclonal phage ELISA analysis (3.3.9.1) of scFv-phage pools from the original library J as well as from scFv-phage pools after each selection round. This allowed a comparison of the number of specific scFv-phage binders via their binding activity. For this panning strategy FG membrane fractions (subtractive antigen) were coated together with L3.6pl membrane fractions (selective antigen) diluted 1 : 100. The scFv-phage pools of eluate and lysis fractions after each selection round were precipitated separately, but mixed together for titer determination and subsequent polyclonal phage ELISA analysis. Figure 4-1 depicts a strong absorption signal for the unselected library J on L3.6pl and FG membranes alike, indicating a large number of potential binders. In contrast to that, a significantly higher binding signal, i. e. 150% increased absorption signal ($p = 0.0016$) was observed for L3.6pl-binding scFv-phage units after the first selection round. Compared to this, binding activity decreased by 59% after the second ($p = 0.0464$) and 150% after the third selection round. Absorption after the final selection round was not significantly different from the value documented for naïve library J. ABTS signals on L3.6pl membrane fractions were

not significantly higher than FG absorption values even though phage pools had been depleted on FG cells before each positive selection.

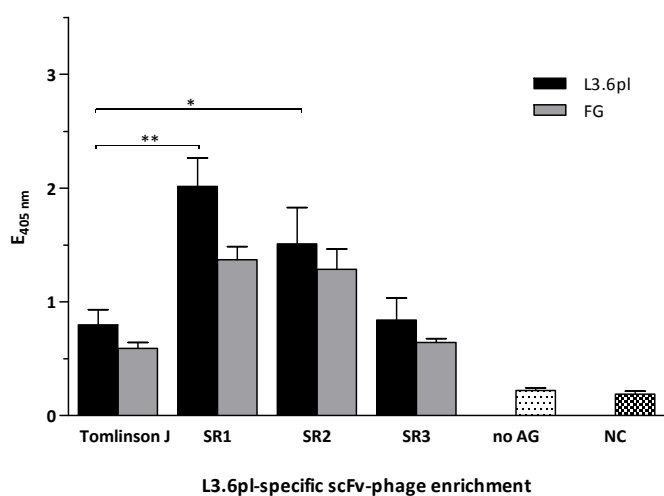


Figure 4-1 Polyclonal phage ELISA after three panning rounds on adherent L3.6pl cells.

Combined phage pools of elution and lysis fractions after each selection round were analyzed for binding activity on membrane fractions of the L3.6pl selection antigen (black) and the FG depletion antigen (grey). Binding activity is displayed via average of ABTS absorption values of three independently performed experiments including error bars for standard deviation. Significant increase/decrease of absorption values between the unselected library J and the selection rounds is indicated by asterisks (**: medium significant difference, *: low significant difference). NC: average absorption value of negative controls, no AG: average absorption value of controls without antigen coating, SR1 – SR3: selection rounds one to three.

Considering the significant increase in binding activity after the first selection round, scFv-phage molecules resulting from the first and third selection round were screened by monoclonal phage ELISA analysis (3.3.9.2, 4.2.4.1).

4.2.2 Enrichment of scFv-phage by suspension panning

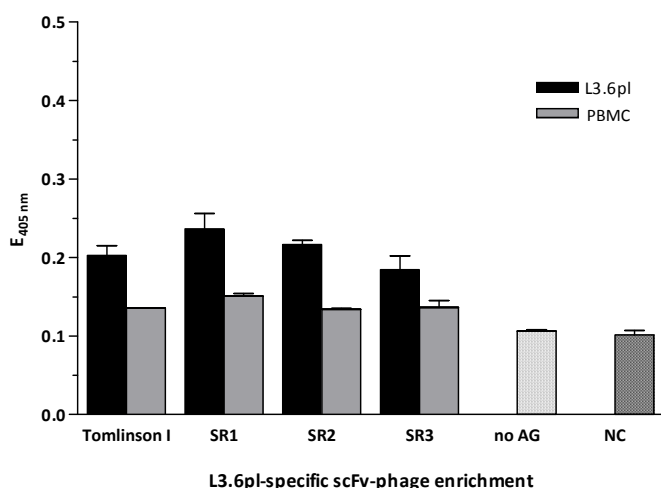
For suspension panning of L3.6pl cells the Tomlinson library I was used (3.4.5.2). All subtractive selection steps were executed on freshly isolated PBMC cells (3.2.4) and the polyvalent M13KO7ΔpIII hyperphage was used for the first selection round. After internalization at 37 °C no elution was performed but surface-bound and incorporated scFv-phage particles were simultaneously recovered by cell lysis. Table 4-4 presents input and output titrations, performed for all panning rounds, thus evaluating enrichment of L3.6pl-binding scFv-phage units. Based on input and output titrations, the enrichment factors (EF) and the actual enrichment (AE) were calculated according to chapter 4.2.1 (Table 4-4). Enrichment factors resulted in an actual enrichment of L3.6pl-binding scFv-phage units of 250-fold after selection round two and an additional 1.5-fold increase after selection round three.

Table 4-4 Input and output titrations of selections on Tomlinson library I on L3.6pl cells in suspension as well as enrichment factors (EF) and actual enrichment (AE) after each selection round.

All input titers showed sufficient scFv-phage concentrations, output titers ranged from 10^5 after the first and second selection round to 10^6 after the third. Enrichment of L3.6pl-binding scFv-phage units was shown. Based on titrations, enrichment factors and actual enrichments were calculated for each panning round.

Selection round	Input [pfu/mL]	Output [pfu/mL]	EF	AE
1	3.1×10^{12}	1.2×10^5	3.9×10^{-8}	-
2	1×10^{11}	9.6×10^5	9.6×10^{-6}	250
3	2.6×10^{11}	3.6×10^6	1.4×10^{-5}	1.5

Even though titrations and resulting actual enrichment indicated an increase of L3.6pl-specific scFv-phage particles, no significant increase in binding activity was documented during polyclonal phage ELISA analysis (3.3.9.1) of consecutive selection rounds (Figure 4-2). For this experiment PBMC membrane fractions (depletion cells) were coated as antigen together with L3.6pl membranes. Despite a slight increase in binding activity of 15% after the first selection round, absorptions values decreased during continued panning rounds. The unselected library I displayed 10% higher ABTS absorption signals on L3.6pl membranes than the phage pool after the third selection round. This indicates a loss of L3.6pl-binding scFv-phage particles. Statistical evaluation showed neither significant increase nor decrease of L3.6pl-specific scFv-phage units throughout all three selection rounds. Compared to absorption values on L3.6pl membrane fractions, signals on PBMC membranes were found to be significantly lower ($p = 0.0424$).

**Figure 4-2 Polyclonal phage ELISA after three selection rounds on L3.6pl cells in suspension.**

Overall ABTS absorption signals were very weak (< 0.25). Signals on PBMC membranes (grey) were considerably weaker than on L3.6pl antigen (black). Binding activity increased after first selection round and then decreased again until the third. Binding activity is displayed as average of ABTS absorption values of three independently performed experiments including error bars for standard deviation. No significant difference was found for binding activities of selection rounds. NC: average absorption value of negative controls, no AG: average absorption value of controls without antigen coating, SR1 – SR3: selection rounds one to three, *: low significant difference.

Based on the titration results, single clones were picked after the third selection round for analysis in a monoclonal phage ELISA (3.3.9.2, 4.2.4.2).

4.2.3 Enrichment of scFv-phage particles on membrane fractions

Solid-phase panning on L3.6pl membrane fractions (3.4.5.3) was performed on both Tomlinson libraries in parallel. Depletion was carried out on PBMC membrane fractions and the polyvalent M13KO7 Δ pIII hyperphage was used for the first selection round. Surface-bound scFv-phage particles were eluted from the membrane antigen, and input and output titers were determined of all three panning rounds for both libraries (Table 4-5). Enrichment factors (EF) and actual enrichment (AE) were calculated from titrations as described in 4.2.1, and are also listed in Table 4-5. All selection rounds showed a constant output of 10^5 for L3.6pl-binding scFv-phage proteins. Actual enrichment of library I was 0.32-fold after panning round two and only 0.07-fold after round three (Table 4-5 A). For library J a 2.3-fold increase of L3.6pl-binding scFv-phage units was observed after selection round two, a 0.02-fold increase after round three (Table 4-5 B).

Table 4-5 Input and output titers as well as enrichment factors (EF) and actual enrichment (AE) of panning rounds with Tomlinson Library I and J on L3.6pl membranes fractions.

All input titers were over the necessary value of 1×10^{11} pfu/mL for a successful selection, output titers reached various values of 10^5 after all selections rounds. (A) Enrichment results of Tomlinson Library I, (B) enrichment results of Tomlinson Library J. A slight enrichment of L3.6pl-binding scFv-phage units was shown for both libraries within three consecutive panning rounds.

(A)	Selection round	Tomlinson I		EF	AE
		Input [pfu/mL]	Output [pfu/mL]		
	1	1.2×10^{11}	2.4×10^5	2×10^{-6}	-
	2	7.6×10^{11}	4.8×10^5	6.3×10^{-7}	0.32
	3	1.1×10^{13}	5.2×10^5	4.7×10^{-8}	0.07

(B)	Selection round	Tomlinson J		EF	AE
		Input [pfu/mL]	Output [pfu/mL]		
	1	2.5×10^{11}	2.8×10^5	1.1×10^{-6}	-
	2	3.8×10^{11}	9.6×10^5	2.5×10^{-6}	2.3
	3	9.3×10^{12}	4×10^5	4.3×10^{-8}	0.02

Polyclonal phage ELISA experiments (3.3.9.1) displayed results for increase of L3.6pl-binding scFv-phage units analogous to titration-based enrichment calculations. For polyclonal phage ELISA, scFv-phage pools of both libraries and of the three continuous selection rounds were tested for binding activity on PBMC (subtractive antigen) and L3.6pl membranes previously used for positive selection.

Tomlinson Library I: In Figure 4-3A, ABTS absorption signals after panning of library I are illustrated after 15 min incubation. A very high binding capacity was measured for the unselected I library on L3.6pl membranes indicating a large amount of potential binders. After the first panning round, absorption values on L3.6pl membranes decreased by 57% when cross-reactive and weak binders had been sorted out via depletion on PBMC membranes. From the first to the second selection round, absorption signals increased again by 88%; after completion of selection round three, an additional increase of 18% was documented. In summary, a low but significant enrichment of L3.6p-specific binders was denoted after panning round two ($p = 0.0287$) and three ($p = 0.0137$) in comparison to the first selection round. Absorption values measured on PBMC membranes after selection round one, were 425% higher than for the naïve library I, and slightly higher (but not significantly) than the values on L3.6pl membranes. Nevertheless, PBMC absorption values decreased after panning rounds two and three indicating the successful elimination of scFv-phage molecules with cross-reactivity towards PBMC membranes.

Tomlinson Library J: Figure 4-3B indicates ABTS absorption values after selection of library J measured after 60 min incubation. A very high binding capacity on L3.6pl membranes was documented for the naïve library J, indicating a large amount of potential binders. After the first selection round, absorption values on L3.6pl membranes decreased by 90% when cross-reactive and weak binders had been sorted out via depletion on PBMC membranes. From the first to the second selection round, absorption signals increased again by 800% but after finishing selection round three only a slight additional increase of L3.6pl-specific binders was found. In summary, a low but significant enrichment was denoted after panning round two ($p = 0.0287$) and the absorption values after round three showed medium significance ($p = 0.0137$) in comparison to the first selection round. Absorption values measured on PBMC membranes were similar throughout the panning process.

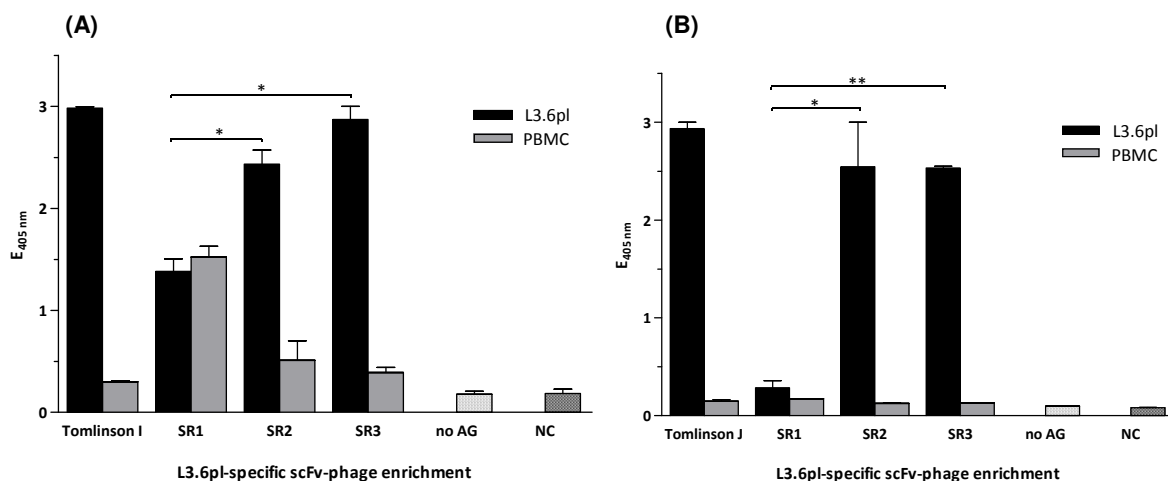


Figure 4-3 Polyclonal phage ELISA after three consecutive panning rounds with Tomlinson libraries I and J on L3.6pl membrane fractions.

(A) Absorption signals for library I measured after 15 min ABTS incubation (signals too strong for TECAN measurement after longer incubation period), (B) absorption signals for library J measured after 60 min ABTS incubation. Absorption values on L3.6pl membranes are illustrated in black, values for PBMC membranes are indicated in grey. For both libraries, binding activity decreases after the first selection round and continuously increases again afterwards. Binding activity is displayed as average of ABTS absorption values of three independently performed experiments including error bars for standard deviation. NC: average absorption value of negative controls, no AG: average absorption value of controls without antigen coating, SR1 – SR3: selection rounds one to three, *: low significant difference, **: medium significant difference.

Based on the assumption that the low increase of L3.6pl-binding scFv-phage particles represented strong binders, as shown during polyclonal phage ELISA experiments, pannings after round three were used for monoclonal phage ELISA analysis (4.2.4.3).

4.2.4 Identification of unique L3.6pl-specific scFv-phage binders

Phage pools with enriched L3.6pl-binding scFv-phage particles were screened for sequence-unique binders via measurement of binding activity in a monoclonal phage ELISA experiment (3.3.9.2). Depending on enrichment results after titration and polyclonal phage ELISA analysis (4.2.1, 4.2.2, 4.2.3), single clones were picked from $LB_{amp,gluc}$ agar plates, transferred into 96-well MTPs and analyzed on immobilized membrane fractions (diluted 1 : 100 in ELISA coating buffer or PBS). All monoclonal phage ELISA experiments were repeated three times to show reproducibility of results. A clone was defined as positive binder when its average absorption value was at least 2.5-times stronger than the negative control (NC) values and background signals measured in reference wells without antigen coating. This defined value, here called NC-reference value, was calculated for every experiment and is graphically indicated by a black vertical line. Following monoclonal phage ELISA analysis, L3.6pl-positive clones were tested for presence of the scFv-insert (length ~950 bp) via colony PCR (3.1.1.2), then the scFv-insert

PCR product was extracted from a preparative agarose gel (3.1.5) and its DNA sequence was analyzed (3.1.4).

4.2.4.1 Monoclonal phage ELISA after selection on adherent cells

Based on results in 4.2.1, scFv-phage pools after the first and third selection round were screened in a monoclonal phage ELISA (3.3.9.2). Figure 4-4A and Figure 4-4B illustrate the screening results of: (a) Two master plates (144 clones) analyzed after the first selection round and (b) two master plates (144 clones) after the third selection round.

Resulting from the first selection round, ten L3.6pl-binding clones displayed binding activity above the NC-reference value of 0.329 and were defined as positive (Figure 4-4A). Three of these clones (A6, B5, and F10) displayed ABTS absorption values twice the NC-reference value. Clone B7 exceeded it even three times.

After the third selection round, only three L3.6pl-binding clones were classified as positive via binding activity above the NC-reference value of 0.509 (Figure 4-4B). All three binders displayed an absorption reading not significantly stronger than the NC-reference value. Clone F7 presented 50% stronger binding on FG than on L3.6pl membranes.

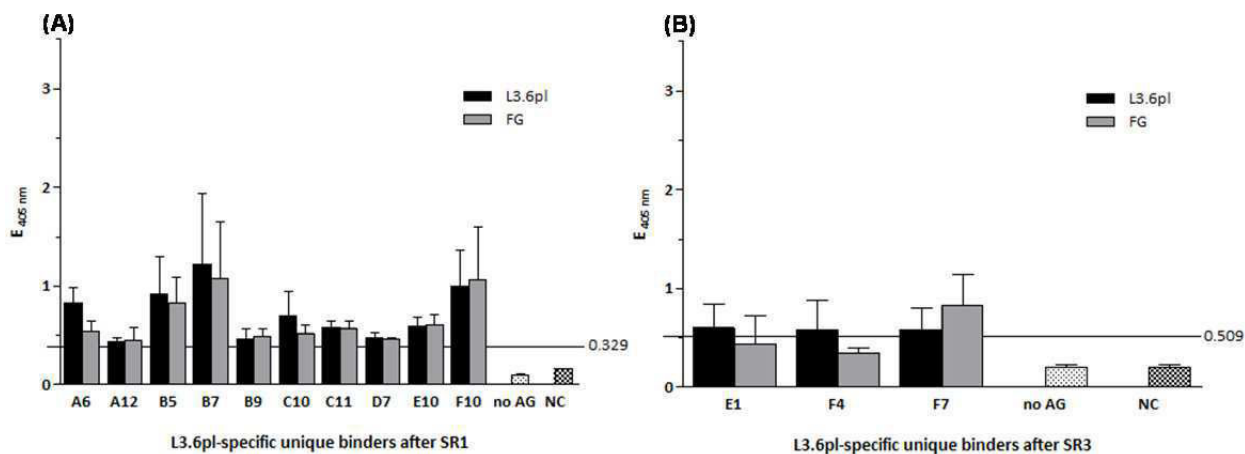


Figure 4-4 Monoclonal phage ELISA after first and third selection round on adherent L3.6pl cells. (A) Ten L3.6pl-positive binders with absorption signals > 0.329 were detected after the first selection round (SR1), (B) three L3.6pl-positive binders with absorption values > 0.509 were identified after the third selection round (SR3). Black bars represent absorption measurements on L3.6pl membranes (positive selection), grey bars show absorption signals on FG membranes (subtractive selection), and the NC-reference value is indicated by the black vertical line. Binding activity is displayed as average of ABTS absorption values of three independently performed experiments including error bars for standard deviation. NC: average absorption value of negative controls, no AG: average absorption value of control wells without antigen coating.

All L3.6pl-positive clones exhibited binding activity above the NC-reference value on FG membrane fractions as well, but except for clones B9, E10 and F10, FG binding activity was weaker than on L3.6pl membranes. High binding activity on FG membranes was expected since the L3.6pl cell line was developed from FG and thus both cell lines share high similarity of surface proteins. Colony PCR and agarose gel electrophoresis revealed that all isolated clones were false-positive binders and none of the 13 positive clones contained a scFv-insert. As a conclusion all clones were discarded.

4.2.4.2 Monoclonal phage ELISA after suspension panning

After the third selection round, 216 single clones were picked onto three master plates to isolate sequence-unique scFv-phage binders. Following the calculation of the NC-reference value of 0.194, a total of three L3.6pl-positive clones were identified. They all displayed very weak overall absorption values (not significantly different from the NC-reference value). PBMC signals were between 50% and 75% of the L3.6pl signals.

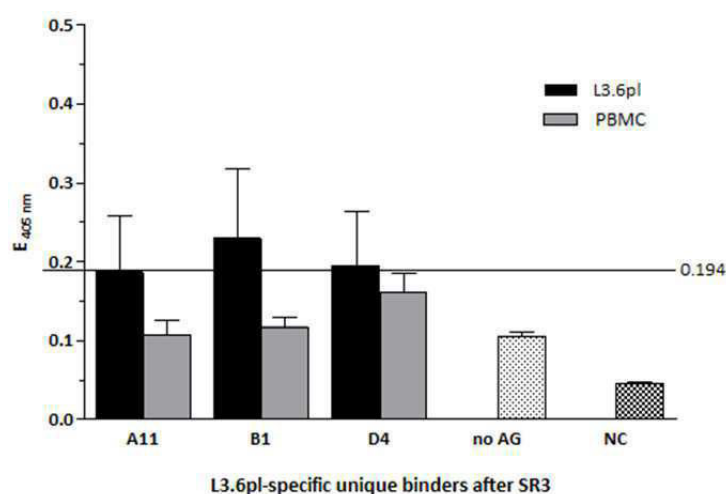


Figure 4-5 Monoclonal phage ELISA after three panning rounds on L3.6pl cells in suspension.

Three L3.6pl-positive binders with absorption values > 0.129 were identified after the third selection round (SR3). Black bars represent absorption measurements on L3.6pl membranes (positive selection), grey bars show absorption signals on PBMC membranes (subtractive selection), and the NC-reference value is indicated by the black vertical line. Binding activity is displayed as average of ABTS absorption values of three independently performed experiments including error bars for standard deviation. NC: average absorption value of negative controls, no AG: average absorption value of control wells without antigen coating.

L3.6pl-positive clones were checked by colony PCR (3.1.1.2), and after DNA analysis clone D4 was the only one identified with an intact insert sequence. Clone B1 had no insert, clone A11 carried a frame shift in CDR2 of the scFv-insert. Hence, both clones were not investigated further.

4.2.4.3 Monoclonal phage ELISA after panning on membrane fractions

Succeeding completed panning and enrichment analysis (4.2.3), eight master plates (576 clones) were picked from the selected Tomlinson library I and another eight master plates from selected Tomlinson library J. After monoclonal phage ELISA analysis, a total of 193 clones was defined as L3.6pl-positive binders. To illustrate this large number of clones, false positive binders and clones containing a frame shift were sorted out by colony PCR and DNA sequence analysis. Only positive clones containing an intact insert sequence are displayed in Figure 4-6.

Figure 4-6A shows eight truly L3.6pl-positive clones were isolated from library I with an absorption value higher than the NC-reference value of 0.210. While clones B12, C5, D8, D12 and F3 showed low absorption values that were 3-times higher than the background, a strong binding activity was measured for clones E5, E7 and F11 exceeding the background by 4-times and more. Clone C1 displayed an absorption value slightly below the NC-reference value but was analyzed exemplary as non-binding control for comparison. DNA sequencing revealed that clones B12 and D12 had the same sequence. Since stronger binding activity was measured for clone D12, it was kept for further experiments, clone B12 was discarded.

Figure 4-6B illustrates absorption values of eleven L3.6pl-positive clones isolated from library J displaying binding activity above the NC-reference value of 0.172. While clones D1, E1 and E3 had low binding activity of twice the background, clones E2, E5 and F1 displayed medium absorption values between twice and 5-times higher than the background. Binders D9 and E8 range between 5 and 10-times over the background whereas the remaining binders (A3 and D5) were measured to have a binding activity over 10-times greater the NC-reference value. DNA sequence analysis revealed that clones E1, E2, E3 and E5 had the same sequence. Based on its high absorption value, clone E3 was applied for all further experiments and clones E1, E2 and E5 were discarded.

Overall ABTS absorption signals on the PBMC membranes were low, displaying values similar to that of the negative controls and wells without coated antigen. The only exception was clones A3 which showed only 20% less binding activity on PBMC than on L3.6pl membranes.

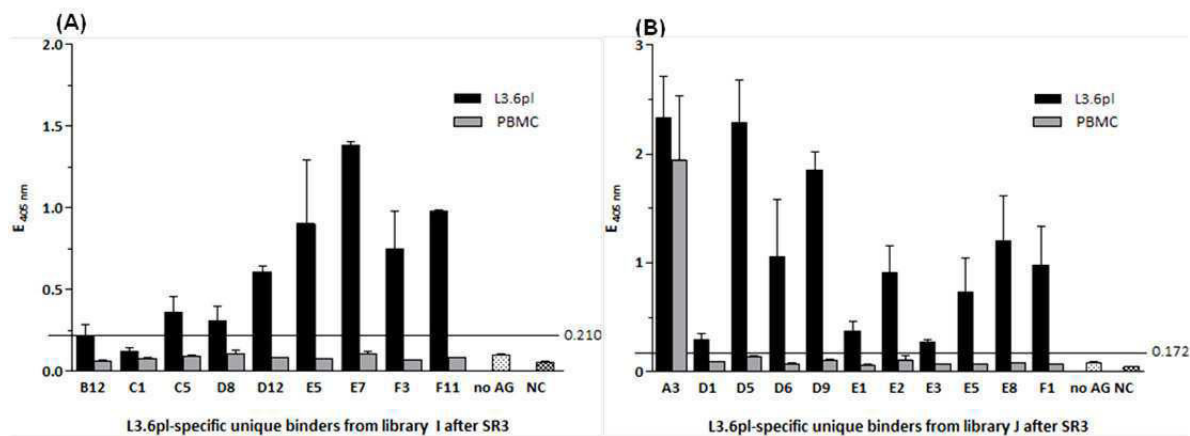


Figure 4-6 Monoclonal phage ELISA after three panning rounds with Tomlinson Library I and J on L3.6pl membrane fractions.

(A) Eight L3.6pl-positive binders isolated from Tomlinson library I, (B) eleven L3.6pl-positive binders isolated from Tomlinson library J. The black columns represent binding on L3.6pl membranes and the grey columns on PBMC membranes whereas the black line marks the NC-reference value defining a clone as positive binder. Binding activity is displayed as average of ABTS absorption values of three independently performed experiments including error bars for standard deviation. NC: average absorption value of negative controls, no AG: average absorption value of control wells without antigen coating.

4.2.5 Monoclonal phage ELISA of 14.1(scFv)

In addition to the Tomlinson-derived clones, monoclonal phage ELISA analysis was performed with the murine single chain antibody 14.1(scFv) isolated by Beate Stadler from a self-made phage display library originated from immunized mice (1.3.7). Prior to this work, the 14.1(scFv) has already been identified as L3.6pl-positive binder on membrane fractions. During this thesis, it was applied to characterization experiments to verify its binding activity on the L3.6pl antigen and to obtain additional characterization data. During the monoclonal phage ELISA, 14.1(scFv) displayed strong binding activity on L3.6pl membrane fractions with an absorption value 8.5-fold over the NC-reference value of 0.210 (Figure 4-7). Absorption readings on PBMC membranes ranged on the level of the negative controls.

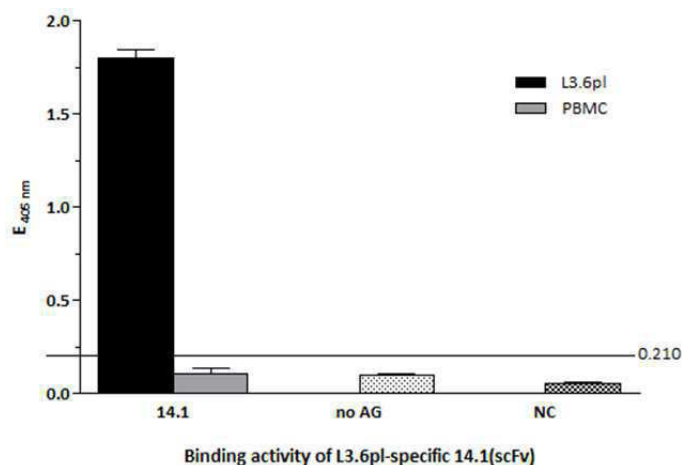


Figure 4-7 Monoclonal phage ELISA of 14.1(scFv) on L3.6pl membrane fractions isolated from the murine self-made from immunized mice after multiple selection rounds on L3.6pl antigen.

The black column represents binding on L3.6pl membranes and the grey column on PBMC membranes. The black line marks the NC-reference value identifying the 14.1(scFv) as L3.6pl-positive binder. Binding activity is displayed as average of ABTS absorption values of three independently performed experiments including error bars for standard deviation. NC: average absorption value of negative controls, no AG: average absorption value of control wells without antigen coating.

4.3 Sequence analysis of isolated L3.6pl-specific scFv

After completion of three consecutive panning rounds performed with three different selection strategies, 16 L3.6pl-specific and sequence-unique binders were isolated from Tomlinson libraries I and J, in addition to the already existing 14.1(scFv) antibody fragment from a self-made murine library (1.3.7). During monoclonal phage ELIA analysis many positive binders were identified as false-positive, projecting a positive absorption signal but were either missing the scFv-insert, had an incomplete sequence or a frame shift in FWR2.

In summary, 23 master plates, containing a total number of single 1656 clones, were picked for screening by monoclonal phage ELISA analysis (Table 4-6). 13 L3.6pl-positive binders were detected after selection on adherent cells, three after panning in suspension and 193 positive clones after membrane selection of both libraries combined. This added up to a total number of 209 L3.6pl-binding clones (12.6% of all picked clones).

Table 4-6 Overview of number of master plates and clones analyzed via monoclonal phage ELISA after three consecutive panning rounds with three different selection strategies, as well as number of resulting L3.6pl-positive binders

Panning strategy	Number of master plates	Number of picked clones	Number of L3.6pl-positive clones
Adherent	4	288	13 (4.5%) ^{a)}
Suspension	3	216	3 (1.4%) ^{a)}
Membranes	16	1152	193 (16.8%) ^{a)}
Total	23	1656	209 (12.6%) ^{a)}

a) Percentage of L3.6pl-positive clones based on number of picked clones

Only 20 clones (9.6% of all ELISA-positive clones) contained an intact insert sequence, meaning that 91.4% of the ELISA-positive clones were false-positive (Table 4-7). Panning on adherent L3.6pl resulted in 100% false-positive clones. From panning in suspension one sequence-correct clone (33.3% of ELISA-positive clones) was isolated, whereas 19 clones (9% of L3.6pl-binding clones) were identified with an intact DNA sequence after panning on membrane fractions.

Table 4-7 Overview of number and proportion of L3.6pl-positive clones identified with an intact DNA insert sequence with respect to different selection strategies.

Panning strategy	Number of sequence-intact clones	Number of false-positive clones
Adherent	0 (0%) ^{b)}	13 (100%) ^{b)}
Suspension	1 (33.3%) ^{b)}	2 (66.6%) ^{b)}
Membranes	19 (9%) ^{b)}	174 (91%) ^{b)}
Total	20 (9.6%) ^{b)}	189 (91.4%) ^{b)}

b) Percentage of sequence intact and false-positive clones based on number of 209 ELISA-positive clones

DNA sequencing revealed that two clones from Tomlinson library I and four clones from library J had identical sequences. This resulted in a total of 16 L3.6pl-positive binders with a unique sequence (Table 4-8). After subtraction of identical clones, eight sequence-unique binders were defined for both libraries.

Table 4-8 Overview of number of L3.6pl-binding clones with intact, identical and unique DNA sequence

Library	Sequence-intact clones	Sequence-identical clones	Sequence-unique clones
I	9	2	8
J	11	4	8
I and J	20	6	16

Unwanted stop codons were located in 14 clones, which corresponds to 87.5% of all sequence-unique clones (Table 4-9). *Amber* stop triplets (TAG) were found in the complementarity determining regions CDR2 or CDR3 of eight clones. An additional six clones contained the *ochre* stop codon triplet TGA in frame work region FWR2. Clones D4 (library I) and E3 (library J) did not carry any stop codon.

Table 4-9 Overview of number and percentage of sequence-unique L3.6pl-positive clones contain *amber* or *ochre* stop codons.

Library	Number of clones with stop codon	<i>Amber</i> stop codons	<i>Ochre</i> stop codons	No stop codon
I	7 (87.5%) ^{c)}	4	3	1
J	7 (87.5%) ^{c)}	4	3	1
I and J	14 (87.5%) ^{c)}	8	6	2

c) Percentage of clones containing an *amber/ochre* stop codons based on number sequence-intact clones

Amino acid sequences of all 16 L3.6pl-positive clones marked according to the distribution of *amber* or *ochre* stop codons are listed in Table 4-10.

Table 4-10 Amino acid sequences of complementarity determining regions (CDRs) in V_H and V_L of 16 scFv antibodies identified as L3.6pl-positive binders during monoclonal phage ELISA analysis.

CDRs were defined using the KABAT database [100, 101]. Clones marked with an asterisk contain an *ochre* stop codon (TGA) in FWR2, clones marked with an x contain an *amber* stop codon in CDR2 or CDR3, whereas clones D4 and E3 lack a stop codon.

	Heavy chain variable region (V _H)			light chain variable region (V _L)		
	CDR1	CDR2	CDR3	CDR1	CDR2	CDR3
A3 ^x		QINPNG*PTKYADSVKG	NKRKFDYS		RASALQS	QQAKKNPTT
C5 ^x		AICNYGSSTS*ADSVKG	TDACFDYS		AASDLQS	QQSSANPTT
D1*		SISNYGSTTSYADSVKG	YYGDFDY		SASALQS	QQTYTAPYT
D4		NISTLGAGTDYADSVKG	NATAFDY		AASWLQS	QQCYSTPKT
D5 ^x		NIYREG*RTSYADSVKG	GAALFDY		VASHLQS	QQVAVTPVT
D6*		TIGYQGHTMYADSVKG	VPYAFDY		SASSLQS	QQSYSTPNT
D8 ^x		YISAAGSNTDYVDSVKG	ANSSFDY		TAS*LQS	QQNSAGPGT
D9 ^x		NIYREG*RTSYANSVKG	GAALFDY		VASHLQS	QQVAVTPVT
D12 ^x	SYAMS	GIS*RGSTTAYVDSVKG	NYTAFDY	RASQSISSYLN	RASRLQS	QQRPPRPRT
E3		SIIGSQGSLTIYADSVKG	HVVAFDY		SASILQS	QQFTRAPPT
E5*		DISTAGATTTYADSVKG	DGYSFDY		ASSLQS	QQTYSAPAT
E7*		NICCGGSSTTYADSVKG	STTSFDY		NASSLQS	QQADNSPTT
E8*		VIGSQSRTAYADSVKG	HVLAFDY		SASILQS	QQYRQSPPT
F1 ^x		SIYS*GNLTIYADSVKG	RPDSFDY		TASTLQS	QQLSRAPST
F3 ^x		SITAYGDTTSYADSVKG	SAT*FDY		ASALQS	QQCCDSPYT
F11*		AISTSGTSTNYADSVKG	NYTSFDY		TASALQS	QQDASSPDT

Except clone A3, none of the L3.6pl-positive clones showed any significant ABTS absorption signal on the PBMC negative control antigen during monoclonal phage ELISA. But all L3.6pl-positive clones depicted positive binding on the FG cell line.

4.3.1 Whole cell ELISA

Screening of sequence-unique L3.6pl-specific binders was performed on membrane fractions which present the still functional antigen on small membrane vesicles [134]. A major drawback of membrane fractions is the formation of vesicles to compensate surface tension. Approximately 50% right-side-out vesicles and 50% inside-out particles, exposing the inner cell membrane during selection and screening, are formed. To ensure binding activity on native surface protein conformations, the isolated binders were tested in a monoclonal phage ELISA on living L3.6pl cells (3.3.9.2). A positive binding signal was measured for some clones but absorption results could not be verified in repeated

experiments. Six repetitions of the monoclonal phage ELISA on whole cells resulted in very inconsistent binding data; different clones displayed positive binding activity with each ELISA repetition (data not shown). To obtain more reproducible binding results, 100% ice-cold EtOH, acetone and 4% PFA were tested as alternative fixation methods. Nevertheless, binding results were dissenting for 100% ice-cold EtOH and acetone, whereas on 4% PFA high and unspecific background was measured after addition of scFv-phage particles. Fixed L3.6pl cells were viewed under a microscope and a substantial cell loss was documented independent of the fixation reagent. It was concluded that L3.6pl cells were very sensitive and difficult to handle during a whole cell ELISA, and consequently the resulting data was not significant. To confirm binding activity on whole L3.6pl cells, positive scFv antibodies were tested as soluble proteins via flow cytometry (3.3.10.1, 4.6.2).

4.3.2 Cross-reactivity analysis

L3.6pl-positive clones were examined for cross-reactive binding to other human pancreatic cancer cell lines by means of monoclonal phage ELISA analysis (3.3.9.2). Binding capacity of 17 clones, tested positive in 4.2.4, was analyzed on membrane fractions of FG, Su86.86, S2-0028 and PT-46 cell lines (Figure 4-8). Cross-reactivity testing was performed in triplicates and repeated three times for each clone and antigen to confirm reproducibility of binding data. A clone was defined as positive binder when its average absorption value was at least 2.5-fold stronger than the mean negative control (NC) and background absorption signals measured in reference wells without antigen coating. This calculated value, here called NC-reference value, was adjusted for each experiment. Weak binding was defined as absorption values up to 2-fold, medium binding activity as 3 to 5-fold, and strong binders as 5 to 10-fold higher than the background.

With the exception of clones D8, 16 binders exhibited positive binding capacity on FG membranes (Figure 4-8A) with absorption signals higher than the NC-reference value of 0.313. Clones D1 and E3 showed weak binding whereas medium absorption readings were recorded for seven clones (C5, D12, F1, F11, D4, E5 and E8). Clones D6, E7, F3, 14.1, D9, A3 and D5 were defined as strong binders. Moreover, Figure 4-8A illustrates positive absorption readings on Su86.86 antigen for eleven clones. Weak absorption values were measured for 6 clones (14.1, D6, D12, E3, E5 and F3), and medium binding activity was demonstrated for clones F1, F11 and D9. Strong absorption readings (up to 6-fold over NC-reference) were recorded for clones D5 and A3.

Figure 4-8B shows binding activity of isolated clones on S2-0028 and PT-46 antigen. Weak binding activity was recorded for clones C5, D5 and D9 on S2-0028 antigen. The remaining clones displayed no binding. On PT-46 antigen, two clones did not demonstrate binding (14.1 and E7), whereas all other clones displayed weak absorption values except for clone D9 which was denoted with medium binding activity. Overall background noise was very high for measurements on S2-0028 and PT-46 antigen.

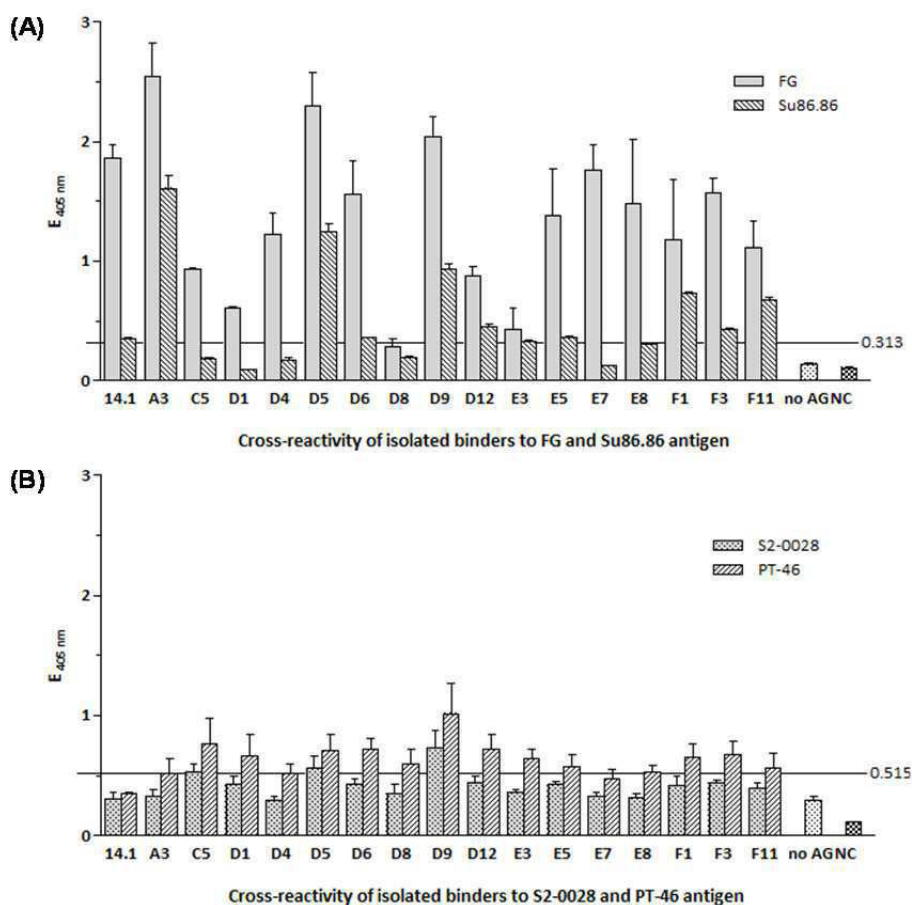


Figure 4-8 Cross-reactivity data of isolated clones and 14.1(scFv) obtained by means of monoclonal phage ELISA analysis on FG, Su86.86, S2-0028 and PT-46 membrane fractions.

(A) Cross-reactivity data towards FG and Su86.86 antigen. The light grey bars present binding data on FG membranes, the bars with left-tilted lines indicate absorption readings on Su86.86 antigen and the NC-reference value of 0.313 is marked by the black line. 16 clones were found with positive binding results on FG membranes and eleven clones displayed binding activity on Su86.86 antigen. (B) Cross-reactivity data towards S2-0028 and PT-46 membrane fractions. The grey dotted bars present binding data on S2-0028 membranes, bars with right-tilted lines indicate absorption readings on PT-46 antigen and the NC-reference value of 0.515 is marked by the black line. 15 clones demonstrated positive absorption signals on the PT-46 antigen but only 3 clones had positive ABTS measurement on S2-0028 membranes. Binding activity is displayed as average of ABTS absorption values of three independently performed experiments including error bars for standard deviation. NC: average absorption value of negative controls, no AG: average absorption value of control wells without antigen coating.

4.4 QuikChange Mutation of stop codons

In order to characterize the isolated L3.6pl binders as soluble proteins, the scFv antibody fragments were expressed without the pIII phage coat protein fusion. Normally, soluble protein expression without pIII is achieved by transformation of pIT2 phagemids into the non-suppressor strain HB2151 *E.coli*. This bacterial strain recognizes the *amber* stop codon and terminates protein translation after the scFv right before the pIII phage coat protein (4.5.1). Here, the artificial NNK triplet diversification of CDRs in the Tomlinson library J (1.3.3) is problematic for the expression of soluble protein, since 3% of the diversifications result in the formation of the *amber* stop codon TAG. Phage display with the *amber*-suppressor strain TG1F+ *E.coli* allowed mistranslation of the *amber* stop codon as glutamine (CAG). Yet, expression of soluble proteins in prokaryotic non-suppressor strains or eukaryotes would result in truncated and non-functional proteins. In this work, eight of 16 positive clones included an *amber* stop codon in their DNA sequence. Moreover, seven clones displayed an abnormal point mutation in FWR2 where the amino acid tryptophan was mutated from triplet TGG to the *ochre* stop codon TGA. Introduction of a stop codon within the scFv sequence leads to an early termination of protein translation ending in an incomplete and non-functional scFv protein. Consequently, all stop codons were eliminated by site-directed mutagenesis with the QuikChange® Site-Directed Mutagenesis Kit (2.6). The *amber* triplet TAG was mutated to CAG, which encodes the amino acid glutamine, and the *ochre* TGA triplets were changed back to the regular framework triplet TGG, coding for tryptophan. As a result, the scFv antibodies could be expressed as soluble prokaryotic protein in *E.coli* HB2151 (3.1.9.4). After subcloning, soluble protein prokaryotic expression in *E.coli* BL21 Rosetta 2 (DE3) (3.1.9.3) and eukaryotic protein expression in HEK293T was feasible as well (3.2.3).

Clone D8 was sorted out during site-directed mutagenesis since the stop codon could not be removed after 10 mutation attempts. Binding activity of mutated clones expressed in TG1F+ *E.coli* on phage level was not tested; instead soluble protein characterization was started directly after site-directed mutagenesis.

4.5 Production and purification of soluble scFv antibodies

After screening of L3.6pl-positive binders by monoclonal phage ELISA (4.2.4), DNA sequencing of unique binders (4.3) and site-directed elimination of stop codons (4.4), 15 remaining binders, in addition to the 14.1(scFv) (1.3.7), were characterized on protein

level. Therefore, scFv antibody fragments were expressed without pIII phage coat protein fusion by means of three different expression methods: (a) Prokaryotic expression in HB2151 *E.coli* using the pIT2 phagemid (4.5.1), (b) prokaryotic expression in Rosetta 2 (DE3) *E.coli* using the T7 promoter-controlled pMT plasmid (4.5.2) [171] and (c) eukaryotic expression in HEK293T cells via the CMV-operated pMS-SNAPMut plasmid (4.5.3) [183]. Expression of soluble scFv protein offers a huge advantage during scFv characterization since the phage coat protein in the original scFv-phage fusion protein may interfere with binding properties on L3.6pl cells or membranes due to protein interactions. The inexact titer determination (all phage particles in a solution are counted including the ones without scFv) is an additional problem during binding analysis on phage level. It is known that only up to 10% of the phage particles in a solution are fused to a scFv [247]. This renders exact quantitative evaluation of the binding activity on phage level impossible. Soluble scFv proteins will be characterized by protein ELISA (4.6.1), flow cytometry (4.6.2) and internalization assays (4.6.3).

4.5.1 Prokaryotic expression in HB2151 *E.coli* via pIT2 phagemid

After stop codon removal by site-directed mutagenesis, the pIT2-phagemids (2.10) were re-transformed into the non-suppressor strain HB2151 *E.coli* (2.3, 3.1.11) for soluble protein expression. Protein expression was initiated via the pHEN-derived lac-operon controlled pIT2 phagemid (Figure 1-4A) by means of IPTG or lactose induction. While still containing the genetic information for the pIII phage coat protein, the unsuppressed *amber* stop codon actively terminated protein translation, thus separating the scFv fragment from pIII. Figure 1-4B shows the expression cassette for production of soluble scFv proteins according to 3.1.9.4.

Due to the low amount of scFv protein secreted into the medium, protein recovery from the bacterial pellet via TES buffer lysis (3.3.5.2) was necessary. Protein yield was analyzed by SDS-PAGE (3.3.1) and Western blot (3.3.2). Several clones displayed protein expression, whereas others did not express any protein. Huge variations in protein concentration were observed for all single clones in consecutive experiments. Each repetition featured different clones with strong protein yield, while others depicted no protein expression despite correct DNA sequence and intact open reading frame (ORF) (data not shown). This inconsistent protein production rendered binding analysis via protein ELISA impossible since absorption results mirrored the non-reproducible protein concentrations which resulted in varying binding activities (data not shown). To obtain more consistent protein

expression, some of the cultivation and experimental parameters were changed: (a) Different IPTG concentrations 0.5, 1, 2, 5 and 10 mM in LB_{amp} medium to induce protein expression, (b) bacterial lysis with lysozyme (3.3.5.1) or sonication (3.3.5.4) for protein recovery instead of TES buffer, (c) LB_{amp} medium and 2 x TY_{amp} medium for cultivation instead of auto-induction medium, (d) use of different detection antibodies directed against His₆-tag and *myc*-tag, and (e) use of different blocking reagents (Chemiblock, 3% BSA/PBS, varying concentrations of milk powder dissolved in PBS (between 1 and 10%)). None of these parameters succeeded in improved protein production and reproducible ELISA results. Only clones A3, D5 and D9 exhibited enough protein yield for repeatedly positive binding analysis in every performed protein ELISA.

4.5.2 Prokaryotic expression in BL21 Rosetta 2 (DE3) via pMT plasmid

As a consequence of 4.5.1, soluble scFv proteins for evaluation of protein binding activity were expressed with a different strategy. Therefore, scFv inserts were subcloned into the pET-27b+-derived pMT vector (2.10) via the compatible restriction sites *Sfi*I and *Not*I (Figure 4-9) and transformed into BL21 Rosetta 2 (DE3) *E.coli* (2.3). This bacterial strain carries the lac-operon controlled gene for the T7 RNA polymerase (T7 promoter). Induction by IPTG or lactose, guarantees a stringent periplasmic expression of the recombinant scFv protein via a *pelB* leader peptide.

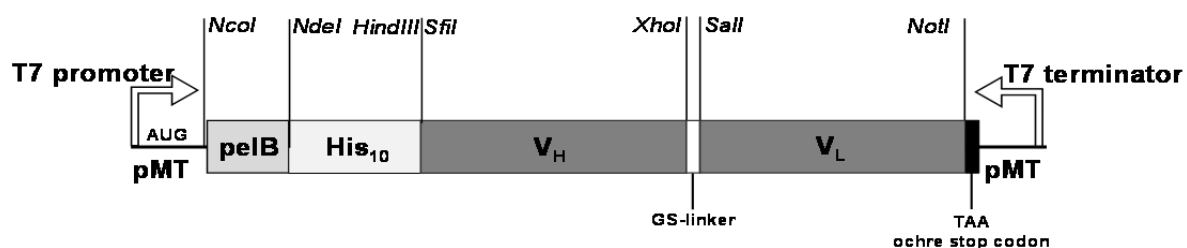


Figure 4-9 Schematic of pMT expression cassette for prokaryotic production of soluble scFv protein in BL21 Rosetta 2 (DE3).

A *pelB* signal peptide and the His₁₀-tag are located up-stream of the scFv sequence. Within the scFv, the heavy chain V_H is connected to the light chain V_L through a glycine-serine (GS) linker peptide. scFv expression is controlled by a T7 promoter inducible with IPTG or lactose. A TAA stop codon terminates the protein translation down-stream of the scFv sequence. The scFv DNA sequence was inserted into the pMT vector through enzymatic restriction sites *Sfi*I and *Not*I.

Recombinant scFv protein was expressed as described in 3.1.9.3. Despite high potential for secretion, only small concentrations of soluble scFv protein were detected in the culture medium. Again the bacterial pellet was lysed using TES buffer (3.3.5.2), then protein yield was investigated by means of SDS-PAGE (3.3.1) and Western blot (3.3.2). Protein expression results displayed similar inconsistency of protein concentrations as in 4.5.1.

Same parameters were changed as variables for the expression in HB2151 to improve expression results; nevertheless, protein yield and ELISA binding results were not reproducible. As a consequence, prokaryotic expression of soluble recombinant scFv antibody fragments was not pursued further.

4.5.3 Eukaryotic expression in HEK293T via pMS-SNAPMut plasmid

To approach eukaryotic expression of soluble scFv antibodies, L3.6pl-positive scFv inserts were transferred into the pSecTag2-based pMS-SNAPMut vector (2.10) via restriction sites *SfiI* and *NotI* (Figure 4-10). 15 L3.6pl-positive clones were successfully transfected into HEK293T cells (3.2.3.1) along with the 14.1(scFv, and 425(scFv) antibody fragments as positive control. Eukaryotic expression was conducted as described in 3.2.3.2.

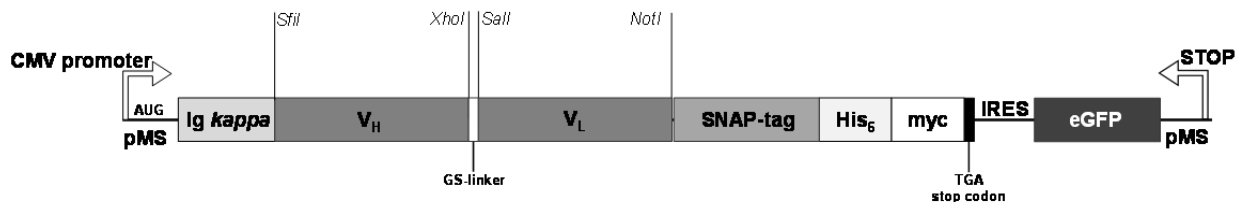


Figure 4-10 Schematic of pMS-SNAPMut expression cassette for eukaryotic expression of soluble scFv-SNAP proteins in transiently transfected HEK293T.

Protein expression is regulated with a CMV promoter. Recombinant scFv proteins, consisting of a heavy chain V_H and light chain V_L connected via a glycine-serine (GS) linker, are secreted into the culture medium via an Igkappa signal sequence up-stream of the scFv. The scFv is genetically fused to a SNAP-tag as well as a His₆-tag and a myc-tag used for detection or fluorescent labeling. Protein expression is terminated by a TGA stop codon. Down-stream of this, the internal ribosomal entry site (IRES) promotes co-translation of enhanced green fluorescent protein (eGFP) in parallel to expression of scFv-SNAP. Visible green fluorescence in transfected HEK293T cells indicates successful scFv-SNAP protein production.

In successfully transfected cells, the bicistronic pMS-SNAPMut vector promotes expression of soluble scFv-SNAP proteins in HEK293T cells simultaneously with eGFP. This fluoresces under the microscope, thus visualizing protein expression. Transfected cells were cultivated under selective pressure of Zeocin for two weeks until $80 \pm 10\%$ of all viable cells featured eGFP as well as scFv-SNAP protein expression; untransfected HEK293T control cells died completely. Produced scFv-SNAP proteins were secreted into the culture medium via an IgG kappa signal sequence and the tissue culture supernatant (TCSN) was examined by SDS-PAGE and Western blot (Figure 4-11). The coomassie-stained SDS-PAGE is not displayed here since the high FBS concentration in the cultivation medium resulted in a protein band at 66 kDa overlaying the scFv-SNAP protein band at 42 kDa. All scFv-SNAP proteins, except E3(scFv)-SNAP, were successfully expressed at the expected protein size. Protein concentrations slightly differed between

clones but all bands were clearly visible, indicating a sufficient scFv-SNAP protein concentration for subsequent experiments.

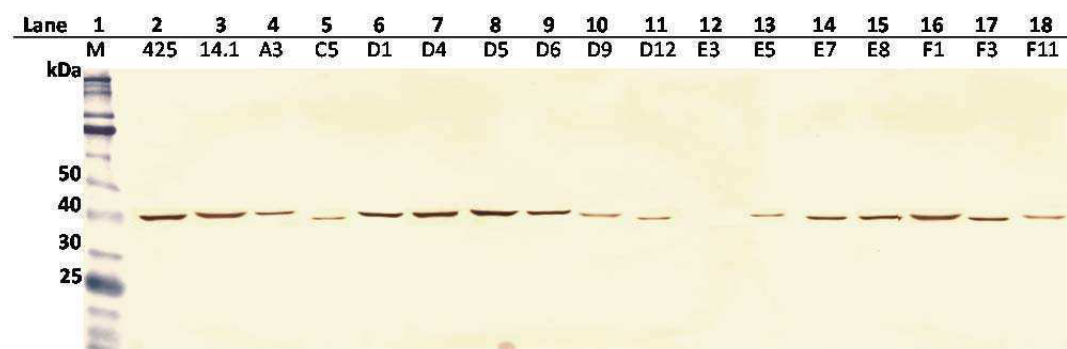


Figure 4-11 Western blot analysis of tissue culture supernatant containing transiently expressed scFv-SNAP proteins.

A protein band at ~42 kDa indicates successful expression of all scFv-SNAP proteins, here detected via a penta-anti-His primary and a GAM-PO secondary antibody followed by signal development with DAB. Lane 2: Expression of the positive control protein 425(scFv)-SNAP, lane 3: protein band of 14.1(scFv)-SNAP expression. No protein band was detected for the E3(scFv)-SNAP protein (lane 12) which despite correct DNA sequence and ORF could not be expressed in HEK293T cells.

Harvested TCSN, containing the scFv-SNAP proteins, was utilized for flow cytometric binding analysis (4.6.2), internalization assays (4.6.3) and IMAC purification combined with SNAP-labeling (4.5.4).

4.5.4 IMAC purification and SNAP-tag labeling with fluorescent dyes

Eukaryotically produced scFv-SNAP proteins were purified by means of immobilized metal-ion affinity chromatography (IMAC) via the C-terminal His₆-tag and if necessary were additionally labeled at the SNAP-tag with benzylguanine(BG)-coupled fluorescent dyes. IMAC purification and fluorescent labeling was exclusively performed with ELISA-positive clones (3.3.4). By this, one set of unlabeled scFv-SNAP antibodies and one labeled with BG-Alexa Fluor 647 (AF647) fluorescent dye was generated. Proteins 14.1(scFv)-SNAP and 425(scFv)-SNAP were purified and labeled likewise. Figure 4-12 illustrates an SDS-PAGE (Figure 4-12A) and Western blot analysis (Figure 4-12B) of successfully purified and AF647-labeled scFv-SNAP proteins. Each purification eluate analysis featured a protein band at approximately 49 kDa. Successful AF647-labeling was verified via image analysis in a VersaDoc device (Figure 4-12C). The presence of the scFv-SNAP antibody within the protein band at 42 kDa was verified via mass spectrometry after comparison to the MASCOT protein data base (data not shown, 3.3.8). Recombinant scFv-SNAP proteins were specifically detected via the His₆-tag or SNAP-tag with DAB during Western blot analysis (Figure 4-12B). Protein concentration of IMAC-purified

scFv-SNAP proteins was calculated by means of densitometric AIDA-based analysis (3.3.3.1) using several BSA protein standard dilutions (50 – 1000 $\mu\text{g}/\text{mL}$) for evaluation. Resulting protein yield of 40 mL TCSN was between 103 $\mu\text{g}/\text{mL}$ (A3(scFv)-SNAP) to 1078 mg/mL (425(scFv)-SNAP). While AF647-labeling was successfully documented (Figure 4-12C), presence of free fluorescent dye (<10 kDa) was not observed on the SDS-PAGE.

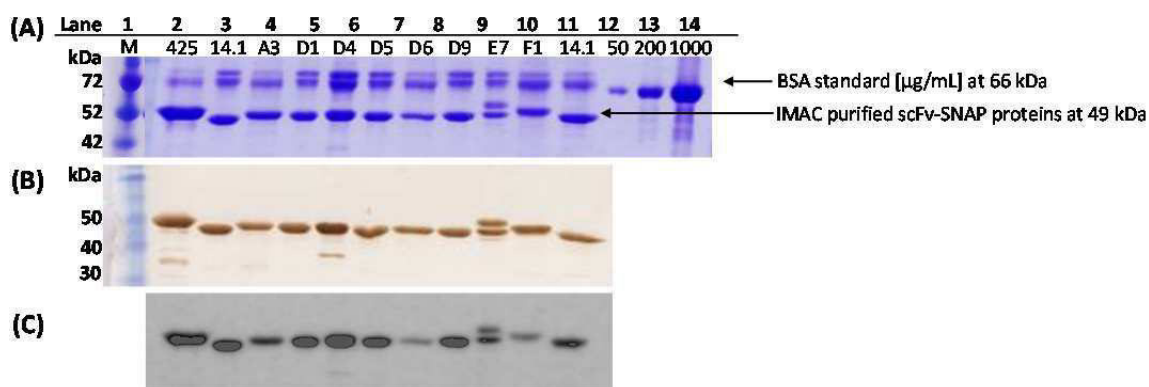


Figure 4-12 SDS-PAGE and Western blot analysis of IMAC-purified scFv-SNAP proteins with subsequent AF647 labeling.

(A) SDS-PAGE after coomassie-staining of all proteins with visible protein band for the scFv-SNAP proteins at 49 kDa and additional protein bands at 66 kDa for the BSA protein standard (lane 12: 50 $\mu\text{g}/\text{mL}$, lane 13: 200 $\mu\text{g}/\text{mL}$, lane 14: 1000 $\mu\text{g}/\text{mL}$). Additional contaminating protein bands are visible around 70 kDa. (B) Western blot with scFv-SNAP proteins at 49 kDa specifically detected via penta-anti-His primary and GAM-PO secondary antibody, developed with DAB substrate. (C) Photograph of scFv-SNAP proteins successfully labeled with AF647 fluorescent dye.

4.6 Characterization of soluble scFv antibodies

Biological functionality of soluble scFv-SNAP proteins was characterized by means of soluble protein ELISA (3.3.9.3), flow cytometry (3.3.10.1) and internalization assays (3.3.11). Binding activity of unpurified, purified, and AF647-labeled scFv-SNAP protein was tested on the pancreatic cancer cell line L3.6pl in combination with internalization behavior. Additional cross-reactive flow cytometric binding analysis was performed on other pancreatic and non-pancreatic cell lines. The EGFR-binding 425(scFv)-SNAP antibody fragment [164] served as a positive control during scFv-SNAP characterization (1.3.6).

4.6.1 Protein ELISA

Binding activity against pancreatic tumor-associated antigen was examined via soluble protein ELISA on L3.6pl, FG and PBMC membrane fractions (3.3.9.3), by applying 2 $\mu\text{g}/\text{well}$ purified but non-labeled scFv-SNAP protein. All clones featuring absorption signals of at least twice the ABTS background value (NC-reference value) of 0.129, were

defined as positive. Figure 4-13 displays positive ABTS absorption values on L3.6pl membranes for eleven scFv-SNAP proteins. Even stronger absorption values were observed on FG membranes but none on PBMC negative control membranes. Clone 14.1(scFv)-SNAP behaved likewise. A3(scFv)-SNAP showed weak but non-significant cross-reaction on PBMC membranes, although this particular absorption value on PBMC antigen was much weaker than during monoclonal phage ELISA analysis (4.2.4.3). Clones C5(scFv)-SNAP, D12(scFv)-SNAP, E3(scFv)-SNAP, E8(scFv)-SNAP and F3(scFv)-SNAP did not bind to L3.6pl membranes on protein level, and were not investigated further. Repetition of the protein ELISA, using TCSN instead of IMAC-purified protein, verified the tendency of results in Figure 4-13; but variations in absorption signals were observed due to differing protein concentrations in the TCSN (data not shown). Overall, stronger ELISA signals were measured with unpurified proteins. Clones D5(scFv)-SNAP and D9(scFv)-SNAP exhibited strong binding (absorption >10-fold of background), clones 14.1(scFv)-SNAP and A3(scFv)-SNAP displayed medium binding between 5- and 10-fold over background, whereas all other L3.6pl-positive clones only showed weak binding activity (2- to 5-fold above background).

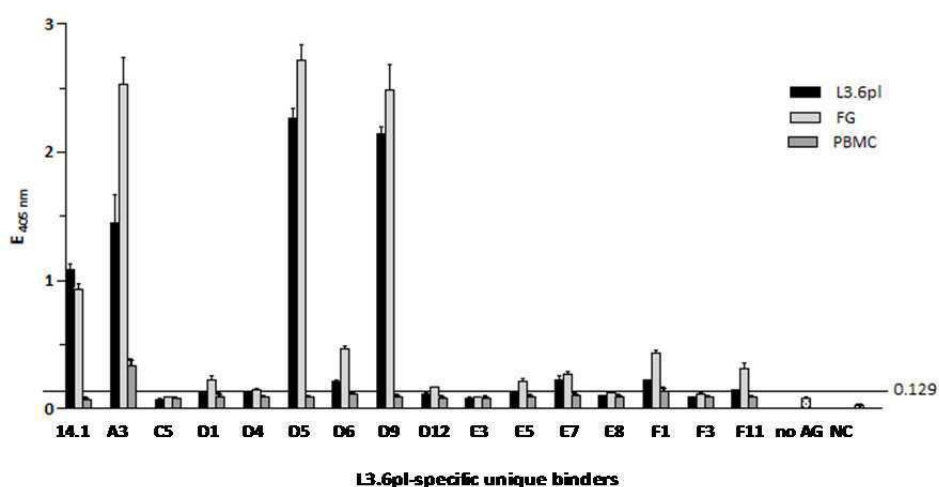


Figure 4-13 Protein ELISA analysis with soluble scFv-SNAP proteins produced in HEK293T cells. Recombinant scFv-SNAP proteins were tested on L3.6pl, FG and PBMC membrane fractions. Bound scFv-SNAP antibodies were detected via polyclonal anti-SNAP-tag primary antibody, a GAM-PO secondary antibody and signal development with ABTS substrate. The average background value was 0.129, defining clones as positive when displaying ABTS absorption signals twice that value and higher.

4.6.2 Flow cytometric analysis

Besides binding analysis on membrane fractions, all eleven positive scFv-SNAP proteins (4.6.1) were tested for binding on living L3.6pl and PBMC cells via flow cytometry. Histograms in Figure 4-14A clearly document binding activity on viable L3.6pl cells, compared to the background fluorescence of the cells. Nine scFv-SNAP proteins, plus the

14.1(scFv)-SNAP, depicted positive binding on the L3.6pl target cell line but none on the PBMC negative control cells (Figure 4-14B). A3(scFv)-SNAP did not bind to the living PBMCs despite positive absorption measurements during ELISA analysis. Figure 4-14C states the percentage of L3.6pl target cells bound by scFv-SNAP antibodies and compares the mean fluorescent intensities (MFI) of each clone against the 425(scFv)-SNAP positive control. Clones E5(scFv)-SNAP and F11(scFv)-SNAP did not bind to living L3.6pl cells during flow cytometry and were discarded. Even though clones D5(scFv)-SNAP and D9(scFv)-SNAP featured very strong ELISA-binding, only very weak binding potential was observed here. Both clones will be discussed separately in 6.1.6. During flow cytometry, it was observed repeatedly that purified and fluorescence-labeled scFv-SNAP proteins depicted weaker binding activity than the unpurified TCSN (data not shown).

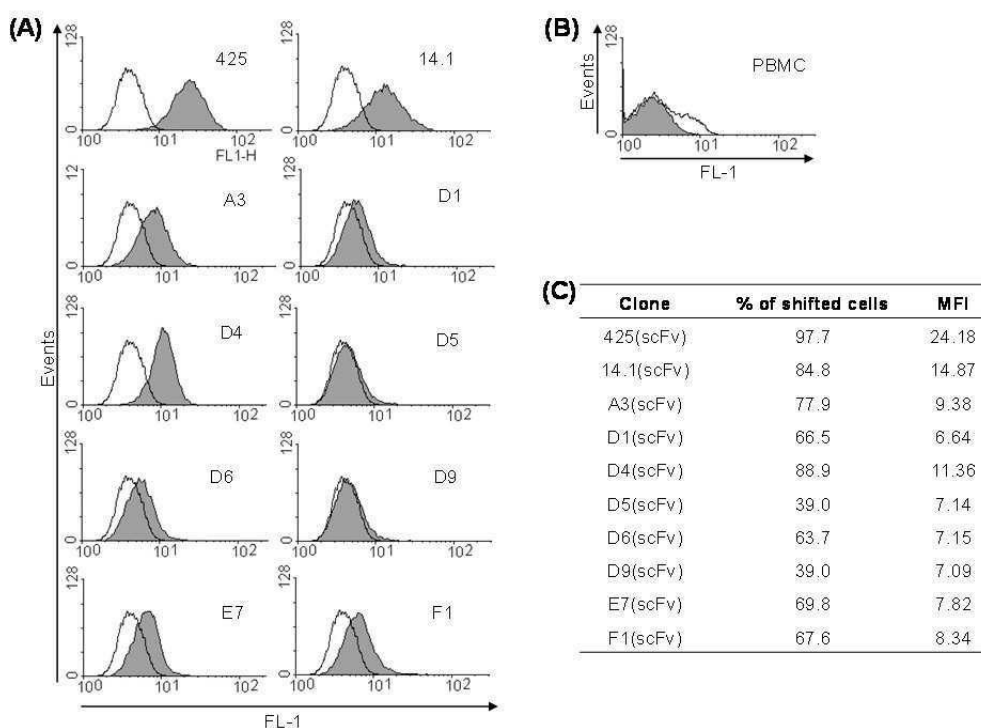


Figure 4-14 Flow cytometric binding activity data of scFv-SNAP proteins on L3.6pl and PBMC cells. (A) Incubation of unpurified TCSN or 2 µg/sample scFv-SNAP fusion protein. The right-shifted grey curve represents bound scFv-SNAP proteins detected with an anti-His AF488-conjugated antibody. The black curve indicates the background fluorescence in comparison. Positive binding was shown for scFv-SNAP clones 14.1, A3, D1, D4, D6, E7 and F1. Clones D5 and D9 showed almost no binding. (B) None of the clones depicted binding on PBMC cells, (C) percentage of cells bound by scFv-SNAP proteins and the corresponding mean fluorescence values (MFI).

D5(scFv) and D9(scFv) both exhibited very strong binding activity on membrane fractions during ELISA analysis on phage (4.2.4.3) and protein level (4.6.1) but merely featured weak binding (39% shifted cells) during flow cytometry (4.6.2). Closer investigations revealed a positive shift of 2.5% (D5(scFv)) and 2% (D9(scFv)) respectively (Figure 4-15),

indicating the possible existence of a certain cell subpopulation within the highly metastasizing L3.6pl cell line .

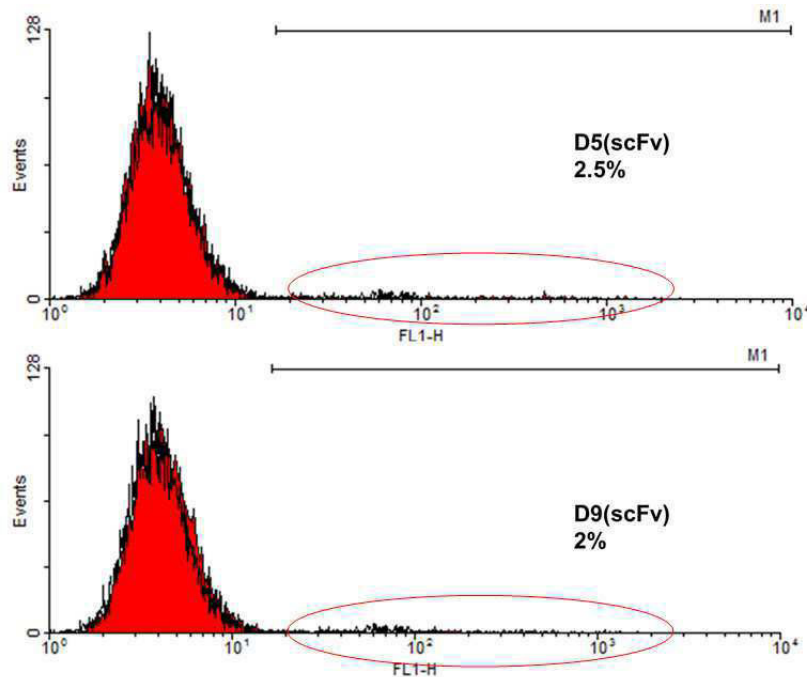


Figure 4-15 Flow cytometric analysis of binding activity of D5(scFv) and D9(scFv) indicating a possible subpopulation within the L3.6pl cell line.

Bound scFv proteins were detected with an anti-His IgG conjugated to AF488 fluorescence dye emitting in fluorescence channel FL-1. The black curve represents the background fluorescence of the detection antibody on the L3.6pl cells, the filled red curve displays the binding activity of D5(scFv) and D9(scFv) on L3.6pl. M1 indicates the area marked for shifted cells.

4.6.2.1 Flow cytometric cross-reactivity analysis

Since scFv-phage particles binding to healthy PBMC cells had already been depleted during panning, no binding was detected on living PBMC cells during flow cytometry. Nevertheless, cross-reactive properties of the L3.6pl-positive scFv-SNAP antibodies was investigated on other pancreatic cancer cell lines as well as on carcinoma cell lines originated from different tissue types (2.4). Existing cross-reactivity might indicate a tumor-associated antigen present on more than one type of cancer.

Cross-reactivity to pancreatic cancer cell lines: Surface binding was examined on the pancreas-derived cell lines FG, Su86.86, MiaPaCa2, PancTuI and PancTuI-*luc* (Table 4-11). All clones displayed positive binding on the PancTuI and PancTuI-*luc* but binding activities differed from the values measured on L3.6pl. For instance, clone D6(scFv)-SNAP bound 25% more PancTuI/PancTuI-*luc* cells, whereas clone 14.1(scFv)-SNAP displayed approximately 50% less binding to PancTuI/PancTuI-*luc* than on L3.6pl. Recombinant scFv-SNAP antibodies 14.1, D1, D4, D6 and F1 also showed

binding activity to the non-metastasizing precursor cell line FG. Moreover, scFv-SNAP clones D1, D4, D6 and F1 bound to MiaPaCa2 and Su86.86, whereas 14.1(scFv)-SNAP did not feature any binding on the latter two cell lines.

Table 4-11 Results of flow cytometric cross-reactivity testing with L3.6pl-positive scFv-SNAP antibody fragments on other pancreatic carcinoma cell lines.

Clone	L3.6pl	FG	MiaPaCa2	Su86.86	PancTu1/PancTu1-luc
14.1(scFv)	+++	+++	-	-	+
A3(scFv)	+++	-	-	-	++
D1(scFv)	++	+	+	+	++
D4(scFv)	+++	+	+	+	+
D5(scFv)	+	-	-	-	+
D6(scFv)	++	+	+	+	+++
D9(scFv)	+	-	-	-	+
E7(scFv)	++	-	-	-	+++
F1(scFv)	++	+	+	+	+++

Definition of percentage of shifted cells: +++ = 100 – 75%, ++ = 75 – 50%, + = 50 – 25%, - = 25 – 0%

Cross-reactivity to non-pancreatic cell lines: Different degrees of cross-reactive binding results on cell lines A431 (human epidermoid carcinoma), LNCaP (human prostate carcinoma), MDA-MB-231 (human breast carcinoma) and SiHa-BHT35 (human cervix carcinoma) are summarized in Table 4-12. All clones except D5(scFv)-SNAP and D9(scFv)-SNAP bound to A431 and MDA-MB-231. Cell line SiHa-BHT35 was tested positive for binding of six scFv-SNAP clones (14.1, D1, D4, D6, D9 and F1), but only four scFv-SNAP proteins (D1, D4, D6 and F1) displayed slightly positive binding on the prostate cancer cell line LNCaP.

Table 4-12 Results of flow cytometric cross-reactivity testing with L3.6pl-positive scFv-SNAP antibodies on cell lines derived from several different cancer types.

Clone	A431	LNCaP	MDA-MB-231	SiHa-BTH35
425(scFv)		+		
14.1(scFv)	+	-	+	++
A3(scFv)	+	-	+	-
D1(scFv)	++	+	++	+
D4(scFv)	+	+	++	+
D5(scFv)	-	-	-	-
D6(scFv)	++	+	++	++
D9(scFv)	-	-	-	+
E7(scFv)	+	-	+	-
F1(scFv)	++	+	++	++

Definition of percentage of shifted cells: +++ = 100 – 75%, ++ = 75 – 50%, + = 50 – 25%, - = 25 – 0%

None of the scFv-SNAP antibodies showed unspecific binding to the eukaryotic expression cell line HEK293T (data not shown).

4.6.3 Internalization assays

Recombinant scFv antibodies isolated in this work are potential candidates for the generation of immunotoxins for application during targeted immunotherapeutic cancer treatment. It is essential for therapeutic antibodies to be transported into the cytosol of a target cell after surface binding. Internalization of fundamentally improves the metabolic uptake and therapeutic effectiveness of recombinant immunotoxins. Based on positive binding activity on viable cells during flow cytometry (4.6.2.1), flow cytometric internalization experiments [244] (4.6.3.1) were performed with scFv-SNAP proteins of clones 14.1, A3, D1, D4, D5, D6, D9, E7 and F1. Candidates with positive internalization behavior during flow cytometric internalization were then further investigated by means of immunofluorescence staining and confocal microscopy in the OPERA live cell imager (4.6.3.2).

4.6.3.1 Internalization analysis via flow cytometry

IMAC-purified scFv-SNAP proteins were labeled with red AF647 fluorescent dye and incubated with L3.6pl cells at 37 °C to induce internalization. In parallel, the identical AF647-labeled scFv-SNAP proteins were incubated at 4 °C to document surface binding instead of internalization. Bound and internalized scFv antibodies marked with AF647 were measured in fluorescence channel FL-4 of a FACScalibur device (Figure 4-16). Positive AF647-binding signals were detected at both temperatures. To distinguish internalized from surface-bound scFv antibodies, the exterior cell proteins were removed by digestion with trypsin. This eliminated the AF647 signal of surface-attached scFv-SNAP proteins, while keeping the internalized fluorescence signal intact. Afterwards fluorescence signals were still measured for clones 14.1, A3, D4 and F1, when previously incubated at 37 °C. Remaining clones did not display a positive fluorescence signal after incubation at 37 °C and trypsination. Following 4 °C incubation, none of the clones depicted a positive AF647 signal after trypsin treatment. Concluding, positive fluorescence signals after trypsin digest were only emitted by AF647-coupled and internalized scFv-SNAP antibodies. Figure 4-16 illustrates, a positive internalization process was measured for clones 14.1, A3, D4 and F1. A positive right-shift (black curve) was shown after incubation at 4 °C as well as 37 °C. Trypsin treatment of L3.6pl cells, after incubation

at 4 °C, resulted in a negative flow cytometric signal. To prove successful internalization, binding of scFv-SNAP proteins at 4 °C and successful trypsinization after internalization were verified by co-incubation with an anti-His-AF488 conjugated detection antibody.

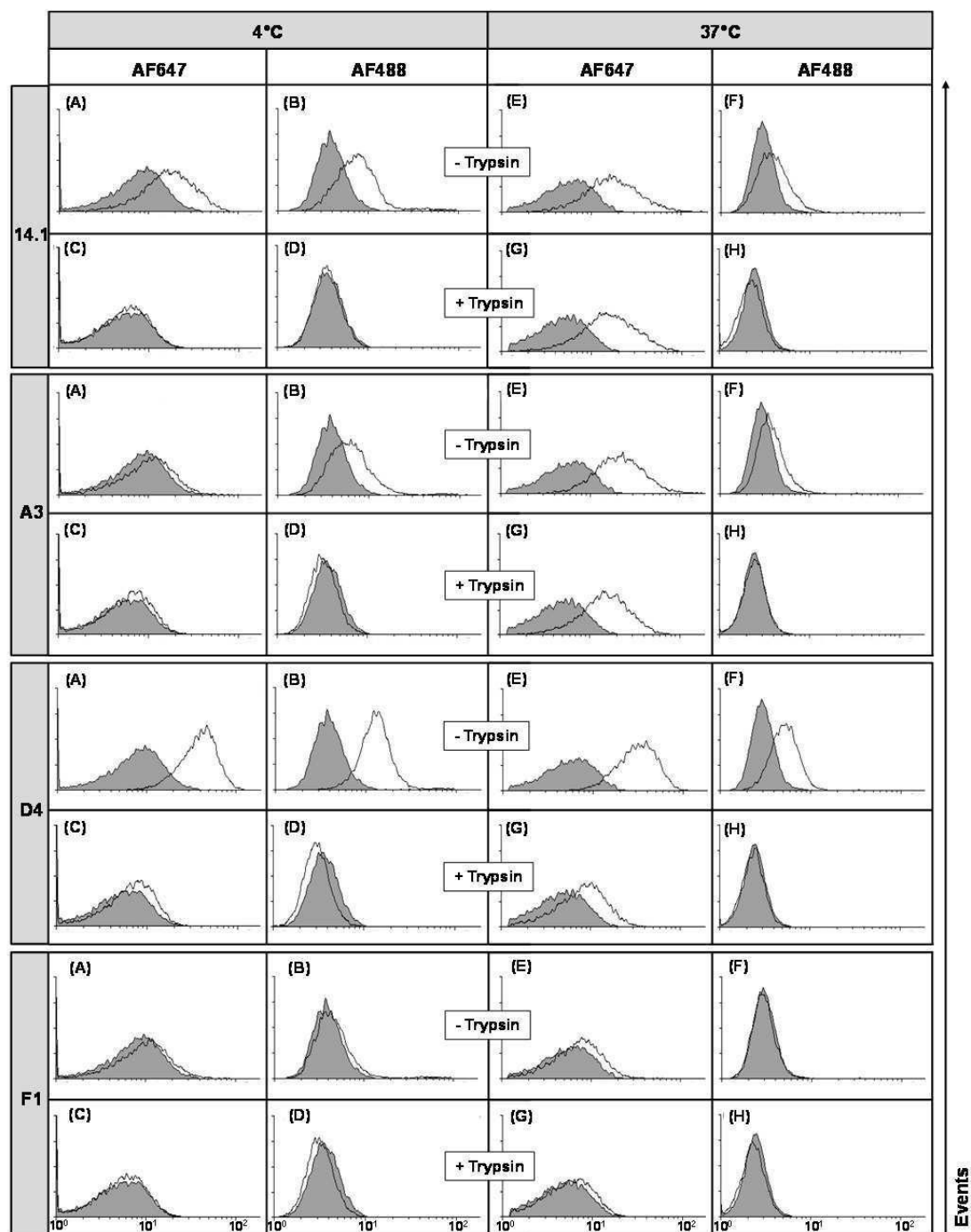


Figure 4-16 Flow cytometric documentation of internalization and binding properties of 14.1(scFv)-SNAP, A3(scFv)-SNAP, D4(scFv)-SNAP and F1(scFv)-SNAP labeled with AF647 on L3.6pl cells.

Binding and successful trypsinization was detected via the His₆-tag and an anti-His-AF488 conjugated detection antibody. (A) and (B) demonstrate binding at 4 °C; (C) and (D) prove elimination of red fluorescence after incubation at 4 °C and trypsinization due to successful removal of surface-bound scFv-SNAP protein; (E) depicts the combined fluorescence signal of surface-bound and internalized scFv-SNAP at 37 °C; (F) shows surface-bound proteins after 37 °C incubation, detected with anti-His-AF488; (G) positive signal of AF647-labeled scFv-SNAP proteins after removal of surface-bound protein after incubation at 37°C; (H) proves that trypsinization of cells measured in (G) has been successful because there is no measurable AF488 signal.

Measurements of trypsinated cells after incubation at 37 °C rendered positive red-fluorescent signals, indicating internalization of AF647-labeled proteins into L3.6pl cells but no signal for the AF488-conjugated detection antibody. Non-trypsinated cells featured an AF488-related fluorescence signal for all clones. Fluorescence intensity of internalized scFv-SNAP antibodies following trypsin treatment was weaker than the signal before trypsination. This was attributed to the removal of surface-bound scFv antibodies from the measurement. In summary, four scFv-SNAP clones (14.1, A3, D4 and F1) depicted a positive internalization signal during flow cytometric internalization analysis. Clones D1, D5, D6, D9 and E7 showed a similar binding performance as in Figure 4-14, but their fluorescence signal was completely eliminated by trypsin treatment after incubation at 37 °C. This led to the conclusion that for said clones merely exterior binding occurred but no internalization.

4.6.3.2 Internalization via OPERA confocal microscopy

Following flow cytometry (4.6.3.1), the four internalization-positive scFv-SNAP proteins 14.1, A3, D4 and F1 were examined by immunofluorescence staining using the OPERA live cell imaging system. In a first experiment, IMAC-purified unlabeled scFv-SNAP proteins were detected via a polyclonal anti-SNAP-tag antibody and an AF647-labeled detection antibody. As second analysis, kinetic measurements were performed with the OPERA device by means of live cell imaging in order to document the internalization process of the AF647-labeled 14.1(scFv)-SNAP antibody fragment into L3.6pl cells.

Immunofluorescence staining of scFv-SNAP proteins: 2 µg/well of IMAC-purified unlabeled scFv-SNAP protein were incubated on L3.6pl cells in a 96-well plate (µ-clear, black, greiner) at 4 °C for 1 h and at 37 °C for different time periods (1, 2, 3, 6 and 12 h) to observe internalization behavior. Since adhesive L3.6pl cells were not detached or treated with trypsin, differently shaped cells were observed to adhere to the bottom of the 96-well plate. Figure 4-17 illustrates the internalization of 14.1(scFv)-SNAP after one to two hours incubation at 37 °C at two different locations in a well.

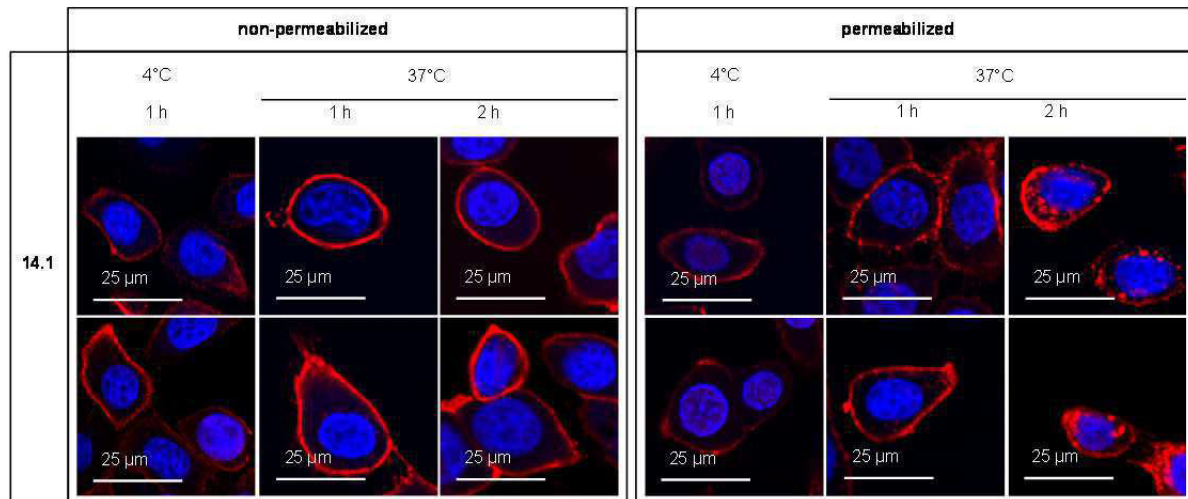


Figure 4-17 Immunofluorescence staining of 14.1(scFv)-SNAP protein incubated on L3.6pl cells at 4°C and 37°C.

Half of the cells were permeabilized with Triton X100 before staining and after fixation with 4% PFA. After 1 h incubation at 4 °C, surface binding was observed. After 1 h at 37°C, binding to cell surface was increased and vesicle formation started in the permeabilized cells. Internalization of vesicles with 14.1(scFv)-SNAP occurred after 1-2 h at 37°C. Vesicles inside the cell became larger and more with time. Non-permeabilized cells do not display the internalization very clearly but the permeabilized cells give a very good impression of the vesicles transported into the L3.6pl cells. Nucleus staining was performed with DAPI, scFv-SNAP detection via a polyclonal anti-SNAP-tag secondary and an AF647-labeled tertiary antibody.

Non-permeabilized cells show excellent binding of the AF647-labeled 14.1(scFv)-SNAP protein, but hardly any internalized antibody. Permeabilized cells, on the other hand, show a large number of internalized vesicles after two hours. In contrast to the other antibodies with internalizing properties, 14.1(scFv)-SNAP bound to the cell surface continuously indicating recognition of a tumor associated target antigen with high expression density.

Figure 4-18 depicts binding and internalization of clone A3(scFv)-SNAP. Binding after 1 h at 4 °C was very weak but binding increased during incubation at 37 °C. In contrast to 14.1(scFv)-SNAP, binding was located in defined spots on the cell surface. Repeatedly, non-permeabilized cells only featured surface binding but permeabilized cells showed visible internalized vesicles three hours incubation at 37 °C.

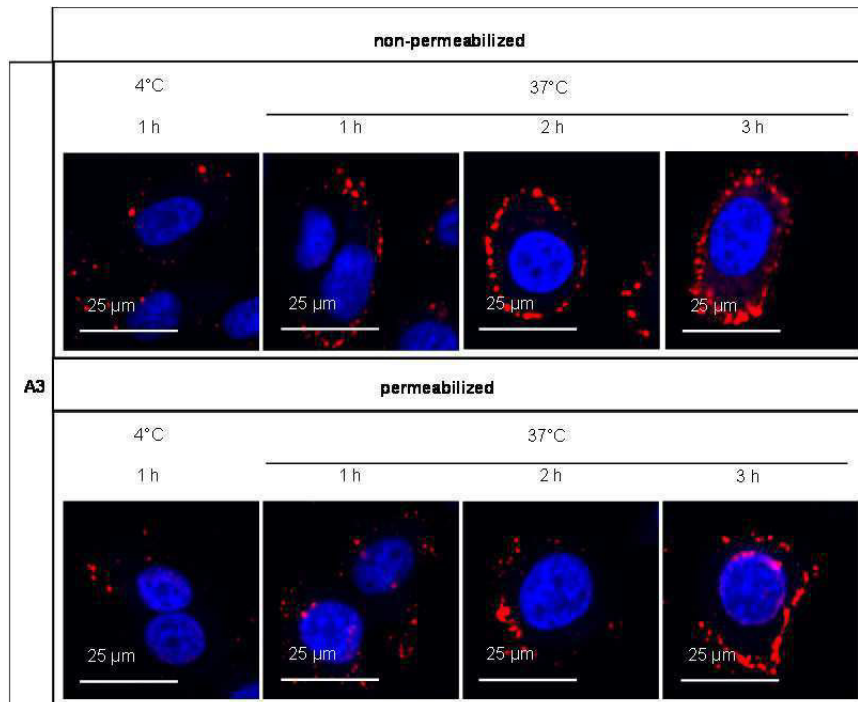


Figure 4-18 Immunofluorescence staining of A3(scFv)-SNAP on L3.6pl cells at 4°C and 37°C.

Half of the cells were permeabilized with Triton X100 before staining and after fixation with 4% PFA. After 1 h incubation at 4 °C, surface binding was observed. After 1 h at 37°C, binding to cell surface was increased and vesicle formation started in the permeabilized cells. Internalization of vesicles with A3(scFv)-SNAP protein occurred after 1-2 h at 37°C. Vesicles inside the cell became larger and more with time. Non-permeabilized cells do not display the internalization very clearly but the permeabilized cells give a very good impression of the vesicles transported into the L3.6pl cells. Nucleus staining was performed with DAPI, scFv-SNAP detection via a polyclonal anti-SNAP-tag secondary and an AF647-labeled tertiary antibody.

For clones D4(scFv)-SNAP and F1(scFv)-SNAP, binding as well as starting internalization were only observed after three to six hours incubation at 37 °C. Both were visualized by a growing number of vesicles with longer incubation time, in parallel to an enlargement of these vesicles over time. The actual internalization process of these two clones took between six and twelve hours. This is clearly documented in Figure 4-19 by the defined and internalized vesicles inside the cell.

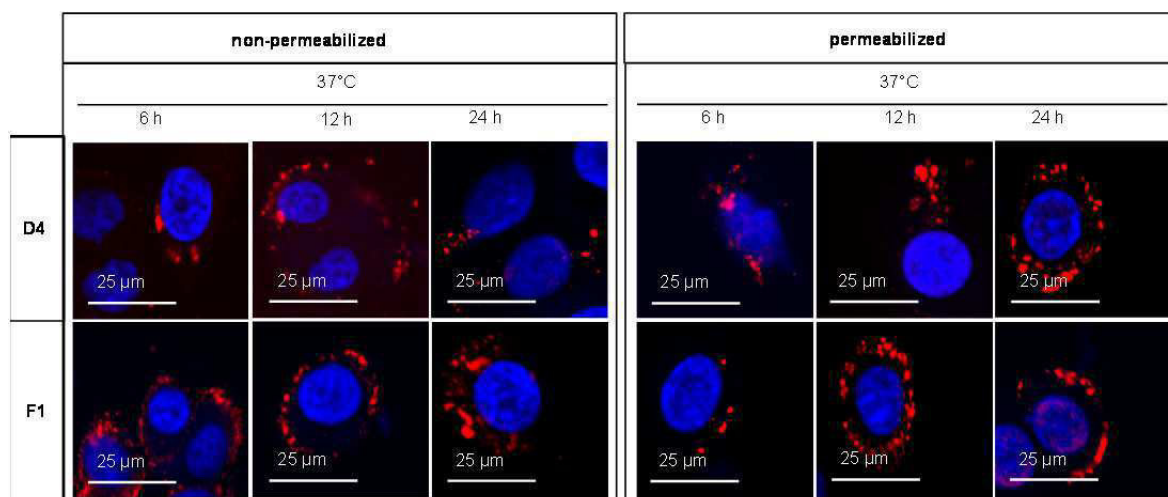


Figure 4-19 Immunofluorescence staining of D4(scFv)-SNAP and F1(scFv)-SNAP incubated on L3.6pl cells at 4°C and 37°C.

Half of the cells were permeabilized with Triton X100 before staining and after fixation with 4% PFA. Binding of both scFv proteins to cell surface was clearly visible after 3 – 6 h incubation at 37 °C. After 12 h at 37 °C binding to cell surface was increased and vesicle formation started. Starting internalization of vesicles with D4 and F1 proteins took place around 12 h at 37°C. Vesicles inside the cell became larger with time. Non-permeabilized cells do not show the internalization very clearly but the permeabilized cells give a very good impression of the vesicles that were transported into the L3.6pl cells. Again both scFv antibodies do not bind to the cell surface continuously but only on certain spots of the cell surface. Starting from these spots, they start to internalize into the cells. Nucleus staining was performed with DAPI, scFv-SNAP detection via a polyclonal anti-SNAP-tag secondary and an AF647-labeled tertiary antibody.

Binding of proteins A3(scFv)-SNAP, D4(scFv)-SNAP and F1(scFv)-SNAP located in small spots on the cell surface indicates that the bound surface antigen is not over-expressed to the same extent of the antigen bound by 14.1(scFv)-SNAP antibody.

Internalization kinetics of 14.1(scFv)-SNAP-AF647: Featuring the fasted internalization rate, IMAC-purified and AF647-labeled 14.1(scFv)-SNAP protein was applied during a kinetic experiment and measured with the OPERA system. Because living L3.6pl cells were very sensitive to any kind of unusual treatment, and tended to detach after two to three hours, fast internalization was essential for this experiment. Sensitivity was observed by rounding of L3.6pl cells which slightly influenced the focus of the OPERA confocal microscope, resulting in blurred photographs. Figure 4-20 documents a kinetic illustration of the internalization process of 14.1(scFv)-SNAP-AF647 at 37°C (concentrated 2 μg/well) at the same position in four wells at different time points (60 min at 4 °C (t = 0), 30 min at 37 °C (t = 30), 60 min at 37 °C (t = 60 min), and 80 min at 37 °C (t = 80 min)). After surface binding, 14.1(scFv)-SNAP-AF647 was internalized via small vesicles. After 80 min incubation at 37 °C, most cells were swimming freely in the wells and the experiment was stopped. No DAPI counter-staining was performed to avoid eventual interference with the AF647 signal and cell sensitivity.

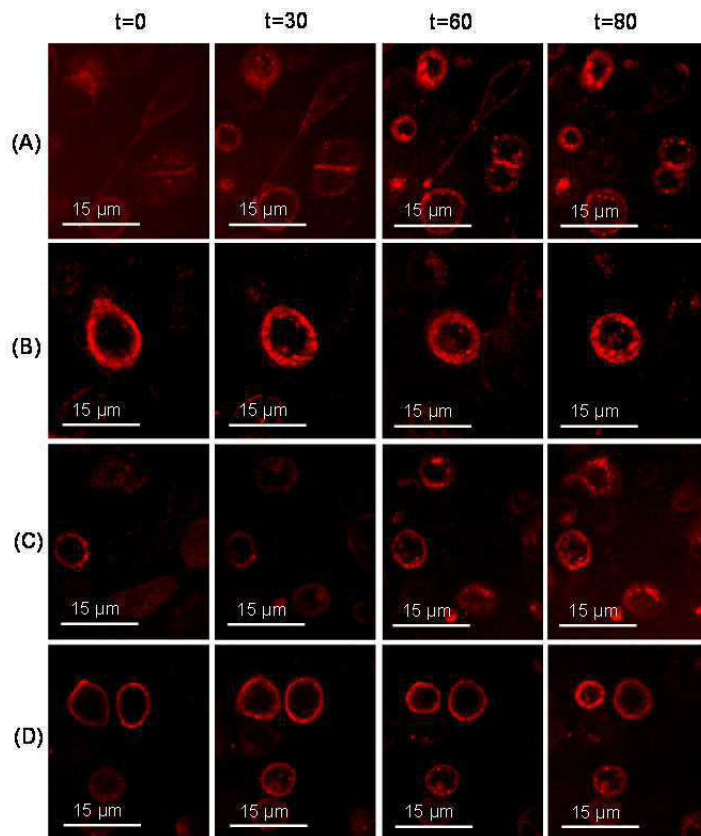


Figure 4-20 Internalization kinetics of 14.1(scFv)-SNAP-AF647 into L3.6pl cells at 37°C at different time points.

A, B, C and D show the internalization behavior of 4 different positions at 37°C. Pictures were taken after 1 h incubation at 4°C ($t = 0$) and after 30 min ($t = 30$), 60 min ($t = 60$) as well as 80 min ($t = 80$) incubation at 37°C. All positions show the process of binding to the cell surface and the internalization of the 14.1(scFv)-SNAP-AF647 protein into the L3.6pl cells. AF647 fluorescence in cells was photographed at 40 x magnification with the confocal OPERA microscope.

5 Results: Design of novel fluorescent W-tag

Efficient production of recombinant therapeutic proteins is another current major area of research. Prospectively, pancreas-specific scFv antibody fragments isolated from the Tomlinson libraries I and J characterized in the work, are promising candidates to serve as binding domain within an immunotoxin. Similar therapeutic results, based on the anti-EGFR single chain 425(scFv) as binding moiety fused to a truncated version of the bacterial toxin *Pseudomonas Exotoxin A'* (ETA'), have previously been described [157, 159]. Being potentially toxic to eukaryotic organisms, such cytotoxic constructs are primarily produced in prokaryotic expression systems, such as *E.coli*. To evaluate the production of such recombinant target constructs more easily, research during the last decade has focussed on non-invasive on-line monitoring systems to observe bacterial cultures during fermentation. One system, called BioLector[®], was developed at the Department of Biochemical Engineering at RWTH Aachen University. It is able to monitor bacterial cultures for product formation through a green fluorescent protein (GFP) reporter tag, measures pH or oxygen content. As an alternative to the commonly used reporter tag GFP, a new protein tag was developed, exploiting the auto-fluorescent characteristics of the aromatic amino acid tryptophan (W) by means of tryptophan clustering. This W-enriched tag, called W-tag, is much shorter than GFP. It offers a possibly advantageous approach for the on-line measurement of protein formation in real-time. Five W-tags with various numbers of tryptophan residues were designed and exemplarily fused to the anti-CD30 receptor single chain Ki-4(scFv) [237]. The anti-Muc1 receptor single chain M12(scFv) [238] was used as a second proof-of-concept protein for the on-line monitoring. The following chapter presents the results of cloning, expression, as well as on-line and off-line analysis regarding those novel W-tags. Additionally, the relation between product formation and tryptophan fluorescence intensity was investigated, followed by the analysis of binding specificity of W-tagged and untagged recombinant protein.

5.1 Generation of W-tag constructs

5.1.1 Sequence design and cloning

Five different W-tag sequences, containing between one and five tryptophan residues (W1 – W5), were developed in co-operation with Dr. Heinrich Delbrück (Fraunhofer IME, Aachen). Accumulated tryptophan residues were embedded into the structure of a naturally occurring protein loop originated from a *Bacillus caldolyticus* cold shock protein

(GenBank accession numbers are: W1-tag – JN107996, W2-tag – JN120907, W3-tag – JN120908, W4-tag – JN120909, W5-tag – JN120910). Table 5-1 gives an overview of the number of tryptophan residues (and other aromatic amino acids) within the W-tags, additionally comparing the lengths of the W-tags and the W-tagged single chain fusion proteins.

Table 5-1 Five different W-tag variations stating the number of tryptophan residues per construct, the construct name, the total number of aromatic amino acids (tryptophan, tyrosine and phenylalanine) as well as the size of the tag region and fusion protein in kDa. [246]

Name	Aromatic amino acids in W-tag	Fusion protein in kDa	W-tag in kDa
EC	0	24.16	1.73
W1	1W 1Y 1F	25.79	3.36
W2	2W 3Y 0F	27.44	5.01
W3	3W 2Y 0F	27.46	5.03
W4	4W 1Y 0F	27.49	5.06
W5	5W 3Y 0F	28	5.57

W-tags were synthesized at GENEART (Regensburg, Germany) and delivered as DNA sequences in plasmids pMA_(amp) and pCR4Blunt-TOPO_(amp,kan), containing the necessary restriction sites (*NcoI*, *NdeI*, *HindIII* and *XbaI*).

Table 5-2 displays the DNA and protein sequence data of the W-tags. DNA triplets of the ordered DNA sequences were optimized for the protein expression in *E.coli*.

Table 5-2 DNA and protein sequences of all five W-tags.

The DNA sequences were ordered from GENEART with *E.coli*-optimized triplets. They were delivered in the vector backbones pMA and pCR4Blunt-TOPO containing all the restriction sites necessary for subsequent cloning into a prokaryotic or eukaryotic expression system.

W-tag	DNA sequence	Protein sequence	Delivery vector
W1	AAA TGG AGC AAC AAC GAA AAA GGC TAT GGC TTT AGC	KWSNNEKGYGFS	pMA
W2	CGC GGC AAA GAA AAA TGG AAA AAC AAC GAA AAA GGC TAT GGC TAT CAG GAA GAT GAA GGC GGC AGC TAT AAA TGG GAA GAT	RGKEKWKNNEKGYGYQEDEGGSYKWED	pMA
W3	CGC GGC AAA GAA AAA TGG AAA AAC AAC GAA AAA GGC TGG GGC TAT CAG GAA GAT GAA GGC GGC AGC TAT AAA TGG GAA GAT	RGKEKWKNNEKGWGYQEDEGGSYKWED	pMA
W4	CGC GGC AAA GAA AAA TGG AAA AAC AAC GAA AAA GGC TGG GGC TAT CAG GAA GAT GAA GGC GGC AGC TGG AAA TGG GAA GAT	RGKEKWKNNEKGWGYQEDEGGSWKWED	pCR4Blunt-TOPO
W5	CGC GGC AAA TAT AAA TGG AAA AAC AAC GAA AAA GGC TGG GGC TAT TGG GAA GAT GAA GGC GGC AGC TGG TAT TGG AAA GAT	RGKYKWKNNEKGWGYWEDEGGSWYWKD	pMA

During W-tag design, the protein sequences were analyzed with the CHARMM software (<http://www.CHARMM.org>) in Discovery Studio (<http://www.accelrys.com>) to minimize the free energy of each model and to create 3D-models for each W-tag protein loop (Figure 5-1). Moreover, all protein sequences were arranged with the same program to ensure that tryptophan residues were positioned on the outside of the protein loop.

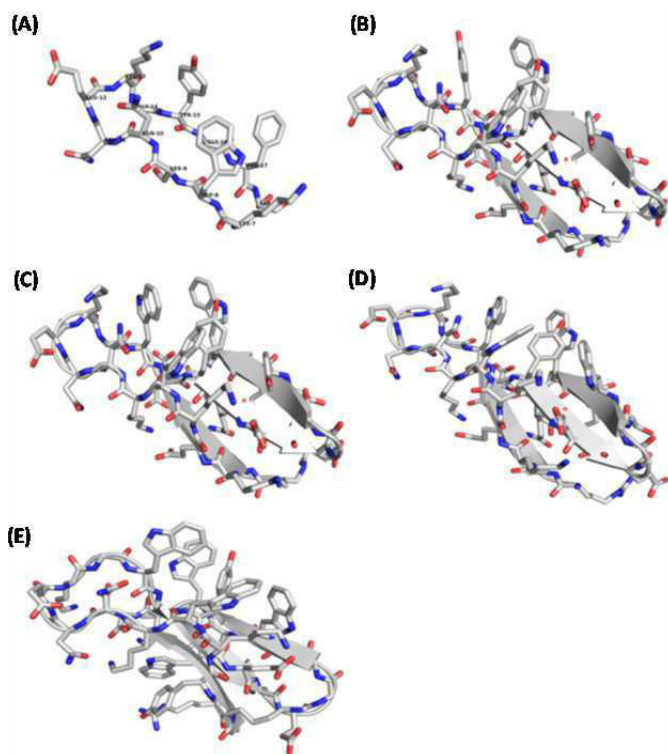


Figure 5-1 3D-models of amino acid sequence structures of all five W-tags.

(A) W1-tag, (B) W2-tag, (C) W3-tag, (D) W4-tag and (E) W5-tag; all structures display the amino acid residues on molecular basis featuring the calculated in- and outward orientation of the amino acids in the protein loop used for the W-tag design.

5.1.2 Vector assembly of W-tag constructs

All five W-tags were successfully subcloned from the pMA and pCR4Blunt-TOPO delivery vectors into the pET-27b+-derived pMT plasmid (2.10, Figure 2-1) used for prokaryotic protein expression in *E.coli*. The pMT expression vector contained a gene encoding the CD30-specific murine single-chain antibody fragment Ki-4(scFv) [237] or the human single chain M12(scFv) [238], supposed to bind against the MucI receptor. Two different constructs were prepared for each W-tag and each recombinant scFv antibodies: (a) One construct carrying a *pelB* leader peptide to produce periplasmic target protein (subcloned via restriction sites *NcoI* and *HindIII*), and (b) one construct without *pelB* leader peptide to produce cytoplasmic protein (transferred through enzymes *NdeI* and *HindIII*).

DNA fragments were ligated into the pMT plasmid to create the expression vector series pMT-W_x-Ki-4(scFv) and pMT-W_x-M12(scFv), where x refers to the number of tryptophan residues in the W-tag. The complete expression cassette (Figure 5-2) comprised a *pelB* leader (or no *pelB* leader respectively), W-tags (W1–W5), a His₆-tag, GS-linkers and a cleavable enterokinase site (EK-site). Recombinant scFv genes were introduced as an in-frame fusion down-stream of the W-tag region exchangeable within the expression cassette via restriction enzymes *SfiI* and *NotI*.

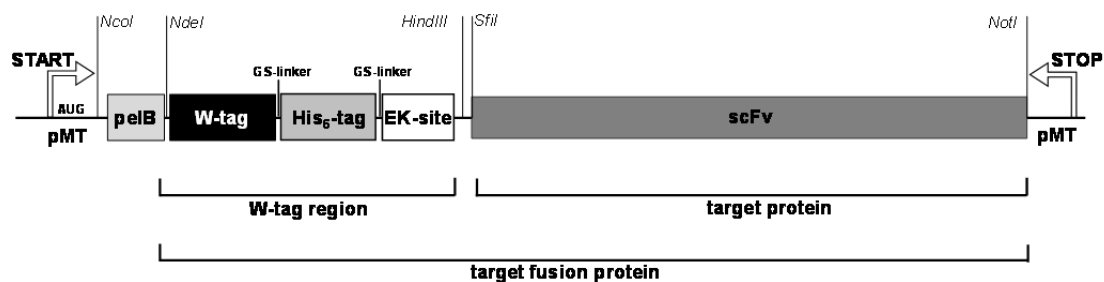


Figure 5-2 Expression cassette for pMT-W_x-Ki-4(scFv) and pMT-W_x-M12(scFv) fusion protein constructs.

The target protein is genetically linked to the W-tag region together forming the target fusion protein. The schematic structure of the W_x-Ki-4(scFv)/M12(scFv) insert in the expression cassette consists of the *pelB* signal peptide inducible with IPTG via the *lac* operator (periplasmic construct), W-tag fused to a His₆-tag by a GS-linker and the scFv target protein linked to the His₆-tag through a potentially cleavable EK-site. The cytoplasmic construct has no *pelB* leader peptide. Restriction sites for constructs with *pelB* leader are *NcoI* and *HindIII*, restriction sites for constructs without *pelB* leader *NdeI* and *HindIII*. The recombinant scFv can be exchanged through *SfiI* and *NotI* restriction sites. [246]

All W-tag constructs were equipped with a His₆-tag for immunodetection and affinity purification as well as an EK-site for potential cleavage of the target protein from the W-tag and His₆-tag. Since all proteins naturally contain some tryptophan residues in their amino acid sequence vectors pMT-Ki-4(scFv) and pMT-M12(scFv) without W-tags were employed as expression controls (EC) to determine the background auto-fluorescence of the untagged single chains. The empty pET-27b+ vector was used as a true negative control (NC).

5.2 Expression of W-tag fusion proteins

5.2.1 Protein expression in bacterial pellet

To illustrate protein expression, W_x-Ki-4(scFv) constructs with *pelB* leader are shown exemplary for all constructs with and without *pelB* leader as well as all corresponding W_x-M12(scFv) constructs. All five W_x-Ki-4(scFv) constructs including controls (EC and NC) were expressed under kanamycin selective pressure in BL21 Rosetta 2 (DE3) *E.coli*

(3.1.9.3) induced with IPTG via the lac operator. Samples were retrieved from bacterial pellet by heat lysis and successful target fusion protein expression was verified via SDS-PAGE and Western blot analysis against the His₆-tag (Figure 5-3). Intense double bands ranging from 25 to 35 kDa were detected, confirming over-expression of the different W-tagged target proteins with and without the *pelB* leader peptide. NC did not show any protein expression on the Western blot. The double bands occurred due to incomplete cleavage of the *pelB* leader when the fusion protein was transported from the cytoplasm to the periplasmic space. The identity of each protein band was confirmed by mass spectrometry (3.3.8) (data not shown). The lower protein band (25 – 30 kDa) corresponded to the calculated weight of the protein, the higher band (30 – 35 kDa) included the uncleaved *pelB* leader peptide. Remaining visible protein bands on the SDS-PAGE were contaminating bacterial proteins.

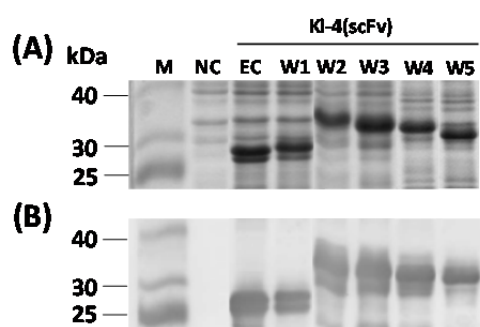


Figure 5-3 Wx-Ki-4(scFv) protein expression analysis on SDS-PAGE and Western blot.

(A) SDS-PAGE: lane 1 – Prestained Broad Range Protein Marker, lane 2 – empty vector as negative control (NC), lane 3 – Ki-4(scFv) expression control (EC), lane 4 – W1-Ki-4(scFv), lane 5 – W2-Ki-4(scFv), lane 6 – W3-Ki-4(scFv), lane 7 – W4-Ki-4(scFv), lane 8 – W5-Ki-4(scFv). (B) Western blot of proteins detected with a monoclonal anti-polyHis IgG antibody, a goat anti-mouse-peroxidase conjugated antibody and DAB. In figures (A) and (B) the proteins are detected as double bands. [246]

The cytoplasmic constructs without *pelB* leader peptide and the Wx-M12(scFv) target fusion proteins were expressed in the pellet likewise (data not shown). [246]

5.2.2 Protein secretion into cultivation medium

Non-tagged Ki-4(scFv) antibody (EC) and the W1-Ki-4(scFv) protein were partially secreted and found in both the supernatant and the cell pellet (Figure 5-4A). Target fusion proteins containing between two and five tryptophan residues within the W-tag were almost exclusively detected in the cell pellet fraction and barely secreted into the medium, displayed by the very weak band visible in the Western blot (Figure 5-4B). Even though the bacterial pellet was thoroughly separated from the medium by centrifugation, these weak bands may be residual protein from cells damaged during centrifugation.

Wx-M12(scFv) constructs showed the same trend of protein secretion during expression as the W-tagged Ki-4(scFv) proteins.

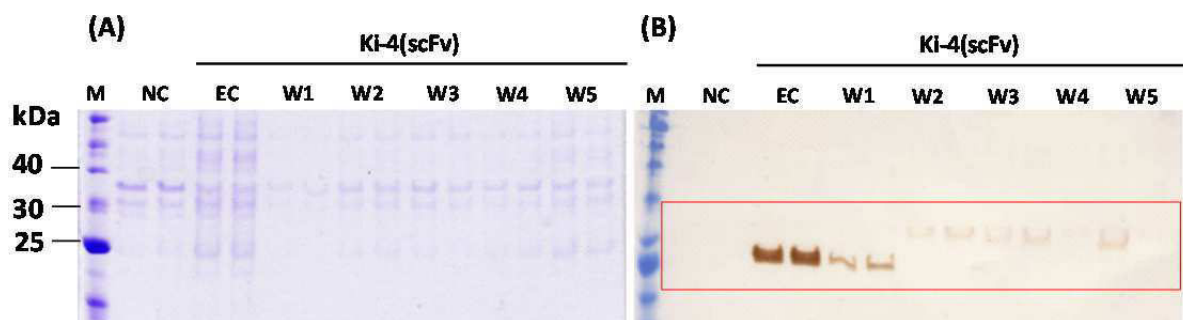


Figure 5-4 SDS-PAGE and Western blot analysis of Wx-Ki-4(scFv) proteins secreted into cultivation medium.

(A) SDS-PAGE and (B) Western Blot of cultivation medium: Lanes 1 and 2 were loaded with the NC showing no protein, lanes 3 and 4 contain the Ki-4(scFv) expression control which was secreted into the cultivation medium (band at ~25kDa). In lane 5 and 6 the W1-Ki-4(scFv) protein secretion into cultivation medium is shown. Lanes 7 to 15 display the Ki-4(scFv) protein tagged with W2 to W5 which were only detected as weak bands in the cultivation medium if at all. All lanes display various bands of bacterial protein.

None of the cytoplasmatically expressed proteins without *pelB* leader were released into the medium since they were not transported to the periplasmic space after translation.

5.2.3 Protein expression in different types of media

Moreover, the proteins were expressed as 5 mL cultures using different media to test for differences in expression: (a) modified Wilm-Reuss synthetic minimal medium (2.3), (b) LB_{kan} medium induced with 1 mM IPTG (2.3) and (c) LB_{kan} auto-induction medium (2.3). Comparing the protein expression in these different types of media, all Wx-Ki-4(scFv) target fusion proteins were over-expressed to a similar degree in all three types of media, although expression in LB_{kan} auto-induction medium sometimes yielded slightly better results (data not shown). As a consequence, modified Wilms-Reuss synthetic medium was chosen for all subsequent fermentations and on-line fluorescence measurements. A huge advantage is that synthetic medium displays lower background fluorescence than complex medium, thus resulting in a clearer signal during measurements.

It was confirmed that control cultures lacking induction with 1 mM IPTG or lactose, never featured any protein expression during any time of cultivation in any cultivation medium.

5.2.4 Percentage of over-expressed Wx-Ki-4(scFv)

To evaluate the time point of maximum target protein over-expression, samples of all induced Wx-Ki-4(scFv) target fusion proteins were taken from a fermentation at five

different time points ($t_0 = 4.44$ h, $t_1 = 6.22$ h, $t_2 = 9.11$ h, $t_3 = 12.2$ h, $t_4 = 26.7$ h) as well as the NC and EC controls. All cultures were induced with 1 mM IPTG after 4.44 h of fermentation when the bacteria entered the exponential growth phase. The bacterial pellet of each sample was harvested and the protein concentration within each pellet was analyzed via SDS-PAGE (3.3.1) and AIDA analysis software (3.3.3.1). After determining the total bacterial protein concentration as well as the concentration of target protein from the respective protein band on the SDS-PAGE, the percentage of the target protein was calculated referring to the total bacterial protein amount. Target protein concentration peaked between 9 and 10 h of cultivation (Figure 5-5). Subsequently target proteins were harvested after 9.5 h of fermentation to obtain optimal yield for further investigations of the target proteins. The graph below clearly shows a lower protein yield for EC and W1-Ki-4(scFv) than for the target proteins. W3-Ki-4(scFv) was produced best. Target protein concentration decreased again between 10 and 12 h of fermentation due to protein degradation or accumulation of biomass without target protein.

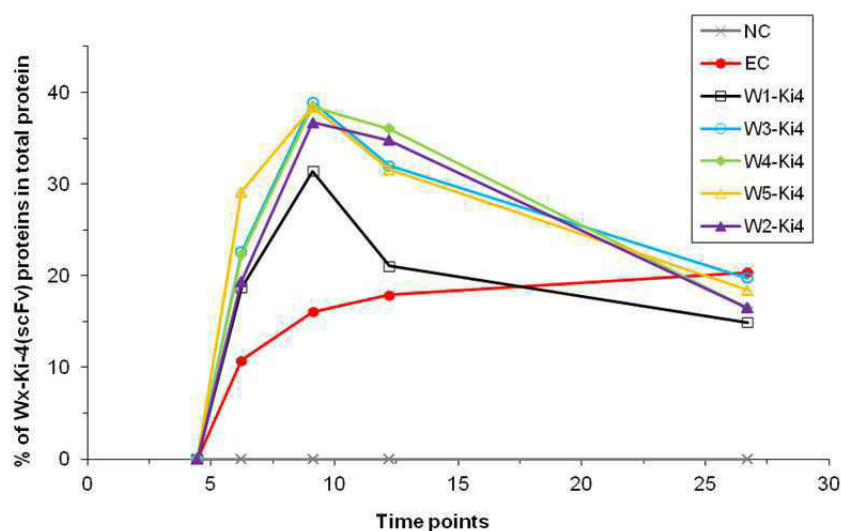


Figure 5-5 Calculated percentage of Wx-Ki-4(scFv) proteins referring to total bacterial protein after determination of protein concentration with AIDA.

NC did not produce any protein. All target proteins reached a peak of over-expression between 9 and 10 h, except EC which kept growing and producing target protein until the fermentation ended. EC and W1-Ki-4(scFv) display lower expression of the target protein than the other constructs. W3-Ki-4(scFv) has the best over-expression at the peak. Between 10 and 12 h of fermentation the target protein concentration decreased.

5.3 On-line measurement data

In the following, W-tagged Ki-4(scFv) and M12(scFv) fusion proteins were examined for bacterial cell growth and cytotoxic effects eventually influencing biomass production using a self-made Respiratory Activity Monitoring System (RAMOS) (data not shown). Additionally, target fusion protein production was monitored on-line with a non-invasive

BioLector-like device via the auto-fluorescence signal of the different W-tags which optically detected protein production in real-time (3.5.1). BioLector on-line measurement data was performed and analyzed by Esther Gartz at the Department of Biochemical Engineering at RWTH Aachen University.

5.3.1 On-line fluorescence intensity measurements

One aim of this thesis was to create a short and optically active protein tag exploiting the auto-fluorescence properties of accumulated tryptophan residues in an on-line measurement set-up with an adapted BioLector® device to simultaneously measure biomass and product formation via tryptophan fluorescence during fermentation of induced and non-induced cultures (Figure 5-6A-D). Fermentation in the BioLector-like apparatus was carried out in 96-well MTPs (3.1.9.3). During cultivation, bacterial growth was determined by measuring the scattered light signal at 620 nm [224]. Tryptophan was excited at 280 nm and its emission was measured at 350 nm in form of a tryptophan fluorescence signal. Mean measurement values of quadruplicate samples of parallel induced and non-induced cultures, representing each Wx-Ki-4(scFv) target fusion protein as well as the EC and NC constructs, are displayed in Figure 5-6A-E. The relative percentage deviation of these measurements was less than 6% (data not shown). [246]

Scattered light signals of the non-induced cultures (Figure 5-6A) similarly increased for all constructs during the exponential growth phase up to 7.5 h of fermentation. At this stage, glucose was almost depleted and the signals then declined until 10 h. For all non-induced clones, the different W-tag clones had no influence on the growth behavior. From 10 h onwards, the scattered light signals increased for the EC and NC cultures and, after a short stationary period, in the other cultures as well (Figure 5-6A). Tryptophan fluorescence curves of the non-induced cultures were comparable to the corresponding scattered light curves (Figure 5-6C) and reached a plateau after 7.5 h, indicating no further growth when the bacteria switched from consuming glucose to the overflow metabolite acetate. The similar curves for scattered light and tryptophan fluorescence suggest that both signals provide data about biomass formation (discussed later in more detail). [246]

A slight increase for scattered light and tryptophan fluorescence signals was also observed in the non-inoculated control wells with pure medium (Figure 5-6A-D). Still no cell growth was detected towards the end of the experiment (no pellet after centrifugation). [246]

Induction of protein expression with 1 mM IPTG in the early exponential phase (after 3.2 h of cultivation) profoundly impacted the resulting growth curves. Only a moderate increase in biomass formation was observed (Figure 5-6B) but tryptophan fluorescence signals of all cultures rapidly increased except the negative control (NC) (Figure 5-6D). It was observed that the W-tags with a higher number of tryptophan residues did not return a proportional increase in fluorescence intensity. Nevertheless, the fluorescence intensity increases even with a stagnating biomass formation apart from the EC which keeps growing until the end of the fermentation (Figure 5-6D). Glucose depletion was observed after 9 – 10 h and at the same time the tryptophan fluorescence intensity declined in all induced cultures. [246]

In the non-induced bacteria (Figure 5-6A and C), the increasing biomass (scattered light signal intensity) and tryptophan fluorescence intensity correlate with each other, and thus with the presence of tryptophan in the biomass. The tryptophan fluorescence was plotted as a function of the scattered light where all data points were almost concurrent with one another (Figure 5-6E). This means that all five W-tag constructs performed in a similar manner with regard to tryptophan fluorescence vs. scattered light intensity in non-induced cultures. The connection between tryptophan fluorescence and scattered light intensity was described using the power function ($\text{fluorescence intensity}_{\text{calc}} = 4780 \cdot [\text{scattered light intensity}_{\text{meas}}]^{0.077} - 7715$). Consequently, tryptophan fluorescence in the non-induced cultures was independent of the W-tag variant and only mirrored the scattered light intensity depicting the amount of cells. This so called fit indicates the effect of the biomass fluorescence signal on the tryptophan fluorescence intensity. Using the biomass signal of the uninduced clones, this factor was subtracted from the tryptophan fluorescence signal (Figure 5-6E). [246]

Thus, tryptophan fluorescence coming from the biomass could be calculated with the power function and was subtracted from the overall tryptophan fluorescence to retrieve the partial tryptophan fluorescence signal actually resulting from the W-tag. This implies no observations of correlation between the quantitative and exact concentration value of target protein and tryptophan fluorescence. Only an increased product formation was documented where the curves of the W-tagged proteins provided a differing signal from the untagged to the W-tagged target fusion proteins. [246]

In the induced cultures, the overall tryptophan fluorescence signal is the sum of the fluorescence signal from the biomass and the fluorescence signal from the W-tagged fusion

proteins. When plotted against time (Figure 5-6F) it became apparent that the fusion protein begins to accumulate after induction only. Fluorescence intensity then increased until about 10 h of cultivation and declined after that, possibly reflecting protein degradation. Containing six tryptophan residues, the EC construct also generated tryptophan fluorescence but its tryptophan signal intensity was substantially lower than that of the W-tagged proteins. [246]

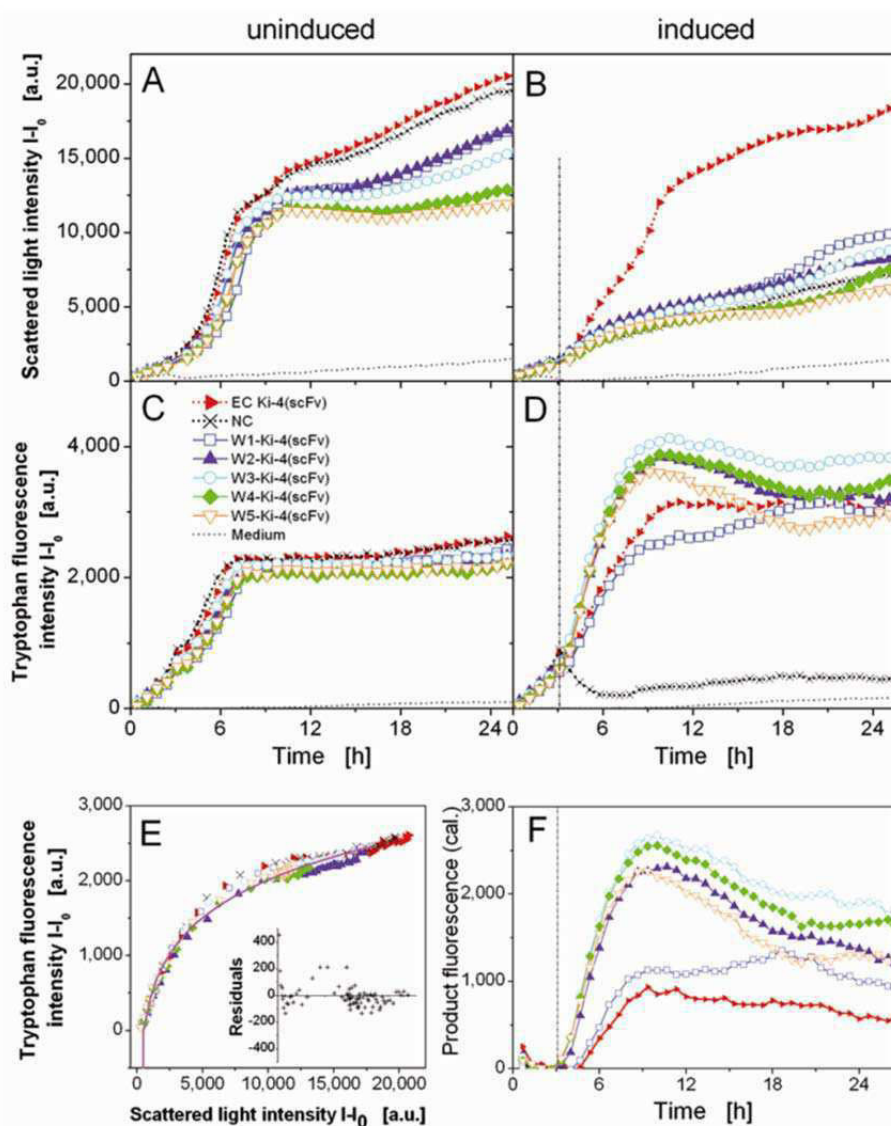


Figure 5-6 On-line detection of biomass formation and production of Wx-Ki-4(scFv) target fusion proteins.

The intensities of (A,B) represent the scattered light (620 nm) and (C,D) tryptophan fluorescence (280/350 nm excitation/emission) and were measured for the non-induced and induced cultures (induction with 1 mM IPTG is indicated by the vertical broken line after 3.2 h). For the non-induced cultures (no product), tryptophan fluorescence is plotted versus scattered light intensity (symbols). (E) The appropriate fit shown as a continuous line (power function: fluorescence intensity_{calc} = 4780·[scattered light intensity_{meas}]^{0.077}-7715). The plot of the residuals between the calculated and the measured fluorescence is displayed within the diagram as an inset box. (F) Product fluorescence intensity calculated by subtracting the biomass fluorescence of the non-induced cultures from the total fluorescence of the induced cultures. Data and figure were provided by Esther Gartz. [246]

To demonstrate the general applicability of the W-tagging concept the on-line measurement experiments were repeated using the second single chain M12(scFv) antibody [238] unrelated to the Ki-4(scFv) (Figure 5-7). This second antibody had been fused to the five different W-tags as well and was expressed in *E.coli* likewise (3.1.9.3). Fluorescence behavior of this antibody and the W-tags were similar to that of the original Ki-4(scFv) model antibody (Figure 5-6) confirming the Wx-Ki-4(scFv) data and thus provided a proof-of-concept of the W-tag as a reporter tag.

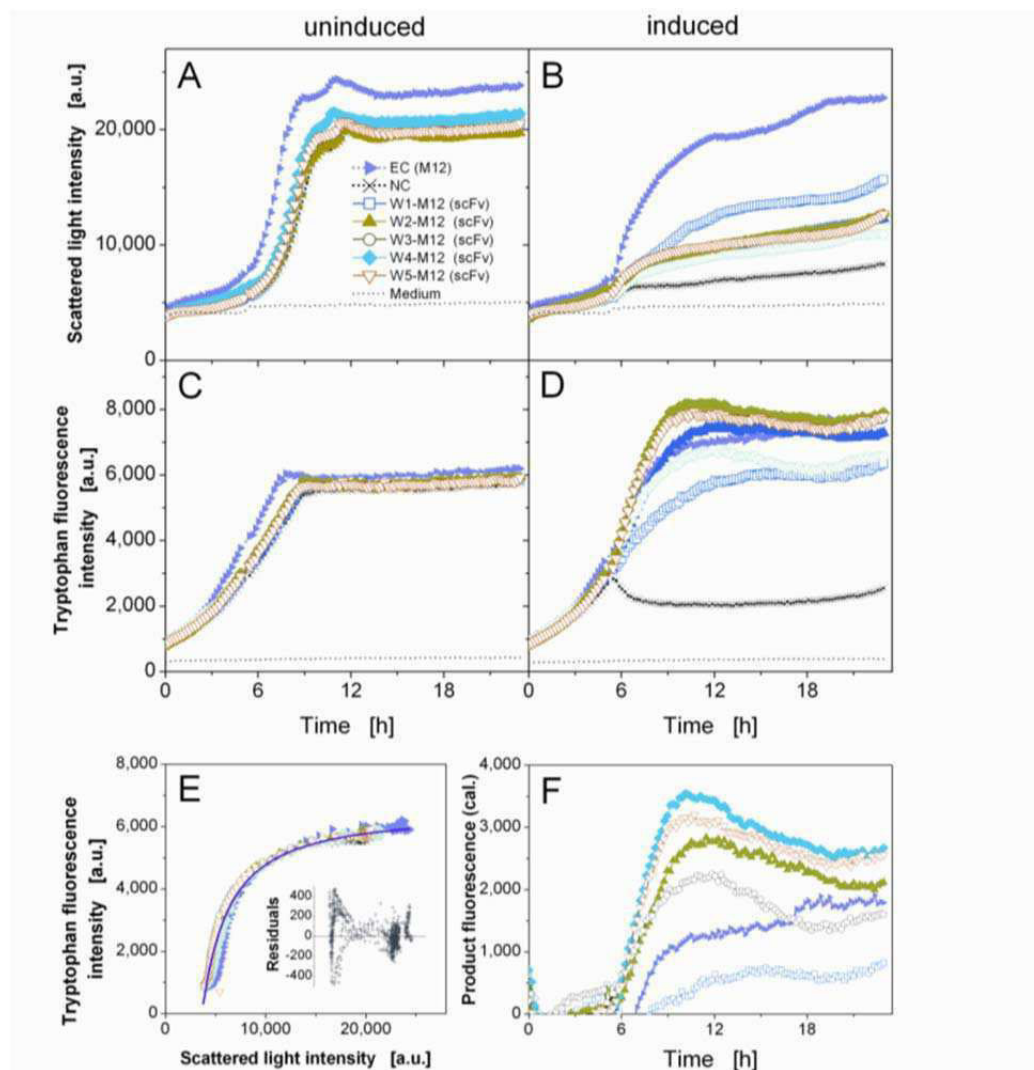


Figure 5-7 On-line detection of biomass formation and production of Wx-M12(scFv) fusion target proteins.

On-line fermentation signals measured with a modified BioLector® device during cultivation of *E.coli* BL21 Rosetta 2 (DE3) expressing the M12 single chain variable fragment in modified Wilms-Reuss medium with 20 g/L glucose using a 96-well microtiter plate. The intensities of (A,B) the scattered light (ex:620 nm/em) and (C,D) tryptophan fluorescence (ex:280 nm/em:350 nm) were measured for the non-induced and induced cultures (induction with 1 mM IPTG: vertical dash-dotted line after 3.2 h of cultivation). For the non-induced cultures (no product), tryptophan fluorescence is plotted versus scattered light intensity (symbols). The appropriate fit is given as the continuous line (power function: $\text{fluorescence intensity}_{\text{calc}} = -4190 \cdot 10^8 \cdot [\text{scattered light intensity}_{\text{meas}}]^{1.35} + 6415$); the plot of the residues between the calculated and the measured fluorescence is displayed within the diagram as inserted. (F) Product fluorescence intensity resulting from the total fluorescence of the induced cultures derived from product and biomass minus the fluorescence originated from biomass calculated from the fit (E) for the uninduced cultures [246]. Data and figure were provided by Esther Gartz.

The W-tagged Ki-4(scFv) and M12(scFv) target proteins without *pelB* leader peptide featured similar curves as in Figure 5-6 and Figure 5-7, except that the overall measured values for the tryptophan fluorescence intensity were weaker than the signal for clones with *pelB* leader (data not shown).

5.4 Protein purification of Wx-Ki-4(scFv) proteins

Different detergents were tested for bacterial lysis and the non-denaturing recovery of over-expressed W-tag target fusion proteins: (a) TES buffer lysis (3.3.5.2), (b) lysozyme (3.3.5.1), (c) NP-40 (3.3.5.3) and (d) sonication (3.3.5.4). Lysis results and yield of protein recovery were examined via SDS-PAGE and Western blotting, and the best recovery method was chosen for down-stream processing and protein preparation for further characterization of W-tagged proteins.

5.4.1 Protein recovery by TES buffer lysis

Non-denatured periplasmic protein was recovered by TES buffer lysis as instructed in (3.3.5.2) and Wx-Ki-4(scFv) proteins were used representatively. Figure 5-8A displays multiple bands of all bacterial proteins as well as the target protein in the TES lysate as a result of a successfully lysed cell pellet. Western blotting (Figure 5-8B) shows protein bands ranging from 25 – 35 kDa specifically staining the Wx-Ki-4(scFv) proteins. EC showed some bands of lower molecular weight from degraded proteins and the band for W5-Ki-4(scFv) was very weak. Apparently the W5-Ki-4(scFv) protein was not released from the bacterial pellet as well as the other proteins.

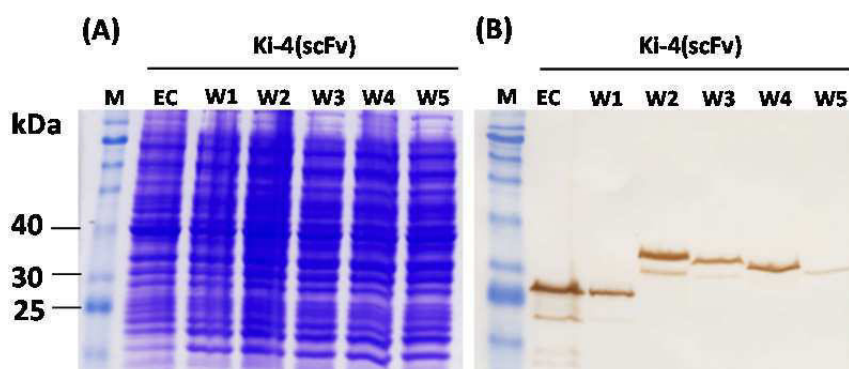


Figure 5-8 SDS-PAGE and Western blot of Wx-Ki-4(scFv) fusion proteins after bacterial lysis with TES buffer.

(A) shows the bacterial total lysate indicating a successful cell lysis by osmotic shock. In (B) the Wx-Ki-4(scFv) target proteins were detected via the His₆-tag using an anti-His mouse IgG and an anti-mouse GAM-PO antibody followed by detection with DAB substrate. Distinctive protein bands between 25 and 35 kDa were visible for all proteins, although the W5-Ki-4(scFv) band was only faint.

A disadvantage of the TES buffer method is the EDTA content of the lysis buffer. EDTA complexes Ni^{2+} and Co^{2+} ions, elutes them from the purification columns and therefore, the His₆-tag intended protein purification would not be able to bind to the purification matrix. To render subsequent protein purification via IMAC (3.3.4.1) with Ni-NTA/Talon columns or further experiments feasible, the EDTA was removed from the bacterial crude lysate.

The EDTA-containing TES buffer was exchanged with PBS via PD10-desalting columns (3.3.6, Figure 5-9). During this process, the sample volume was increased so that the target protein concentration was diluted. Proteins W4-Ki-(scFv) and W5-Ki-4(scFv) were not detected during immunoblot analysis after dialysis and it was assumed that elution from the PD10-desalting columns had been unsuccessful. EC and W1-Ki-4(scFv) were recovered at a high protein concentration (lane 2 and 3) but W2-Ki-4(scFv) and W3-Ki-4(scFv) showed weak protein concentrations in the PBS eluate.

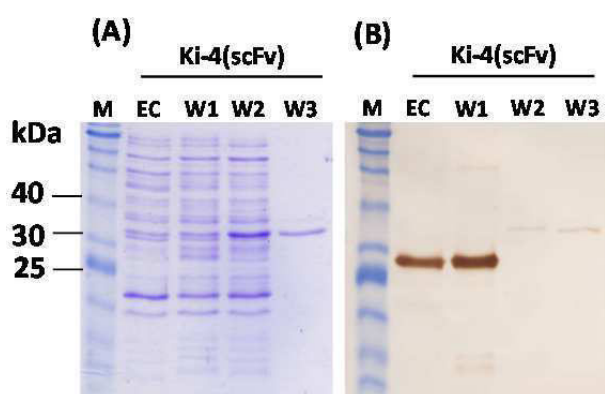


Figure 5-9 Documentation of protein dialysis with SDS-PAGE and Western blot analysis of EC, W1-Ki-4(scFv), W2-Ki-4(scFv) and W3-Ki-4(scFv) after TES lysis and buffer exchange to PBS.

(A) Crude lysate with all bacterial proteins stained via coomassie. (B) shows the Western Blot analysis of EC, W1-Ki-4(scFv), W2-Ki 4(scFv) and W3-Ki-4(scFv) detected via the His₆-tag. EC and W1-Ki-4(scFv) show a high amount of protein in the sample whereas W2-Ki-4(scFv) and W3-Ki-4(scFv) reach only a weak protein concentration in the PBS eluate. The W4-Ki-4(scFv) and W5-Ki-4(scFv) proteins got lost on the PD10-desalting columns.

For further protein analysis the sample concentration of EC, W1-Ki-4(scFv), W2-Ki-4(scFv) and W3-Ki-4(scFv) was increased with Vivaspin 6 or Vivaspin 20 columns depending on the sample volume. Protein recovery by other lysis methods was not successful.

5.4.2 IMAC protein purification

Subsequently, the IMAC purification potential of the recovered native proteins was examined using the standard IMAC purification protocol (3.3.4.1) via His₆-tag and Talon or Ni-NTA columns. For binding analysis or other applications of the target protein, it

would be ideal to use purified Wx-Ki-4(scFv) or Wx-M12(scFv) proteins with few contaminating substances as possible. Non-tagged expression control proteins Ki-4(scFv) and M12(scFv) were successfully purified with the IMAC method via Ni-NTA and talon columns. For the purification, W1 and W3 tagged constructs of Ki-4(scFv) and M12(scFv) were applied to the IMAC columns. Both W1 constructs resulted in successful protein purification with a decent amount of protein in the sample (data not shown), W3-tagged constructs could not be purified by IMAC. No protein was eluted from the talon or Ni-NTA columns, neither during elution nor during washing steps. The procedure was repeated at pH 7 and pH 8, with different imidazole concentrations (10, 20, 50, 75, 100, 150, 200, 250 and 500 mM for elution but with without positive result.

5.5 Measurement of protein binding activity

Due to unsuccessful IMAC purification, the bacterial crude lysate after TES buffer lysis and dialyzed into PBS was applied for analysis of target protein binding activity. Biological functionality as well as the binding specificity of the W-tagged target proteins were examined. As shown in 5.4.1, only EC, W1-Ki-4(scFv), W2-Ki-4(scFv) and W3-Ki-4(scFv) could be used for binding analysis. The concentration of the W-tagged target proteins in the dialyzed samples was calculated to be between 3 and 40 µg/mL which was enough for the subsequent analysis experiments.

5.5.1 Wx-M12(scFv) binding analysis on MCF7 and MDA-MB-231

Flow cytometric binding analysis with the Wx-M12(scFv) fusion proteins was not successful since the M12(scFv) fragment antibody, even without W-tag, did not display binding on the MCF7 or MDA-MB-231 cells, neither during flow cytometry nor in a protein binding ELISA on MCF-7 membranes. Consequently, both cell lines were tested for the presence of the MucI surface protein which was detected to be positive on both cell lines with a commercially available anti-(human)MucI mouse IgG antibody (Abcam, Cambridge, dilution 1 : 150 in PBS) and goat-anti-mouse-FITC conjugated IgG antibody. A flow cytometric experiment verified MucI expression on the cell lines by a clear shift of 75% of the cells (data not shown).

It was concluded that the M12(scFv) fragment antibody simply does not bind to the MucI antigen unlike described by Wong et al., 2001 [238]. Binding analysis of M12(scFv) was not investigated further.

5.5.2 Protein ELISA of Wx-Ki-4(scFv) fusion proteins

Binding activity of Wx-Ki-4(scFv) target fusion proteins was tested in a protein ELISA (3.3.9.3) on L540cy membrane fractions via ABTS detection at 405 nm. PBMC membrane fractions were used as negative control antigen. Wx-Ki-4(scFv) proteins were applied as TES lysates without further processing at a concentration of 3 µg/mL protein per well (Figure 5-10). The untagged EC showed sufficient binding on the L540cy membrane fractions. Binding of W1-Ki-4(scFv) was present on L540cy membranes significantly reduced by 25% compared to EC. Binding activity further decreased for the W2-Ki-4(scFv) (by 40%) and W3-Ki-4(scFv) (by 50%) constructs, although binding for the W3-tagged version was slightly stronger. ABTS absorption signals were even more diminished for W4 and W5 tagged proteins, displayed absorption values equal to the PBMC negative control measurements. As a general observation, binding activity decreases with increasing number of tryptophan residues in the W-tag.

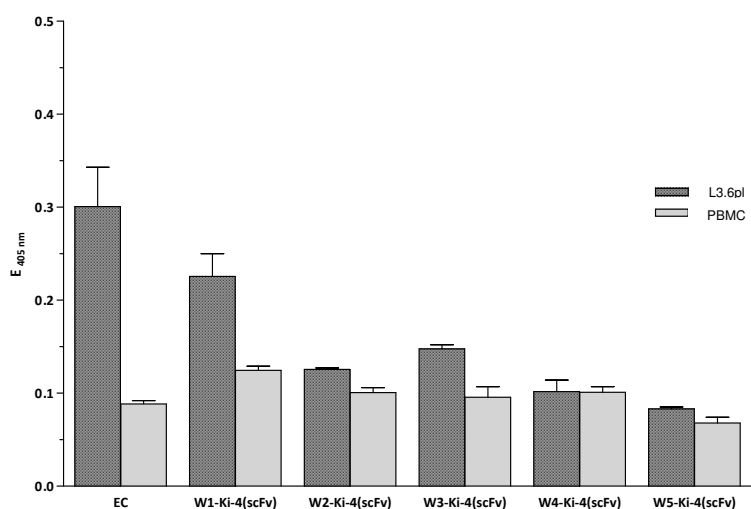


Figure 5-10 Protein ELISA binding analysis of dialyzed TES crude lysate containing all five Wx-Ki-4(scFv) fusion proteins.

Protein binding was detected via His₆-tag, anti-His mouse IgG and GAM-PO antibodies and ABTS substrate. EC displays strong binding of untagged Ki-4(scFv) protein on L540cy membrane fractions. But amount of binding continuously decreases from W1-Ki-4(scFv) to W5-Ki-4(scFv) almost reaching ABTS absorption level of the PBMC negative controls, indicating no binding activity. Overall absorption values were weak (<0.3).

5.5.3 Flow cytometric analysis of Wx-Ki-4(scFv) on L540cy

Binding activity of Wx-Ki-4(scFv) target fusion proteins was analyzed by flow cytometry using the untagged Ki-4(scFv) antibody (EC) and the W-tag constructs with one, two and three tryptophan residues as dialyzed TES lysis crude extracts. W1-Ki-4(scFv), W2-Ki-4(scFv) and the W3-Ki-4(scFv) as well as the untagged EC antibody bound to

CD30-positive L540cy cells (Figure 5-11). The W-tagged fusion protein variants showed a slightly lower binding activity than EC indicated by a slightly lower fluorescent signal of the anti-His-AF488 conjugated detection antibody.

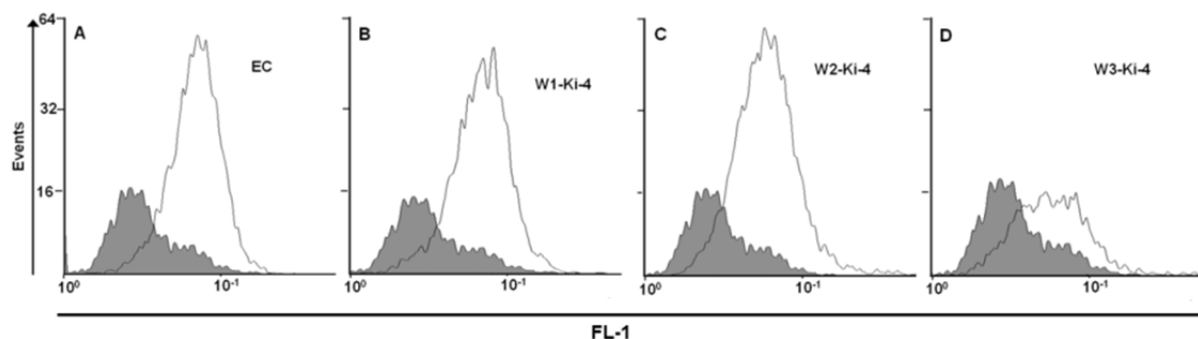


Figure 5-11 Flow cytometric binding analysis of Wx-Ki-4(scFv) fusion proteins on L540cy cells.

(A) EC (Ki-4(scFv)), (B) W1-Ki-4(scFv), (C) W2-Ki-4(scFv) and (D) W3-Ki-4(scFv). The black curve represents L540cy cells incubated with only the secondary antibody (background). The grey curve represents the different versions of the Wx-Ki-4(scFv) proteins. The signal shift to the right means increased fluorescence intensity in relation to the black curve as the antibody binds to the CD30 receptor.

Moreover, the mean fluorescence intensity (MFI) was slightly lower for W-tagged fusion proteins when EC was assumed to be 100% binding activity (Table 5-3). This reconfirmed that binding between the fusion proteins and CD30 is slightly weaker than the corresponding interaction involving untagged Ki-4(scFv).

Table 5-3 Mean fluorescence intensity (MFI) values and geometrical mean of the fusion proteins.

The MFI of the W-tagged fusion proteins is only marginally reduced compared to the MFI of the Ki-4(scFv), which is arbitrarily set at 100%. The same tendency is illustrated with the geometrical mean values. The similar mean fluorescence of the W-tagged fusion proteins compared to EC indicates that the binding of the Ki-4(scFv) is reduced when a W-tag is present.

(scFv) protein	Mean Fluorescence Intensity	% G-mean
Ki-4(scFv) (EC)	7.13	100
W1-Ki-4(scFv)	6.67	93.6
W2-Ki-4(scFv)	6.73	94.4
W3-Ki-4(scFv)	6.69	93.8

For this experiment, HEK293T cells were used as negative control cell line. As expected neither the Ki-4(scFv) without W-tag nor the W-tagged fusion proteins displayed any binding on HEK293T cells.

5.5.4 Competitive FACS

In addition, a competitive flow cytometric analysis was performed to prove that even though the binding activity was effected, specificity of Ki-4(scFv) binding was not impaired by the presence of the W-tags (Figure 5-12). Increasing concentrations of the

hybridoma-derived bivalent Ki-4 full length antibody were incubated on L540cy cells parallel to the Wx-Ki-4(scFv) proteins thus replacing the monovalent single chain fragment variable by the full length antibody. It was shown that the fluorescence intensity, indicating specific binding of the Wx-Ki-4(scFv) fusion proteins, decreased with an increasing concentration of Ki-4 full length antibody. As a result the binding curves of Ki-4(scFv) shifted to the left displaying lower fluorescence intensity. Binding of the Ki-4(scFv) and W1-Ki-4(scFv) was stronger so that higher concentrations of the Ki-4 full length antibody were necessary to suppress single chain binding than the binding of the W2-Ki-4(scFv) and W3-Ki-4(scFv). It was concluded that the Wx-Ki-4(scFv) fusion proteins still possessed active and specific binding ability. Although, the binding specificity of the fusion proteins was not impaired, a higher number of tryptophan residues results had a negative influence on the binding affinity. This was shown by deletion of the Ki-4(scFv) binding signal with a lower concentration of full length antibody for W2 and W3. [246]

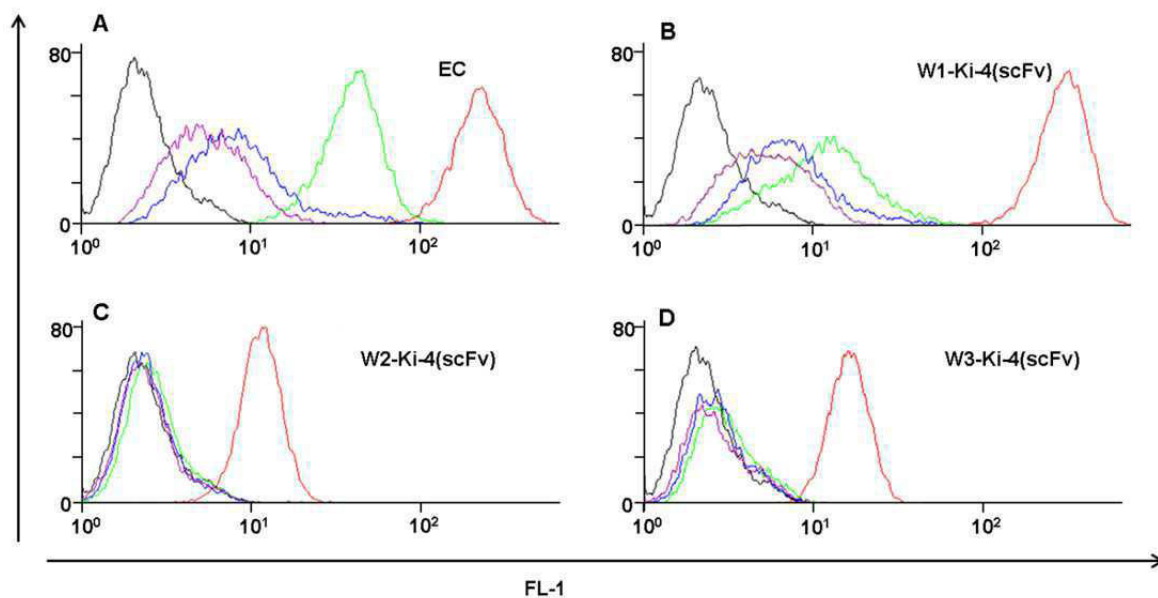


Figure 5-12 Competitive flow cytometry of Ki-4(scFv), W1-Ki-4(scFv), W2-Ki-4(scFv), W3-Ki-4(scFv) against a monoclonal Ki-4 full length antibody.

(A) Ki-4(scFv), (B) W1-Ki-4(scFv), (C) W2-Ki-4(scFv) and (D) W3-Ki-4(scFv). The black curve displays the measurement of the L540cy cells incubated with the secondary antibody α -His AlexaFluor 488 (Qiagen, Germany), the red curve presents the binding measurement of the Wx-Ki-4(scFv) protein detected via the α -His AlexaFluor 488 antibody without competitive addition of the monoclonal Ki-4 full length antibody. The green curve displays the fluorescence intensity of the Wx-Ki-4(scFv) proteins after adding and co-incubation with 0.5 μ g Ki-4 full length antibody. The blue curve presents the fluorescence intensity of the Wx-Ki-4(scFv) proteins after adding and co-incubation with 2 μ g Ki-4 full length antibody and the purple curve after the addition of 5 μ g Ki-4 full length antibody. [246]

5.6 2D fluorescence measurement of Wx-Ki-4(scFv)

To ensure that the W-tagged target fusion proteins maintained their ability to fluoresce after TES buffer extraction and buffer exchange to PBS, extracts containing the W1-Ki-4(scFv), W2-Ki-4(scFv), W3-Ki-4(scFv) and EC constructs were analyzed by two-dimensional (2D) fluorescence intensity scanning in a suitable MTP using a protein concentration of 3 $\mu\text{g/mL}$ in 200 μL volume. Only dialyzed fusion proteins, containing one to three tryptophan residues plus the lysate of the EC, were analyzed since the protein concentration for the W4 and W5 constructs was too low. Tryptophan fluorescence was excited between 250-300 nm and the resulting emission was detected in a range from 300-400 nm, using 2 nm steps for multiple measurement points. It was observed that the fluorescence intensity correlated with the number of tryptophan residues in the tag. Whereas no fluorescence was detected in empty wells (Figure 5-13A) or wells containing pure PBS (Figure 5-13B), the fluorescence intensity increased visibly from the EC (Figure 5-13C) over W1-Ki-4(scFv), W2-Ki-4(scFv) and W3-Ki-4(scFv) (Figure 5-13D-F). All crude extracts generated maximum fluorescence values at comparable excitation/emission wavelengths of 290/338 nm. [246]

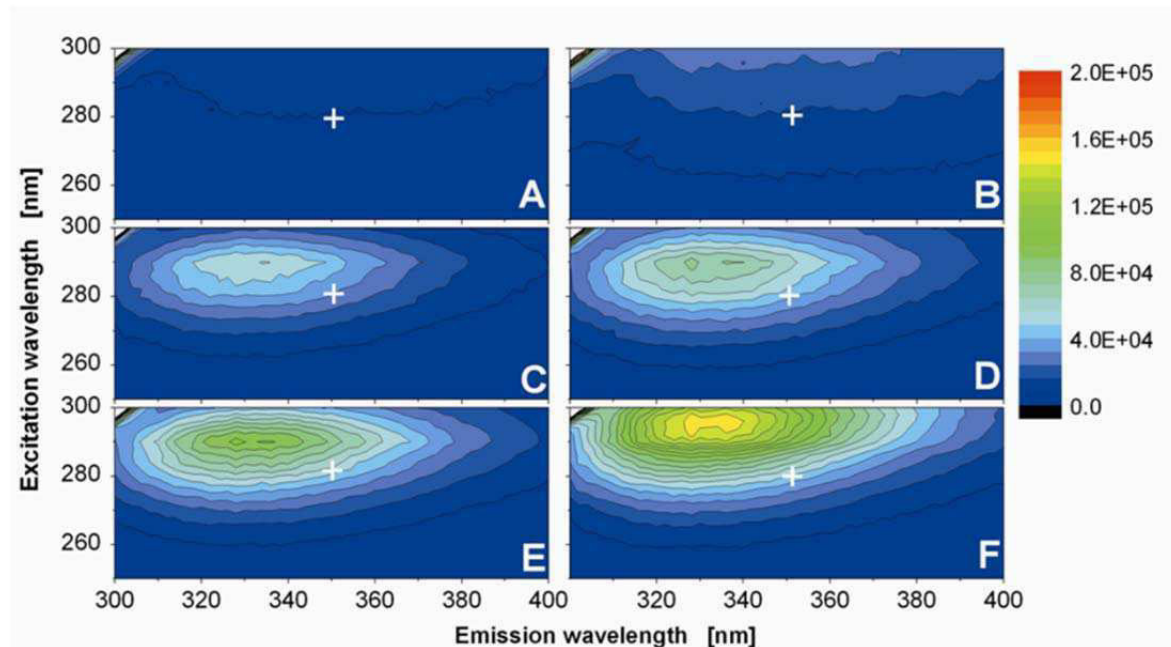


Figure 5-13 Two-dimensional fluorescence intensity scan of concentrated Ki-4(scFv) tagged with different Wx-tags.

Depicted are fluorescence measurements of (A) an empty well, (B) 100% PBS buffer, (C) EC Ki-4(scFv), (D) W1-Ki-4(scFv), (E) W2-Ki-4(scFv) and (F) W3-Ki-4(scFv). For each well, the concentration of the Ki-4(scFv) and Wx-Ki-4(scFv) fusion proteins amounts to 3 $\mu\text{g/mL}$, harvested after 10 h cultivation. The 2D scan shows that the increased fluorescence depends on the number of tryptophan residues in the tag. The empty well and PBS buffer do not generate significant signals. The cross in the diagram denotes the wavelength combination (280/350 nm excitation/emission) applied for the measurements [246].

6 Discussion

6.1 Isolation and characterization of pancreas-specific scFv antibodies

Identification of novel recombinant monoclonal antibodies specifically binding tumor-associated antigens on metastasizing pancreatic cancer cells was a major aim of this thesis. New cancer targets are desperately needed to advance potential immunotherapeutic for targeted tumor elimination and removal of residual malignant cells to improve prognosis of patients. Additionally, reliable tools for early diagnosis and follow-up examinations are essential for a solid prognosis. Using phage display technology [145] a combination of different panning strategies was applied, for the *in vitro* isolation of specific human scFv antibodies against the metastasizing pancreatic carcinoma cell line L3.6pl [155, 156]. In the process, subtractive and positive selection [138] of the human naïve Tomlinson libraries I and J [135, 136, 142] was performed under selective pressure for internalizing scFv-phage particles [138, 139, 248] or supporting surface-displayed cancer targets only [134]. The ability for internalization is favorable for a direct drug-delivery of therapeutic agents to ensure their translocation to an intracellular specific target of action. Isolation was followed by monoclonal phage ELISA screening on L3.6pl antigen. In addition to the already existing 14.1(scFv) antibody fragment isolated from an immunized murine phage display library (1.3.7), the successively eliminating characterization process of this thesis identified:

- (1) Nine novel and sequence-unique L3.6pl-specific scFv antibody fragments featured surface binding and thus are promising for potential use as diagnostics and therapeutics.
- (2) Four of these scFv antibody fragments displayed internalizing properties which renders them excellent candidates for in-cell delivery of therapeutic cytolytic fusion proteins.

In the following chapters, results will be discussed with respect to the state-of-the-art as well as to certain discrepancies and difficulties which occurred during experiments and data analysis.

6.1.1 Enrichment of L3.6pl-specific binders

Successful enrichment of antigen-specific phage particles mostly depends on three basic parameters:

- (a) The antigen source (purified protein, membrane fractions, viable cells),
- (b) the selection method (internalizing conditions, washing stringency, antigen dilution, phage valency) and
- (c) the scFv-phage library (naïve/immunized, diversity, insert-carrying phage).

Each selection round, independent of panning strategy, was started with a scFv-phage concentration between 1×10^{11} pfu/mL and 5×10^{12} pfu/mL, but selection results varied widely.

6.1.1.1 Influence of antigen presentation on enrichment

Solid-phase panning on adherent L3.6pl cells [138, 248, 249] was adopted to select pancreas-specific scFv-phage particles with explicitly internalizing potential. Whole adherent cells present their antigens in a native form and thus allow the identification of antibodies against proteins with complex conformations, such as multiple membrane-spanning regions or protein interaction domains as well as glycosylation or post-translational modifications and non-proteinogene targets [250] in their natural active form [138, 251, 252]. To eliminate irrelevant or non-specific scFv-phage particles binding to the many abundant immunogenic cell-surface epitopes regardless of tumor specificity, a competitive selection approach on non-metastasizing FG cells was applied to remove unspecific scFv antibodies from the phage pool [138, 253] before positive selection the L3.6pl target cell line (1.3.4). Competition cells (FG) and selection cells (L3.6pl) were adherently grown in tissue culture flasks to maintain cell surface appearance during panning as original as possible [248]. Intact outer-membrane protein structure and intracellular metabolic functions were supposed to favor internalization of scFv-phage particles during incubation at 37 °C under internalization pressure (3.4.5.1). Conditions for internalizing selection protocol were chosen to favor metabolically active uptake of surface-bound scFv-phage molecules into viable cells through translocation mechanisms of surface receptors [254]. Yet, using FG cells as competitive cell line proved problematic since no positive scFv binders without non-sense mutation emerged from this panning strategy. FG and L3.6pl cells feature a great similarity since the metastasizing L3.6pl cell line was directly derived, from the progenitor cell line FG, after several passages of pancreas-liver transplantations in nude mice [155, 156]. Originally exactly this similarity

should be exploited to isolate unique and extremely specific scFv binders against metastasizing and advanced forms of pancreatic cancer by application of a very stringent selection protocol. But even though a rigorous depletion of non-homogeneously presented universal background antigens is obligatory, the expression pattern on both cell lines was apparently related too closely for distinguished isolation of specific scFv binders. Consequently, potential tumor-specific binders were removed from the panning system during subtractive selection and were hence lost for the positive selection process.

During panning on L3.6pl cells in suspension, unspecific binders were excluded from the system by introducing peripheral blood mononuclear cells (PBMCs) for negative selection. Although PBMCs are of non-epithelial origin [138] and do not represent healthy pancreas tissue, they typify a highly essential cell type in the human body. Unspecific cross-reactivity of a monoclonal antibody of clinical relevance to PBMCs has to be avoided on any account. But owing to lower competitive pressure during subtraction on PBMCs, isolated clones may feature less affinity. Nevertheless, this selection method resulted in one L3.6pl-positive binder that exhibited strong binding and internalization potential.

One possibly problematic aspect of suspension panning, using originally adherent L3.6pl cells is the treatment with the enzyme-containing solution Accutase[®] for cell detachment and singularisation before panning [255]. Even though Accutase[®] is gentler than trypsin-EDTA and enhances cell viability, it still digests the protein anchorage of adherent cells thus altering their surface structure. Destruction of complex surface conformations during the singularisation process may result in isolation of scFv antibody fragments that are unable to bind antigens with intact outer protein structure. To circumvent this problematic aspect of cell manipulation by Accutase[®] treatment in the course of this thesis, cryo sections of primary pancreatic tumor tissue were introduced for phage display selection of antigens expressed *in situ* [256]. However, no enrichment of pancreas-specific scFv-phage particles was documented (data not shown) and the method was not investigated further.

Alternatively, selection antigen can be presented in form of membrane fractions (3.4.5.3), which almost behave like isolated and purified protein [134]. Those membrane vesicles were immobilized on artificial surfaces, such as Maxisorb plastic tubes or MTPs by means of hydrophobic interactions. Even though this protein presentation is uncomplicated and reliable during panning, hydrophobic immobilization may lead to exposure of

non-physiological epitopes on those synthetic surfaces. Especially membrane proteins only exist in their optimal conformation within the lipid membrane. This may result in the isolation of scFv antibodies unable to recognize the native protein in its natural surrounding [257, 258]. Moreover, the imbalanced surface-to-length ratio of the membrane fractions holds another problem since it may favor the formation of inside-out particles to compensate surface tension. Literature states that vesicles exposing the apoplasmic surface right-side-out are formed initially, but repeated thawing and freezing cycles promote formation of vesicles turning out their cytoplasmic side [134]. Selection of unspecific scFv fragments binding to cell-internal proteins may be the consequence. During monoclonal phage ELISA and protein ELISA analysis inverted membrane vesicles resulted in seven false-positive clones, whose target proteins only existed inside the cells but was presented on the surface of wrong-side out membrane particles. Consequently, there was no guarantee that living cells during flow cytometry analysis were recognized by those binders. A drawback of membrane-based panning is that the selection pressure is automatically on surface-binding scFvs antibodies. Nevertheless, three clones also displaying internalizing properties were isolated by that panning strategy.

6.1.1.2 Influence of washing stringency and buffers on enrichment

Moreover, variety and quantity of washing steps are important criteria for a successful selection process. Even though basic phage display principles are universal, it is difficult to transfer protocols to any selection antigen. Ideal panning conditions have to be determined empirically before starting a selection to ensure that cells are still intact after washing and elution [259]. Application of intensive washing steps with detergent-complemented buffers (e.g. 0.05% Tween20) might impair antigen immobilization during selection rounds. Adherently grown L3.6pl cells turned out to be very sensitive towards buffers, pH value (pH 2.2 of elution buffer) as well as shearing stress or the combination of all three parameters. Continuously changing incubation, washing and elution buffers during the panning, as well as constant motion of the liquid in the shaken vessels, had a negative effect on cell adhesiveness and membrane stability. By the second washing step, cell clusters detached from the plastic surface and burst cells were lost by partial lysis. As a result, proteases were set free from inside the cells which again had an adverse proteolytic effect on the structure of the cell surface proteins and the scFv-phage proteins itself. Hence, binding of scFv-phage particles to tumor-associated cell surface protein might have been impaired by damaged protein structures on both sides resulting in a negative panning

outcome and repetition of panning round to obtain a sufficient output titer. Tests with different buffers such as PBS, PBST, RPMI medium or NaCl (4.1.2) confirmed the sensitive nature of the L3.6pl selection cell line. Although the non-ionic detergent Tween20 destabilizes lipids and destroys membrane proteins at high concentrations [260], it resulted in the least sensitive reaction of L3.6pl cells. FG and PBMC subtraction cells were not affected since the depletion time was limited to one hour. Fixation of L3.6pl cells with 4% PFA resulted in PFA-binding scFv antibody fragments and did not solve the problem. Implementing acetone or 100% ice-cold ethanol for cell fixation was not sufficient to oppose shearing stress and cells still detached during washing steps. While permanent fixation of sensitive living cells on plastic was challenging, no antigen detachment was observed with membrane fractions due to the highly affine immobilization on the MTP plastic surface. However, varying fixation of membrane fractions was observed depending on pH of coating buffers and cell line. Experiments demonstrated that PBMC membranes reached better immobilization with PBS (pH 7.4) whereas L3.6pl and FG membranes displayed optimal adsorption to the MTP surface using standard ELISA coating buffer (pH 9.6).

Nevertheless, the number of washing steps defines selective stringency. Isolation of clones with high specificity usually fails if washing steps are not stringent enough and results in enrichment of unspecific clones [261]. Respectively, washing intensity and related optimal enrichment strongly depends on the cell line and practical realization.

Normally, ideal washing conditions are determined according to quantity of excess scFv-phage particles detectable in washing waste. But destruction of cells and release of internalized scFv-phage particles into the surrounding medium before panning was completed rendered this impossible. Consequently, selection stringency was adapted to cell sensitivity even though optimal selectivity was not achieved.

6.1.1.3 Internalizing selection conditions

Besides specific antigen recognition, development of therapeutic antibodies requires a direct or indirect effector function (1.2) [68-70]. Direct effects are induced only by antibody binding performance which can alter signal transduction pathways via cross-linking or disruption of receptor-ligand interactions, thus suppressing or stimulating cell proliferation [262]. An effector molecule fusion to a proapoptotic protein can enhance the therapeutic effect of the indirect antibody binding function. Therefore, it is essential that the recombinant antibody is transported to the target-site of pharmaceutical action located

inside of a malignant cell [83, 263]. This increases effective therapeutic concentration at the target-site and reduces systemic side-effects.

In this work, a direct method for selection of internalizing scFv antibodies was employed [138, 139] where intact L3.6pl cells were incubated at 37°C to induce internalization instead of a 4°C incubation step for surface-binding scFv antibodies. Originally, elution buffer (pH 2.2) was utilized to recover surface-bound scFv-phage before collecting internalized scFv-phage particles via cell lysis at pH 12. Even though the acidic pH was supposed to remove only surface-bound scFv-phage molecules, it also caused partial lysis of the sensitive L3.6pl cells. Hence, it was impossible to distinguish between eluted and internalized phage and difficulties occurred during output titer determination of lysis fractions after previous elution. To improve output titer results, the elution step was skipped during suspension panning to ensure that L3.6pl cells were not affected by the acidic milieu of the elution buffer and that the whole pool of binding and internalized scFv-phage particles was rescued after final cell lysis (pH 12) without loss.

6.1.1.4 Enrichment analysis by titer determination

A selection progress during panning rounds is commonly determined by analyzing the input and output titers before and after each selection round, as well as calculation of the resulting enrichment factor. However, this parameter is only suitable to a limited extent to inform about enrichment of specific scFv clones. Phage titer was determined using the plaque method which has some significant limitations, such as a limited dynamic range, dependence on environmental conditions on media resulting in decreased infectivity, viability of host cells, visual counting errors, and multiple pipetting and dilution steps as errors source [264]. Other methods for titer determination have been investigated in literature but even though it is quite time-consuming, the plaque assay is still most easily to realize without expensive equipment. Frequently, a considerable decrease of phage output titer is observed after the first panning round due to removal of unspecific scFv-phage particles. An increase in phage output titer is monitored after the second panning round caused by amplification of specific binders and continuing elimination of unspecific ones [265]. Results of this work could not confirm these findings for titer development during panning. No enrichment was observed by titer development for any of the selection strategies. By dividing input and output titer results of the same selection round, the enrichment factor was calculated ($EF = \text{output [pfu/mL]} / \text{input [pfu/mL]}$). Enrichment factors of two selection rounds were divided to obtain the actual enrichment of

L3.6pl-specific scFv-phage particles ($AE = EF_x / EF_{x-1}$). These factors allowed a better interpretation of enrichment by means of titration.

As expected, during panning on adherent L3.6pl cells, lysis and elution output titers after the first selection round were much less than the input titer, output titers after all selection rounds decreased further, documenting potential loss of binding phage (4.2.1). These calculations are consistent with the observations of cell sensitivity during panning and may explain the negative screening result. Aside from the plaque method as error source, these results suggest that due to their high sensitivity selection on adherent L3.6pl cells is not the most suitable method to isolate scFv fragments from the Tomlinson phage library.

Panning on L3.6pl cells in suspension was performed without the elution step before lysis. The calculated output titer after the first selection round decreased according to literature. Output titers of selection rounds two and three increased slightly, indicating a gain of binding scFv-phage particles (4.2.2). Additional panning rounds did not improve the amount of rescued phage particles (data not shown). It was concluded that suspension panning followed by cell lysis without preceding elution step was the better choice for panning on whole L3.6pl cells with internalization pressure.

Comparing input and output titers as well as enrichment after selection on membrane fractions displayed unexpected results. Both libraries exhibited only a slight increase of L3.6pl-binding scFv fragments throughout the three selection rounds (4.2.3). The attempt to increase stringency by applying a fourth selection round with even more stringent washing conditions resulted in “over-panning” without any determinable output titer. When merely considering the enrichment results, selection on membrane fractions seems to be a non-feasible panning strategy. Nevertheless, 16 L3.6pl-binding clones resulted from this selection strategy.

6.1.1.5 Enrichment analysis by polyclonal phage ELISA

Titer and enrichment calculations (4.2, 0) might not be necessarily significant. Even a small number of isolated binders could represent a set of scFv fragments with strong affinity and high specificity but still project a low output titer. To further evaluate successful and successive enrichment of specific scFv antibodies during selection rounds, a polyclonal phage ELISA (4.2) was performed, on L3.6pl selection membranes using PBMC or FG membranes as negative control. Thus, specifically L3.6pl-binding scFv-

phage particles were quantitatively analyzed from precipitated phage pools after each panning round by measuring ABTS absorption signals at 405 nm.

For the non-metastatic FG cell line generally less binding signal was observed than for L3.6pl during panning on adherent cells. Even though the cell lines are directly related this was expected since FG cells were used for negative selection. Binding signals of the unselected library J were quite strong pointing towards a large number of potential binders. Selection round one displayed a significant increase of binders of 150%. Compared to the first selection round, quantity of binding phage decreased by 25% after the second round and over 50% after the third round, which may be attributed to cell loss by lysis caused by buffers and shear stress. Nevertheless, the negative selection outcome might partially be due to morphological changes of the target cell line after too many passages. Moreover, it is problematic that ELISA experiments were always carried out on membrane fractions instead of whole cells as employed during panning. Presence of inside-out vesicles also might have tampered with the results when isolated scFv antibodies were unable to bind [134].

Regarding the observed enrichment of L3.6pl-binding scFv-phage units after suspension panning, the polyclonal phage ELISA displayed a contradicting result. Again absorption values of library I were very high and a 15% increase of binding scFv-phage particles was observed after the first selection round. In contrast to enrichment calculations, the amount of binders decreased by 10% during the second selection round and by another 10% during the third. One explanation for this contradiction may be the use of membrane fractions instead of whole cells [134]. In addition the Accutase[®] treatment might have had an altering effect on the surface antigen conformation of suspended cells. PBMC absorption values did not change during selection rounds but were about 25% lower than L3.6pl absorption measurements. Consequently, either general overall absorption values obtained of library I were very low or may reflect a poor quality of the new batch of L3.6pl membrane fractions used during this experiment.

During panning on membrane fractions, titer and enrichment calculations stated a slight increase of L3.6pl-binding scFv-phage units for both libraries. However, data analysis of binding documentation by polyclonal phage ELISA was able to display growing numbers of L3.6pl-binding scFv-phage particles with continuing selection. Repeatedly, absorption values of both unselected libraries were very high. After the first selection round, a 57% decrease of binders was reported for the library I and 90% decrease for the library J. After

panning round two, quantitative binding increased by 88% for library I and by 800% for library J. L3.6pl-positive binders increased another 20% for library I whereas the third selection round showed no significant increase of binders for the J library. For the library J no significant binding was observed on PBMC membranes. Very unexpected, binding value even slightly higher than the respective one for L3.6pl was measured on PBMC membranes after the first selection round. That implies that during this selection round scFv fragments binding against a universal epitope were selected. Still, the ELISA absorption values for PBMCs decreased after the second selection round indicating successful depletion of these ubiquitous surface proteins.

Tendency of polyclonal absorption values after selections of both libraries on L3.6pl membranes (4.2.3) varied from values measured after selection on whole cells (4.2.2, 4.2.3). Observed overall absorption values are much stronger than after selection on whole cells. This discrepancy may be caused by morphological alterations of cells processed for a different batch of membrane preparations of L3.6pl cells and coated for membrane panning as well as all subsequent polyclonal and monoclonal phage ELISA experiments.

6.1.1.6 Influence of phage valency

The semi-synthetic Tomlinson phage library was employed to generate recombinant scFv antibodies targeting pancreatic cancer cells. To avoid the presence of empty phage particles, which occur during production of monovalent phage [129], the polyvalent M13KO7 Δ pIII hyperphage was utilized during the first panning round and only substituted by the monovalent M13KO7 helperphage during following selection rounds [266, 267]. The polyvalent phage particle presents scFv molecules on all five pIII coat proteins and is supposed to improve selection efficiency [130] due to its increased avidity as a result of the multiplied valence-related affinity of the five binding sites. To isolate high-affinity scFv binders, the monovalent M13KO7 helperphage was applied during the second and third panning round. This monovalent structure displays strong intrinsic affinity and accuracy of fit towards a single surface epitope, whereas the multivalent phage particles may still feature strong binding activity attributable to inaccurate fit at multiple sites. By comparing of the bacterial infection rate of multivalent and monovalent phage particles via input titer calculation, no negative influence was observed. By combining these two phage valences, the first selection was supposed to retain as many L3.6pl-specific binders as possible after cross-reactivity elimination on PBMC antigen. Selections with the monovalent phage on the other hand had the aim to hold only the highly affine binders.

ELISA experiments performed with polyvalent phage particles always displayed much higher absorption signal (up to twice as high) than when performed with monovalent ones, even though the trend of binding activity was identical. This effect is due to the higher avidity of the multivalent phage format [254].

6.1.2 The Tomlinson Phage Library

6.1.2.1 Single clone analysis via monoclonal phage ELISA

After panning and enrichment analysis, single clones were picked and screened in a monoclonal phage ELISA for binding activity on L3.6pl membrane fractions. Clones with absorption signal at least 2.5-fold stronger than the background were defined positive. In summary, 1656 single clones were tested of which 12.6% were identified as L3.6pl-positive binders. Thus the overall percentage of positive scFv antibody fragments was much lower than the 50% documented in literature [267, 268].

Whole adherent cells: Of 288 picked single clones only 13 were identified as ELISA-positive binders after solid-phase panning on whole adherent cells. On the one hand, the low number of positive binders was attributed to the close relation the of FG as competition cell line to L3.6pl, and on the other hand, to the selection strategy itself being not compatible with the sensitive L3.6pl selection cell line regarding washing, blocking and elution steps as well as shear stress.

Whole cells in suspension: Merely three positive binders evolved from 216 picked clones. Although subtractive FG cells had been replaced by PBMCs, cell damage during washing was still assumed to be too severe to create optimal selective conditions even though scFv-phage enrichment was documented.

Membrane fractions: Starting with 576 clones from both libraries, best selection results were observed during panning on membrane fractions with an outcome of 193 ELISA-positive clones. A variation of ABTS absorption intensities was measured resulting in seven weak binders (absorption twice the background), six medium binders (absorption 2 – 5 x background) and seven strong binders (absorption 5 – 10 x background).

The large number of 1447 L3.6pl-negative clones (87.4%) during screening is conspicuous and suggests an ineffective and insufficiently stringent selection. As discussed in 0, reasons therefore might be the L3.6pl cell line as antigen source or non-compatible selection strategies concerning this special antigen source. Laboratory intern observations indicate

that such a low selection rate is very untypical. When compared to other selection processes with the Tomlinson Library generally only 20% of the picked clones were identified as negative during screening by monoclonal phage ELISA after application of the same panning protocols.

6.1.2.2 Sequence analysis of single clones

After screening via monoclonal phage ELISA, the scFv insert was investigated by colony PCR (3.1.1.2) and DNA sequence analysis (3.1.4). Subsequent to PCR analysis, 137 clones were found without intact scFv insert but false-positive ELISA signals. DNA sequencing identified 72 clones carrying a scFv insert, but only 20 clones containing an insert without a frame shift.

Table 4-10 shows, the localization of hypervariable CDRs in V_H and V_L numbered after Kabat [100]. For all clones, conserved framework regions (FWR) were identical [146] but alignment revealed varying amino acid sequences in CDRs. During artificial library synthesis diversification were limited to positions H50, H52, H52a, H53, H55, H56, H58, H95, H96, H97, H98 of the heavy chain, and to positions L50, L53, L91, L92, L93, L94, L96 of the light chain [146].

Moreover, the amount of 137 false-positive clones not carrying a scFv-insert (65% of 209 positive clones) was high [133] considering that only 4% of library I and 12% of library J are initially insert-free [135]. Apparently, insert-free phagemid vectors have a selective advantage [133]. One reason may be the contamination of the Tomlinson library with scFv-free vectors [133] or incomplete restriction, as well as phagemid self-ligation during library cloning [133]. In addition, low efficiency of helperphage-dependent packing of phage particles during phage rescue may lead to generation of phage particles without incorporation of scFv-pIII fusion proteins. Since the majority of phage proteins just expresses native pIII protein phage enrichment by non-specific binding activity to any antigen is favored. Besides that, a reduced vector size diminishes enrichment of specific phage. All these reasons result in a growth advantage of insert-free phage that cannot always be compensated by choice of selection strategy [133]. Selection of clones without ORF could be avoided when exclusively using the hyperphage with pIII deletion for selection [269]. Limited library size caused by a growth advantage of insert-free or defective clones results in their enrichment and may lead to an unsuccessful selection and failed enrichment during panning for all selection strategies.

Summarized, only 20 of 1656 analyzed clones displayed an intact DNA sequence for the scFv insert. Sequence analysis revealed that 8 clones contained an *amber* stop codon (TAG) within CDR 2 of V_H. TAG triplets were formed during synthetic triplet generation in CDRs of library J according to the NNK distribution (1.3.3) [147]. Library I has been produced using DVT triplet distribution (1.3.3), and thus random TAG triplet formation should not occur during library synthesis. Nevertheless, stop triplets were detected in isolated clones. This phenomenon has not been described in literature before but was observed during all selections performed with Tomlinson library I by the AG Barth. Literature states, that only 3% of the scFv antibody fragments in the original Tomlinson phage library carry an *amber* stop codon. But after screening, 90% of the isolated clones were found with TAG triplet. Still, high percentage of *amber* stop codon containing clones after selection from the Tomlinson libraries has been shown by several other groups before [153, 154, 270-272]. The *amber*-suppressor strain TG1F+ *E.coli* used for phage propagation was suspected to be the source of this phenomenon [154]. During panning this strain translates the *amber* stop codon as CAG, encoding for glutamine, instead of TAG. Clones that bind to a target antigen and contain *amber* stop codons have a considerable growth advantage in TG1F+ *E.coli* [153, 269]. Propagation for stock amplification and distribution before panning, results in evolutionary changed scFv-phage pools and subsequent selections were started with more clones carrying stop codons than the original library. Consequently, each growth cycle additionally created even more clones with stop codons. But this was not investigated further.

Aside from that, six clones were detected with *ochre* stop codons (TGA) in the conserved framework region FWR2 of V_H in isolated clones from both libraries. For their characterization, TGA triplets were therefore mutated back to TGG, encoding for tryptophan, according to the actual framework sequence documented for the Tomlinson library. It is proposed that these framework mutations could be caused by spontaneous mutation [273]. They occur always at the same position in the FWR2. Apart from spontaneous mutations, this also suggests a systemic problem which might have already existed in the initially purchased Tomlinson library.

Another explanation for the presence of TAG, as well as TGA stop codons, is the occurrence of mutations during PCR amplification reactions. DNA of positive clones was not sequenced from the phagemid vector directly but amplified first by colony PCR whose product was sequenced. When using *goTaq* polymerase without a proof-reading function for PCR reactions, the enzyme creates an error about every 9000 bases. In 30 reaction

cycles this statistically adds up to an incorrect base every 300 bases. Thus, the application of a non-proof-reading polymerase enzyme during PCR amplifications may also account for integration of TAG and TGA stop codons. Besides, inaccurate PCR amplification products might be an explanation for the 52 ELISA-positive scFv binders found with frame shift in CDR2. Resulting characteristics of single clone analysis and DNA sequencing are summarized in Figure 6-1.

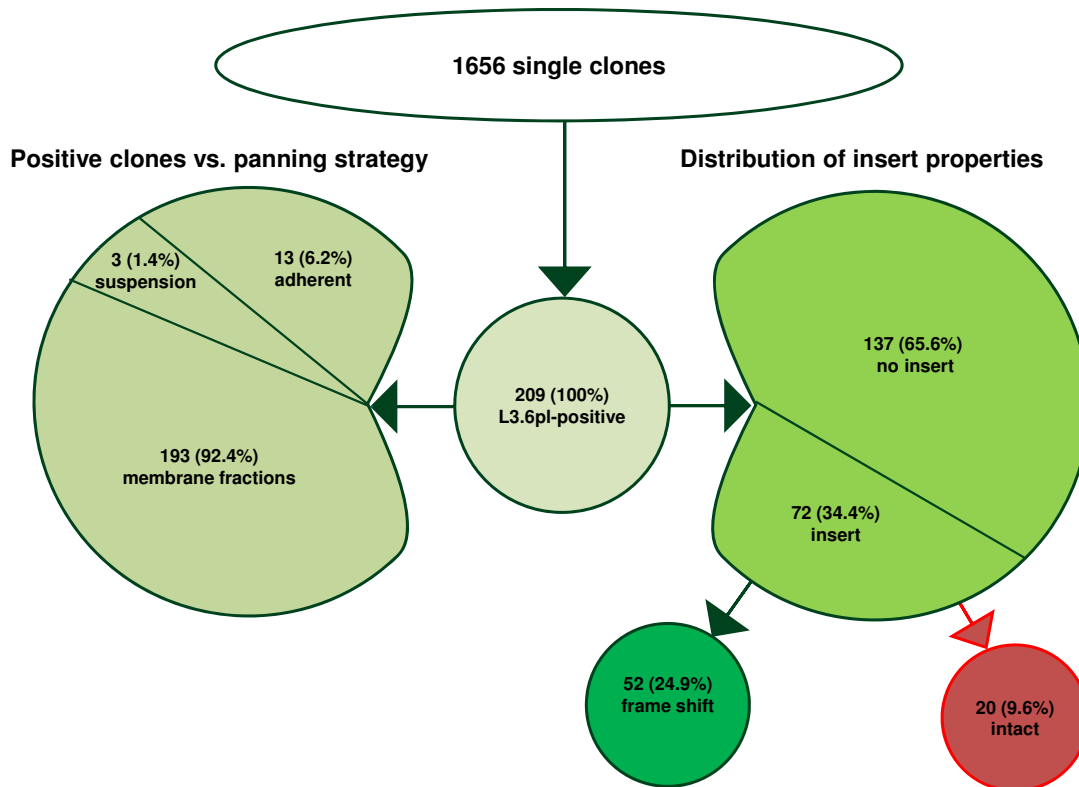


Figure 6-1 Illustrated distribution of L3.6pl-positive clones with regard to panning strategy and characteristics of scFv insert.

Colony PCR revealed 137 false-positive clones (65.6%) without scFv insert. Of the 72 clones carrying a scFv insert, 52 clones contained a frame shift in CDR2 whereas DNA sequencing verified 20 clones (marked in red) with an intact scFv sequence which could be applied for further analysis.

Moreover, clone diversity of isolated L3.6pl-positive scFv antibodies was analyzed by DNA sequencing. A total number 16 unique L3.6pl-specific binders was identified from 20 positive clones of all three selection strategies. The sequence of clone E3 was found four times and clone D12 twice. Normally, much stronger enrichment of sequence-identical clones is expected during selection on complex heterogeneous epitopes as literature states for other cell systems [274].

6.1.3 Protein Expression

After analyzing of binding activity on phage-level and DNA sequencing to identify unique binders, L3.6pl-positive scFv clones were expressed as soluble proteins in order to evaluate binding independent of phage proteins in further characterization experiments. According to the Tomlinson protocol [135], it is possible to express library-derived scFv antibodies after transformation of the pIT2 phagemid into the non-suppressor strain HB2151 *E.coli* after removal of CDR-internal stop codons. This HB2151 non-suppressor strain reads the TAG stop codon down-stream of the genetic information for the scFv antibody and terminates translation before pIII expression. Consequently, soluble scFv proteins are produced without the pIII fusion protein and are then transported into the periplasmic space via the *pelB* leader peptide and are ideally secreted into the surrounding medium. The oxidizing milieu of the periplasm favors correct protein folding (chaperones) and formation of disulfide bonds [172]. In contrast to the Tomlinson protocol, experiments, using the HB2151 for soluble protein expression and subsequent ELISA binding analysis, showed very inconsistent results. Clones tested positive during monoclonal phage ELISA analysis did not display reproducible binding as soluble protein.

SDS-PAGE and Western blot analysis showed that soluble scFv proteins were secreted only partially. Osmotic lysis of bacteria (TES buffer) to free enriched scFv proteins present in the periplasmic space did not yield better results. Generally, protein production in HB2151 bacteria was observed to be very low and inconsistent.

Expression of clones was strongly dependent on time point of IPTG-induction of the *lacZ* gene which controls the *lac* promoter. Moreover, shaking radius and velocity during cultivation were not ideal since the surface tension, as a result of a small culture volume, prevents sufficient oxygenation capacity [223]. This means that not all clones were induced properly and were therefore unable to express enough protein for repeatable and comparable binding results.

To solve this problem, the scFv were subcloned into the pET-derived pMT vector for prokaryotic protein expression in the BL21 Rosetta 2 (DE3) *E.coli* strain [171]. This expression system is under the control of the IPTG-inducible T7 promoter. Additionally, these bacteria carry the pRARE plasmid which enables them to translate DNA triplets of human origin. Nevertheless, an improvement in terms of reproducibility of protein expression and subsequent binding data was not achieved.

Therefore, and because prokaryotes are generally not able to form glycosylation or other post-translational modifications, soluble scFv proteins were expressed in a mammalian expression system [172]. Eukaryotic glycosylation also improves correct folding and conformation essential for production of functional proteins and also leads to better solubility [172]. For eukaryotic expression, the scFv genes were subcloned into the bicistronic pMS-SNAPMut vector [183] which was transfected into HEK293T cells and cultivated under Zeocin selection pressure (3.2.3). Successful transfection was monitored directly under the fluorescence microscope through co-translated eGFP down-stream of the IRES sequence. Production of scFv-SNAP fusion protein and its secretion into the tissue culture supernatant (TCSN) was evaluated via SDS-PAGE, where the prominent FBS band did not allow protein detection, and Western blotting. Therefore, protein concentration in the unpurified TCSN could not be quantified via AIDA-analysis (3.3.3.1) before scFv-SNAP proteins had been purified by means of IMAC (3.3.4). Thus, binding activity in relation to protein concentration could only be determined with pure protein. Nevertheless, presence of FBS in the unpurified TCSN favored scFv-SNAP protein stability in the HEK293T supernatant during long-term storage.

Moreover, flow cytometric binding analysis with unpurified TCSN containing scFv-SNAP displayed even better binding results than the purified scFv-SNAP proteins.

6.1.4 Soluble protein ELISA analysis

Clones identified as positive by means of monoclonal phage ELISA and sequencing, were produced as soluble proteins in HEK293T cells via the eukaryotic pMS expression system [183]. Specific binding was analyzed by indirect ELISA against functional membrane fractions of the target cell line [134].

Here, only eleven of the 16 clones, showing reproducible binding activity during monoclonal phage ELISA analysis, were identified as positive binders after soluble protein expression. Five clones did not display positive binding activity when tested in a soluble protein ELISA. This loss in functionality may be attributed to the separation of the scFv fragment from the pIII phage coat protein during subcloning into the pMS-SNAPMut vector [183]. It is possible that the phage protein had a stabilizing effect on the scFv which is now missing on the C-terminal end so that the V_L chain, normally adjoining the constant region, is now exposed to non-physiological buffers. Another reason might be the expression in HEK293T cells which rendered post-translational modifications and

glycosylation possible which did not exist during phage display selection in TG1F+ bacteria before [172]. Such post-translational changes of surface patterns may result in different binding behavior.

6.1.5 Flow cytometric binding and cross-reactivity observations

It is crucial for therapeutic applications that isolated scFv antibodies recognize the target antigen in its natural conformation (1.3.2). Most scFv antibody fragments were isolated on membrane fractions which display still functional proteins in a slightly changed conformation [134]. Another disadvantage of selection on membrane fractions is the possibility that isolated scFv candidates may bind to cytolytic epitopes on inside-out vesicles [134]. To ensure epitope recognition of native protein conformations, flow cytometric binding analysis was performed on viable L3.6pl cells. Nine out of eleven clones were tested positive on intact L3.6pl cells, only clones E5(scFv)-SNAP and F11(scFv)-SNAP did not bind to living L3.6pl cells. Loss of binding was attributed to the artificial antigen presentation of membrane fractions lacking the original complex protein conformation of intact cells (glycosylation, post-translational modifications) [138]. Moreover, isolation of scFv-phage binders to inside-out membrane particles had resulted in false-positive binding activity during previous monoclonal phage ELISA and soluble protein ELISA analysis [134].

A normalized amount of 2 µg total protein per sample demonstrated various degrees of binding strength on viable L3.6pl cells (4.6.2), caused by recognition of different surface epitopes with varying expression density. A high percentage of right-shifted cells in the histogram implied a high receptor density. Pointed curves indicated homogenous antigen expression whereas broad and flat curves implied highly variable antigen expression within the measured cell population [275]. Gating around living cells ensured evaluation of binding activity on viable cells only, apart from dead ones or cell debris.

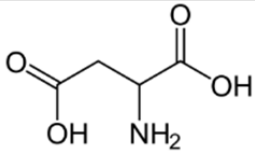
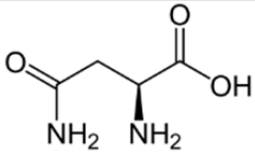
Even though binding reactions are highly specific, it is possible that recognized epitopes are also present on tumor cells of different origin. This cross-reactivity may lead to the identification of a ubiquitously expressed tumor-associated antigen (TAA) as potential new cancer target. Selected clones displayed cross-reactive binding on various cell lines to different degrees, since tumor-associated antigens vary in differentiation and activation in different organ-derived tissue. Very interesting was the binding activity on the pancreatic

carcinoma cell line PancTuI/PancTuI-*luc* [189] since clones featuring strong L3.6pl-binding were only weak binders on PancTuI/PancTuI-*luc* and vice versa (4.6.2.1).

6.1.6 Hypothesis on clones D5(scFv) and D9(scFv)

When comparing all DNA sequences of the unique scFv clones, a general sequence similarity of 93% was found. In the course of this, clones D5(scFv) and D9(scFv) attracted special attention since their sequence only differed by one amino acid in CDR2 of V_H due to one changed base pair in the DNA sequence. D5(scFv) contains aspartic acid (D) at the same position where asparagine (N) is found in D9(scFv). These amino acids are similar in atomic structure and properties (Figure 6-1).

Table 6-1 Comparing illustration of structure and characteristics of aspartic acid and asparagine.

	D5(scFv)	D9(scFv)
Amino acid	Aspartic acid (D)	Asparagine (N)
Molecular structure	 MW = 133.10 g/mol	 MW = 132.12 g/mol
Molecular formula	C ₄ H ₇ NO ₄	C ₄ H ₈ N ₂ O ₃
Properties	Acidic	Polar but uncharged side chains
	Negatively charged via proton dissociation	Electronegative groups
	Hydrophilic	Hydrophilic

Aspartic acid is formed via hydrolysis of the highly polar side chains of asparagine exchanging the amide group at to a carboxyl group. Hydrolysis generally occurs when a weak acid, such as an amino acid, is dissolved in an aqueous milieu. H₂O is constantly subjected to spontaneous ionization into hydroxyl and hydrogen ions thus promoting hydrolysis of polar substances. This fact does support the theory that D5(scFv) and D9(scFv) not only share high similarity but might even be transformed into identical molecules when exposed to an appropriate environment [276].

Highly similar or even equal amino acid sequences are likely to share the same protein fold. This can be analyzed by homology modeling based on the assumption that unknown proteins of similar molecular structure are also predicted with a similar protein fold, as it may be the case for the CDR2 regions of D5(scFv) and D9(scFv) [277]. Proteins featuring identical 3D structures are expected to recognize similar or even the same antigen target

structures. Binding behaviors of both clones during monoclonal phage ELISA as well as the protein ELISA and flow cytometric experiments were almost identical.

As already described in 4.6.2, clones D5(scFv) and D9(scFv) feature a strong right-shifted cell group comprising only 2.5% and 2% of the cell population, respectively (Figure 4-15), which could indicate existence of a certain cell subpopulation within the highly metastasizing L3.6pl cell line .

Very specific characteristics of pancreatic cancer are its high potential to metastasize and its resistance against standard chemotherapy and radiotherapy. Recent findings indicate cancer stem cells (CSC) may assume a function in the aggressive development and progression of tumors [278-282]. This stem cell hypothesis has been explored in pancreatic cancer [283] and literature describes the specific identification of CSC within digested human pancreatic tumor tissue decisively featuring the expression of CD133 [284]. Moreover, a reproducible number of CD133+ cells (1 – 2%) were identified within the human pancreatic cancer cell line L3.6pl which possesses highly metastatic properties and succeeds in inducing tumor formation after orthotopic implantation with only 10^3 cells [284]. The *in vitro* resistance of the CD133+ cells is mediated by the Chk1/Chk2 pathway, and CD133+ cells were observed to preferentially activate the DNA damage apparatus. Through up-regulation of DNA damage checkpoint response activation, CD133+ cells were able to more efficiently repair radiation-induced DNA damage than CD133- cells [285]. It is also described in literature that treatment with the first-line agent gemcitabine leads to enrichment of the CD133+ subpopulation in the L3.6pl cells cell line [284].

The hypothesis is proposed that clones D5(scFv) and D9(scFv) may recognize that CD133+ cancer stem cell subpopulation within L3.6pl (7.1). Both could be an excellent target for further investigations to remove residual and aggressively metastasizing cells following surgical tumor removal or to identify tumor antigens associated with tumor migration and proliferation.

6.1.7 Internalization behavior

Internalizing properties are a critical factor for the development of novel potentially therapeutic immunotoxins, as their effectiveness depends on the drugs' delivery and uptake into the cell metabolism [83].

Internalization was clearly verified for the murine clone 14.1(scFv), originated from a self-made immunized phage library (1.3.7) and for clones A3(scFv)-SNAP,

D4(scFv)-SNAP and F1(scFv)-SNAP isolated from the Tomlinson phage library by means flow cytometry (4.6.3.1), immunofluorescence staining and confocal-based internalization assays (4.6.3.2). Those three internalization-positive clones, originating from the Tomlinson library, represent only 2.1% of the 193 ELISA-positive clones (4.3). Literature states that phage particles with multiple scFv copies undergo receptor-mediated endocytosis more efficiently than monovalent ones since they are able to cross-link receptors [254]. Nevertheless, this effect was not confirmed for panning processes under internalization pressure within this work since only clone D4(scFv)-SNAP is the result on internalizing selections. Clones 14.1(scFv)-SNAP, A3(scFv)-SNAP and F1(scFv)-SNAP on the other hand display internalization potential despite isolation on membrane fractions.

Different patterns of surface binding and internalization were observed for the murine 14.1(scFv)-SNAP and the human clones A3(scFv)-SNAP, D4(scFv)-SNAP and F1(scFv)-SNAP. All Tomlinson-derived clones featured a spotted binding pattern on L3.6pl cells whereas the 14.1(scFv)-SNAP protein bound to the cell surface continuously (4.6.3.2). These variations of binding pattern may be caused by varying expression regulation of surface antigens or unequal distribution of receptor density. Recognition of different surface epitopes may result in different internalization mechanisms and up-take rates during translocation into the cytosol.

Observed intracellular internalization pattern was the same for all four clones. Small vesicles were transported from the cell membrane towards a location in the cell center (4.6.3.2). Internalization periods varied between 1 – 2 h for clone 14.1(scFv), ranging over clone A3(scFv) with 3 – 4 h, to clones D4(scFv) and F1(scFv) with an internalization time of 6 – 12 h. This suggests at least three different target proteins presenting different surface receptors, different internalization mechanisms or a combination of both. Generally, internalization of fusion proteins is mediated by endocytosis [286]. Receptor-mediated internalization occurs in most cases by clathrin-mediated endocytosis but many other proteins are internalized by clathrin-independent cholesterol-dependent endocytic pathways with involvement of caveolin (cholesterol, glycolipids) [83, 287]. Such lipid rafts may in consequence account for the vesicle-like spotted binding to the cell surface. The three main ways of endocytosis are: (a) Phagocytosis, (b) clathrin-dependent receptor/ligand-mediated endocytosis (also extracellular fluids), and (c) clathrin-independent endocytosis [286-288].

During internalization, scFv antibodies undergo endocytosis by entering endosomal compartments which provide an environment for sorting entering molecules. Endosomes regulate targeting of different destinations before lysosomal degradation, avoid degradation through translocation to the Golgi apparatus via retrograde trafficking pathways or relocation to the plasma membrane [287-289]. Following endocytosis, endosomal compartments are created which often fuse with lysosomes where enzymes degrade the present proteins. Thus, phage particles are either already lost during phage display selection or potential therapeutic scFv antibodies becomes useless. Besides retrograde transport ways, clathrin-independent endocytosis is sometimes able to bypass the endosome-to-lysosome pathway by offering pathogens an alternative route to avoid lysosomal enzymes [287].

Phage molecules eventually lost through lysosomal degradation during panning can be rescued by rolling circle amplification which recovers the phagemid DNA instead of the complete phage particles [290]. Thereby recovered scFv antibodies can still be used for diagnostic applications but not for clinical treatment since the lysosomal transport way might end in degradation of the therapeutic agent. Nevertheless, the conducted internalization experiments did not hint at lysosomal uptake since no diffuse fluorescent background signal was measured in L3.6pl cells during confocal microscopy.

6.2 Design of optically active W-tags

Screening of numerous large-scale cultures in parallel during production of recombinant proteins is a huge challenge when cell growth and target protein quantification have to be assessed simultaneously without disturbing the actual cultivation process. Micro-scale fermentation in MTPs [224, 228] is a very convenient technique to evaluate efficient production of enzymes or other pharmaceutically relevant target proteins. Product quantification is usually achieved by sampling and off-line analysis, e. g. by measuring enzymatic activity [231] or performing an enzyme-linked immunosorbent assay (ELISA). Still, non-invasive on-line detection systems are preferable over sampling with subsequent separate sample analysis. Using representative parameters such as optical density (OD_{600}), oxygen transfer rate (OTR) or culture fluorescence [223, 245] for monitoring, clones with optimal performance can be identified. Here, product quantification can be achieved in real-time by measuring intrinsic protein fluorescence or by expressing the target protein tagged with a fluorescent marker [231], e. g. a conventional fluorescent protein such as GFP [191] or a FMN-based fluorescent proteins [196, 200]. The second aim of this thesis

has been the design, development and characterization of a novel short and optically active reporter tag for on-line measurement purposes. Results of tag design, expression, purification and its use for the on-line monitoring of product formation in micro-scale bacterial cultures, as an alternative to GFP or FMN-based fluorescent proteins, are discussed below. [246]

6.2.1 W-tag design

A major drawback of GFP and its derivatives is the molecular large size, which may increase metabolic stress, inhibit protein folding or interfere with protein secretion into the supernatant. Moreover its ability to fluoresce is fully dependent on an aerobic environment since an anaerobic surrounding leads to a delay between expression and fluorescence development and thus its detection [191, 194, 196, 291]. In contrast to GFP, FMN-binding proteins are approximately half the size of GFP and do not depend on oxygen, but they may still cause metabolic stress and interfere with the folding of small target proteins. On the other hand, the short-chained W-tags developed in this thesis, are very small with comparatively 5-11% of the molecular weight referring to GFP. Tryptophan is known for its ability to auto-fluoresce and it does not need oxygen to mature like GFP. Therefore, it was presumed that the W-tags have full functionality even under oxygen-limited conditions. This renders them suitable for the multiplex parallel on-line analysis of bacterial cultures producing fusion proteins without any of the disadvantages caused by larger tags. Unfortunately, tryptophan is also counted to the hydrophobic amino acids. First approaches to design a tryptophan tag as imitation of the His₆-tag, with several tryptophan residues simply in series, were not pursued any further since the accumulation of highly hydrophobic properties was assumed to be problematic during expression and purification. Therefore, the tryptophan residues were embedded in the originally occurring natural structure of a protein loop derived from a cold shock protein (BcCsp) of *Bacillus caldolyticus* [236]. The natural structure was meant to compensate for the hydrophobic quality of tryptophan through neighboring residues (Figure 5-1).

With the assistance of Dr. Heinrich Delbrück (Fraunhofer IME, Aachen), energetically ideal W-tags were developed *in silico* using modeling software tools (CHARMM (www.charmm.org) in Discovery Studio (www.accelrys.com)). Corresponding DNA sequences were optimized by triplet configuration for expression in *E.coli* and then fused genetically in-frame with the coding sequence for the Ki-4(scFv) [237] or M12(scFv) [238], respectively. The tightly regulated IPTG-inducible expression vector pMT [171],

based on the pET expression system [292], was used as plasmid backbone to be able to compare non-induced cultures lacking the recombinant protein production to cultures expressing different W-tagged forms of the same recombinant antibody (Figure 5-2). [246]

6.2.2 W-tag protein expression and purification

6.2.2.1 Over-expression of W-tagged fusion proteins

SDS-PAGE and Western blot analysis of W-tagged scFv target fusion proteins after fermentation showed a generally strong over-expression of W_X-Ki-4(scFv) and W_X-M12(scFv) proteins in 96-well micro-scale cultures as well as in larger culturing volumes. Very peculiar are the protein bands in Figure 5-4 since their molecular weights do not correspond to the calculated values. The molecular mass of the W-tagged proteins containing two to five tryptophan residues, show a continuously decreasing trend in size on the immunoblot even though molecular weight should increase with higher residue number (Table 5-1). The migration of proteins during SDS-PAGE analysis strongly depends on the negative charge attached to the protein as well as its length. Electrophoresis running buffer is supplemented with the ionic detergent SDS which binds to the hydrophobic protein regions. SDS places a negative charge on proteins with a constant charge-to-mass ratio, and in addition disrupts secondary and tertiary structures. Since tryptophan contains the hydrophobic indole ring system as side chain, it was assumed that proteins with more tryptophan residues and consequently increased hydrophobicity are surrounded by a higher negative charge, and simply move faster despite their higher molecular mass. But this phenomenon could also be explained by incomplete denaturation of some W-tagged proteins resulting in limited mobility at this certain polyacrylamide content. Addition of more reducing agents, such as β -mercaptoethanol or DTT, into the protein loading buffer could solve this problem [293].

Expression evaluation of the W-tags revealed that fusion proteins were not secreted into the medium which essentially complicated protein retrieval and quantification. Lacking secretion was probably caused by the hydrophobicity of the tryptophan residues and their placement on the outer shell of the protein loop. High amounts of protein were detected in the bacterial pellet for periplasmic as well as cytoplasmic expression of W-tagged proteins (5.2.1). The double bands during immunoblot analysis (Figure 5-3) occurred due to the incomplete cleavage of the *pelB* leader when the fusion protein was transported from the cytoplasm to the periplasmic space. The identity of each protein band has been confirmed

by mass spectrometry (data not shown). The oxidizing environment of the periplasmic space promotes the correct disulfide bond formation and folding [172] of recoverable proteins in a soluble state.

Nevertheless, excessively produced proteins, especially when expressed in the cytoplasm, may be present as insoluble precipitate, called inclusion bodies (IBs). These protein aggregates, consisting mostly of incorrect or only partially folded proteins, can reach a diameter of 0.2 – 1.5 μm , so that a single IB may fill out a single cell. IBs feature a porous but defined conformation and can accumulate up to 50% of the total amount of cell protein [178, 294, 295]. The proportion of biologically active protein within a cell can vary widely depending on the production organism and the target protein. To rescue inactive protein from IBs, often requires labor-intensive and expensive protein back-folding during down-stream processing. Even though the formation of IBs is very likely to occur in the neutral and aqueous milieu of the cytoplasm during expression, this possibility was not investigated further [178, 294, 295].

Considering observations of protein formation over time (Figure 5-5), it was found that the target protein concentration in MTP cultures peaked between 9 and 10 h of fermentation but decreased afterwards. A possible explanation is that the W-tagged proteins are degraded by the temperature used for fermentation (37 °C), or that the bacteria simply kept growing and produced more biomass but no target protein. Since the target protein content was calculated referring to the total bacterial protein concentration, this would account for the diminished quantity. [246]

6.2.2.2 W-tag fusion protein recovery and purification

Extraction of soluble Wx-Ki-4(scFv) and Wx-M12(scFv) protein with EDTA-containing TES buffer resulted in the partial release of proteins, tagged with W1, W2 and W3, from the cell pellet. W-tagged fusion proteins with four and five tryptophan residues (W4, W5) could not be detached from the bacterial pellet and were consequently analyzed by neither flow cytometry nor 2D-fluorescence intensity scanning. It was assumed, that the protein recovery rate decreased with increasing number of tryptophan residues in the W-tags due to increased adherence to the cell membranes as a result of enhanced hydrophobicity. Since the negative hydrophobic effects of tryptophan become stronger with the accumulation of residues, it can be said that protein yield is strongly dependent on the number of tryptophan in the W-tag. Application of stronger lysis buffers with different detergents might improve the recovery of soluble target fusion protein in the future [221].

Purification of the tagged recombinant proteins by immobilized metal ion chromatography (IMAC) was unsuccessful. This was attributed to the close proximity of the W-tag to the His₆-tag under the assumption that the affinity tag was obscured by the larger tryptophan-rich tag. Another possibility is the incomplete removal of EDTA from the TES lysis buffer via dialysis. EDTA can form complexes with Co²⁺ ions and elute them from the IMAC resin, thus preventing the capture of His₆-tagged proteins. Moreover, steric hindrance might prevent protein recovery by IMAC which leads to potential solutions that include switching the order of the His₆-tag and W-tag, separating them with an intervening linker, or appending them to different termini. If the presence of EDTA is preventing sufficient recovery, then a potential solution would be to replace the His₆-tag, for example with a FLAG epitope [186]. This would also prevent EDTA disrupting down-stream purification strategies involving the use of Ni-NTA or talon columns.

Difficulties during IMAC purification could also be caused by the formation of dimeric complexes between the accumulated tryptophan residues and the positively-charged Co²⁺ and Ni²⁺ metal ions [296]. Such interactions of the negative end of the indole ring system with double-charged metal cations play a role in some ion channels (e.g. gramicidin-A channel [297]). Both metal ions applied via IMAC columns form so-called open-shell monomeric or dimeric complexes with tryptophan, but Ni²⁺ complexes are by far more stable [296]. Even though the IMAC purification system exploits binding of histidine-based affinity tags to the Ni²⁺ or Co²⁺ purification matrix, the strong binding and very stable complexes might be a problem during elution. Since none of the target protein was detected in the flowthrough, it was assumed that the W-tagged target proteins containing two to five tryptophan residues potentially complexed with the metal ion matrix to such a degree that rendered a successful protein recovery impossible.

This purification problem could eventually be solved by aqueous two-phase extraction as described by Nilson et al. [221, 298, 299], where the hydrophobicity of accumulated tryptophan residues is utilized to specifically concentrate those tryptophan-enriched target proteins within an organic solvent by extraction. [246]

6.2.3 Online measurement of fluorescence intensity

During non-invasive on-line measurements of micro-scale fermentations in 96-well MTPs (3.1.9.3, 5.3.1), the induced cultures showed a strong over-expression of the Wx-Ki-4(scFv) fusion proteins. Target fusion proteins equipped with the different tags could be distinguished according to the intensity of the fluorescence signal in comparison

to the untagged protein. Statistically, every cell contains proteins that include tryptophan residues, resulting in a mixed fluorescence signal which is produced by all induced cultures expressing W-tagged recombinant target proteins. This signal is composed of the fluorescence intensity of both, the product fusion protein and the biomass. Therefore, induced and non-induced cultures had to be cultivated in parallel to determine the biomass signal, which was then subtracted from the total fluorescence to calculate the signal for the W-tagged recombinant target protein alone (Figure 5-6E). Normally, this would double the number of assays required for one experiment as well as the number of wells occupied in MTPs. However, since the correlation between fluorescence intensity and scattered light intensity for the non-induced cultures was the same for all fusion protein variants, it should be sufficient to cultivate just one of the variants as a non-induced control to determine biomass fluorescence. Moreover, fluorescence intensity of each fusion protein was substantially greater than that of the corresponding untagged target protein (Figure 5-6F), even when that protein contained multiple tryptophan residues [300-302].

This calculated product fluorescence intensity increased with the number of tryptophan residues from EC over W1 to W3. Even though W4 and W5 comprise a higher number of tryptophan residues they featured slightly weaker fluorescence intensity than W3. Supposedly, the enhanced hydrophobicity of the accumulated tryptophan residues resulted in a preferential interaction of the fusion proteins with the cell membranes, which may have caused partial quenching of fluorescence intensity. However, instead of hydrophobicity, the formation of exciplexes presents another probable explanation for the quenched fluorescence signals. Exciplexes are photo-induced electron transfer reactions, which occur during bimolecular encounter of an excited molecule and a quencher [303, 304]. The dense packing of tryptophan residues in W4 and W5, as well as the increasing target product concentration towards the end of the fermentation, may support exciplex formation. Quenching, and thus a decrease in fluorescence signal intensity may be a consequence of that effect. Nevertheless, when comparing protein expression by means of immunoblotting and fluorescence intensity development via on-line monitoring, it could be confirmed that an increase in fluorescence intensity was equivalent to protein product formation.

Slightly increased scattered light and tryptophan fluorescence signals were monitored during MTP fermentation, but no bacterial growth was detected. Even though the MTPs were sealed with a gas permeable membrane, some small degree of evaporation was

present. Consequently, the medium components became more concentrated and the signals, especially the scattered light signal, increased.

From 10 h onwards, the scattered light signals increased for the EC and NC cultures and, after a short stationary period, in the other cultures as well (Figure 5-6A). This occurrence may reflect morphological changes of the bacteria [305].

The W-tagged Ki-4(scFv) and M12(scFv) target proteins produced without *peIB* leader peptide, featured similar curves as cultures with *peIB* leader in Figure 5-6 and Figure 5-7, except that the overall measured values for the tryptophan fluorescence intensity were weaker than the signal for clones with *peIB* leader (data not shown). This is a logic result since, without *peIB* leader, the proteins are transported into the cytoplasm inside the bacterial cells and not to the periplasmic space which is located between the outer and inner cell membrane.

Identical results for the on-line analysis in MTPs were obtained with a second but unrelated M12(scFv) antibody fragment [238], demonstrating that the W-tagging concept is generally applicable. But bearing in mind that the W-tags described in this thesis are prototypes only, it is also possible that their general performance could be improved by additional structural modifications. [246]

6.2.4 2D-scans

Dialyzed crude cell lysates of EC and Ki-4(scFv) tagged with W1 to W3 were analyzed by two-dimensional scanning (5.6) to prove whether W-tagged target proteins outside the cell display similar fluorescence behavior than within bacterial cultures. It is known, that excitation and emission properties of tryptophan are strongly influenced by other compounds in the solution [302]. During on-line monitoring, tryptophan fluorescence was excited at 280 nm and fluorescence emission was recorded at 350 nm. Unfortunately, these wavelengths could not be adopted for the tryptophan fluorescence 2D scans of dialyzed crude extracts (Figure 5-13). Instead, maxima were observed at 292 nm (excitation) and 338 nm (emission). This discrepancy was attributed to the different ionic strength (polarity) and buffer composition, resulting from the surrounding solution during the cultivation (Wilms-Reuss medium, (2.3)) and the off-line measurement of the 2D-analysis (PBS, (2.7)). Nevertheless, these differences in the excitation and emission wavelengths do not principally affect the values of the data, but it is necessary to determine optimal

measurement wavelengths on a case-by-case basis for individual fusion proteins, media compositions, pH values and other parameters.

6.2.5 Flow cytometric binding analysis

Binding activity of the Ki-4(scFv) target fusion proteins was tested for the untagged EC as well as for the W-tagged versions comprising one, two and three tryptophan residues using dialyzed TES lysis extracts (5.5.3). The binding activity of Ki-4 (scFv) [237] was not affected by the presence of the W-tags. All different W-tagged versions of the Ki-4(scFv) antibody fragment were able to bind the L540cy cell line that over-expresses the corresponding CD30 receptor. The slight decrease of fluorescence signal (especially for W3-Ki-4(scFv)), illustrated by the MFI and geometrical mean (%G-mean), may result from the binding of the secondary antibody to the His₆-tag of the fusion proteins (Figure 5-11). It is possible that the His₆-tag is partially obscured by the W-tag, or that the W-tag folding itself causes this change (Table 5-3). It may also be that the W-tag negatively influences binding activity with increasing number of tryptophan residues in the tag as already shown in Figure 5-11.

Binding of the W-tagged M12(scFv) antibody fragment could not be tested due to non-existent binding activity on the mamma-derived carcinoma cell lines MCF-7 and MDA-MB-231, despite proven presence of the MucI receptor on the cell surface.

Competitive flow cytometry revealed that, notwithstanding adverse effects binding activity, the binding specificity against CD30 was not influenced by the W-tags (5.5.4) but that the binding affinity of W2-Ki-4(scFv) and W3-Ki-4(scFv) was lower when incubated against a Ki-4 full length antibody.

7 Outlook

7.1 Pancreas-specific scFv antibody fragments

Evaluation of the generated L3.6pl-positive antibody fragments (4.6.2) for application in diagnostic pathology could provide data on early tumor diagnosis. The detailed functional binding activity of the scFv-SNAP antibodies could be tested on primary human tumor material, using cryo-preserved and paraffin-embedded tissue blocks alike. Immunohistochemistry staining on as many different patient tissues as possible would lead to valuable conclusions on their clinical relevance. Co-staining with known tumor markers, such as CA19-9 (gold standard), CA 124 or CEA [19, 50, 306] could verify or exclude binding to tumorous tissues and possibly classify new ubiquitous tumor antigens.

Additional prospective experiments may focus on the antigen identification of the tumor-associated epitopes bound by the pancreas-specific scFv antibodies. Since the isolated ligands were selected on undefined antigen binding sources, this could pave the way for the categorization of novel diagnostic cancer targets and insights into the structure of cancerous surface proteins used as potential immunotherapeutic targets. Therefore, conventional cell lysis followed by immunoprecipitation and Western blot analysis [233] with subsequent mass spectrometry is exploited before analysis of the antigen molecules using the MASCOT protein data base (Matrix Science, London, UK). Another method is the generation of a cDNA library originated of the mRNA from L3.6pl cells [307]. Antigens expressed from cDNA-carrying vectors are screened for binding activity by means of ELISA and analyzed via comparison in protein data banks after PCR amplification. Mammalian-based libraries have the advantage of antigen presentation in a natural surrounding including post-translational modification whereas prokaryotic expression libraries are more diverse but do not always fold proteins to their native conformation.

Ligands with the biological function for internalization are promising candidates for immunotoxin fusions, prospectively used during targeted therapeutic approaches. Their small size is ideal for delivery to a target location within the cytosol resulting in a high value for adjuvant therapy and the focused elimination of residual cancerous cells. *In vitro* examinations of immunotoxin fusions of the scFv antibodies to the truncated version of *Pseudomonas aeruginosa* Exotoxin A' (ETA') [157, 159, 171, 175] for binding activity and cytotoxicity on L3.6pl and PancTuI-*luc* cell lines (XTT assay) will indicate whether or

not one of the ligands at hand are therapeutically relevant. Compared to other toxins, ETA' is very efficient so that the internalization of one to ten molecules into the cytosol is theoretically enough to destroy the cell [85, 87]. As a drawback, ETA' is not a human toxin and will provoke an immune response during repeated application. Systemic application of ETA' fusion proteins may lead to several dosage-dependent side effects [88, 308], caused by the high immunogenicity. Human enzymes with cytotoxic effector domains, such as the human RNaseA (angiogenine) [89], the serine protease GranzymeB [91, 92] or DAPKinase [90] can be used instead.

Succeeding *in vitro* analysis, recombinant immunotoxins will be characterized *in vivo*. This includes an analysis of the *in vivo* toxicity by establishing the maximum tolerable dosis [309, 310] as well as investigations of the effect of the novel recombinant immunotoxins on subcutaneous tumor growth during treatment in comparison to Gemcitabine. A pre-clinical orthotopic mouse model (SCID or NOD-SCID strains) based on the PancTuI cell line marked with click-beetle red luciferase (PancTuI-*luc*) [189] can be used for investigations on targeted tumor imaging.

Therapeutic recombinant antibody-SNAP fusions not only hold the potential for *in vivo* optical imaging techniques after fluorescence-labeling [158, 211] but can also be applied as theranostics when for example coupled to Fe-particles. Here, the SNAP-tag technology could be applied to generate scFv fusion antibodies, labeled with supermagnetic iron oxide nanoparticles. This would create a non-invasive *in vivo* detection system, combining tumor localization as well as treatment and post-operative monitoring. For diagnosis, the molecules can be detected by MRI [311] without radiolabeling [312], and then an alternating magnetic field (AMF) can be used to induce mild heating [313], raising the temperature of the targeted cancer cells above 42.5°C and thus destroying the cells through a combination of protein denaturation and aggregation, cytoskeletal disruption, inhibition of DNA, RNA and protein synthesis, lipid peroxidation and inhibition of repair.

7.2 Characterization of optically active W-tag

Optically active reporter tags are essential tools for the on-line monitoring of product formation during fermentation of recombinant target proteins. The W-tags, newly developed during this work, show great promise. Due to their high fluorescence intensity compared to untagged recombinant proteins, future research may focus on optimizing the presented W-tags to improve secretion or ways to release the W-tagged proteins from the

bacterial pellet. Empirical switching of number and order of the tryptophan residues might result in optimized fluorescence intensity during on-line measurement and increase protein recovery yield. Apart from free energy calculations (CHARMM (www.charmm.org) in Discovery Studio (www.accelrys.com)), it is very difficult to predict fluorescence and expression behavior of newly designed W-tags and their protein fusions by means of software analysis and additional empirical data collection is unavoidable.

Protein extraction via aqueous two-phase extraction techniques [221, 298] could solve the problematic of low to non-existent protein yield during purification via the IMAC method. The highly hydrophobic character of the W-tags posed a huge disadvantage throughout the experiments of this thesis. Here, the capability of the aromatic ring system to interact with a long-chained organic solvent might actually be advantageous to the extraction process which could result in highly concentrated W-tagged recombinant proteins in the hydrophobic phase. Afterwards, enterokinase digest could cleave the tag-region from the recombinant protein and finally functionalize the target protein for potential therapeutic approaches, such as immunotoxin treatment during targeted cancer therapy.

Adaptation of the W-tags to a eukaryotic expression system offers the benefit of incorporated glycosylation and other posttranslational modifications within proteins of mammalian origin. Appropriate enzyme restriction sites (*XbaI*) to insert the W-tag into the pMS-SNAPMut expression vector [183] have already been included into the cloning constructs ordered from GENEART. Subsequent transfection and expression in HEK293T cells would reveal information about the applicability of the novel W-tags in eukaryotes.

Small size and repeated insertion of tryptophan residues within short distance, makes the W-tags potentially suitable for the application as affinity tag. Phage display selection against the purified W-tag protein [314, 315] could generate a highly specific antibody for use during immunodetection.

8 Summary

Pancreatic cancer is a most aggressive type of neoplasia characterized by its high potential for metastasis with a most devastating prognosis. Initial stages are almost asymptomatic, thus preventing early detection before local tissue invasion due to the lack of reliable diagnostics. Surgical removal in combination with standard first-line chemotherapeutic Gemcitabine treatment and radiation-based therapy are merely life-prolonging options. High resistance towards conventional therapeutics and the huge metastasizing potential leaves minimal residual micrometastasis accountable for an enormously high relapse rate. Despite its low incidence (3%), pancreatic cancer is the 4th leading cause of death caused by malignant diseases. Therefore, the first aim of this thesis was to develop novel tumor-specific human single chain antibody fragments (scFv) for possible future application as cytolytic therapeutics for adjuvant treatment of metastasizing pancreatic cancer, as well as more efficient molecular tools for early diagnosis. Antibody-based approaches using highly specific scFv fragments present a promising alternative to conventionally applied therapies. Phage display technology was employed to generate pancreas-specific scFv-phage antibodies from the naïve human Tomlinson phage libraries I and J binding against unknown tumor-associated antigen. Highly specific scFv-phage ligands were isolated in a two-step panning strategy via depletion on human peripheral blood mononuclear cells (PBMC), followed by a positive selection on the metastatic pancreatic cancer cell line L3.6pl. Monoclonal phage ELISA identified 16 unique L3.6pl-positive scFv binders, subsequently expressed in eukaryotic HEK293T cells as soluble scFv proteins fused to the SNAP-tag (scFv-SNAP). Additionally, clone 14.1(scFv)-SNAP, originally isolated from a laboratory-own murine immunized phage display library, was included into the expression and characterization process. Analysis of binding specificity of IMAC-purified scFv-SNAP proteins by soluble protein ELISA and flow cytometry identified nine clones recognizing L3.6pl cells with differing cross-reactivity to various pancreas-derived cell lines. Of these, four clones displayed internalizing properties during flow cytometric and OPERA-based internalization tests. All positive candidates are clinically relevant pancreatic carcinoma specific scFvs and may provide the prospect of a tumor-targeted cancer therapy to eliminate residual cancer cells. Moreover, they are highly promising candidates for diagnostic *in vivo* imaging tools besides an additional application as theranostics.

To produce recombinant pharmaceutically relevant proteins on large scale, highly efficient screening technologies have been developed to characterize optimum cultivation

conditions for bacterial growth and production formation. Microtiter plates (MTPs), in combination with measurement systems such as the BioLector[®], are a practical tool for non-invasive on-line monitoring of product formation of continuously shaken microbial cultures on lab-scale. Conventional reporter proteins for on-line monitoring, such as GFP and its derivatives or flavin mononucleotide (FMN)-based fluorescent proteins, are very large (26.9 kDa and 15.7 kDa, respectively) which possibly imposes stress on the host organism. Additionally, GFP strongly depends on an oxygen-saturated environment for fluorophore formation. To circumvent mentioned drawbacks of conventional reporter tags, short but still optically active reporter tag for on-line detection were designed in this thesis. These novel reporter tags (W-tags) are based on the auto-fluorescence of the aromatic amino acid tryptophan (W). Using *in silico* techniques, between one and five tryptophan residues (W1 - W5) were accumulated in the naturally occurring protein loop of the cold shock protein (Bc Csp), originated from *Bacillus caldolyticus*, to have equilibrated charges with the tryptophan residues presented on the outer side of the loop. Genetic fusions of these five different W-tags (MW = 3.4 to 5.6 kDa) to the anti-CD30 Ki-4(scFv) as well as the anti-MucI M12(scFv) antibody fragment were produced in the pET-derived prokaryotic pMT expression system. Analysis of on-line product fluorescence intensity during fermentation in MTPs followed by molecular biological flow cytometric binding analysis showed that more tryptophan residues within a W-tag generated a stronger tryptophan fluorescence signal gaining intensity corresponding to product formation. Nevertheless, an increase in tryptophan residues also complicated concentration of W-tagged proteins in the cell lysate. Protein recovery was only possible for W-tagged constructs containing one to three tryptophan residues. W4 and W5 remained in the cell pellet due to highly hydrophobic properties of the accumulated tryptophan molecules. Normal and comparative flow cytometry of W-tagged Ki-4(scFv) proteins on L540cy cells, in combination with a Ki-4 full length antibody, confirmed that binding specificity was not influenced whereas W-tags with more than one tryptophan residue seemed to have a negative effect on binding activity and affinity. Lacking the main drawbacks of conventional reporter proteins, the novel W-tags are a generally applicable alternative during non-invasive monitoring of recombinant product formation. They present the possibility for rapid and qualitative on-line measurement during large-scale production of pharmaceutically relevant target proteins.

9 References

1. (Hrsg), R.K.-I.H.u.d.G.d.e.K.i.D.e.V., *Krebs in Deutschland 2007/2008*, 2012: Berlin.
2. Bray, F., et al., *Global estimates of cancer prevalence for 27 sites in the adult population in 2008*. Int J Cancer, 2013. 132(5): p. 1133-45.
3. Ferlay, J., et al., *Estimates of worldwide burden of cancer in 2008: GLOBOCAN 2008*. Int J Cancer, 2010. 127(12): p. 2893-917.
4. Hanahan, D. and R.A. Weinberg, *The hallmarks of cancer*. Cell, 2000. 100(1): p. 57-70.
5. Hanahan, D. and R.A. Weinberg, *Hallmarks of cancer: the next generation*. Cell, 2011. 144(5): p. 646-74.
6. Burkhart, D.L. and J. Sage, *Cellular mechanisms of tumour suppression by the retinoblastoma gene*. Nat Rev Cancer, 2008. 8(9): p. 671-82.
7. Junttila, M.R. and G.I. Evan, *p53--a Jack of all trades but master of none*. Nat Rev Cancer, 2009. 9(11): p. 821-9.
8. Levine, B. and G. Kroemer, *Autophagy in the pathogenesis of disease*. Cell, 2008. 132(1): p. 27-42.
9. Adams, J.M. and S. Cory, *Bcl-2-regulated apoptosis: mechanism and therapeutic potential*. Curr Opin Immunol, 2007. 19(5): p. 488-96.
10. Cory, A.H. and J.G. Cory, *Understanding interactions between and among apoptosis inducing pathways in tumor cells*. In Vivo, 2007. 21(2): p. 245-9.
11. Blasco, M.A., *Telomeres and human disease: ageing, cancer and beyond*. Nat Rev Genet, 2005. 6(8): p. 611-22.
12. Baeriswyl, V. and G. Christofori, *The angiogenic switch in carcinogenesis*. Semin Cancer Biol, 2009. 19(5): p. 329-37.
13. Berx, G. and F. van Roy, *Involvement of members of the cadherin superfamily in cancer*. Cold Spring Harb Perspect Biol, 2009. 1(6): p. a003129.
14. Bergfeld, S.A. and Y.A. DeClerck, *Bone marrow-derived mesenchymal stem cells and the tumor microenvironment*. Cancer Metastasis Rev, 2010. 29(2): p. 249-61.
15. Fang, S. and P. Salven, *Stem cells in tumor angiogenesis*. J Mol Cell Cardiol, 2011. 50(2): p. 290-5.
16. Beger, H.G., *The pancreas : an integrated textbook of basic science, medicine, and surgery*. 2nd ed2008, Malden, Mass. ; Oxford: Blackwell Pub. xv, 1006 p.
17. Society, A.C. 2012.
18. Beger, H.G., et al., *Treatment of pancreatic cancer: challenge of the facts*. World J Surg, 2003. 27(10): p. 1075-84.
19. Maitra, A. and R.H. Hruban, *Pancreatic cancer*. Annu Rev Pathol, 2008. 3: p. 157-88.
20. Jemal, A., et al., *Global patterns of cancer incidence and mortality rates and trends*. Cancer Epidemiol Biomarkers Prev, 2010. 19(8): p. 1893-907.
21. Jemal, A., et al., *Cancer statistics, 2010*. CA Cancer J Clin, 2010. 60(5): p. 277-300.
22. Lynch, S.M., et al., *Cigarette smoking and pancreatic cancer: a pooled analysis from the pancreatic cancer cohort consortium*. Am J Epidemiol, 2009. 170(4): p. 403-13.
23. Olson, S.H. and R.C. Kurtz, *Epidemiology of pancreatic cancer and the role of family history*. J Surg Oncol, 2013. 107(1): p. 1-7.

24. O'Rorke, M.A., et al., *Can physical activity modulate pancreatic cancer risk? a systematic review and meta-analysis*. International Journal of Cancer, 2010. 126(12): p. 2957-2968.
25. Howes, N., et al., *Clinical and genetic characteristics of hereditary pancreatitis in Europe*. Clin Gastroenterol Hepatol, 2004. 2(3): p. 252-61.
26. Guerra, C., et al., *Chronic pancreatitis is essential for induction of pancreatic ductal adenocarcinoma by K-Ras oncogenes in adult mice*. Cancer Cell, 2007. 11(3): p. 291-302.
27. Brune, K., et al., *Genetic and epigenetic alterations of familial pancreatic cancers*. Cancer Epidemiol Biomarkers Prev, 2008. 17(12): p. 3536-42.
28. Brune, K.A., et al., *Importance of age of onset in pancreatic cancer kindreds*. J Natl Cancer Inst, 2010. 102(2): p. 119-26.
29. Edge, S.B. and C.C. Compton, *The American Joint Committee on Cancer: the 7th edition of the AJCC cancer staging manual and the future of TNM*. Ann Surg Oncol, 2010. 17(6): p. 1471-4.
30. Brand, R., *The diagnosis of pancreatic cancer*. Cancer J, 2001. 7(4): p. 287-97.
31. Koido, S., et al., *Current immunotherapeutic approaches in pancreatic cancer*. Clin Dev Immunol, 2011. 2011: p. 267539.
32. Schramm, H., *[Pancreatic cancer--diagnostics and therapy]*. Zentralbl Chir, 2003. 128(5): p. 367.
33. Henne-Bruns, D., et al., *Surgery for ductal adenocarcinoma of the pancreatic head: staging, complications, and survival after regional versus extended lymphadenectomy*. World J Surg, 2000. 24(5): p. 595-601; discussion 601-2.
34. Lim, J.E., M.W. Chien, and C.C. Earle, *Prognostic factors following curative resection for pancreatic adenocarcinoma: a population-based, linked database analysis of 396 patients*. Ann Surg, 2003. 237(1): p. 74-85.
35. You, D.D., et al., *Prognostic factors and adjuvant chemoradiation therapy after pancreaticoduodenectomy for pancreatic adenocarcinoma*. J Gastrointest Surg, 2009. 13(9): p. 1699-706.
36. Prost, P., M. Ychou, and D. Azria, *[Gemcitabine and pancreatic cancer]*. Bull Cancer, 2002. 89 Spec No: p. S91-5.
37. Toyama, Y., et al., *Successful adjuvant bi-weekly gemcitabine chemotherapy for pancreatic cancer without impairing patients' quality of life*. World J Surg Oncol, 2013. 11: p. 3.
38. Gligorov, J., et al., *[Updates on gemcitabine at the American Society of Clinical Oncology congress (ASCO, 2002)]*. Bull Cancer, 2002. 89 Spec No: p. S134-44.
39. Burris, H.A., 3rd, et al., *Improvements in survival and clinical benefit with gemcitabine as first-line therapy for patients with advanced pancreas cancer: a randomized trial*. J Clin Oncol, 1997. 15(6): p. 2403-13.
40. Rothenberg, M.L., et al., *A rationale for expanding the endpoints for clinical trials in advanced pancreatic carcinoma*. Cancer, 1996. 78(3 Suppl): p. 627-32.
41. Moore, M.J., et al., *Erlotinib plus gemcitabine compared with gemcitabine alone in patients with advanced pancreatic cancer: a phase III trial of the National Cancer Institute of Canada Clinical Trials Group*. J Clin Oncol, 2007. 25(15): p. 1960-6.
42. Welch, S.A. and M.J. Moore, *Erlotinib: success of a molecularly targeted agent for the treatment of advanced pancreatic cancer*. Future Oncol, 2007. 3(3): p. 247-54.
43. Hazard, L., *The role of radiation therapy in pancreas cancer*. Gastrointest Cancer Res, 2009. 3(1): p. 20-8.
44. Hidalgo, M., *Pancreatic cancer*. N Engl J Med, 2010. 362(17): p. 1605-17.

45. Haag, C. and G. Ehninger, [*Indications for chemotherapy in cancers of the esophagus, stomach and pancreas*]. *Z Gastroenterol*, 2002. 40 Suppl 1: p. S68-S70.
46. Linskens, R.K., et al., *Severe acute lung injury induced by gemcitabine*. *Neth J Med*, 2000. 56(6): p. 232-5.
47. Nissim, A. and Y. Chernajovsky, *Historical development of monoclonal antibody therapeutics*. *Handb Exp Pharmacol*, 2008(181): p. 3-18.
48. Holubec, L., et al., *The role of cetuximab in the treatment of metastatic colorectal cancer*. *Anticancer Res*, 2012. 32(9): p. 4007-11.
49. Arteaga, C.L., et al., *Treatment of HER2-positive breast cancer: current status and future perspectives*. *Nat Rev Clin Oncol*, 2012. 9(1): p. 16-32.
50. Girgis, M.D., et al., *Anti-CA19-9 diabody as a PET imaging probe for pancreas cancer*. *J Surg Res*, 2011. 170(2): p. 169-78.
51. Okamoto, O.K. and J.F. Perez, *Targeting cancer stem cells with monoclonal antibodies: a new perspective in cancer therapy and diagnosis*. *Expert Rev Mol Diagn*, 2008. 8(4): p. 387-93.
52. Yong, K.T., et al., *Imaging pancreatic cancer using bioconjugated InP quantum dots*. *ACS Nano*, 2009. 3(3): p. 502-10.
53. Waldmann, T.A., *Immunotherapy: past, present and future*. *Nat Med*, 2003. 9(3): p. 269-77.
54. Steinman, R.M. and J. Swanson, *The endocytic activity of dendritic cells*. *J Exp Med*, 1995. 182(2): p. 283-8.
55. Steinman, R.M., *The dendritic cell system and its role in immunogenicity*. *Annu Rev Immunol*, 1991. 9: p. 271-96.
56. Banchereau, J. and R.M. Steinman, *Dendritic cells and the control of immunity*. *Nature*, 1998. 392(6673): p. 245-52.
57. Abou-Alfa, G.K., et al., *Targeting mutated K-ras in pancreatic adenocarcinoma using an adjuvant vaccine*. *Am J Clin Oncol*, 2011. 34(3): p. 321-5.
58. Yamaguchi, K., M. Enjoji, and M. Tsuneyoshi, *Pancreatoduodenal carcinoma: a clinicopathologic study of 304 patients and immunohistochemical observation for CEA and CA19-9*. *J Surg Oncol*, 1991. 47(3): p. 148-54.
59. Maacke, H., et al., *Overexpression of p53 protein during pancreatitis*. *Br J Cancer*, 1997. 75(10): p. 1501-4.
60. Seki, K., et al., *Diagnosis of pancreatic adenocarcinoma by detection of human telomerase reverse transcriptase messenger RNA in pancreatic juice with sample qualification*. *Clin Cancer Res*, 2001. 7(7): p. 1976-81.
61. Koido, S., et al., *Regulation of tumor immunity by tumor/dendritic cell fusions*. *Clin Dev Immunol*, 2010. 2010: p. 516768.
62. Ragnhammar, P., *Anti-tumoral effect of GM-CSF with or without cytokines and monoclonal antibodies in solid tumors*. *Med Oncol*, 1996. 13(3): p. 167-76.
63. Pardoll, D.M., *Paracrine cytokine adjuvants in cancer immunotherapy*. *Annu Rev Immunol*, 1995. 13: p. 399-415.
64. Hellstrom, K.E., P. Gladstone, and I. Hellstrom, *Cancer vaccines: challenges and potential solutions*. *Mol Med Today*, 1997. 3(7): p. 286-90.
65. Bartels, C.J., S.A. Rosenberg, and J.C. Yang, *Adoptive cellular immunotherapy of cancer in mice using allogeneic T-cells*. *Ann Surg Oncol*, 1996. 3(1): p. 67-73.

66. Chan, B., et al., *Adoptive cellular immunotherapy for non-small cell lung cancer: a pilot study*. Cytotherapy, 2003. 5(1): p. 46-54.
67. Winter, H. and B.A. Fox, *Adoptive cellular immunotherapy of cancer*. Curr Opin Mol Ther, 1999. 1(1): p. 89-97.
68. Dienstmann, R., B. Markman, and J. Tabernero, *Application of monoclonal antibodies as cancer therapy in solid tumors*. Curr Clin Pharmacol, 2012. 7(2): p. 137-45.
69. Scott, A.M., J.P. Allison, and J.D. Wolchok, *Monoclonal antibodies in cancer therapy*. Cancer Immun, 2012. 12: p. 14.
70. Di Gaetano, N., et al., *Complement activation determines the therapeutic activity of rituximab in vivo*. J Immunol, 2003. 171(3): p. 1581-7.
71. Clynes, R.A., et al., *Inhibitory Fc receptors modulate in vivo cytotoxicity against tumor targets*. Nat Med, 2000. 6(4): p. 443-6.
72. Bondeson, J. and R.N. Maini, *Tumour necrosis factor as a therapeutic target in rheumatoid arthritis and other chronic inflammatory diseases: the clinical experience with infliximab (REMICADE)*. Int J Clin Pract, 2001. 55(3): p. 211-6.
73. Navarro-Sarabia, F., et al., *Adalimumab for treating rheumatoid arthritis*. J Rheumatol, 2006. 33(6): p. 1075-81.
74. Henry, M.L. and A. Rajab, *The use of basiliximab in solid organ transplantation*. Expert Opin Pharmacother, 2002. 3(11): p. 1657-63.
75. Olyaei, A.J., et al., *Use of basiliximab and daclizumab in kidney transplantation*. Prog Transplant, 2001. 11(1): p. 33-7; quiz 38-9.
76. Ferrara, N., K.J. Hillan, and W. Novotny, *Bevacizumab (Avastin), a humanized anti-VEGF monoclonal antibody for cancer therapy*. Biochem Biophys Res Commun, 2005. 333(2): p. 328-35.
77. Institut, P.E., *Bundesanzeiger Arzneimittel*. Veröffentlichungsnummer 376, 2012.
78. Keating, G.M., *Rituximab: a review of its use in chronic lymphocytic leukaemia, low-grade or follicular lymphoma and diffuse large B-cell lymphoma*. Drugs, 2010. 70(11): p. 1445-76.
79. Kan, R.W., et al., *Update on yttrium-90-based radio-embolization for treatment of hepatocellular carcinoma*. ANZ J Surg, 2012. 82(7-8): p. 505-9.
80. Lee, S.L., *Radioactive iodine therapy*. Curr Opin Endocrinol Diabetes Obes, 2012. 19(5): p. 420-8.
81. Pastan, I., et al., *Immunotoxin therapy of cancer*. Nat Rev Cancer, 2006. 6(7): p. 559-65.
82. Madhumathi, J. and R.S. Verma, *Therapeutic targets and recent advances in protein immunotoxins*. Curr Opin Microbiol, 2012. 15(3): p. 300-9.
83. Weidle, U.H., G. Georges, and U. Brinkmann, *Fully human targeted cytotoxic fusion proteins: new anticancer agents on the horizon*. Cancer Genomics Proteomics, 2012. 9(3): p. 119-33.
84. Adkins, I., et al., *Bacteria and their Toxins Tamed for Immunotherapy*. Curr Pharm Biotechnol, 2012. 13(8): p. 1446-1473.
85. Weldon, J.E. and I. Pastan, *A guide to taming a toxin--recombinant immunotoxins constructed from Pseudomonas exotoxin A for the treatment of cancer*. FEBS J, 2011. 278(23): p. 4683-700.
86. Barth, S., *Recombinant immunotoxins--the next generation*. Curr Pharm Des, 2009. 15(23): p. 2650-1.
87. Kessler, S.P. and D.R. Galloway, *Pseudomonas aeruginosa exotoxin A interaction with eucaryotic elongation factor 2. Role of the His426 residue*. J Biol Chem, 1992. 267(27): p. 19107-11.
88. Kreitman, R.J., *Toxin-labeled monoclonal antibodies*. Curr Pharm Biotechnol, 2001. 2(4): p. 313-25.

89. Huhn, M., et al., *Human angiogenin fused to human CD30 ligand (Ang-CD30L) exhibits specific cytotoxicity against CD30-positive lymphoma*. *Cancer Res*, 2001. 61(24): p. 8737-42.
90. Tur, M.K., et al., *Targeted restoration of down-regulated DAPK2 tumor suppressor activity induces apoptosis in Hodgkin lymphoma cells*. *J Immunother*, 2009. 32(5): p. 431-41.
91. Rosenblum, M.G. and S. Barth, *Development of novel, highly cytotoxic fusion constructs containing granzyme B: unique mechanisms and functions*. *Curr Pharm Des*, 2009. 15(23): p. 2676-92.
92. Stahnke, B., et al., *Granzyme B-H22(scFv), a human immunotoxin targeting CD64 in acute myeloid leukemia of monocytic subtypes*. *Mol Cancer Ther*, 2008. 7(9): p. 2924-32.
93. Laheru, D. and E.M. Jaffee, *Immunotherapy for pancreatic cancer - science driving clinical progress*. *Nat Rev Cancer*, 2005. 5(6): p. 459-67.
94. Plate, J., *Clinical trials of vaccines for immunotherapy in pancreatic cancer*. *Expert Rev Vaccines*, 2011. 10(6): p. 825-36.
95. Puri, S., et al., *A review of studies on targeting interleukin 4 receptor for central nervous system malignancy*. *Curr Mol Med*, 2009. 9(6): p. 732-9.
96. Strumberg, D., et al., *Phase II study of nimotuzumab, a humanized monoclonal anti-epidermal growth factor receptor (EGFR) antibody, in patients with locally advanced or metastatic pancreatic cancer*. *Invest New Drugs*, 2012. 30(3): p. 1138-43.
97. Murphy, K., et al., *Janeway's immunobiology*. 8th ed 2012, New York: Garland Science. xix, 868 p.
98. Strebhardt, K. and A. Ullrich, *Paul Ehrlich's magic bullet concept: 100 years of progress*. *Nat Rev Cancer*, 2008. 8(6): p. 473-80.
99. Kohler, G. and C. Milstein, *Continuous cultures of fused cells secreting antibody of predefined specificity*. *Nature*, 1975. 256(5517): p. 495-7.
100. Kabat, E.A. and T.T. Wu, *Identical V region amino acid sequences and segments of sequences in antibodies of different specificities. Relative contributions of VH and VL genes, minigenes, and complementarity-determining regions to binding of antibody-combining sites*. *J Immunol*, 1991. 147(5): p. 1709-19.
101. Johnson, G. and T.T. Wu, *Kabat database and its applications: 30 years after the first variability plot*. *Nucleic Acids Res*, 2000. 28(1): p. 214-8.
102. Tjandra, J.J., L. Ramadi, and I.F. McKenzie, *Development of human anti-murine antibody (HAMA) response in patients*. *Immunol Cell Biol*, 1990. 68 (Pt 6): p. 367-76.
103. LoBuglio, A.F. and M.N. Saleh, *Monoclonal antibody therapy of cancer*. *Crit Rev Oncol Hematol*, 1992. 13(3): p. 271-82.
104. Yokota, T., et al., *Rapid tumor penetration of a single-chain Fv and comparison with other immunoglobulin forms*. *Cancer Res*, 1992. 52(12): p. 3402-8.
105. Porter, R.R., *The hydrolysis of rabbit y-globulin and antibodies with crystalline papain*. *Biochem J*, 1959. 73: p. 119-26.
106. Inbar, D., J. Hochman, and D. Givol, *Localization of antibody-combining sites within the variable portions of heavy and light chains*. *Proc Natl Acad Sci U S A*, 1972. 69(9): p. 2659-62.
107. Mirick, G.R., et al., *A review of human anti-globulin antibody (HAGA, HAMA, HACA, HAHA) responses to monoclonal antibodies. Not four letter words*. *Q J Nucl Med Mol Imaging*, 2004. 48(4): p. 251-7.
108. Qu, Z., et al., *Development of humanized antibodies as cancer therapeutics*. *Methods*, 2005. 36(1): p. 84-95.

109. Lonberg, N., et al., *Antigen-specific human antibodies from mice comprising four distinct genetic modifications*. Nature, 1994. 368(6474): p. 856-9.
110. Hoogenboom, H.R. and G. Winter, *By-passing immunisation. Human antibodies from synthetic repertoires of germline VH gene segments rearranged in vitro*. Journal of Molecular Biology, 1992. 227(2): p. 381-8.
111. Hoogenboom, H.R., *Selecting and screening recombinant antibody libraries*. Nat Biotechnol, 2005. 23(9): p. 1105-16.
112. Fagerholm, U., *Prediction of human pharmacokinetics - renal metabolic and excretion clearance*. J Pharm Pharmacol, 2007. 59(11): p. 1463-71.
113. Fagerholm, U., *Prediction of human pharmacokinetics-biliary and intestinal clearance and enterohepatic circulation*. J Pharm Pharmacol, 2008. 60(5): p. 535-42.
114. Benedict, C.A., A.J. MacKrell, and W.F. Anderson, *Determination of the binding affinity of an anti-CD34 single-chain antibody using a novel, flow cytometry based assay*. J Immunol Methods, 1997. 201(2): p. 223-31.
115. Zhao, X., et al., *Selection and characterization of an internalizing epidermal-growth-factor-receptor antibody*. Biotechnol Appl Biochem, 2007. 46(Pt 1): p. 27-33.
116. Adams, G.P., et al., *High affinity restricts the localization and tumor penetration of single-chain fv antibody molecules*. Cancer Res, 2001. 61(12): p. 4750-5.
117. Hoogenboom, H.R. and P. Chames, *Natural and designer binding sites made by phage display technology*. Immunol Today, 2000. 21(8): p. 371-8.
118. Carmen, S. and L. Jermutus, *Concepts in antibody phage display*. Brief Funct Genomic Proteomic, 2002. 1(2): p. 189-203.
119. Marks, J.D., et al., *By-passing immunization. Human antibodies from V-gene libraries displayed on phage*. Journal of Molecular Biology, 1991. 222(3): p. 581-97.
120. Aina, O.H., et al., *From combinatorial chemistry to cancer-targeting peptides*. Mol Pharm, 2007. 4(5): p. 631-51.
121. Li, M., *Applications of display technology in protein analysis*. Nat Biotechnol, 2000. 18(12): p. 1251-6.
122. Kay, B.K., J. Winter, and J. McCafferty, *Phage display of peptides and proteins : a laboratory manual*1996, San Diego: Academic Press. xxii, 344 p.
123. Arap, M.A., *Phage display technology - Applications and innovations*. Genetics and Molecular Biology, 2005. 28(1): p. 1-9.
124. Click, E.M. and R.E. Webster, *The TolQRA proteins are required for membrane insertion of the major capsid protein of the filamentous phage phi during infection*. J Bacteriol, 1998. 180(7): p. 1723-8.
125. Russel, M., *Filamentous phage assembly*. Mol Microbiol, 1991. 5(7): p. 1607-13.
126. Vieira, J. and J. Messing, *Production of single-stranded plasmid DNA*. Methods Enzymol, 1987. 153: p. 3-11.
127. <http://www.daviddarling.info/encyclopedia/P/pilus.html>.
128. Barbas, C.F., 3rd, et al., *Assembly of combinatorial antibody libraries on phage surfaces: the gene III site*. Proc Natl Acad Sci U S A, 1991. 88(18): p. 7978-82.
129. Viti, F., et al., *Design and use of phage display libraries for the selection of antibodies and enzymes*. Methods Enzymol, 2000. 326: p. 480-505.
130. Soltes, G., et al., *A new helper phage and phagemid vector system improves viral display of antibody Fab fragments and avoids propagation of insert-less virions*. J Immunol Methods, 2003. 274(1-2): p. 233-44.

131. O'Connell, D., et al., *Phage versus phagemid libraries for generation of human monoclonal antibodies*. Journal of Molecular Biology, 2002. 321(1): p. 49-56.
132. Klimka, A., et al., *Human anti-CD30 recombinant antibodies by guided phage antibody selection using cell panning*. Br J Cancer, 2000. 83(2): p. 252-60.
133. Tur, M.K., et al., *Selection of scFv phages on intact cells under low pH conditions leads to a significant loss of insert-free phages*. Biotechniques, 2001. 30(2): p. 404-8, 410, 412-3.
134. Tur, M.K., et al., *A novel approach for immunization, screening and characterization of selected scFv libraries using membrane fractions of tumor cells*. Int J Mol Med, 2003. 11(4): p. 523-7.
135. <http://www.lifesciences.sourcebioscience.com/media/143421/tomlinsonij.pdf>.
136. Winter, G., et al., *Making antibodies by phage display technology*. Annu Rev Immunol, 1994. 12: p. 433-55.
137. Hust, M., et al., *A human scFv antibody generation pipeline for proteome research*. J Biotechnol, 2011. 152(4): p. 159-70.
138. Siva, A.C., et al., *Selection of anti-cancer antibodies from combinatorial libraries by whole-cell panning and stringent subtraction with human blood cells*. J Immunol Methods, 2008. 330(1-2): p. 109-19.
139. Gao, C., et al., *De novo identification of tumor-specific internalizing human antibody-receptor pairs by phage-display methods*. J Immunol Methods, 2003. 274(1-2): p. 185-97.
140. Soderlind, E., et al., *Recombining germline-derived CDR sequences for creating diverse single-framework antibody libraries*. Nat Biotechnol, 2000. 18(8): p. 852-6.
141. Nissim, A., et al., *Antibody fragments from a 'single pot' phage display library as immunochemical reagents*. EMBO J, 1994. 13(3): p. 692-8.
142. Griffiths, A.D., et al., *Isolation of high affinity human antibodies directly from large synthetic repertoires*. EMBO J, 1994. 13(14): p. 3245-60.
143. Sheets, M.D., et al., *Efficient construction of a large nonimmune phage antibody library: the production of high-affinity human single-chain antibodies to protein antigens*. Proc Natl Acad Sci U S A, 1998. 95(11): p. 6157-62.
144. An, F., et al., *Targeted drug delivery to mesothelioma cells using functionally selected internalizing human single-chain antibodies*. Mol Cancer Ther, 2008. 7(3): p. 569-78.
145. Poul, M.A., et al., *Selection of tumor-specific internalizing human antibodies from phage libraries*. Journal of Molecular Biology, 2000. 301(5): p. 1149-61.
146. Tomlinson I.M., W.G., *Method of screen phage display libraries with different ligands*, 2005, Domantis Limited, Cambridge (GB): United States Patent.
147. Cwirla, S.E., et al., *Peptides on phage: a vast library of peptides for identifying ligands*. Proc Natl Acad Sci U S A, 1990. 87(16): p. 6378-82.
148. Tomlinson, I.M., et al., *The repertoire of human germline VH sequences reveals about fifty groups of VH segments with different hypervariable loops*. Journal of Molecular Biology, 1992. 227(3): p. 776-98.
149. de Wildt, R.M., et al., *Antibody arrays for high-throughput screening of antibody-antigen interactions*. Nat Biotechnol, 2000. 18(9): p. 989-94.
150. Cox, J.P., I.M. Tomlinson, and G. Winter, *A directory of human germ-line V kappa segments reveals a strong bias in their usage*. Eur J Immunol, 1994. 24(4): p. 827-36.
151. Suzuki, I., et al., *Representation of rearranged VH gene segments in the human adult antibody repertoire*. J Immunol, 1995. 154(8): p. 3902-11.

152. Koch, H., et al., *Direct selection of antibodies from complex libraries with the protein fragment complementation assay*. Journal of Molecular Biology, 2006. 357(2): p. 427-41.
153. Marcus, W.D., S.M. Lindsay, and M.R. Sierks, *Identification and repair of positive binding antibodies containing randomly generated amber codons from synthetic phage display libraries*. Biotechnol Prog, 2006. 22(3): p. 919-22.
154. Pokorny, N.J., et al., *Inhibition of Cryptosporidium parvum infection of a mammalian cell culture by recombinant scFv antibodies*. Antonie Van Leeuwenhoek, 2008. 94(3): p. 353-64.
155. Bruns, C.J., et al., *In vivo selection and characterization of metastatic variants from human pancreatic adenocarcinoma by using orthotopic implantation in nude mice*. Neoplasia, 1999. 1(1): p. 50-62.
156. Vezeridis, M.P., et al., *In vivo selection of a highly metastatic cell line from a human pancreatic carcinoma in the nude mouse*. Cancer, 1992. 69(8): p. 2060-3.
157. Bruell, D., et al., *Recombinant anti-EGFR immunotoxin 425(scFv)-ETA' demonstrates anti-tumor activity against disseminated human pancreatic cancer in nude mice*. Int J Mol Med, 2005. 15(2): p. 305-13.
158. Kampmeier, F., et al., *Rapid optical imaging of EGF receptor expression with a single-chain antibody SNAP-tag fusion protein*. Eur J Nucl Med Mol Imaging, 2010. 37(10): p. 1926-34.
159. Bruell, D., et al., *The recombinant anti-EGF receptor immunotoxin 425(scFv)-ETA' suppresses growth of a highly metastatic pancreatic carcinoma cell line*. Int J Oncol, 2003. 23(4): p. 1179-86.
160. Herbst, R.S., *Review of epidermal growth factor receptor biology*. Int J Radiat Oncol Biol Phys, 2004. 59(2 Suppl): p. 21-6.
161. Jorissen, R.N., et al., *Epidermal growth factor receptor: mechanisms of activation and signalling*. Exp Cell Res, 2003. 284(1): p. 31-53.
162. Saito, T., et al., *Differential activation of epidermal growth factor (EGF) receptor downstream signaling pathways by betacellulin and EGF*. Endocrinology, 2004. 145(9): p. 4232-43.
163. Stang, E., et al., *Cbl-dependent ubiquitination is required for progression of EGF receptors into clathrin-coated pits*. Mol Biol Cell, 2004. 15(8): p. 3591-604.
164. Haisma, H.J., et al., *Targeting of adenoviral vectors through a bispecific single-chain antibody*. Cancer Gene Ther, 2000. 7(6): p. 901-4.
165. Mendelsohn, J., *Epidermal growth factor receptor inhibition by a monoclonal antibody as anticancer therapy*. Clin Cancer Res, 1997. 3(12 Pt 2): p. 2703-7.
166. Modjtahedi, H., et al., *Antitumor activity of combinations of antibodies directed against different epitopes on the extracellular domain of the human EGF receptor*. Cell Biophys, 1993. 22(1-3): p. 129-46.
167. Masui, H., et al., *Growth inhibition of human tumor cells in athymic mice by anti-epidermal growth factor receptor monoclonal antibodies*. Cancer Res, 1984. 44(3): p. 1002-7.
168. Kamat, V., et al., *Enhanced EGFR inhibition and distinct epitope recognition by EGFR antagonistic mAbs C225 and 425*. Cancer Biology & Therapy, 2008. 7(5): p. 726-733.
169. Pardo, A., et al., *In vivo imaging of immunotoxin treatment using Katushka-transfected A-431 cells in a murine xenograft tumour model*. Cancer Immunol Immunother, 2012. 61(10): p. 1617-26.
170. Baneyx, F., *Recombinant protein expression in Escherichia coli*. Curr Opin Biotechnol, 1999. 10(5): p. 411-21.
171. Matthey, B., et al., *A new series of pET-derived vectors for high efficiency expression of Pseudomonas exotoxin-based fusion proteins*. Gene, 1999. 229(1-2): p. 145-53.

172. de Marco, A., *Strategies for successful recombinant expression of disulfide bond-dependent proteins in Escherichia coli*. Microb Cell Fact, 2009. 8: p. 26.
173. Schlapschy, M. and A. Skerra, *Periplasmic chaperones used to enhance functional secretion of proteins in E. coli*. Methods Mol Biol, 2011. 705: p. 211-24.
174. Talmadge, K. and W. Gilbert, *Cellular location affects protein stability in Escherichia coli*. Proc Natl Acad Sci U S A, 1982. 79(6): p. 1830-3.
175. Barth, S., et al., *Compatible-solute-supported periplasmic expression of functional recombinant proteins under stress conditions*. Appl Environ Microbiol, 2000. 66(4): p. 1572-9.
176. Gao, J., et al., *Preparation, cloning, and high level expression in E. coli of interleukin 2-pseudomonas exotoxin fusion genes*. Chin J Biotechnol, 1996. 12(2): p. 81-7.
177. Sanchez, L., et al., *High cytoplasmic expression in E. coli, purification, and in vitro refolding of a single chain Fv antibody fragment against the hepatitis B surface antigen*. J Biotechnol, 1999. 72(1-2): p. 13-20.
178. Ventura, S. and A. Villaverde, *Protein quality in bacterial inclusion bodies*. Trends in Biotechnology, 2006. 24(4): p. 179-85.
179. Benhar, I. and I. Pastan, *Cloning, expression and characterization of the Fv fragments of the anti-carbohydrate mAbs B1 and B5 as single-chain immunotoxins*. Protein Engineering, 1994. 7(12): p. 1509-15.
180. Swamy, K.H. and A.L. Goldberg, *Subcellular distribution of various proteases in Escherichia coli*. J Bacteriol, 1982. 149(3): p. 1027-33.
181. Wall, J.G. and A. Pluckthun, *The hierarchy of mutations influencing the folding of antibody domains in Escherichia coli*. Protein Engineering, 1999. 12(7): p. 605-11.
182. Kane, J.F., *Effects of rare codon clusters on high-level expression of heterologous proteins in Escherichia coli*. Curr Opin Biotechnol, 1995. 6(5): p. 494-500.
183. Stocker, M., et al., *Secretion of functional anti-CD30-angiogenin immunotoxins into the supernatant of transfected 293T-cells*. Protein Expr Purif, 2003. 28(2): p. 211-9.
184. Liu, Y.Y., et al., *Expression of an anti-CD3 single-chain immunotoxin with a truncated diphtheria toxin in a mutant CHO cell line*. Protein Expr Purif, 2000. 19(2): p. 304-11.
185. Ribbert, T., et al., *Recombinant, ETA'-based CD64 immunotoxins: improved efficacy by increased valency, both in vitro and in vivo in a chronic cutaneous inflammation model in human CD64 transgenic mice*. Br J Dermatol, 2010. 163(2): p. 279-86.
186. Terpe, K., *Overview of tag protein fusions: from molecular and biochemical fundamentals to commercial systems*. Appl Microbiol Biotechnol, 2003. 60(5): p. 523-33.
187. Casadaban, M.J., J. Chou, and S.N. Cohen, *In vitro gene fusions that join an enzymatically active beta-galactosidase segment to amino-terminal fragments of exogenous proteins: Escherichia coli plasmid vectors for the detection and cloning of translational initiation signals*. J Bacteriol, 1980. 143(2): p. 971-80.
188. Wood, K.V., *Marker proteins for gene expression*. Curr Opin Biotechnol, 1995. 6(1): p. 50-8.
189. Egberts, J.H., et al., *Anti-tumor necrosis factor therapy inhibits pancreatic tumor growth and metastasis*. Cancer Res, 2008. 68(5): p. 1443-50.
190. Ghim, C.M., et al., *The art of reporter proteins in science: past, present and future applications*. BMB Rep, 2010. 43(7): p. 451-60.
191. Tsien, R.Y., *The green fluorescent protein*. Annu Rev Biochem, 1998. 67: p. 509-44.

192. Shimomura, O., F.H. Johnson, and Y. Saiga, *Extraction, purification and properties of aequorin, a bioluminescent protein from the luminous hydromedusan, Aequorea*. J Cell Comp Physiol, 1962. 59: p. 223-39.
193. Shimomura, O., *The discovery of aequorin and green fluorescent protein*. J Microsc, 2005. 217(Pt 1): p. 1-15.
194. Shaner, N.C., P.A. Steinbach, and R.Y. Tsien, *A guide to choosing fluorescent proteins*. Nat Methods, 2005. 2(12): p. 905-9.
195. Shaner, N.C., P.A. Steinbach, and R.Y. Tsien, *A guide to choosing fluorescent proteins*. Nature Methods, 2005. 2(12): p. 905-909.
196. Drepper, T., et al., *Flavin mononucleotide-based fluorescent reporter proteins outperform green fluorescent protein-like proteins as quantitative in vivo real-time reporters*. Appl Environ Microbiol, 2010. 76(17): p. 5990-4.
197. Zimmer, M., *Green fluorescent protein (GFP): Applications, structure, and related photophysical behavior*. Chemical Reviews, 2002. 102(3): p. 759-781.
198. Briggs, W.R. and J.M. Christie, *Phototropins 1 and 2: versatile plant blue-light receptors*. Trends Plant Sci, 2002. 7(5): p. 204-10.
199. Losi, A., *The bacterial counterparts of plant phototropins*. Photochem Photobiol Sci, 2004. 3(6): p. 566-74.
200. Drepper, T., et al., *Reporter proteins for in vivo fluorescence without oxygen*. Nat Biotechnol, 2007. 25(4): p. 443-5.
201. Losi, A., et al., *Mutational effects on protein structural changes and interdomain interactions in the blue-light sensing LOV protein YtvA*. Photochem Photobiol, 2005. 81(5): p. 1145-52.
202. Potzkei, J., et al., *Real-time determination of intracellular oxygen in bacteria using a genetically encoded FRET-based biosensor*. BMC Biology 2012. 10(28).
203. www.tsienlab.ucsd.edu.
204. Hearps, A.C., et al., *The biarsenical dye Lumio exhibits a reduced ability to specifically detect tetracycline-containing proteins within live cells*. J Fluoresc, 2007. 17(6): p. 593-7.
205. Los, G.V., et al., *HaloTag: a novel protein labeling technology for cell imaging and protein analysis*. ACS Chem Biol, 2008. 3(6): p. 373-82.
206. Beckett, D., E. Kovaleva, and P.J. Schatz, *A minimal peptide substrate in biotin holoenzyme synthetase-catalyzed biotinylation*. Protein Sci, 1999. 8(4): p. 921-9.
207. Antos, J.M., et al., *Site-specific N- and C-terminal labeling of a single polypeptide using sortases of different specificity*. Journal of the American Chemical Society, 2009. 131(31): p. 10800-1.
208. Yin, J., et al., *Genetically encoded short peptide tag for versatile protein labeling by Sfp phosphopantetheinyl transferase*. Proc Natl Acad Sci U S A, 2005. 102(44): p. 15815-20.
209. Keppler, A., et al., *Labeling of fusion proteins of O6-alkylguanine-DNA alkyltransferase with small molecules in vivo and in vitro*. Methods, 2004. 32(4): p. 437-44.
210. Gronemeyer, T., et al., *Directed evolution of O6-alkylguanine-DNA alkyltransferase for applications in protein labeling*. Protein Eng Des Sel, 2006. 19(7): p. 309-16.
211. Kampmeier, F., et al., *Site-specific, covalent labeling of recombinant antibody fragments via fusion to an engineered version of 6-O-alkylguanine DNA alkyltransferase*. Bioconjug Chem, 2009. 20(5): p. 1010-5.
212. Keppler, A., et al., *Labeling of fusion proteins with synthetic fluorophores in live cells*. Proc Natl Acad Sci U S A, 2004. 101(27): p. 9955-9.

213. Pegg, A.E., *Mammalian O6-alkylguanine-DNA alkyltransferase: regulation and importance in response to alkylating carcinogenic and therapeutic agents*. *Cancer Res*, 1990. 50(19): p. 6119-29.
214. www.neb.com
215. Kindermann, M., et al., *Covalent and selective immobilization of fusion proteins*. *Journal of the American Chemical Society*, 2003. 125(26): p. 7810-1.
216. Gautier, A., et al., *An engineered protein tag for multiprotein labeling in living cells*. *Chem Biol*, 2008. 15(2): p. 128-36.
217. Lakowicz, J.R., *Principles of fluorescence spectroscopy*. 2nd ed1999, New York: Kluwer Academic/Plenum Publisher.
218. Vivian, J.T. and P.R. Callis, *Mechanisms of tryptophan fluorescence shifts in proteins*. *Biophys J*, 2001. 80(5): p. 2093-109.
219. Chen, X., et al., *Proton-regulated electron transfers from tyrosine to tryptophan in proteins: through-bond mechanism versus long-range hopping mechanism*. *J Phys Chem B*, 2009. 113(52): p. 16681-8.
220. Jones, D.T., W.R. Taylor, and J.M. Thornton, *The rapid generation of mutation data matrices from protein sequences*. *Comput Appl Biosci*, 1992. 8(3): p. 275-82.
221. Nilsson, A., et al., *Tryptophan-tagged cutinase studied by steady state fluorescence for understanding of tag interactions in aqueous two-phase systems*. *Biochimica Et Biophysica Acta*, 2003. 1646(1-2): p. 57-66.
222. Silacci, M., et al., *Design, construction, and characterization of a large synthetic human antibody phage display library*. *Proteomics*, 2005. 5(9): p. 2340-50.
223. Samorski, M., G. Muller-Newen, and J. Buchs, *Quasi-continuous combined scattered light and fluorescence measurements: a novel measurement technique for shaken microtiter plates*. *Biotechnol Bioeng*, 2005. 92(1): p. 61-8.
224. Kensy, F., et al., *Validation of a high-throughput fermentation system based on online monitoring of biomass and fluorescence in continuously shaken microtiter plates*. *Microb Cell Fact*, 2009. 8: p. 31.
225. Klockner, W. and J. Buchs, *Advances in shaking technologies*. *Trends in Biotechnology*, 2012. 30(6): p. 307-14.
226. Weuster-Botz, D., J. Altenbach-Rehm, and M. Arnold, *Parallel substrate feeding and pH-control in shaking-flasks*. *Biochem Eng J*, 2001. 7(2): p. 163-170.
227. Anderlei, T., et al., *Online respiration activity measurement (OTR, CTR, RQ) in shake flasks*. *Biochem Eng J*, 2004. 17(3): p. 187-194.
228. Duetz, W.A., *Microtiter plates as mini-bioreactors: miniaturization of fermentation methods*. *Trends in Microbiology*, 2007. 15(10): p. 469-475.
229. Betts, J.I. and F. Baganz, *Miniature bioreactors: current practices and future opportunities*. *Microb Cell Fact*, 2006. 5.
230. Isett, K., et al., *Twenty-four-well plate miniature Bioreactor high-throughput system: Assessment for microbial cultivations*. *Biotechnol Bioeng*, 2007. 98(5): p. 1017-1028.
231. DeLisa, M.P., et al., *Generic model control of induced protein expression in high cell density cultivation of Escherichia coli using on-line GFP-fusion monitoring*. *Bioprocess Biosyst Eng*, 2001. 24(2): p. 83-91.
232. Scheidle, M., Klinger, J., Büchs, J., *Combination of On-line pH and Oxygen Transfer Rate Measurement in Shake Flasks by Fiber Optical Technique and Respirations Activity Monitoring System (RAMOS)*. *Sensors*, 2007. 7(12): p. 9.

233. Sambrook, J. and D.W. Russell, *Molecular cloning : a laboratory manual*. 3rd ed 2001, Cold Spring Harbor, N.Y.: Cold Spring Harbor Laboratory Press.
234. Saiki, R.K., et al., *Enzymatic amplification of beta-globin genomic sequences and restriction site analysis for diagnosis of sickle cell anemia*. *Science*, 1985. 230(4732): p. 1350-4.
235. Sanger, F., S. Nicklen, and A.R. Coulson, *DNA sequencing with chain-terminating inhibitors*. *Proc Natl Acad Sci U S A*, 1977. 74(12): p. 5463-7.
236. Mueller, U., et al., *Thermal stability and atomic-resolution crystal structure of the Bacillus caldolyticus cold shock protein*. *Journal of Molecular Biology*, 2000. 297(4): p. 975-88.
237. Klimka, A., et al., *An anti-CD30 single-chain Fv selected by phage display and fused to Pseudomonas exotoxin A (Ki-4(scFv)-ETA') is a potent immunotoxin against a Hodgkin-derived cell line*. *Br J Cancer*, 1999. 80(8): p. 1214-22.
238. Wong, C., et al., *Human scFv antibody fragments specific for the epithelial tumour marker MUC-1, selected by phage display on living cells*. *Cancer Immunol Immunother*, 2001. 50(2): p. 93-101.
239. Maier, U. and J. Buchs, *Characterisation of the gas-liquid mass transfer in shaking bioreactors*. *Biochem Eng J*, 2001. 7(2): p. 99-106.
240. Hermann, R., M. Lehmann, and J. Buchs, *Characterization of gas-liquid mass transfer phenomena in microtiter plates*. *Biotechnol Bioeng*, 2003. 81(2): p. 178-86.
241. Studier, F.W., *Protein production by auto-induction in high density shaking cultures*. *Protein Expr Purif*, 2005. 41(1): p. 207-34.
242. Felgner, P.L., et al., *Lipofection: a highly efficient, lipid-mediated DNA-transfection procedure*. *Proc Natl Acad Sci U S A*, 1987. 84(21): p. 7413-7.
243. Porath, J., et al., *Metal chelate affinity chromatography, a new approach to protein fractionation*. *Nature*, 1975. 258(5536): p. 598-9.
244. Xiao, Z., et al., *Cell-specific internalization study of an aptamer from whole cell selection*. *Chemistry*, 2008. 14(6): p. 1769-75.
245. Kensy, F., et al., *Oxygen transfer phenomena in 48-well microtiter plates: determination by optical monitoring of sulfite oxidation and verification by real-time measurement during microbial growth*. *Biotechnol Bioeng*, 2005. 89(6): p. 698-708.
246. Siepert, E.M., et al., *Short-chain fluorescent tryptophan tags for on-line detection of functional recombinant proteins*. *BMC Biotechnol*, 2012. 12(1): p. 65.
247. Russel, M., Lowman, H. B., Clackson, T., and Al, E. T., *Chapter 1: Introduction to phage biology and phage display*, 2004, Oxford University Press, New York. p. 1-26.
248. Tordsson, J., et al., *A3--a novel colon and pancreatic cancer reactive antibody from a primate phage library selected using intact tumour cells*. *Int J Cancer*, 2000. 87(4): p. 559-68.
249. Popkov, M., C. Rader, and C.F. Barbas, 3rd, *Isolation of human prostate cancer cell reactive antibodies using phage display technology*. *J Immunol Methods*, 2004. 291(1-2): p. 137-51.
250. Dantas-Barbosa, C., et al., *Isolation of osteosarcoma-associated human antibodies from a combinatorial Fab phage display library*. *J Biomed Biotechnol*, 2009. 2009: p. 157531.
251. Kristensen, P., et al., *Applying phage display technology in aging research*. *Biogerontology*, 2000. 1(1): p. 67-78.
252. Sawyer, C., J. Embleton, and C. Dean, *Methodology for selection of human antibodies to membrane proteins from a phage-display library*. *J Immunol Methods*, 1997. 204(2): p. 193-203.

253. Eisenhardt, S.U., et al., *Subtractive single-chain antibody (scFv) phage-display: tailoring phage-display for high specificity against function-specific conformations of cell membrane molecules*. Nat Protoc, 2007. 2(12): p. 3063-73.
254. Becerril, B., M.A. Poul, and J.D. Marks, *Toward selection of internalizing antibodies from phage libraries*. Biochem Biophys Res Commun, 1999. 255(2): p. 386-93.
255. Loring, J.F. and S.E. Peterson, *Human stem cell manual : a laboratory guide*. 2nd ed 2012, London, UK ; Waltham, MA: Elsevier/Academic Press. xxxi, 619 p.
256. Tordsson, J., et al., *Efficient selection of scFv antibody phage by adsorption to in situ expressed antigens in tissue sections*. J Immunol Methods, 1997. 210(1): p. 11-23.
257. Hegmans, J.P., et al., *A model system for optimising the selection of membrane antigen-specific human antibodies on intact cells using phage antibody display technology*. J Immunol Methods, 2002. 262(1-2): p. 191-204.
258. Mutuberría, R., et al., *Model systems to study the parameters determining the success of phage antibody selections on complex antigens*. J Immunol Methods, 1999. 231(1-2): p. 65-81.
259. Lou, J., et al., *Antibodies in haystacks: how selection strategy influences the outcome of selection from molecular diversity libraries*. J Immunol Methods, 2001. 253(1-2): p. 233-42.
260. Carter, D.M., et al., *Phage display reveals multiple contact sites between FhuA, an outer membrane receptor of Escherichia coli, and TonB*. Journal of Molecular Biology, 2006. 357(1): p. 236-51.
261. Hawkins, R.E., S.J. Russell, and G. Winter, *Selection of phage antibodies by binding affinity. Mimicking affinity maturation*. Journal of Molecular Biology, 1992. 226(3): p. 889-96.
262. Hicklin, D.J., et al., *Monoclonal antibody strategies to block angiogenesis*. Drug Discov Today, 2001. 6(10): p. 517-528.
263. Allen, T.M., *Ligand-targeted therapeutics in anticancer therapy*. Nat Rev Cancer, 2002. 2(10): p. 750-63.
264. Edelman, D.C. and J. Barletta, *Real-time PCR provides improved detection and titer determination of bacteriophage*. Biotechniques, 2003. 35(2): p. 368-75.
265. de Kruif, J., et al., *Rapid selection of cell subpopulation-specific human monoclonal antibodies from a synthetic phage antibody library*. Proc Natl Acad Sci U S A, 1995. 92(9): p. 3938-42.
266. Bratkovic, T., *Progress in phage display: evolution of the technique and its application*. Cell Mol Life Sci, 2010. 67(5): p. 749-67.
267. Rondot, S., et al., *A helper phage to improve single-chain antibody presentation in phage display*. Nat Biotechnol, 2001. 19(1): p. 75-8.
268. Jensen, K.B., et al., *Identification of keratinocyte-specific markers using phage display and mass spectrometry*. Mol Cell Proteomics, 2003. 2(2): p. 61-9.
269. Hust, M., et al., *Enrichment of open reading frames presented on bacteriophage M13 using hyperphage*. Biotechniques, 2006. 41(3): p. 335-42.
270. Boulter-Bitzer, J.I., H. Lee, and J.T. Trevors, *Single-chain variable fragment antibodies selected by phage display against the sporozoite surface antigen P23 Of Cryptosporidium parvum*. J Parasitol, 2009. 95(1): p. 75-81.
271. Eteshola, E., *Isolation of scFv fragments specific for monokine induced by interferon-gamma (MIG) using phage display*. J Immunol Methods, 2010. 358(1-2): p. 104-10.
272. Wu, S., A. Ke, and J.A. Doudna, *A fast and efficient procedure to produce scFvs specific for large macromolecular complexes*. J Immunol Methods, 2007. 318(1-2): p. 95-101.

273. Brinkmann, U., et al., *Phage display of disulfide-stabilized Fv fragments*. J Immunol Methods, 1995. 182(1): p. 41-50.
274. Hoogenboom, H.R., et al., *Selection-dominant and nonaccessible epitopes on cell-surface receptors revealed by cell-panning with a large phage antibody library*. European Journal of Biochemistry, 1999. 260(3): p. 774-84.
275. Schmidt, M.M., G.M. Thurber, and K.D. Wittrup, *Kinetics of anti-carcinoembryonic antigen antibody internalization: effects of affinity, bivalency, and stability*. Cancer Immunol Immunother, 2008. 57(12): p. 1879-90.
276. Chelius, D., D.S. Rehder, and P.V. Bondarenko, *Identification and characterization of deamidation sites in the conserved regions of human immunoglobulin gamma antibodies*. Analytical Chemistry, 2005. 77(18): p. 6004-11.
277. Piana, S., et al., *Predicting the effect of a point mutation on a protein fold: the villin and advillin headpieces and their Pro62Ala mutants*. Journal of Molecular Biology, 2008. 375(2): p. 460-70.
278. Ricci-Vitiani, L., et al., *Identification and expansion of human colon-cancer-initiating cells*. Nature, 2007. 445(7123): p. 111-5.
279. Jordan, C.T., M.L. Guzman, and M. Noble, *Cancer stem cells*. N Engl J Med, 2006. 355(12): p. 1253-61.
280. Hermann, P.C., S.L. Huber, and C. Heeschen, *Metastatic cancer stem cells: a new target for anti-cancer therapy?* Cell Cycle, 2008. 7(2): p. 188-93.
281. Clarke, R.B., *Ovarian steroids and the human breast: regulation of stem cells and cell proliferation*. Maturitas, 2006. 54(4): p. 327-34.
282. Bao, S., et al., *Stem cell-like glioma cells promote tumor angiogenesis through vascular endothelial growth factor*. Cancer Res, 2006. 66(16): p. 7843-8.
283. Li, C., et al., *Identification of pancreatic cancer stem cells*. Cancer Res, 2007. 67(3): p. 1030-7.
284. Hermann, P.C., et al., *Distinct populations of cancer stem cells determine tumor growth and metastatic activity in human pancreatic cancer*. Cell Stem Cell, 2007. 1(3): p. 313-23.
285. Bao, S., et al., *Glioma stem cells promote radioresistance by preferential activation of the DNA damage response*. Nature, 2006. 444(7120): p. 756-60.
286. Conner, S.D. and S.L. Schmid, *Regulated portals of entry into the cell*. Nature, 2003. 422(6927): p. 37-44.
287. Doherty, G.J. and H.T. McMahon, *Mechanisms of endocytosis*. Annu Rev Biochem, 2009. 78: p. 857-902.
288. Mellman, I., *Endocytosis and molecular sorting*. Annu Rev Cell Dev Biol, 1996. 12: p. 575-625.
289. Molenaar, T.J., et al., *Uptake and processing of modified bacteriophage M13 in mice: implications for phage display*. Virology, 2002. 293(1): p. 182-91.
290. Burg, M., et al., *Selection of internalizing ligand-display phage using rolling circle amplification for phage recovery*. DNA Cell Biol, 2004. 23(7): p. 457-62.
291. Zimmer, M., *Green fluorescent protein (GFP): applications, structure, and related photophysical behavior*. Chem Rev, 2002. 102(3): p. 759-81.
292. Studier, F.W. and B.A. Moffatt, *Use of bacteriophage T7 RNA polymerase to direct selective high-level expression of cloned genes*. Journal of Molecular Biology, 1986. 189(1): p. 113-30.
293. Hames, B.D., *Gel electrophoresis of proteins : a practical approach*. 3rd ed. Practical approach series 1998, Oxford ; New York: Oxford University Press. xx, 352 p.

294. Baneyx, F. and M. Mujacic, *Recombinant protein folding and misfolding in Escherichia coli*. Nat Biotechnol, 2004. 22(11): p. 1399-408.
295. de Groot, N.S. and S. Ventura, *Effect of temperature on protein quality in bacterial inclusion bodies*. FEBS Lett, 2006. 580(27): p. 6471-6.
296. Dunbar, R.C., et al., *Dimeric complexes of tryptophan with M²⁺ metal ions*. J Phys Chem A, 2009. 113(5): p. 845-51.
297. Durrant, J.D., D. Caywood, and D.D. Busath, *Tryptophan contributions to the empirical free-energy profile in gramicidin A/M heterodimer channels*. Biophysical Journal, 2006. 91(9): p. 3230-41.
298. Nilsson, A., et al., *Partitioning of peptide-tagged proteins in aqueous two-phase systems using hydrophobically modified micelle-forming thermoseparating polymer*. Biochimica Et Biophysica Acta, 2002. 1601(2): p. 138-48.
299. Fexby, S. and L. Bulow, *Hydrophobic peptide tags as tools in bioseparation*. Trends in Biotechnology, 2004. 22(10): p. 511-516.
300. Chen, J., et al., *Mechanism of the highly efficient quenching of tryptophan fluorescence in human gammaD-crystallin*. Biochemistry, 2006. 45(38): p. 11552-63.
301. Chen, Y. and M.D. Barkley, *Toward understanding tryptophan fluorescence in proteins*. Biochemistry, 1998. 37(28): p. 9976-82.
302. Vivian, J.T. and P.R. Callis, *Mechanisms of tryptophan fluorescence shifts in proteins*. Biophysical Journal, 2001. 80(5): p. 2093-109.
303. Gould, I.R., et al., *Mechanisms of Exciplex Formation - Roles of Superexchange, Solvent Polarity, and Driving-Force for Electron-Transfer*. Journal of the American Chemical Society, 1994. 116(18): p. 8176-8187.
304. Reshetnyak, Y.K., Y. Koshevnik, and E.A. Burstein, *Decomposition of protein tryptophan fluorescence spectra into log-normal components. III. Correlation between fluorescence and microenvironment parameters of individual tryptophan residues*. Biophysical Journal, 2001. 81(3): p. 1735-1758.
305. Nystrom, T., *Stationary-phase physiology*. Annual review of microbiology, 2004. 58: p. 161-81.
306. Robert Grützmann, M.D., *Tumormarker und Biomarker beim Bauchspeicheldrüsenkrebs*, in *M&K kompakt "Medica 2012", Supplement 2012*, GIT Verlag.
307. *CHAPTER 5: Construction of Recombinant DNA Libraries*, in *Current Protocols in Molecular Biology 2012*, Wiley-VCH.
308. Posey, J.A., et al., *A phase I trial of the single-chain immunotoxin SGN-10 (BR96 sFv-PE40) in patients with advanced solid tumors*. Clin Cancer Res, 2002. 8(10): p. 3092-9.
309. Barth, S., et al., *Recombinant anti-CD25 immunotoxin RFT5(scFv)-ETA ' demonstrates successful elimination of disseminated human Hodgkin lymphoma in SCID mice*. International Journal of Cancer, 2000. 86(5): p. 718-724.
310. Barth, S., et al., *Ki-4(scFv)-ETA ', a new recombinant anti-CD30 immunotoxin with highly specific cytotoxic activity against disseminated Hodgkin tumors in SCID mice*. Blood, 2000. 95(12): p. 3909-3914.
311. Otsuji, E., et al., *Monoclonal antibody A7 coupled to magnetic particles as a contrast enhancing agent for magnetic resonance imaging of human colorectal carcinoma*. Cancer Immunol Immunother, 2006. 55(6): p. 728-33.
312. Toma, A., et al., *Monoclonal antibody A7-superparamagnetic iron oxide as contrast agent of MR imaging of rectal carcinoma*. Br J Cancer, 2005. 93(1): p. 131-6.
313. Shido, Y., et al., *Targeted hyperthermia using magnetite cationic liposomes and an alternating magnetic field in a mouse osteosarcoma model*. J Bone Joint Surg Br, 2010. 92(4): p. 580-5.

314. Thie, H., et al., *Phage display derived therapeutic antibodies*. *Curr Pharm Biotechnol*, 2008. 9(6): p. 439-46.
315. Schirrmann, T. and M. Hust, *Construction of human antibody gene libraries and selection of antibodies by phage display*. *Methods Mol Biol*, 2010. 651: p. 177-209.

10 Appendix

10.1 QuikChange Mutagenesis primers

Table 10-1 Individual primer sequences for site-directed QuikChange Mutagenesis

Clone	Forward primer 5'-->3'	Reverse primer 5'-->3'
A3	GGGTCTCACAGATTAATCCTAATG GTCAGCCGACAAAGTACGC	GCGTACTTTGTCGGCTGACCATTAGG ATTAATCTGTGAGACCC
C5	GGTTCTAGTACATCTCAGGCAG ACTCCGTGAAGGGCCGG	CCGGCCCTTCACGGAGTCTGCCTG AGATGTACTAGAACC
D1	GGGAAGGGGCTGGAGTGGGTC TCAAGTATTTCTAATTATGG	CCATAATTAGAAATACTTGAGAC CCACTCCAGCCCCTTCCC
D4	No stop codon!	
D5	CGGGAGGGTTCAGAGGACAAGTTAC GCAGACTCCG	CGGAGTCTGCGTAACTTGTCTCTGA CCCTCCCG
D6	GGGAAAGGGCTGGAGTGGGTCTC AACGATTGAGTATCGG	CCGATACTCAATCGTTGAGACCCACT CCAGCCCTTTCCC
D9	GGGTCTCAAATATTTATCGGGAGG GTCAGAGGACAAGTTACGCAAACCTCC	GGAGTTTTCGTAACCTTGTCTCTGAC CCTCCCGATAAATATTTGAGACCC
D12	GGGTCTCAGGTATTTGGCAGCG GGGTTCTACTACAGC	GCTGTAGTAGAACCCGCTGCCA AATACCTGAGACCC
E3	No stop codon!	
E5	GGGAAGGGGCTGGAGTGGGTCT CAGATATTTCTACTGCTGG	CCAGCAGTAGAAATATCTGAGACC CACTCCAGCCCCTTCCC
E7	GGGTCCCTGAGACTCTCTGCG CAGCCTCTGGATTACCC	GGTGAATCCAGAGGCTGCGCAGG AGAGTCTCAGGGACCC
E8	CCAGGGAAGGGGCTGGAGTGGG TCTCAGTTATTGGG	CCCAATAACTGAGACCCACTCCAG CCCCTTCCCCTGG
F1	GGGCTGGAGTGGGTCTCAAGTAT TTATTTCGAGGGTAATCTTACAATTTACGC	GCGTAAATTGTAAGATTACCCTGCG AATAAATACTTGAGACCCACTCCAGCCC
F3	GCGAAAAGTGCTACTCAGTTTG ACTACTGGGGCCAGGG	CCCTGGCCCCAGTAGTCAAACCTG AGTAGCACTTTTTCGC
F11	GGGAAGGGGCTGGAGTGGGTCT CAGCTATTAGTACTTCTGG	CCAGAAGTACTAATAGCTGAGACC CACTCCAGCCCCTTCCC

Table 10-2 Overview of amber and ochre stop codons found in isolated scFv antibody fragments.

Clone	Length	Stop codon	Location of stop	GC content	Tm temperature
A3	43 bp	TAG-->CAG	CDR2	46,50%	82,6 °C
C5	39 bp	TAA-->CAG	CDR2	59,00%	85,8 °C
D1	41 bp	TGA-->TGG	FWR2	48,78%	82,6 °C
D4	No stop codon!				
D5	34 bp	TAG-->CAG	CDR2	58,80%	82,8 °C
D6	39 bp	TGA-->TGG	FWR2	53,80%	83,7 °C
D9	50 bp	TAG-->CAG	CDR2	46,00%	84,7 °C
D12	37 bp	TAG-->CAG	CDR2	54,05%	82,7 °C
E3	No stop codon!				
E5	41 bp	TGA-->TGG	FWR2	53,60%	84,6 °C
E7	39 bp	TGA-->TGC	FWR1	64,10%	87,9 °C
E8	36 bp	TGA-->TGG	FWR2	58,30%	83,9 °C
F1	53 bp	TAG-->CAG	CDR2	43,40%	84,7 °C
F3	38 bp	TAG-->CAG	CDR3	52,63%	82,6 °C
F11	41 bp	TGA-->TGG	FWR2	53,60%	84,6 °C

10.2 Amino acids (IUPC letter codes)

Table 10-3 Overview of codes for amino acids

Amino acid	3-letter code	1-letter code	Triplets coding for amino acid
Alanine	Ala	A	GCT, GCC, GCA, GCG
Arginine	Arg	R	CGT, CGC, CGA, CGG, AGA, AGG
Asparagine	Asn	N	AAT, AAC,
Aspartic acid	Asp	D	GAT, GAC
Cysteine	Cys	C	TGT, TGC,
Glutamine	Gln	Q	CAG, CAA,
Glutamic acid	Glu	E	GAA, GAG
Glycine	Gly	G	GGT, GGC, GGA, GGG
Histidine	His	H	CAT, CAC,
Isoleucine	Ile	I	ATT, ATC, ATA
Leucine	Leu	L	CTT, CTC, CTA, CTG
Lysine	Lys	K	AAA, AAG
Methionine	Met	M	ATG
Phenylalanine	Phe	F	TTT, TTC,
Proline	Pro	P	CCT, CCC, CCA, CCG
Serine	Ser	S	TCT, TCC, AGT, AGC
Threonine	Thr	T	ACT, ACC, ACA, ACG
Tryptophan	Trp	W	TGG
Tyrosine	Tyr	Y	TAT, TAC,
Valine	Val	V	GTT, GTC, GTA, GTG

10.3 List of approved therapeutic mABs in Germany

Table 10-4 List of recombinant antibodies approved for treatment in Europe. [77]

Name of mAB	Type	Target of Action	Condition	Approved
Arzerra (Ofatumumab)	Human	Anti-CD20	Chronic lymphatic leukemia	2010
Avastin (Bevacizumab)	Humanized	Anti-VEGF	Advanced colorectal, lung, breast, kidney and cervix carcinoma	2005
Benlysta (Belimumab)	Human	Inhibits B-cell activating factor (BAFF)	Systemic lupus erythematosus	2011
Cimzia (Certolizumab)	Humanized Fab	Anti-TNF α	Inflammatory gastro-intestinal disease, Crohn's disease, rheumatoid arthritis	2009
Erbix (Cetuximab)	Chimeric	Anti-EGFR	Metastatic colorectal cancer, and head and neck cancer	2004
Herceptin (Trastuzumab)	Humanized	Anti-HER2	Breast cancer and stomach cancer	2000
Humira (Adalimumab)	Human	Anti-TNF α	Rheumatoid arthritis, psoriasis-arthritis, spondylitis aknylosans, Crohn's disease, colitis ulcerosa	2003
ILARIS (Canakinumab)	Human	Anti-IL-1 β	autoinflammatory syndromes including familial cold autoinflammatory syndrome, Muckle-Wells syndrome, and neonatal-onset multisystem inflammatory disease	2009
Lucentis (Ranibizumab)	Mouse Fab	Anti-VEGF	"wet" type of age-related macular degeneration (AMD, also ARMD), a common form of age-related	2007

			vision loss	
MabCampath (Alemtuzumab)	Humanized	Anti-CD52	chronic lymphocytic leukemia, cutaneous T-cell lymphoma and T-cell lymphoma, conditioning regimens for bone marrow transplantation, kidney transplantation and Islet cell transplantation	2001
Mabthera (Rituximab)	chimeric	Anti-CD20	Attacks B-cells, lymphomas, leukemias, transplant rejection, and some autoimmune disorders	1998
Prolia (Denosumab)	Human	Anti-RANKL	osteoporosis, treatment-induced bone loss, bone metastases, rheumatoid arthritis, multiple myeloma, and giant cell tumor of bone	2010
Remicade (Infliximab)	Chimeric	Anti-TNF α	Autoimmune diseases	1999
Removab (Catumaxomab)	Hybrid	Bispecific anti-CD3, anti-EpCAM	malignant ascites, a condition occurring in patients with metastasizing cancer	2009
Reopro (Abciximab)	Chimeric	Anti-GPIIb/IIIa	platelet aggregation inhibitor during and after coronary artery procedures like angioplasty to prevent blood clots formation within the coronary artery	1995/2005
Rilonacept Regeneron	Dimer	IL-1 receptor inhibitor	cryopyrin-associated periodic syndromes, including familial cold autoinflammatory syndrome, Muckle-Wells syndrome and neonatal onset multisystem inflammatory disease	2009
RoActemra (Tocilizumab)	Humanized	Anti-IL-6	rheumatoid arthritis and systemic juvenile idiopathic arthritis	2009
Simponi (Golimumab)	Human	Anti-TNF α	severely active rheumatoid arthritis, psoriatic arthritis, and ankylosing spondylitis	2009
Simulect (Basiliximab)	Chimeric	Anti-CD25	prevent rejection in organ transplantation (kidney transplants)	1998
Soliris (Eculizumab)	Humanized	Anti-complement C5	paroxysmal nocturnal hemoglobinuria (PNH), atypical hemolytic-uremic syndrome	2007
Stelara (Ustekinumab)	Human	Anti-IL-12/23	moderate to severe plaque psoriasis	2009
Synagis (Palivizumab)	Humanized	Anti-RS-virus	prevention of respiratory syncytial virus infections	1999
Tysabri (Natalizumab)	Humanized	Anti- α 4-integrin	multiple sclerosis and Crohn's disease	2006
Vectibix (Panitumumab)	Human	Anti-EGFR	EGFR-expressing metastatic colorectal cancer	2007
Xgeva (Denosumab)	Human	Anti-RANKL	osteoporosis, treatment-induced bone loss, bone metastases, rheumatoid arthritis, multiple myeloma, and giant cell tumor of bone	2011
Xolair (Omalizumab)	Humanized	Anti-IgE	severe, persistent allergic asthma	2005
Yervoy (Ipilimumab)	Human	Anti-CTLA-4	turns off this inhibitory mechanism in cells and allows cytotoxic T-lymphocytes to continue to destroy cancer cells	2011
Zevalin (Ibritumomab)	Mouse	Anti-CD20	radioimmunotherapy treatment for relapsed or refractory, low grade or transformed B cell non-Hodgkin's lymphoma	2004

(12 approved recombinant antibodies against carcinoma are marked in grey)

10.4 Abbreviations

Abbreviation	Explanation
♀	Female
♂	Male
	percent
x g	times gravity
<	smaller
>	larger
°C	degree Celsius
∞	infinite
2D	two-dimensional
²	squared
3D	three-dimensional
α	alpha
β	beta
Δ	delta
λ	lamda
μ	micro
Ω	ohm
A	adenine
ABTS	2,2'-azino-bis(3-ethylbenzothiazoline-6-sulphonic acid)
ad	fill volume up to
ADC	antibody-drug-conjugate
AE	actual enrichment
AF	Alexa Fluor
AG	antigen
AIDA	Advanced Image Data Analyzer
AJCC	American Joint Committee on Cancer
AME	Institute for Applied Biomedical Engineering
amp	Ampicillin
AmpR	Ampicillin resistance
APS	ammonium persulfate
ATP	adenosine triphosphate
AUG	RNA triplet coding for methionine
BC	bicinchoninic acid (also: BCA)
BG	benzylguanine
bp	base pairs
BSA	bovine serum albumine
C	cytosine
CA	carbohydrate antigen
CAG	DNA triplet coding for glutamine
CD	cluster of differentiation
cDNA	copy DNA
CDR	complementarity determining region
CEA	carcinoembryonic antigen
CFP	cyan fluorescent protein
cm	centi meter

CMV	cytomegalovirus
ColE1	origin of replication for <i>E.coli</i>
CSC	cancer stem cells
CT	computed tomography scan
CTR	carbon dioxide transfer rate
Da	Dalton
DAB	3,3',4,4'-Tetraaminobiphenyltetrahydrochlorid
DAPI	4',6-diamidino-2-phenylindole
DAPK	death-associated protein kinase
ddH ₂ O	bi-distilled/double distilled water
DF	dilution factor
DMEM	Dulbecco's Modified Eagle Medium
DMSO	Dimethylsuloxide
DNA	desoxyribonucleic acid
dNTP	desoxyribonucleoside triphosphate
DOT	dissolved oxygen tension
DPBS	Dulbecco's Phosphate Buffered Saline
dsDNA	double-stranded DNA
DTT	dithiothreitol
DVT	D = adenine, guanine or thymine, V = adenine, guanine or cytosine, T = thymine
E ₄₀₅	extinction measured at 405 nm
EC	expression control
<i>E.coli</i>	<i>Escherichia coli</i> bacterial strain
EDTA	ethylenediaminetetraacetic acid
EF	enrichment factor
e.g.	"exempli gratia" (for example)
eGFP	enhanced green fluorescencet protein
EGFR	epidermal growth factor receptor
EK	enterokinase
ELISA	enzyme-linked immunosorbent assay
ER	endoplasmic reticulum
ESI/MS	electrospray ionization mass spectroscopy
ETA'	trunated version of <i>Pseudomonas Exotoxin A</i>
EtOH	ethanol
EU/mL	endotoxin units per mL
F	fertility factor
f1 ori	origin of replication for f1 phage
Fab	fragment antigen binding
FACS	Fluorescence activated cell sorting
FbFP	FMN-based fluorescent protein
FBS	fetal bovine serum
Fc	fragment crystallizable
FDA	Food and Drug Association
FhG	Fraunhofer Gesellschaft
FITC	fluorescein isothiocyanate
FMN	flavin mononucleotide-binding protein
FP	fluorescent protein
FU	fluorouracil

FWR	framework region
g	gram
G	guanine
GAM	goat-anti-mouse
GFP	green fluorescent protein
gluc	glucose
G-mean	geometrical mean
GS-linker	glycine-serine linker
h	hour
HACA	human anti-chimeric antibody
hAGT	human O ₆ -alkylguanine DNA alkyltransferase repair enzyme
HAHA	human anti-human antibody
HAMA	human anti-mouse antibody
HEK	human embryo kidney
His	histidine
His ₆ -tag	protein affinity tag consisting of six histidine residues
HPLC	high pressure liquid chromatography
HRP	horseradish peroxidase
I	intensity
IDA	iminodiacetic acid
i.e.	“id est” (that is)
IgG	immunoglobulin G
IF	immunofluorescence
IHC	immunohistochemistry
IMAC	Immobilized metal-ion affinity chromatography
IME	Institute for Molecular Biology and Ecology
IMRT	intensity-modulated radiation therapy
IPTG	isopropyl β-D-1-thiogalactopyranoside
IRES	internal ribosomal entry sequence
IT	immunotoxin
IVS	intervening sequence
kan	Kanamycin
KanR	Kanamycin resistance
kb	kilo bases
KBE/mL	“koloniebildende Einheiten“ per mL
L	liter
LB medium	Lysogeny Broth medium
LOV	light-oxygen-voltage
<i>Luc</i>	cell line transfected with click-beetle red luciferase
m	milli
M	mega
M	molar
mAB	monoclonal antibody
MFI	mean fluorescence intensity
min	minute
MOI	multiplicity of infection
mol	moles
MOPS	3-(N-morpholino)propanesulfonic acid

MRC	Medical Research Council
MRD	minimal residual disease
MRI	magnetic resonance imaging
MTP	microtiter plate
MW	molecular weight
<i>myc</i>	myelocytomatosis oncogen
n	nano
NC	negative control
NNK	N = refers to any base, K = cytosine or guanine
NOD	non-obese diabetic
NTA	Nitrioltriactic acid
OD ₆₀₀	optical density measured at 600 nm
O/N	over night
OPERA	Oscillation Project with Emulsion-tRacking Apparatus
ORF	open reading frame
OTR	oxygen transfer rate
p	pico
p	p-value, probability, statistical significance
pI – pXI	M13 phage coat proteins
PAA	polyacrylamide
PCR	polymerase chain reaction
<i>pelB</i>	pectate lyase B
PET	positron emission tomography
PBMC	peripheral blood mononuclear cell
PBS	phosphate buffered saline
PBST	Phosphate buffered saline supplemented with 0.05% Tween20
PCR	polymerase chain reaction
PEG	polyethylene glycol
PFA	paraformaldehyde
pfu	plaque forming unit
<i>pfiTurbo</i>	DNA polymerase from <i>Pyrococcus furiosus</i>
PO	peroxidase
pSV40	origin of replication for SV40
Q-TOF	quadrupole time-of-flight mass analyzer
RAMOS	Respiration Activity Monitoring System
RB	retinoblastoma-associated
RBS	ribosomal binding site
RNA	ribonucleic acid
rpm	revolutions per minute
RPMI	Roswell Park Memorial Institute
RQ	respiratory quotient
RT	room temperature
s	second
SBP	streptavidin binding peptide
scFv	Single chain fragment variable
SCID	Severe Combined Immunodeficiency
SDS-PAGE	sodium dodecylsulfate polyacrylamide gel electrophoresis
SOC	SOB (Super Optimal Broth) containing 20 mM glucose

SOE	Splicing by overlap extension
SR	selection round
ssDNA	single-stranded DNA
SV40	Simian vacuolating virus 40
SV40 pA	SV40 polyadenylation signal
t	time
T	temperature
T	thymine
TAA	tumor-associated antigen
TAE	Tris-Acetate-EDTA buffer
TAG	<i>amber</i> stop codon
TCSN	tissue culture supernatant
TEA	triethylamide
TEMED	tetramethylethylenediamine
TES	Tris-EDTA-sucrose buffer
TGA	<i>ochre</i> stop codon
TGG	DNA triplet coding for tryptophan
T _m	melting temperature
TSP-1	thrombospondin-1
TY medium	tryptone-yeast medium
UKA	University Hospital Aachen
UKGM	University Hospital Giessen and Marburg
UV	ultraviolet
V	volt
VEGF-A	vascular endothelial growth factor A
VG	Vista Green
V _H	heavy chain variable region
V _L	light chain variable region
vs.	versus
v/v	volume per volume
v/w	volume per weight
W	tryptophan
W1 – W5	one to five tryptophan
Wx-tag	short reporter tag containing accumulated tryptophan
WB	Western blot
w/v	weight per volume
XTT	2,3-bis-(2-methoxy-4-nitro-5-sulfophenyl)-2H-tetrazolium-5-carboxanilide salt
YFP	yellow fluorescent protein
Zeo	Zeocin
ZeoR	Zeocin resistance

10.5 List of figures

Figure 1-1	Schematic drawing of monoclonal antibody, F(ab') ₂ fragment and scFv to illustrate the structure of immunoglobulins (Ig) and derived antibody fragments.	11
Figure 1-2	Schematic of filamentous M13 bacteriophage and E.coli with F-pili.	14
Figure 1-3	General schematic illustration of phage display panning procedure for the selection of specific scFv-phage particles.	15
Figure 1-4	Schematic illustration of pIT2 phagemid and corresponding expression cassette for production of scFv-phage particles.	18
Figure 1-5	Illustrated protein structure of GFP and YtvA LOV domain from <i>Bacillus subtilis</i> exemplarily for the FMN-based fluorescent proteins. (A) Figure displays the 11-stranded β -barrel (green) and the chromophore attached to the α -helix in its center (brown) [203]. (B) Its FMN-binding domain consists of five β -sheet structures (blue) that are flanked by two α -helices (red and yellow). The chromophore is indicated in green, and the photoactive cysteine in the center is colored red [200].	26
Figure 1-6	Schematic illustration of SNAP-tag coupling mechanism. [214]	27
Figure 1-7	Flow chart illustrating the two objectives of this thesis and their experimental approach.	32
Figure 2-1	Schematic drawing of plasmid maps of expression vectors pMT and pMS-SNAPMut.	40
Figure 3-1	Schematic for phage display selection on adherent whole L3.6pl cells.	69
Figure 3-2	Schematic for phage display selection on L3.6pl cells in suspension.	70
Figure 3-3	Schematic for phage display selection on L3.6pl membrane fractions.	72
Figure 4-1	Polyclonal phage ELISA after three panning rounds on adherent L3.6pl cells.	81
Figure 4-2	Polyclonal phage ELISA after three selection rounds on L3.6pl cells in suspension.	82
Figure 4-3	Polyclonal phage ELISA after three consecutive panning rounds with Tomlinson libraries I and J on L3.6pl membrane fractions.	85
Figure 4-4	Monoclonal phage ELISA after first and third selection round on adherent L3.6pl cells.	86
Figure 4-5	Monoclonal phage ELISA after three panning rounds on L3.6pl cells in suspension.	87
Figure 4-6	Monoclonal phage ELISA after three panning rounds with Tomlinson Library I and J on L3.6pl membrane fractions.	89

Figure 4-7	Monoclonal phage ELISA of 14.1(scFv) on L3.6pl membrane fractions isolated from the murine self-made from immunized mice after multiple selection rounds on L3.6pl antigen.	90
Figure 4-8	Cross-reactivity data of isolated clones and 14.1(scFv) obtained by means of monoclonal phage ELISA analysis on FG, Su86.86, S2-0028 and PT-46 membrane fractions.	94
Figure 4-9	Schematic of pMT expression cassette for prokaryotic production of soluble scFv protein in BL21 Rosetta 2 (DE3).	97
Figure 4-10	Schematic of pMS-SNAPMut expression cassette for eukaryotic expression of soluble scFv-SNAP proteins in transiently transfected HEK293T.	98
Figure 4-11	Western blot analysis of tissue culture supernatant containing transiently expressed scFv-SNAP proteins.	99
Figure 4-12	SDS-PAGE and Western blot analysis of IMAC-purified scFv-SNAP proteins with subsequent AF647 labeling.	100
Figure 4-13	Protein ELISA analysis with soluble scFv-SNAP proteins produced in HEK293T cells.	101
Figure 4-14	Flow cytometric binding activity data of scFv-SNAP proteins on L3.6pl and PBMC cells.	102
Figure 4-15	Flow cytometric analysis of binding activity of D5(scFv) and D9(scFv) indicating a possible subpopulation within the L3.6pl cell line.	103
Figure 4-16	Flow cytometric documentation of internalization and binding properties of 14.1(scFv)-SNAP, A3(scFv)-SNAP, D4(scFv)-SNAP and F1(scFv)-SNAP labeled with AF647 on L3.6pl cells.	106
Figure 4-17	Immunofluorescence staining of 14.1(scFv)-SNAP protein incubated on L3.6pl cells at 4°C and 37°C.	108
Figure 4-18	Immunofluorescence staining of A3(scFv)-SNAP on L3.6pl cells at 4°C and 37°C.	109
Figure 4-19	Immunofluorescence staining of D4(scFv)-SNAP and F1(scFv)-SNAP incubated on L3.6pl cells at 4°C and 37°C.	110
Figure 4-20	Internalization kinetics of 14.1(scFv)-SNAP-AF647 into L3.6pl cells at 37°C at different time points.	111
Figure 5-1	3D-models of amino acid sequence structures of all five W-tags.	114
Figure 5-2	Expression cassette for pMT-Wx-Ki-4(scFv) and pMT-Wx-M12(scFv) fusion protein constructs.	115
Figure 5-3	Wx-Ki-4(scFv) protein expression analysis on SDS-PAGE and Western blot.	116

Figure 5-4	SDS-PAGE and Western blot analysis of Wx-Ki-4(scFv) proteins secreted into cultivation medium.	117
Figure 5-5	Calculated percentage of Wx-Ki-4(scFv) proteins referring to total bacterial protein after determination of protein concentration with AIDA.....	118
Figure 5-6	On-line detection of biomass formation and production of Wx-Ki-4(scFv) target fusion proteins.....	121
Figure 5-7	On-line detection of biomass formation and production of Wx-M12(scFv) fusion target proteins.	122
Figure 5-8	SDS-PAGE and Western blot of Wx-Ki-4(scFv) fusion proteins after bacterial lysis with TES buffer.	123
Figure 5-9	Documentation of protein dialysis with SDS-PAGE and Western blot analysis of EC, W1-Ki-4(scFv), W2-Ki-4(scFv) and W3-Ki-4(scFv) after TES lysis and buffer exchange to PBS.	124
Figure 5-10	Protein ELISA binding analysis of dialyzed TES crude lysate containing all five Wx-Ki-4(scFv) fusion proteins.	126
Figure 5-11	Flow cytometric binding analysis of Wx-Ki-4(scFv) fusion proteins on L540cy cells.	127
Figure 5-12	Competitive flow cytometry of Ki-4(scFv), W1-Ki-4(scFv), W2-Ki-4(scFv), W3-Ki-4(scFv) against a monoclonal Ki-4 full length antibody.....	128
Figure 5-13	Two-dimensional fluorescence intensity scan of concentrated Ki-4(scFv) tagged with different Wx-tags.	129
Figure 6-1	Illustrated distribution of L3.6pl-positive clones with regard to panning strategy and characteristics of scFv insert.	142

10.6 List of tables

Table 1-1	Six generally applicable characteristics for development of malignant tumor cells. [4, 5]	1
Table 1-2	Statistical data on pancreatic cancer in Germany in 2008 with a prognosis for 2012. [1].....	2
Table 1-3	List of approved exemplarily mABs with a direct and indirect effector mechanisms.....	8
Table 1-4	List of common affinity tags including matrices, sequences and molecular size [186].....	23
Table 2-1	List of software, its application and corresponding supplier.....	33
Table 2-2	List of hardware with corresponding suppliers.....	34
Table 2-3	List of <i>E.coli</i> strains, their genotypes and corresponding suppliers.....	35
Table 2-4	List of cultivation media and agars and their exact formulae	35
Table 2-5	List of cell lines, their originating tissue, supplier and cultivation medium	36
Table 2-6	List of tissue culture media and supplementary components for tissue culture	36
Table 2-7	List of enzymes and corresponding suppliers	37
Table 2-8	List of commercially available kits and corresponding suppliers	37
Table 2-9	List of composition of buffers and solutions.....	38
Table 2-10	List of antibiotics	39
Table 2-11	List of antibodies for immunological analysis	39
Table 2-12	Primer sequences and corresponding vectors for sequencing and PCR.....	39
Table 2-13	Plasmid vectors/phagemids, corresponding background information and suppliers.....	40
Table 2-14	Molecular DNA and protein markers and corresponding suppliers.....	41
Table 2-15	Description of different types of phage particles and corresponding suppliers	41
Table 3-1	Reaction conditions of DNA template-based PCR amplification reaction.	43
Table 3-2	Reaction conditions of colony-based PCR amplification reaction.....	43
Table 3-3	Washing steps with increasing stringency applied during solid phase selection on adherent whole cells.....	68
Table 3-4	Washing steps with increasing stringency used for selection rounds one, two and three during suspension panning with whole L3.6pl cells	70
Table 3-5	Dilution of membrane fraction antigen used for selection rounds one, two and three.	71

Table 3-6	Washing steps with increasing stringency applied during selections rounds one to three for all modes of selection.	71
Table 3-7	Reaction conditions of site-directed mutagenesis of <i>amber</i> stop codons using the QuikChange Site-Directed Mutagenesis Kit.	73
Table 4-1	Five different blocking/washing reagents tested for their adverse effects on L3.6pl cells	78
Table 4-2	Documentation of negative effects for five different washing reagents tested on the cell line L3.6pl using panning conditions of third selection round.	78
Table 4-3	Input and output titer of elution and lysis fractions during three consecutive panning rounds on adherent L3.6pl cells.	80
Table 4-4	Input and output titrations of selections on Tomlinson library I on L3.6pl cells in suspension as well as enrichment factors (EF) and actual enrichment (AE) after each selection round.	82
Table 4-5	Input and output titers as well as enrichment factors (EF) and actual enrichment (AE) of panning rounds with Tomlinson Library I and J on L3.6pl membranes fractions.	83
Table 4-6	Overview of number of master plates and clones analyzed via monoclonal phage ELISA after three consecutive panning rounds with three different selection strategies, as well as number of resulting L3.6pl-positive binders.	90
Table 4-7	Overview of number and proportion of L3.6pl-positive clones identified with an intact DNA insert sequence with respect to different selection strategies.	91
Table 4-8	Overview of number of L3.6pl-binding clones with intact, identical and unique DNA sequence	91
Table 4-9	Overview of number and percentage of sequence-unique L3.6pl-positive clones contain <i>amber</i> or <i>ochre</i> stop codons.	91
Table 4-10	Amino acid sequences of complementarity determining regions (CDRs) in V _H and V _L of 16 scFv antibodies identified as L3.6pl-positive binders during monoclonal phage ELISA analysis.	92
Table 4-11	Results of flow cytometric cross-reactivity testing with L3.6pl-positive scFv-SNAP antibody fragments on other pancreatic carcinoma cell lines.	104
Table 4-12	Results of flow cytometric cross-reactivity testing with L3.6pl-positive scFv-SNAP antibodies on cell lines derived from several different cancer types.	104
Table 5-1	Five different W-tag variations stating the number of tryptophan residues per construct, the construct name, the total number of aromatic amino acids (tryptophan, tyrosine and phenylalanine) as well as the size of the tag region and fusion protein in kDa. [246].	113

Table 5-2	DNA and protein sequences of all five W-tags.....	113
Table 5-3	Mean fluorescence intensity (MFI) values and geometrical mean of the fusion proteins.	127
Table 6-1	Comparing illustration of structure and characteristics of aspartic acid and asparagine.	146
Table 10-1	Individual primer sequences for site-directed QuikChange Mutagenesis.....	178
Table 10-2	Overview of <i>amber</i> and <i>ochre</i> stop codons found in isolated scFv antibody fragments.	178
Table 10-3	Overview of codes for amino acids.....	179
Table 10-4	List of recombinant antibodies approved for treatment in Europe. [77].....	179

10.7 Publications, presentations and posters

1. Siepert, E.M., Gartz E., Tur M.K., Delbrück H., Barth S., Büchs J. *Short-chain fluorescent tryptophan tags for on-line detection of functional recombinant proteins.* **BMC Biotechnol**, 2012. 12(1): p. 65.
2. Siepert E.-M., Füllmann C., Barth S., Tur M.K. – Generating scFv antibodies against pancreatic carcinoma from naïve human Phage Display Libraries for clinical application. **Abstract, Kongressband 30. Deutscher Krebskongress 2012, Berlin**
3. Siepert E.-M., Roesgen C., Barth S., Tur M.K. – Generation of scFv antibodies against pancreatic carcinoma using a naïve human Phage Display Library. **Abstract, Kongressband 29. Deutscher Krebskongress 2010, Berlin**
4. Siepert E.-M., Roesgen C., Barth S., Tur M.K. – Isolation of scFv antibodies against unknown internalizing TAA on pancreatic cancer cells using a human antibody Phage Display Library. **Biomedica 2009, Liège (Belgien)**
5. Siepert E.-M. – Isolation and characterization of scFv antibodies against pancreatic carcinoma from naïve human Phage Display Libraries for clinical application. **ScieTalk NRW 2012, Münster**

10.8 Curriculum Vitae

Eva-Maria Siefert (M.Sc.)

Luisenstraße 26

52070 Aachen

Telefon: 0176-2456-5217

E-Mail: e_m_siefert@yahoo.de

geboren am: 16. September 1981 in Bad Säckingen

Staatsangehörigkeit: deutsch

Familienstand: ledig

Berufstätigkeit

- | | |
|------------------|--|
| 10/2012 – 6/2013 | Pharmedartis GmbH in Aachen, Research Associate , Herstellung und Entwicklung humaner und bakterieller Immuntoxine für die therapeutische Anwendung |
| 10/2011 – 9/2012 | Helmholtz Institut für Angewandte Medizintechnik der RWTH Aachen, wissenschaftliche Mitarbeiterin im Projekt „ForSaTum“ : Isolierung von spezifischen single chain Fragmenten (scFv) gegen Pankreaskarzinom mittels Phage Display Technologie, |
| 9/2007 – 9/2011 | Helmholtz Institut für Angewandte Medizintechnik der RWTH Aachen, wissenschaftliche Mitarbeiterin, Molekularbiologische Projektverantwortung eines DFG-geförderten Projektes: „Online-Messung von rekombinanten Proteinen mit kurzen Tags“ <ul style="list-style-type: none">• Betreuung von Diplom-/Masterstudenten und Forschungspraktikanten• Beantragung von Drittmitteln, eigenständige Antragsstellung |

Ausbildung und Studium

- | | |
|------------------|--|
| 9/2007 – 11/2013 | Promotionsstudium in Biologie
RWTH Aachen, Prüfungsdatum: 22. November 2013 |
| 10/2005 – 2/2007 | Englischsprachiges Masterstudium in Biotechnology an der Hochschule Mannheim, Master of Science (M.Sc.), Note 1,5 |
| 10/2002 – 6/2005 | Internationales Bachelorstudium in Chemistry with Marketing an der HS Reutlingen, Bachelor of Chemical Engineering (BEng), Note 1,6 |
| 9/1992 – 6/2001 | Hochrhein Gymnasium Waldshut, Allgemeine Hochschulreife, Note 2,0 |

Praktische Erfahrung und Praktika

3/2012	Erwerb des FELASA-B-Zertifikats zur eigenständigen Durchführung von tierexperimentellen Arbeiten
9/2006 – 2/2007	Tierexperimentelle Arbeit im Rahmen der Masterthesis an der Washington University, St. Louis (USA) : “Investigations to identify a Candidate Gene thought to cause the rapunzel Phenotype in Zebrafish using Transgenesis and Mammalian Cell Culture”
8/2004 – 1/2005	Praxissemester bei Merck KGaA , Darmstadt in der Abteilung New Venture Materials, Projekt: Ionic Liquids

Auslandserfahrung

9/2006 – 2/2007	Masterthesis an der Washington University, St. Louis, im Labor von Matthew I. Goldsmith, Department of Pediatrics and Genetics
2/2004 – 6/2004	Theoretisches Semester an der Dublin City University (Irland)
8/2001 – 8/2002	Au-Pair bei einer Familie mit drei Kindern in Raleigh, NC (USA)

Stipendien

10/2010 – 6/2011	Abschluss-Stipendium der Graduiertenförderung, RWTH Aachen
9/2006 – 2/2007	Stipendium der Washington University, St. Louis (USA)
2/2004 – 6/2004	ERASMUS-Stipendium

EDV – und sonstige fachliche Kenntnisse

- Protein-Datenverarbeitung: WIN-MDI, FLOWing, AIDA
- DNA-Datenverarbeitung: DNASTAR LaserGene, vector NTI, Geneious, CloneManager,
- GraphPadPrism, MS-Office
- Bioreaktorsimulation: MADONNA Berkley

Sprachkenntnisse

Deutsch	Muttersprache
Englisch	fließend in Wort und Schrift
Französisch, Spanisch	Grundkenntnisse
Latein	Großes Latinum

Hobbies

Tanzen (Standard/Latein), Ballett, Klettern, Segeln und Reisen

10.9 Acknowledgement

The success of any project largely depends on the encouragement and guidelines of many people. I take this opportunity to express my gratitude to the people who have been instrumental for the completion of my thesis.

I would like to thank my supervisor Prof. Dr. Dr. Stefan Barth for the opportunity to pursue my PhD thesis as part of his research group *Experimental Medicine and Immunotherapy (EMI)* at the Helmholtz Institute for Applied Biomedical Engineering. His support during all stages of my thesis, as well as creative suggestions, were very helpful for my work.

Furthermore, I would like to thank Prof. Dr. Lothar Elling for co-supervising my thesis as second examiner.

I also would like to thank Dr. Mehmet K. Tur for supervising the laboratory work of this thesis. His valuable suggestions and advice in the preparation of this dissertation and his trouble-shooting during the experimental part of this work were of great help.

Thanks also go to our co-operation partner from the Department of Biochemical Engineering at RWTH Aachen University, Prof. Dr. Jochen Büchs and Esther Gartz. This excellent collaboration and exchange of scientific knowledge gave me a keen insight into on-line fermentation methods and helped me gather important measurement data. In this context, I would also like to thank Dr. Heinrich Delbrück for his help with the protein design of the W-tags.

Many thanks go to the German Research Foundation (DFG) for partially funding this thesis.

Special thanks go to my closest colleagues Jenny Fitting, Claudia Füllmann, Pamela Bogner and Tobias Blume. I very much appreciate the discussions we had, the motivation they gave me, their understanding and of course our good friendship that goes beyond everyday work. Also many thanks go to my co-workers at IME, EMI and Pharmedartis for their co-operation in the laboratory and an inspiring working atmosphere.

Special thanks go to my family. Thank you very much for believing in me!

Finally, I want to express my deepest gratitude to my fiancé Felix Allmendinger for his encouragement and support during the past years.